Topics in Current Chemistry 319

Markus Albrecht
F. Ekkehardt Hahn *Editors*

Chemistry of Nanocontainers

Springer

319

Topics in Current Chemistry

Topics in Current Chemistry

Recently Published and Forthcoming Volumes

Chemistry of Nanocontainers
Volume Editors: Markus Albrecht, F. Ekkehardt Hahn
Vol. 319, 2012

Liquid Crystals: Materials Design and Self-Assembly
Volume Editor: Carsten Tschierske
Vol. 318, 2012

Fragment-Based Drug Discovery and X-Ray Crystallography
Volume Editors: Thomas G. Davies, Marko Hyvönen
Vol. 317, 2012

Novel Sampling Approaches in Higher Dimensional NMR
Volume Editors: Martin Billeter, Vladislav Orekhov
Vol. 316, 2012

Advanced X-Ray Crystallography
Volume Editor: Kari Rissanen
Vol. 315, 2012

Pyrethroids: From Chrysanthemum to Modern Industrial Insecticide
Volume Editors: Noritada Matsuo, Tatsuya Mori
Vol. 314, 2012

Unimolecular and Supramolecular Electronics II
Volume Editor: Robert M. Metzger
Vol. 313, 2012

Unimolecular and Supramolecular Electronics I
Volume Editor: Robert M. Metzger
Vol. 312, 2012

Bismuth-Mediated Organic Reactions
Volume Editor: Thierry Ollevier
Vol. 311, 2012

Peptide-Based Materials
Volume Editor: Timothy Deming
Vol. 310, 2012

Alkaloid Synthesis
Volume Editor: Hans-Joachim Knölker
Vol. 309, 2012

Fluorous Chemistry
Volume Editor: István T. Horváth
Vol. 308, 2012

Multiscale Molecular Methods in Applied Chemistry
Volume Editors: Barbara Kirchner, Jadran Vrabec
Vol. 307, 2012

Solid State NMR
Volume Editor: Jerry C. C. Chan
Vol. 306, 2012

Prion Proteins
Volume Editor: Jörg Tatzelt
Vol. 305, 2011

Microfluidics: Technologies and Applications
Volume Editor: Bingcheng Lin
Vol. 304, 2011

Photocatalysis
Volume Editor: Carlo Alberto Bignozzi
Vol. 303, 2011

Computational Mechanisms of Au and Pt Catalyzed Reactions
Volume Editors: Elena Soriano, José Marco-Contelles
Vol. 302, 2011

Reactivity Tuning in Oligosaccharide Assembly
Volume Editors: Bert Fraser-Reid, J. Cristóbal López
Vol. 301, 2011

Chemistry of Nanocontainers

Volume Editors: Markus Albrecht · F. Ekkehardt Hahn

With Contributions by

D. Ajami · S. Kubik · J. Mattay · I.M. Oppel · J. Rebek · R.W. Saalfrank · S.N. Sahu · A. Scheurer · T. Schröder · A.C. Schulze · B. Therrien

Editors
Prof. Dr. Markus Albrecht
Institut für Organische Chemie
RWTH Aachen
Landoltweg 1
52074 Aachen
Germany
markus.albrecht@oc.rwth-aachen.de

Prof. Dr. F. Ekkehardt Hahn
Institut für Anorganische und
Analytische Chemie
University Münster
Corrensstraße 28/30
48149 Münster
Germany
fehahn@uni-muenster.de

ISSN 0340-1022 e-ISSN 1436-5049
ISBN 978-3-642-28058-0 e-ISBN 978-3-642-28059-7
DOI 10.1007/978-3-642-28059-7
Springer Heidelberg Dordrecht London New York

Library of Congress Control Number: 2012931150

Printed on acid-free paper

Springer is part of Springer Science+Business Media (www.springer.com)

Volume Editors

Prof. Dr. Markus Albrecht

Institut für Organische Chemie
RWTH Aachen
Landoltweg 1
52074 Aachen
Germany
markus.albrecht@oc.rwth-aachen.de

Prof. Dr. F. Ekkehardt Hahn

Institut für Anorganische und
Analytische Chemie
University Münster
Corrensstraße 28/30
48149 Münster
Germany
fehahn@uni-muenster.de

Editorial Board

Topics in Current Chemistry Also Available Electronically

Topics in Current Chemistry is included in Springer's eBook package *Chemistry and Materials Science*. If a library does not opt for the whole package the book series may be bought on a subscription basis. Also, all back volumes are available electronically.

For all customers with a print standing order we offer free access to the electronic volumes of the series published in the current year.

If you do not have access, you can still view the table of contents of each volume and the abstract of each article by going to the SpringerLink homepage, clicking on "Chemistry and Materials Science," under Subject Collection, then "Book Series," under Content Type and finally by selecting *Topics in Current Chemistry*.

You will find information about the

– Editorial Board
– Aims and Scope
– Instructions for Authors
– Sample Contribution

at springer.com using the search function by typing in *Topics in Current Chemistry*.

Color figures are published in full color in the electronic version on SpringerLink.

Aims and Scope

The series *Topics in Current Chemistry* presents critical reviews of the present and future trends in modern chemical research. The scope includes all areas of chemical science, including the interfaces with related disciplines such as biology, medicine, and materials science.

The objective of each thematic volume is to give the non-specialist reader, whether at the university or in industry, a comprehensive overview of an area where new insights of interest to a larger scientific audience are emerging.

Thus each review within the volume critically surveys one aspect of that topic and places it within the context of the volume as a whole. The most significant developments of the last 5–10 years are presented, using selected examples to illustrate the principles discussed. A description of the laboratory procedures involved is often useful to the reader. The coverage is not exhaustive in data, but rather conceptual, concentrating on the methodological thinking that will allow the non-specialist reader to understand the information presented.

Discussion of possible future research directions in the area is welcome.

Review articles for the individual volumes are invited by the volume editors.

In references *Topics in Current Chemistry* is abbreviated *Top Curr Chem* and is cited as a journal.

Impact Factor 2010: 2.067; Section "Chemistry, Multidisciplinary": Rank 44 of 144

Preface

Recently, "nanosphere", "nanocontainer", "nanovessel" or "nanoflask" have become keywords in a fast developing area of supramolecular chemistry. This vivid chemistry was developed based on Donald Cram's early vision to make molecules with a huge internal cavity able to incorporate guest species. Today's approaches to preparing container molecules follow different strategies. One option is to prepare covalently connected derivatives step-by-step using "classical" synthetic methodologies. Another way is to use self-assembly processes which allow easy access to the desired derivatives. In this case, non-covalent linkages (hydrogen bonding, metal coordination or electrostatics) or weak covalent bonds (imines or disulfides) keep the supramolecular entities together. Due to the different natures of the connections, the obtained aggregates are more or less stable.

In addition to their beauty, many of the described nanovessels also show interesting endo/exo chemistry ("inside" and "outside"). In the interior, species can be bound, and highly reactive intermediates can be stabilized, or chemical reactions supported or catalyzed. In the latter case, unusual reactivity or selectivity might be observed. Thus, container molecules act as homogeneous equivalents of heterogeneous porous materials like zeolites or MOFs.

Due to the immense interest in this type of chemistry, the field has rapidly expanded and diversified over the last two decades. In this volume, some of the most prominent scientists in the field contribute extensive reviews, which show the versatility of approaches towards nanocontainers, and give some examples of processes occurring in their interior. The science of nanovessels is still in its infancy and therefore this field is expected to emerge further and develop a high impact in future chemistry. With the size and the special properties of the described derivatives, it bridges the gap between "traditional" chemistry and nanotechnology.

Markus Albrecht
F. Ekkehardt Hahn

Contents

Top Curr Chem (2012) 319: 1–34
DOI: 10.1007/128_2011_244

Published online: 28 September 2011

Molecular Cages and Capsules with Functionalized Inner Surfaces

Stefan Kubik

Abstract Molecular containers enclose a well defined cavity in which an appropriate guest molecule can be included. The corresponding complexes are generally characterized by high kinetic stability. Thermodynamic stability can be rather low, however, because attractive interactions are largely missing between host and guest causing binding to be mainly due to entropic factors. This situation can be improved by distributing appropriate binding sites across the inner surface of a molecular container to which an included guest can bind. This approach, while being conceptually simple, is not straightforward since the incorporation of converging binding sites into a concave surface is difficult and usually requires receptors architectures that differ from those of conventional covalently assembled molecular containers. Therefore, the term molecular cage rather than molecular container is often more appropriate for such types of receptors. In this overview, a selection of cage-type receptors is presented whose inner cavity is functionalized with groups that can engage in directed interactions with an included guest. These receptors, classified according to the type of interaction responsible for guest binding, were chosen to illustrate effects of the inwardly directed binding sites on receptor affinity, selectivity, or other binding properties.

Keywords Molecular cages · Molecular capsules · Molecular containers · Molecular recognition · Noncovalent interactions

Contents

S. Kubik
Technische Universität Kaiserslautern, Fachbereich Chemie – Organische Chemie,
Erwin-Schrödinger-Straße, 67663 Kaiserslautern, Germany
e-mail: kubik@chemie.uni-kl.de

Abbreviations

DBU	Diaza(1,3)bicyclo[5.4.0]undecene
DMA	*N*,*N*-Dimethylacetamide
DMF	*N*,*N*-Dimethylformamide
DMSO	Dimethylsulfoxide
TfO	Trifluoromethylsulfonate
TREN	Tris(2-aminoethyl)amine

1 Introduction

A container is an object with a convex outer surface that encloses a certain volume of space in which other objects complementary in size and shape can be included. Once closed, a container entraps the included object and can hold it practically indefinitely. Every aspect of this definition of macroscopic containers can be transferred into the nanoscopic molecular dimension as perfectly demonstrated by Cram's *carcerands* [1, 2]. These compounds, a prototype of which is **1**, contain incarcerated small molecules such as DMSO, DMF, or DMA when isolated which were present during synthesis (and usually templated carcerand formation). Guest release from these complexes is virtually impossible without breaking covalent bonds because the portals distributed across the carcerand surface are far too small. Many other examples for carcerand complexes, so-called *carceplexes*, structurally relate to **1**, but also include endohedral fullerenes [3, 4].

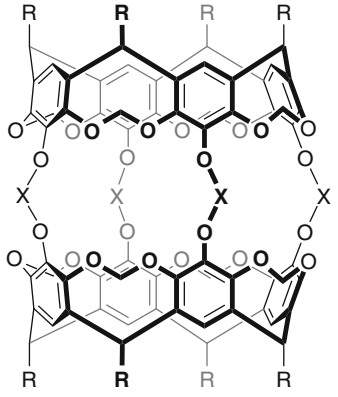

1 (X = CH_2, R = CH_2CH_2Ph)

2 (X = 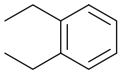 , R = CH_2CH_2Ph)

Since containers that only release their content when destroyed are somewhat impractical, derivatives of **1** with larger portals have been devised that allow reversible guest exchange. A straightforward strategy to increase portal size involved incorporation of longer linkers between the two resorcarene-derived hemispheres [1]. Such compounds have the additional advantage of enclosing a larger cavity, thus allowing the inclusion of more sizeable guests. By definition, they are termed *hemicarcerands* if a reasonable rate of guest exchange can be achieved at elevated temperatures while kinetically inert complexes (*hemicarceplexes*) are formed at room temperature. Systematic characterization of the binding equilibria has shown that complex dissociation and formation of hemicarcerands, an example of which is **2**, are associated with a considerable activation barrier [5]. This barrier is due to strain induced in the linkers or in the guest when the latter squeezes through the portals while entering or leaving the cavity. To describe the kinetic stability of hemicarcerands on a more quantitative basis, Cram has introduced the concept of *constrictive binding* [5, 6]. This term describes the free energy of the transition state for association relative to the free energy of the uncomplexed state (Fig. 1). In other words, constrictive binding refers to the free energy, which must be provided to reach the transition state of dissociation from the associated state minus the intrinsic binding free energy of the binding partners.

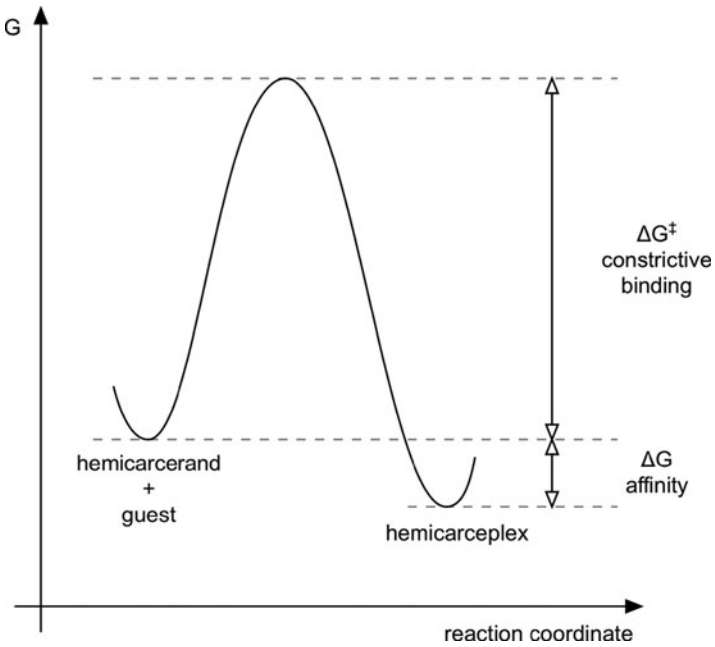

Fig. 1 Energy profile of a hemicarceplex formation illustrating the energy barrier imposed by *constrictive binding*

Detailed binding studies demonstrated that constrictive binding generally takes the larger share of the overall free energy required for a hemicarceplex to reach the transition state when dissociating. For instance, by following the rate with which DMA enters or leaves the cavity of hemicarcerand **2**, the free activation energy of association (constrictive binding) was determined to amount to 98.4 kJ mol^{-1} and the free activation energy of dissociation to 113.9 kJ mol^{-1} (in *o*-xylene-d_{10} at 100 °C) [5]. Thus, the intrinsic binding energy ΔG which describes the thermodynamic stability of DMA $\subset$ **2** is -15.5 kJ mol^{-1}, corresponding to an association constant K_a of 150 M^{-1}. Breaking down this thermodynamic stability into the enthalpic and entropic contribution furthermore shows that both parameters contribute roughly equally to the overall complex stability ($\Delta H = -6.3$ kJ mol^{-1}, $T\Delta S = 9.2$ kJ mol^{-1}) [5]. Thus, attractive interactions between the guest and groups lining the inner wall of **2** play a minor role for hemicarceplex stability. Such interactions sometimes provide a rationale for effects of guest structure on the stability of hemicarceplexes, and they have been invoked to explain differences in the templating ability of structurally related guests [1], but the largest share of the reluctance of a hemicarcerand to release its guest generally stems from kinetic effects.

The deep cavitand **3** described by Rebek and coworkers exhibits similar properties. This compound, although strictly not a molecular container because it lacks the lid, forms kinetically surprisingly stable complexes with, for example, adamantane in *p*-xylene-d_{10} [7]. The activation barrier for the exchange between free and complexed guest was determined by EXSY NMR spectroscopy to amount to 70.6 $\pm$ 1.7 kJ mol^{-1} at 22 °C. Thermodynamically, however, the complex is only 8.4 $\pm$ 1.3 kJ mol^{-1} more stable than the free components ($K_a = 40 \pm 10$ M^{-1}). Again, the kinetic stability of this complex is not due to attractive interactions between host and guest, but to a special mechanism of complex dissociation. In this case, dissociation involves the energy costly cleavage of four hydrogen bonds along the seam of the cavitand followed by a conformational reorganization of **3** from the closed *vase* to the open *kite* conformation. Direct exchange of adamantane for a solvent molecule in the *vase* conformation is impossible because the opening of the cavitand in this conformation is too small for two molecules to squeeze past each other [8].

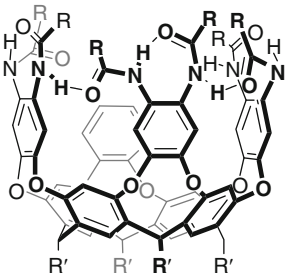

3 (R = C_6H_{13}, R′ = $C_{11}H_{23}$)

The relatively low thermodynamic stability of complexes of hemicarcerands or other container-type hosts is a direct consequence of structural aspects of the walls that make up the inner surface of such compounds. These walls are lined by aromatic subunits while free electron pairs of heteroatoms such as those of the ether oxygen atoms are preferentially oriented to the outside. Complexes are therefore enthalpically stabilized only by weak dispersive interactions. In the case of positively charged guests cation–π interactions can contribute to binding enthalpy as in a self-assembled calixarene-derived capsule [9], but directed interactions such as hydrogen-bonding interactions are usually absent.

It can be expected that incorporation of functional groups into the cavity of a molecular container that allow directed interactions should cause a considerable increase in thermodynamic complex stability and potentially also induce binding selectivity. Another attractive aspect of this concept would be that it should give access to hollow host molecules whose interiors closely mimic active sites buried deeply within globular proteins. To arrange functional groups able to serve as binding sites in a converging manner along the concave inner surface of a hollow molecule is not easy, however. Molecular containers with functionalized inner surfaces therefore usually derive from other types of hosts than carcerands.

Among the earliest examples of synthetic receptors with a three-dimensional molecular framework that can fully encapsulate a guest are the cryptands developed by Lehn and coworkers [10]. These receptors, prototypes of which are bicyclic **4** and tricyclic **5**, are sufficiently flexible to arrange the oxygen atoms in a fashion around the cavity that allows attractive ion–dipole interactions with an included cation. Similarly, protonated versions of these compounds or of derivatives with only amino groups distributed along the cavity (polyaza cryptands) allow the binding of anionic guests by a combination of attractive Coulomb interactions and hydrogen bond formation between the NH groups and the substrates [11, 12]. Related to polyaza cryptands is macrobicyclic receptor **6**, which belongs to a family of anion receptors termed *katapinands* [13].

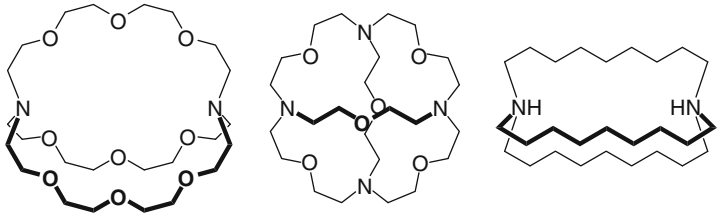

4 **5** **6**

The terms cryptand, derived from Latin crypta (cavity), and katapinand, from Greek καταπίνω (to swallow, to engulf), were chosen to illustrate that complex formation involves complete incorporation of the guests into the receptor cavity. This inclusion, in combination with attractive interactions inside the cavity, generally causes appreciable thermodynamic stability of the corresponding complexes, correlating with the strength and number of possible interactions. In addition,

complexation/decomplexation kinetics is slower than that of receptors with binding sites more exposed to the solvent.

Since portal size is too large to completely impair guest entrance and egress the term molecular container for these types of receptors is not appropriate. However, cryptands have certainly inspired the development of structurally related systems featuring more closed molecular frameworks and binding sites inside the cavity. Most of these receptors have been constructed covalently, although there are also a few examples of noncovalently assembled systems. Hallmarks of such receptors are strong binding, sometimes exceptionally strong, combined with slow binding kinetics, at least on the NMR time-scale.

Since the term cryptand only refers to crown ether derived polycyclic receptors, polycyclic systems deriving from other structural motifs are commonly termed molecular cages or molecular capsules, although other names such as nanospheres, nanoflasks, temple-type receptors, etc., can also be found. The word cage well illustrates the overall architecture of many of these receptors, consisting of a floor and a roof connected by at least three bars.[1] For self-assembled receptors, on the other hand, the term molecular capsule is often more appropriate.

In the following sections, a selection of cage-type receptors, mostly from the more recent literature, is presented whose inner cavity is functionalized with appropriate groups that can engage in directed interactions with an included guest. These examples were chosen to illustrate promising receptor architectures or effects of receptor structure on the thermodynamics and/or kinetics of complex formation. They have been classified according to the type of interaction responsible for guest binding into:

- Receptors containing metal centers along the inner cavity
- Receptors containing hydrogen bond acceptors
- Receptors containing hydrogen bond donors
- Receptors containing hydrogen bond acceptors and donors

2 Cage-Type Receptors Containing Metal Ions

The controlled self-assembly of appropriate ligands and metal ions to yield large hollow coordination cages has become a popular approach in the programmed synthesis of nano-sized objects, some of which possess interesting inclusion properties [14]. Important contributions in this context came from the groups of Albrecht [15], Dalcanale [16], Fujita [17], Nitschke [18], Raymond [19], Saalfrank

[1] Guest binding in molecular cages is usually thermodynamically favorable; in other words, the guest likes to be bound inside the cage. This situation obviously differs from that in the macroscopic world where a prisoner prefers to reside outside rather than inside a cage. The term cage is therefore a good analogy for the architecture and the function of a certain class of receptors but not for the binding event itself.

[20], Stang [21], Ward [22], and others. One of the many examples is cage **7** that was recently described by the Lindoy group [23].

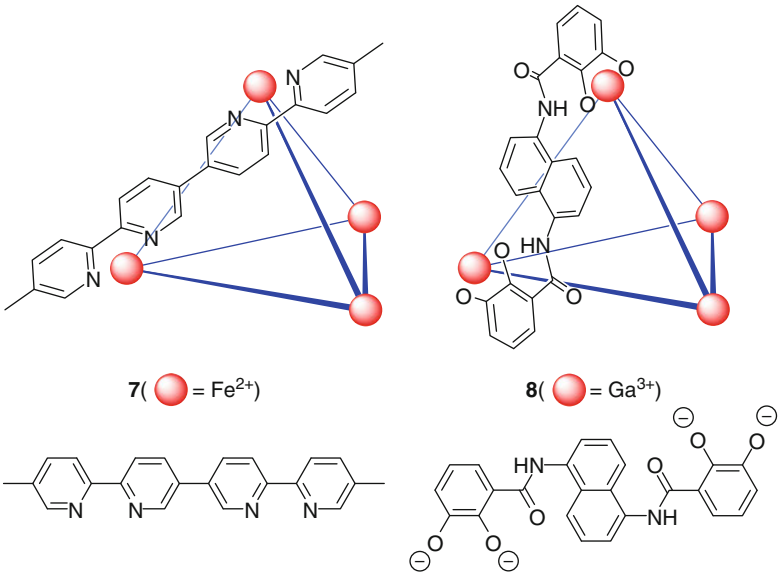

Compound **7** is highly positively charged due to the presence of four Fe(II) ions connecting the six neutral ligands. This cage was shown to bind anions such as BF_4^- or PF_6^- in its interior with the latter anion forming the more stable complex. Complexation/decomplexation equilibrium of the $BF_4^- \subset$ **7** complex is fast on the NMR time-scale while that of the $PF_6^- \subset$ **7** complex is slow. The smaller anion obviously experiences no difficulty in squeezing through the openings of the cage while PF_6^- anions may require a partial disruption of the cage in order to enter or leave it. Although no quantitative data for the thermodynamic stability of these complexes is reported it is reasonable to assume that a major driving force for anion binding of this and other coordination cages [16, 24] derives from electrostatic interactions between the included anion and the positively charged metal ions surrounding the cavity. Conversely, negatively charged cages such as that described by Raymond et al. (**8**) were shown to bind cations [19]. Coulomb interactions obviously stabilize such complexes, but since electrostatic interactions lack directionality, binding of charged guests is not restricted to the cage interior and ions residing outside the cage, for example the excess ions required to compensate the overall charge of the cage, also experience attractive interactions. In this context it is important to note that a detailed microcalorimetric investigation performed to characterize the interaction of tetraethylammonium ions with **8** has revealed striking thermodynamic differences if the anion is bound outside and inside the cage [25]. External binding is enthalpy driven while encapsulation, although also enthalpically favorable, is strongly driven by entropy. Thus, external binding seems to be associated with a loss of (translational) freedom but favored by attractive

interactions between the guests and the exterior surface of the assembly while encapsulation is additionally promoted by desolvation of the guest and release of solvent molecules from the host cavity. The enthalpic and entropic stabilization of the inclusion complex $NEt^+ \subset$ **8** causes an appreciable overall stability amounting to a log K_a of 4.4 at 25 °C in water (0.1 M KCl). It should also be pointed out that cage **7** structurally resembles the metal-free bicyclic cages described by Schmidtchen, which contain quaternary ammonium ions at the vertices and also bind anions by electrostatic interactions in their interior [26].

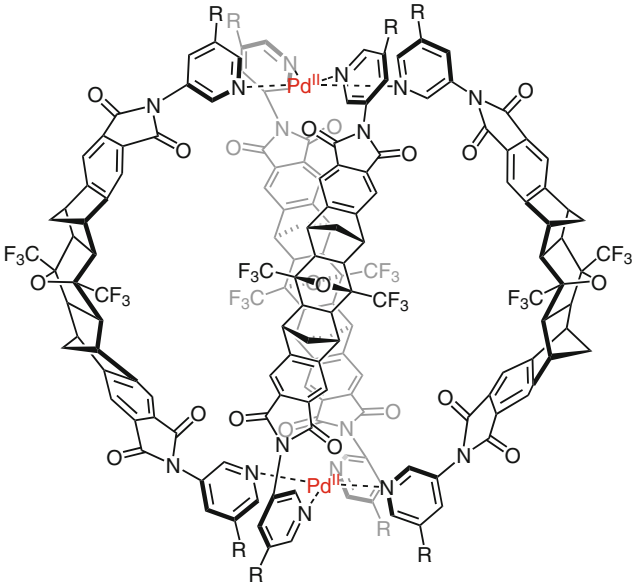

9a R = H
9b R = —≡—O(CH$_2$CH$_2$O)$_3$CH$_3$

The thermodynamics of complex formation of **8** suggests that coordination cages whose overall charge can be fully compensated by a single anion should preferentially bind the guest in the interior where it is entropically stabilized and can engage in interactions with the surrounding metal ions. A step in this direction is the dimetallic cage **9a** described by Shionoya and coworkers [27].

The fourfold positive charge of this cage, assembled by coordination of four banana-shaped ligands to two Pd^{2+} ions, is compensated by four BF_4^- anions. In the crystal, two of these anions reside inside the cage and two outside. The two internal BF_4^- anions can selectively and quantitatively be replaced in solution by guest molecules that contain two negatively charged sulfonate groups matching the BF_4^-–BF_4^- distance found in the crystal structure. Suitable guests that fulfil this criterion are, for example, 1,1′-ferrocene bis(sulfonate) [27] or *cis*-4,4′-azobenzene bis(sulfonate) [28]. Interestingly, the *trans*-isomer of the latter guests does not fit into the cage. As a consequence, the guest is expelled from the complex upon photochemical isomerization of *cis*-4,4′-azobenzene bis(sulfonate) into the

corresponding *trans*-form. This process is reversible; switching the guest back to its *cis*-form restores the complex.

Two other strategies to restrict binding of a guest to the interior of a coordination cage have been realized, the first one involving the introduction of additional functional groups in the linkers that can interact with the included guest, and the second one incorporation of metal ions that are coordinatively unsaturated or contain weakly bound ligands to which the guests can bind.

An example of the first strategy is coordination cage **10** described by Custelcean et al., in which six ligands each containing a urea moiety between two 2,2′-bipyridine moieties are assembled around four nickel(II) ions [29]. This cage was designed by using de novo structure-based computational methods as implemented in the *HostDesigner* software [30]. Starting from the optimized structure of a complex between a sulfate ion and 6 urea units stabilized by the maximum number of 12 intermolecular hydrogen bonds, this program searched for optimal linkers to connect the urea units with 4 Ni(II)bipy$_3$ complexes located at the corners of a tetragon without affecting the geometry of the central anion-(urea)$_6$ core. Subsequently, the most promising ligand resulting from these calculations was synthesized and binding to sulfate was investigated. As predicted, cage **10** is indeed able to include a sulfate ion as shown by X-ray crystallography. Complex stability of the sulfate complex in water could not be determined exactly, but precipitation experiments using $Sr(NO_3)_2$ and $Ba(NO_3)_2$ provided an estimate for the apparent binding constant of $6 \pm 1 \times 10^6$ M^{-1} similar to that of the sulfate-binding protein. In contrast to the protein, however, which binds the substrate solely by hydrogen-bonding interactions, electrostatic interactions between the positively charged cage and the negatively charged substrate can be assumed to contribute significantly to the overall affinity.

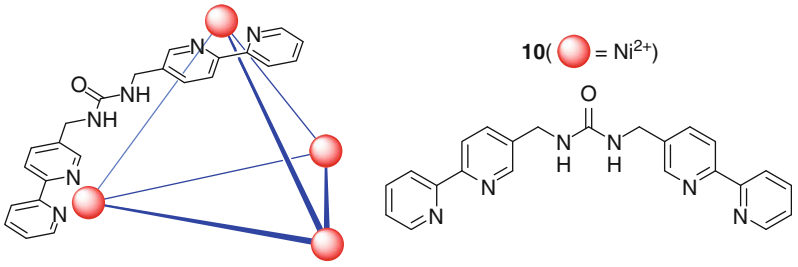

The anion-binding carcerand **11** was described by the Amouri group [31]. This complex contains a tetrafluoroborate anion coordinated to two cobalt(II) ions. Each cobalt ion adopts a square–pyramidal geometry. Four benzimidazole arms of the bridging ligands fill the equatorial positions, and solvent molecules (acetonitrile) coordinate to the outside axial positions. Inside the complex the included tetrafluoroborate anions interacts with the cobalt ions whose inside axial positions are otherwise coordinatively unsaturated. No exchange of the anion was observed even at 60 °C. A detailed study of the anion-binding properties in the crystal state of similar metalla-macrotricyclic cryptands has been performed by Adarsh et al. [32].

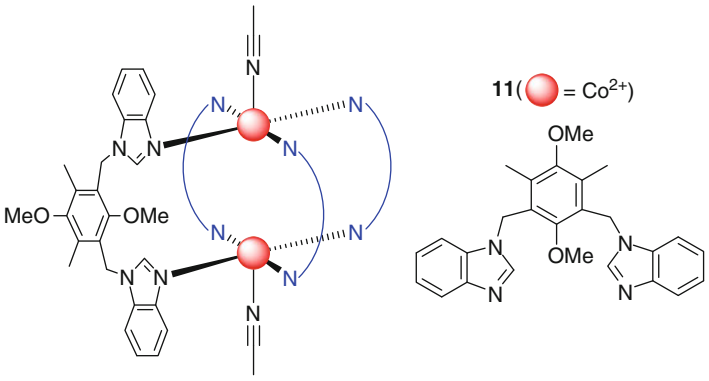

Another example of a cage that allows coordinative interactions of the guests to metal ions has recently been described by Hiraoka et al. [33]. The corresponding compound **12** contains six mercury ions at the vertices, each of which possesses an octahedral coordination geometry with the equatorial positions occupied by the ring nitrogen atoms of the ligands, which make up the faces of the cage. Trifluoromethyl sulfonate anions occupy the axial positions with one anion residing on the outside and the other on the inside of the cage. Overall, **12** therefore contains six trifluoromethyl sulfonate anions in its interior, which can be replaced by other anions. The authors showed that **12**, whose exact composition can be denoted as [**12**·$(TfO_{in})_6$·$(TfO_{out})_6$], is able to incorporated appropriate disulfonates, for example **13**, if the distance of the sulfonate groups is large enough to connect two metal ions internally. Ligand exchange inside the corresponding capsule [**12**·$\mathbf{13}_{in}$·$(TfO_{in})_4$·$(TfO_{out})_6$] is fast on the NMR time-scale at 293 K whereas the exchange of internally bound **13** for external trifluoromethyl sulfonate anions is slow. Interestingly, incorporation of two disulfonate anions yielding complex [**12**·$(\mathbf{13}_{in})_2$·$(TfO_{in})_2$·$(TfO_{out})_6$] could also be achieved. Thermodynamic stability of these complexes clearly benefits from the direct coordination of the internally bound anions to the metal ions.

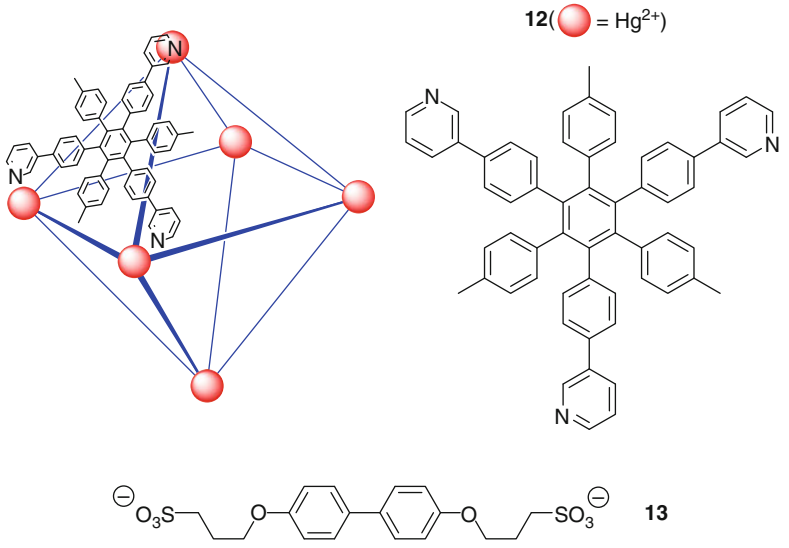

Another strategy to devise metal containing cages that allow an included guest to coordinate to metal centers relies on cryptand-type ligands containing two tris (2-aminoethyl)amine (TREN) subunits at opposing ends. These TREN units can coordinate to a metal ion such as copper(II) or zinc(II) in a trigonal bipyramidal binding mode leaving one axial coordination site at the metal unsaturated or saturated with an only weakly bound solvent molecule or counterion. As a consequence, incorporation of two metal ions into a TREN-derived cryptand yields hosts in which the two metal centers are appropriately positioned to engage cooperatively in interactions with a Lewis-basic guest. If the guest is large enough to bridge the two metal ions a so-called cascade complex is formed. Stability of such complexes depends on the complementarity between size of the anion and the host cavity.

Pioneering work in this area was carried out by the groups of Lehn and Martell [34, 35]. One example of a metal containing cryptand is dicopper(II) complex **14** which was shown to interact with various anions such as N_3^-, OCN^-, SCN^-, SO_4^{2-}, $HCOO^-$, CH_3COO^-, HCO_3^-, and NO_3^- [36]. Complex formation can easily be detected by the color change of an aqueous solution of the receptor from blue in the absence of suitable anionic substrates to green in their presence.

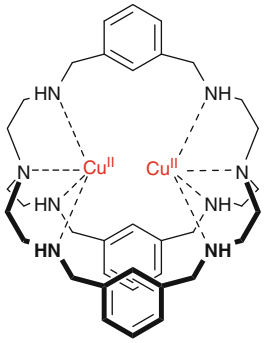

14

Compound **14** forms the most stable complex with N_3^- ($\log K_a = 4.78$) followed by OCN^- ($\log K_a = 4.60$) and HCO_3^- ($\log K_a = 4.56$), a result that was rationalized by the almost perfect fit of azide and, to a lesser extent, hydrogencarbonate and cyanate between the two copper centers. All other anions studied, even the twofold charged sulfate or the strongly coordinating thiocyanate, are bound considerably less tightly, leading to the conclusion that the host does not recognize the donor tendencies or the shape, but the bite length of the anionic guest. Structural variation of ligand structure has made available a large number of structurally related dimetallic hosts possessing affinity not only for inorganic but also for organic anions including nucleotides and dicarboxylates. The extensive work in this area will not be summarized here and the interested reader is referred to relevant reviews [37, 38].

3 Cage-Type Receptors Containing Hydrogen Bond Acceptors

The prototypes of cages with inwardly directed hydrogen bond acceptors are cryptands, for example **4** and **5**. These compounds efficiently interact with cations included into the cavity via ion–dipole interactions. Macrotricyclic cryptand **5**, for example, whose spherical cavity is lined with four nitrogen atoms located at the corners of a tetrahedron and with six oxygens at the corners of an octahedron, was shown to complex large alkali metal ions (K^+, Rb^+, Cs^+) with a 1:1 stoichiometry in chloroform and in water [39]. Complexes are kinetically stable on the NMR time-scale with free energies of activation for the cation exchange derived from temperature-dependent NMR measurements amounting to 64.8 (at 28 °C), 69.8 (at 51 °C), and 67.3 (at 41 °C) kJ mol^{-1} for the K^+, Rb^+, and Cs^+ complexes, respectively. In addition, thermodynamic stability of these complexes is high as illustrated by the stability constants log K_a which range between 3.4 (for the K^+ and Cs^+ complexes) and 4.2 (for the Rb^+ complex) in water at 25 °C.

More important in the context of this chapter is that the nitrogen and oxygen atoms arranged around the cavity of cryptands can also serve as hydrogen bond acceptors, allowing the complexation of ammonium ions [40]. A crystal structure of the complex between **5** and NH_4I together with results from NMR spectroscopic investigations and computational studies indicated, for example, that complexation of the NH_4^+ cation involves four hydrogen bonds to the four bridgehead nitrogen atoms. For this interaction to occur, the receptor adopts a conformation with four inwardly directed nitrogen atoms, somewhat flattened along one axis giving a binding pattern with one shorter and three longer hydrogen bonds. This pattern is complemented by 12 electrostatic interactions between the charged guest and the six ether oxygens, which may be considered as 12 weaker, bent N–H···O hydrogen bonds. In combination, these attractive interactions cause the NH_4^+ complex of **5** to be ca. 500 times more stable than the K^+ complex (log $K_a = 6.1$ vs 3.4 in water at 25 °C). In addition, the energy barrier to NH_4^+ exchange is also very high, amounting to ca. 71.1 kJ mol^{-1}. This large hindrance to cation exchange was ascribed to two main factors: the resistance of the triply connected faces of the macrotricyclic cryptand to deformation and the hindrance to stepwise cation solvation in the transition state as the cation slips through a face of the structure.

Comparison of the binding properties of **5** with those of structural related analogs **15** and **16** demonstrated that the high affinity of **5** for the NH_4^+ cation is mainly due to the good structural complementarity between host and guest [40].

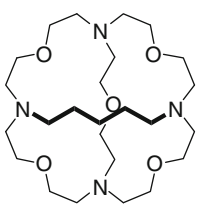

15

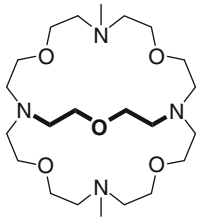

16

By replacement of just one oxygen atom in **5** by a methylene group, affinity of the corresponding cryptand **15** to NH_4^+ decreases by a factor of ca. 100 ($NH_4^+ \subset$ **15** log $K_a = 4.3$). The macrobicycle **16** has almost completely lost the complexation ability and the selectivity of **5** ($NH_4^+ \subset$ **16** log $K_a = 1.7$). This dramatic effect results from the removal of one bridge of **5**, i.e., from a decrease in cyclic order from the tricyclic to the bicyclic ring system, demonstrating the importance of the spherical macrotricyclic structure for the binding properties of **5**.

Unfortunately, distributing inwardly directed hydrogen bond acceptors along the surface of a cage with an even more confined cavity is not straightforward, which is the reason why there are relatively few hosts belonging to this class of molecular cages or capsules. Five examples should be presented. The first is based on the superbowls introduced by the Sherburn group [41, 42]. These large cage-type structures enclose a cavity with an internal volume of over 1,000 $Å^3$. They can thus easily accommodate several small guest molecules. Still, interaction of superbowl **17a** with aspirin leads to a defined 1:1 complex [43].

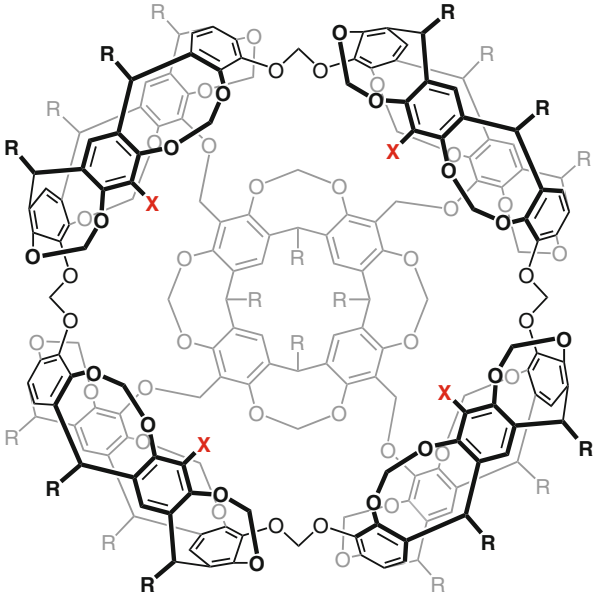

R = C_5H_{11}

17a X = H
17b X = Br
17c X = CH_3
17d X = C_2H_5

Since neither benzoic acid nor phenyl acetate, the two compounds containing only one of aspirin's substituents, nor the *meta* or *para* isomer of aspirin display detectable binding, it appears that both –CO_2H and –OAc functionalities of the guest are required and that these groups must be arranged in an *ortho*-disposition for complex formation to take place. Based on these results the authors proposed a two-point binding mode for the complexation of aspirin within **17a** comprising (1) hydrogen-bonding between the guest's –CO_2H group and the ether oxygen of the host's base-wall –CH_2O– linkers and (2) C–H···π interactions between the guest's –OAc methyl group and the cavity of the base cavitand (Fig. 2).

Substituents around the rim of the host have a profound influence on the stability of the aspirin complex. For instance, while affinity of **17a** for aspirin amounts to 309 M^{-1} (in chloroform at 25 °C), the tetrabromo analog **17b** exhibits no detectable

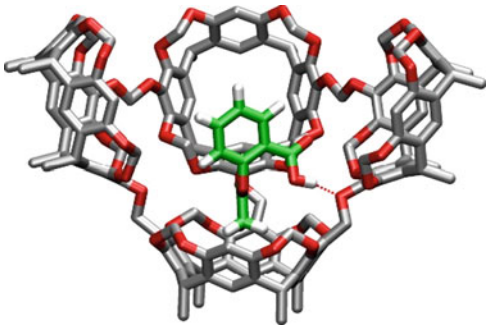

Fig. 2 Representation of the proposed two point binding mode of aspirin (*green*) inside superbowl **17a**. The front wall cavitand of **17a**, hydrogen atoms and *n*-pentyl feet are omitted for clarity

binding. Complex formation of the tetramethyl derivative **17c**, on the other hand, is associated with a larger binding constant of 485 M^{-1}. This higher affinity was attributed to attractive C–H···π interactions between the rim methyl groups and the guest, which hinder guest egress, thereby stabilizing the complex. Superbowl **17d** with even larger substituents along the rim is unable to form a complex, which presumably results from inhibition of guest exchange by steric shielding.

The second type of cage presenting hydrogen bond acceptors into the interior of the cavity, in this case the ring nitrogen atoms of 2,2′-bipyridine units in the three linkers, is compound **18** described by Vögtle and coworkers [44]. This compound and some structurally related derivatives were shown to bind aromatic phenols in methylene chloride. Comparison of the affinity of **18** for trihydroxybenzenes differing in the positions of the three hydroxy groups strongly indicates that host–guest interactions involve hydrogen bond formation between the OH-groups of the guests and the nitrogen atoms in the linkers. The most stable complex turned out to be that between **18** and 1,3,5-trihydroxybenzene, for which a stability constant of 11,000 M^{-1} in dichloromethane was determined.

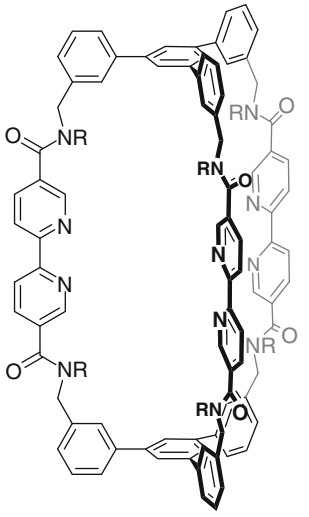

18 (R = CH_2Ph)

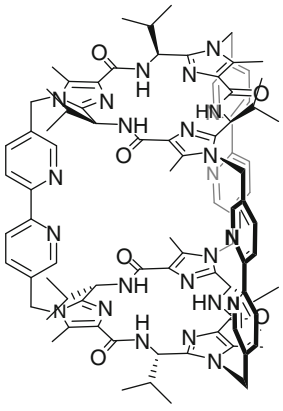

19

The structurally related receptor **19** was described by the Haberhauer group [45]. In this receptor, three 2,2′-bipyridine linkers connect two cyclopeptide-derived scaffolds. Compound **19** also binds to 1,3,5-trihydroxybenzene albeit, with respect to **18**, with a significantly lower K_a of 150 M^{-1} in 10% $CD_3CN/CDCl_3$. Interestingly, a derivative of **19** containing three 2,2′-bipyridine units connected to a single cyclopeptide ring binds the same substrate significantly stronger under the same conditions ($K_a = 680$ M^{-1}) despite the fact that **19** should be much better preorganized for complex formation. This result was attributed to the fact that the inner cavity of **19** is slightly too small to allow for efficient interactions with the guest. While the open analog can easily adapt its cavity dimensions to the steric requirements of 1,3,5-trihydroxybenzene, this is much more difficult for the cage in which the mutual arrangement of the bipyridine linkers is fixed.

In a somewhat related study, the group around Ahn compared the binding properties of cage-type receptor **20** containing the nitrogen atoms of oxazoline residues as hydrogen bond acceptors with those of the previously described tripodal analog **21** lacking the capping aromatic residue [46].

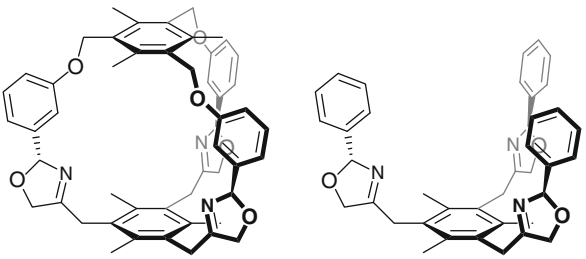

20 **21**

Compound **21** allows the enantioselective recognition of chiral ammonium ions with interactions primarily involving hydrogen bonds between the ammonium NH groups and the nitrogen atoms on the oxazoline rings. The same binding motif was detected crystallographically in the complex between **20** and (*R*)-2-phenylethylammonium perchlorate. As in the case of **19**, closing the cage does not necessarily improve binding properties. Enantioselectivity of **20** in the recognition of racemic 2-phenylethylammonium ions is, for example, lower than that of **21**. The differentiation of the enantiomers of alanine methyl ester is, however, associated with a higher selectivity. Calculations revealed that steric effects of the aromatic roof of **20** prevent the optimal arrangement of an included 2-phenylethylammonium ion. Stability of the complex of **20** with (*R*)-2-phenylethylammonium perchlorate in $CDCl_3/CD_3CN$ (3:1) amounts to 6,170 M^{-1} while that of the complex with the corresponding (*S*)-enantiomer is 2,920 M^{-1}.

That receptors **22a** and **22b** contain an inwardly directed hydrogen bond acceptor is not directly evident. These compounds structurally relate to cavitand **3** in that they contain amide groups at three aromatic resides, which stabilize the cavitand's *vase* conformation by intramolecular hydrogen bond formation. The remaining aromatic wall contains an appended Kemp's triacid residue such that its free carboxyl group is oriented toward the inside of the cavity.

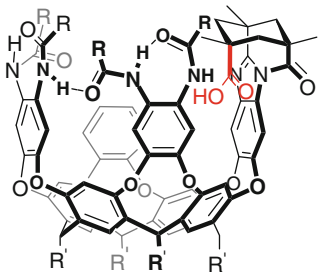

22a (R = C_7H_{15}, R' = $C_{11}H_{23}$)
22b (R = $(CH_2)_3NH_3Cl$, R' = $C_{11}H_{23}$)

Both receptors **22a** and **22b** interact with amines, which are protonated upon complex formation [47, 48]. Since binding involves formation of an ion pair inside the cavity of the receptor, electrostatic interaction between the oppositely charged guest and the introverted carboxylate group most likely dominate the overall affinity. However, cooperative effects of hydrogen bonds between the carboxylate group as a hydrogen bond acceptor and the ammonium proton(s) on the guest have also to be considered.

Cavitand **22a** was shown to bind primary amines such as isobutylamine and 1-aminoadamantane, and tertiary amines such as triethylamine, *S*-nicotine, and 3-picoline in chloroform [48]. Binding is so tight that accurate quantification by NMR titrations proved to be impossible. In contrast, cavitand **3** lacking the inwardly directed carboxylate group does not bind triethylamine, isobutylamine, nicotine, or picoline. Only 1-aminoadamantane is also recognized by **3**, but with a different complex geometry. While this guest is bound inside **3** with the amino group directed toward the floor of the cavity it is included into **22a** with the opposite orientation, namely with the amino group in contact with the acid. Thus, attractive interactions between the guest and the carboxylate group inside the cavity of **22a** stabilize the complex and induce a predictable mutual arrangement of the two binding partners.

Charged cavitand **22b** allowed binding to be studied in water [47]. The ^{1}H NMR spectrum of **22b** in the absence of potential guests shows a poorly resolved and complicated spectrum, indicating the open *kite* conformation. This spectrum sharpens upon addition of quinuclidinium hydrochloride, which is consistent with a conformational reorganization of **22b** to give the *vase* conformation. The significant difference in the affinity of **22b** for quinuclidinium hydrochloride (K_a = 1,300 M^{-1}) and for *N*-methylquinuclidinium chloride (K_a = 18 M^{-1}) in D_2O was attributed to the loss of a buried hydrogen bond in the complex of the quaternary ammonium ion, a result which gives support to the assumption that **22a** and **22b** can be regarded as receptors with inwardly directed hydrogen bond acceptors. Comparison of the binding properties of **22b** with those of a water soluble analog of unfunctionalized cavitand **3** allowed the strength of the ionic hydrogen bond between the introverted carboxylate and the quinuclidinium cation to be quantified. The energy thus determined (−11.3 kJ mol^{-1}) is significantly larger than what would be expected from solvent exposed salt bridges (between −0.8 and −6.3 kJ mol^{-1}), clearly demonstrating the strengthening of the interactions in the hydrophobic interior of the cavitand.

The influence of the introverted acid on the guest exchange kinetics was investigated by exchange spectroscopy (EXSY NMR). According to these measurements, the complex between **22b** and the quinuclidinium ion has a dissociation barrier of 79.4 kJ mol^{-1} in D_2O, ca. 8 kJ mol^{-1} larger than the dissociation barrier of complexes of unfunctionalized cavitands (e.g., **3**) in organic solvents. Complexes of **3** and **22b** were therefore assumed to dissociate along a similar reaction path, involving the *vase* to *kite* conformational shift of the cavitand and the rupture of the upper rim hydrogen bonds. The larger barrier determined for **22b** reflects the additional energy required to break the ionic interaction between host and guest, as well as increased physical constraints imparted on the guest by the introverted acid.

4 Cage-Type Receptors Containing Hydrogen Bond Donors

Cage-type receptors with inwardly directed hydrogen bond donors are easily accessible by protonation of polyazamacrocycles. In the absence of suitable guests, ammonium groups along macrocyclic or polycyclic molecular frameworks prefer more extended conformations with the proton located on the outside. Binding of an anion then causes a conformational reorganization to allow for hydrogen-bonding interactions between the guest and the protonated host (Fig. 3).

The versatile nature of cryptands to serve as cation or anion receptors is clearly evident when taking **5** as an example. Interaction of this cryptand with cations has already been described in the previous section. Anion binding, on the other hand, can be achieved by successive protonation of the bridge-head nitrogen atoms [49]. If HCl is used as the acid, the addition of 1 equiv. to a solution of **5** in CD_3OD furnishes the (empty) diprotonated species **5**·H_2^{2+} (along with unprotonated **5**). Addition of the next equivalent of HCl causes full conversion into **5**·H_2^{2+}, and further HCl addition then induces the formation of the tetraprotonated cryptand **5**·H_4^{4+} whose cavity contains a chloride anion. In this complex, the anion is held tightly by a tetrahedral array of N–H···Cl^- hydrogen bonds, as clearly shown in the corresponding crystal structure [50]. Fluoride and bromide complexes of **5**·H_4^{4+} could be prepared in a similar manner. Iodide is too large, however, to enter the cavity and therefore fails to produce an inclusion complex. Stability of the chloride complex is high, amounting to a log K_a of >4 in water at pH 1.5. The authors ascribed this stability and the high

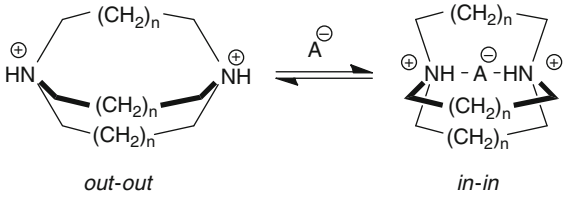

Fig. 3 Equilibria between the different conformers of a diprotonated bicyclic diaza host. The *in–in* conformation is optimal for anion binding

selectivity of $\mathbf{5}{\cdot}H_4^{4+}$ for chloride over other halides to the well-defined and rigid cavity of the host.

After these groundbreaking initial studies there has been extensive research activity to develop receptors on the basis of polyammonium cryptands for other anions such as carbonate, sulfate, phosphate, di- and triphosphate, nucleotides, or other inorganic and organic anionic guests. In this context, effects of a wide variety of structural parameters on anion binding properties were studied including changing the number of binding sites, the overall receptor symmetry or topology, or introducing rigid aromatic subunits. These investigations also involved the characterization of the binding properties of *azacyclophanes* such as **23** [51], or of neutral tricyclic polyamides such as **24** [52]. The latter type of anion receptors also features NH protons as inwardly directed hydrogen bond donors. These macrobicyclic lactams are often well organized for anion binding and they do not suffer from the pH dependent anion affinity observed for polyammonium cryptands, for example the direct structural analog of **24**, copper-free ligand **14**. Since anion binding only relies on hydrogen-bonding without an additional contribution from Coulomb attraction, these receptors are usually only active in organic media, however.

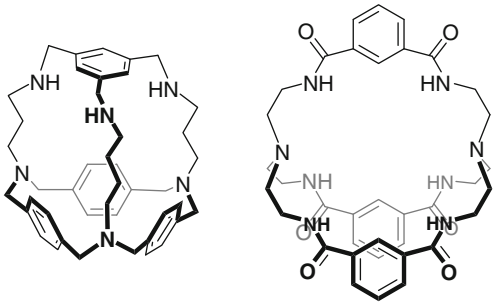

23 **24**

Polyammonium cryptands and tricyclic lactams probably represent the largest family of cryptand-type anion receptors known today and a detailed overview of the properties of these compounds lies outside the scope of this review. The interested reader is therefore referred to two recent reviews [11, 53]. Compound **35b** in the following section is the only polyammonium cryptand besides **5** whose properties are described in this review in more detail to illustrate the effect of the incorporation of additional hydrogen bond acceptor sites on binding properties.

Structurally somewhat related to **24** are the carbohydrate receptors introduced by Davis et al. featuring the so-called temple architecture, for example, compound **25a** [54]. The roof and the floor of the temple in these tricyclic polyamides are made up of aromatic moieties, which serve to engage in CH···π interactions with the ring faces of an included guest. Four isophthalamides, representing the pillars, prevent the cavity from collapsing even in polar solvents and contain functional groups to interact with the guests.

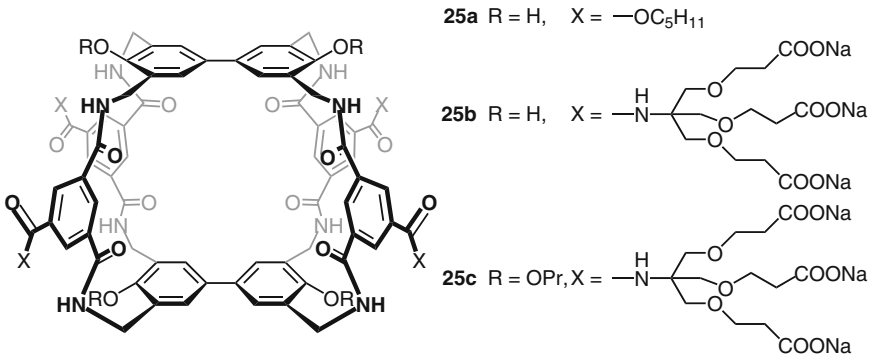

Receptor **25a** has been shown to bind preferentially all-equatorial carbohydrates because unfavorable steric interactions of axial substituents in the substrate with the walls of the receptor cavity cause destabilization of the corresponding complexes. 1-*O*-Octyl β-D-glucopyranoside is bound in 5% $CD_3OD/CDCl_3$ with an association constant determined by NMR titration of 980 M^{-1}, for example, while affinity of **25a** for the corresponding α-anomer or for 1-*O*-octyl β-D-galactopyranoside proved to be significantly lower (1-*O*-octyl α-D-glucopyranoside ⊂ **25a** in 5% $CD_3OD/CDCl_3$ $K_a = 20\ M^{-1}$ and 1-*O*-octyl β-D-galactopyranoside ⊂ **25a** $K_a = 220\ M^{-1}$) [55].

By decorating these temple receptors with polar substituents, binding studies could also be performed in aqueous media. These investigations showed that **25b** possesses appreciable affinity for glucose even in water (1-*O*-methyl β-D-glucopyranoside ⊂ **25a** in 93:7 (*v*/*v*) H_2O/D_2O $K_a = 28\ M^{-1}$) [56]. Interestingly, affinity for certain glucose derivatives, in particular *N*-acetylaminosugars, is substantially higher. *N*-Acetyl-1-*O*-methyl-β-D-glucosamine is, for example, bound with a K_a of 630 M^{-1} [57]. This complex is thus more than one order of magnitude more stable than that of the methyl glucoside or of D-glucose. In addition, binding is highly selective. Of altogether 21 other monosaccharide derivatives studied in water, only four bind to **25b** with an association constant >10 M^{-1} and stability of none of these four complexes exceeds 60 M^{-1}.

Structural characterization of the complex between **25b** and *N*-acetyl-1-*O*-methyl-β-D-glucosamine using a combination of NMR spectroscopy and molecular modeling revealed that the substrate occupies the cavity between the two aromatic rings aligned parallel to each other. Hydrogen bonds and C–H···π interactions ensure an efficient and well-defined binding and, although the isophthalamide pillars could in principle serve as hydrogen bond donors with their NH groups, and as hydrogen bond acceptors with their C=O groups, only the NH groups seem to be involved in substrate binding. The *N*-acetyl group is located between two isophthalamide linkers at one of the smaller portals of the cavity where it is held tightly by several hydrophobic contacts, two hydrogen bonds to the carbonyl oxygen atom, as well as NH···π interactions. These multiple attractive interactions are presumably the reason for the higher affinity of **25b** for monosaccharides containing an *N*-acetylamino group in the 2-position.

Binding selectivity of such temple receptors can also be controlled by introducing alkoxy substituents in 4- and 4′-positions of the biphenyl subunits whose alkyl chains enter the cavity in aqueous solution through the narrow portals [58]. As a consequence, binding of *N*-acetyl-1-*O*-methyl-β-D-glucosamine is significantly impaired because the optimal complex geometry with the *N*-acetyl group of the substrate located at a narrow portal is not accessible, an effect which is the more pronounced the longer the alkyl chains on the receptor become. Interestingly, introduction of the substituents increases D-glucose affinity with a maximum for the *n*-propyloxy substituted receptor **25c**. For comparison, **25c** binds to *N*-acetyl-1-*O*-methyl-β-D-glucosamine with a K_a of only 43 M^{-1} while 1-*O*-methyl β-D-glucopyranoside affinity amounts to 130 M^{-1}. Replacing the biphenyl residues in these temple receptors with larger aromatic moieties such as terphenyl derivatives increases cavity size, thus yielding receptors for disaccharides [59–61].

Inspired by the well-known anion-binding properties of calixpyrroles [62], two cryptand-like derivatives have recently been developed. Compound **26** contains nine pyrrole moieties whose NH groups should induce affinity for small inorganic anions [63]. Indeed, significant signal shifts in the ^{1}H NMR of **26** upon addition of tetrabutylammonium fluoride to a CD_2Cl_2 solution were observed. Specifically, the signals located at 7.49 and 7.67 ppm accounting for six and three NH protons, respectively, gave rise to four signals at 6.78, 7.97, 10.56, and 11.99 ppm in a 1:2:2:4 relative intensity after the addition of 1 equiv. of the salt. The splitting of the shifts indicated that fluoride is not bound within the cryptand interacting with all NH groups simultaneously. Instead, two of the three cryptand arms combine to form a single large pocket that allows six calixpyrrole-like NH groups to be hydrogen-bonded to the anion. Larger anions such as chloride ions form complexes with **26** of higher stoichiometry.

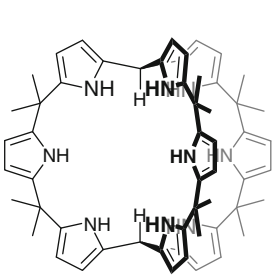

26

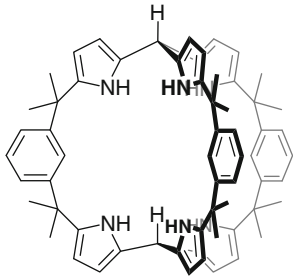

27

Cryptand-like calixpyrrole **27** has a larger cavity than **26** because of the *in/out* configuration at the two opposing methyne groups [64]. This receptor also binds fluoride but, in contrast to **26**, incorporates the anion within the cavity. However, of the six NH groups of **27** only those of the pyrrole moieties at the tripyrrolemethane subunits with the *out*-configuration interact with the anion. According to molecular modeling studies, the other three NH groups are directed into the cavity, but are not involved in anion binding. The stability constant K_a of the fluoride complex of **27** in CD_2Cl_2 amounts to 1,562 M^{-1}.

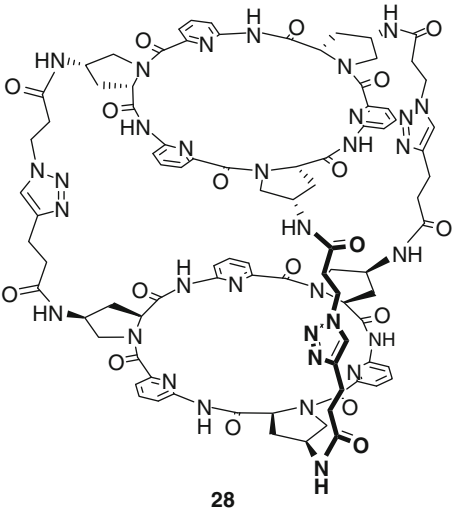

28

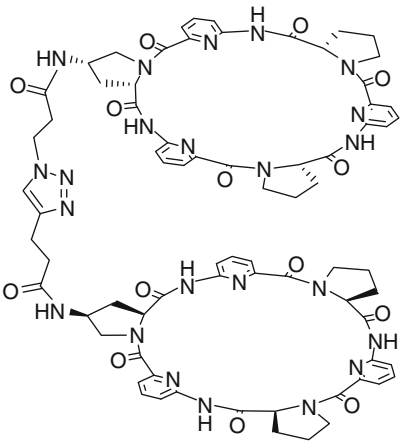

29

Another promising building block for the construction of cage-type receptors with internal binding sites is the anion-binding cyclic hexapeptide described by the Kubik group. This peptide, which contains alternating L-proline and 6-aminopicolinic acid subunits, binds inorganic anions such as sulfate or halides in competitive aqueous solvent mixtures [65]. Complex formation involves inclusion of the anion into the cavity between two cyclopeptide rings where it interacts with six peptide NH groups distributed along the cavity's inner surface. Introduction of one linker between two cyclopeptide moieties has furnished bis(cyclopeptides) that bind to anions in a 1:1 fashion [66–68]. In a logical extension of this approach, cage-type receptors can be obtained by incorporation of three linkers between the cyclopeptide rings. A bis (cyclopeptide) representing this receptor-type is compound **28**, which was prepared by coupling a tris-alkyne and a tris-azide derivative of the monocyclic parent peptide via copper-catalyzed azide–alkyne cycloaddition [69].

Pronounced shifts of cyclopeptide signals in the ^{1}H NMR spectrum caused by adding sodium sulfate to a solution of **28** in D_2O/CD_3OD 1:1 (*v*/*v*) clearly indicated that the anion is bound inside the cage. Force-field calculations provided a picture of the structure of the complex formed, which is stabilized by a well-defined array of hydrogen bonds (Fig. 4).

As expected, binding kinetics of this complex differ significantly from those of bis (cyclopeptide) **29** containing only one linker in that the rate of guest exchange is considerably slower. Thermodynamically, the stability of the sulfate complex of **28** approaches an appreciable log K_a of 6 in H_2O/CH_3OH 1:1 (*v*/*v*) which is, however, only ca. one order of magnitude larger than affinity of the more flexible mono-linked analog. The much better preorganization for complex formation of the triply linked bis (cyclopeptide) therefore does not translate into significantly higher complex stability.

Titration calorimetry revealed that, with respect to **29**, the unexpected low sulfate affinity of **28** is mainly due to profound differences in the thermodynamics

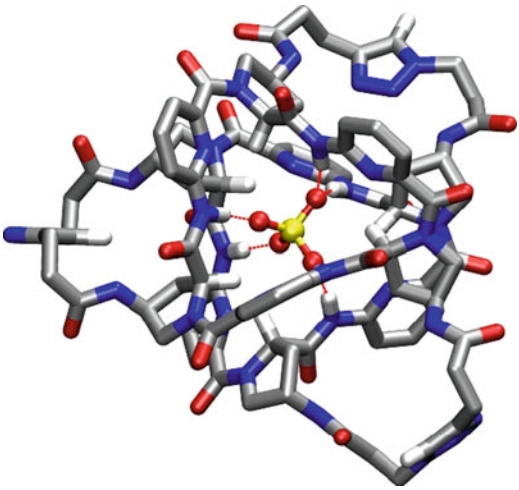

Fig. 4 Calculated structure of the sulfate complex of **28**. Nonacidic hydrogen atoms are omitted for clarity except the ones on the proline α-C atoms. Hydrogen bonds are indicated by dotted lines

of complex formation of both receptors. Sulfate binding of **29** is associated with favorable enthalpic and entropic terms and, although the entropic contribution to complex formation is significant larger in the case of **28**, this advantage is largely canceled out by the unfavorable positive enthalpy of binding. As a result, complex stability of the sulfate complex of **28** is controlled by entropy only. Structural investigations indicated that the endothermicity of the sulfate binding of **28** has most probably structural reasons (the three linkers in **28** adopt energetically unfavorable conformations in the complex), possibly in combination with solvation effects (desolvation of the receptor in aqueous solution is energetically costly). These investigations therefore showed that closing a cage does not necessarily lead to a significant improvement in binding properties if it simultaneously causes pronounced changes in the energetics of complex formation.

Besides these covalently constructed cage-type receptors a number of self-assembled capsules with hydrogen bond donors protruding to the inside have also been described. An early example was reported by Atwood et al. This system makes use of the well known properties of resorcin[4]arene **30a** and pyrogallol[4]arene **30b** to form hexameric spherical capsules in the solid state and, in the case of **30b**, also in solution.

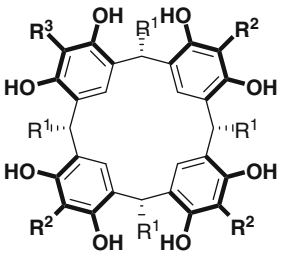

30a R^1 = methyl, $R^2 = R^3 = H$
30b R^1 = *iso*-butyl, $R^2 = R^3 = OH$
30c R^1 = *iso*-butyl, $R^2 = OH$, $R^3 = H$

In the hexameric capsule of **30b** 48 of the 72 potential hydrogen bond donors are used in intramolecular hydrogen bonds to seam the capsule together [70, 71]. The remaining 24 hydrogen bond donors are used in intramolecular hydrogen bonds

between adjacent rings in the macrocyclic building blocks. All hydrogen bond donors are therefore used in completing the hydrogen bond arrangement that forms the capsule and, as a consequence, guests included into the capsules are not ordered. The capsule deriving from **30a** has the composition $[(\mathbf{30a})_6(H_2O)_8]$ [72]. This capsule possesses an excess of four hydrogen bond donors, but these donors are positioned such that they project to the outside of the aggregate and they are therefore incapable of effecting organization of guests within the capsule. The hexameric capsule deriving from the unsymmetrical macrocycle **30c**, however, has a significantly different structure [73]. Of the altogether 66 hydrogen bond donors of $[(\mathbf{30c})_6]$, 24 hydrogen donors are used in intermolecular hydrogen bonds and 24 are used in intramolecular hydrogen bonds. Of the 18 remaining hydrogen bond donors, 6 are oriented to the inside and 6 to the outside of the capsule. The remaining six hydrogen bond donors are not involved in the array of hydrogen bonds stabilizing the aggregate and are located externally. The void of the capsule $[(\mathbf{30c})_6]$ is filled with six diethyl ether molecules in the solid state, but, in contrast to guest molecules included into capsules $[(\mathbf{30a})_6]$ or $[(\mathbf{30a})_6(H_2O)_8]$, these solvent molecules are ordered due to specific interactions of their oxygen atoms with the inwardly directed hydrogen bond donors.

Structurally somewhat related to recorcin[4]arene derivatives **30a–c** is the calix[4]pyrrole derivative **31** described by the Ballester group [74].

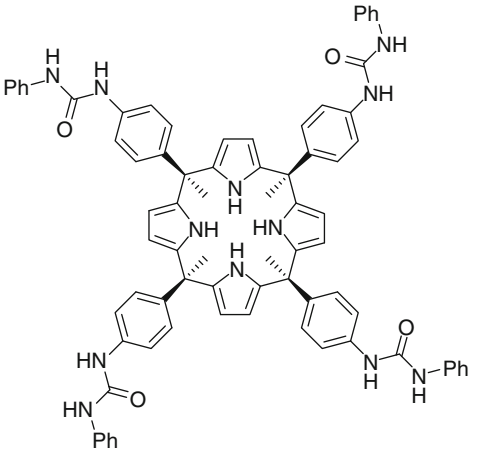

31

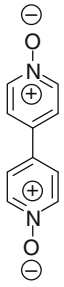

32

This tetrakis-urea was expected to self-assemble in apolar media by hydrogen bond formation between urea moieties of two different units. The analogous behavior of calix[4]arene tetrakis-ureas is well documented [75], but, in contrast to the corresponding calix[4]arene capsules, those deriving from **31** would feature hydrogen bond donor sites within the cavity (Fig. 5).

In the absence of suitable guests no self-assembly of **31** was observed, presumably because the calix[4]pyrrole core is not sufficiently well preorganized for dimerization and the entropic and enthalpic energy terms associated with the required conformational reorganization are not compensated by the formation of the 16 hydrogen bonds

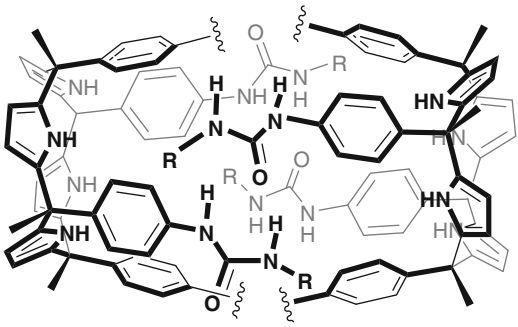

Fig. 5 Schematic representation of the dimeric capsule deriving from calix[4]pyrrole **31**

in the assembled system. However, addition of a suitable guest, namely 4,4′-bipyridine bis-*N*,*N*′-oxide **32**, induces capsule formation due to binding of the two *N*-oxide oxygen atoms to the NH groups of the two calix[4]pyrrole rings. This binding event concomitantly induces hydrogen bond formation between the urea groups along the seam of the capsule leading to a thermodynamically ($K_a > 10^7$ M^{-2}) as well as kinetically very stable complex. Kinetic stability was demonstrated by an elegant competition experiment. When a 1:1 mixture of two derivatives of **31**, differing in the substituent at the urea groups, was treated with an excess of **32** in CD_2Cl_2, the formation of three capsules, two homodimers and one heterodimer, was observed NMR spectroscopically. However, if the two homodimers were preformed individually and then mixed they predominate in solution. Thermodynamic equilibrium with all three capsules present is reached only after several hours.

A similar guest induced dimerization was observed for the disubstituted calix[4]pyrrole derivative **33** [76]. In the presence of 4-hydroxybenzoic acid, 1,4-benzenedicarboxylic acid, or the corresponding 1,3-disubstituted analog and 2 equiv. of each a base and **33**, a molecular capsule is formed in which a dianionic guest bridges two units of **33** by hydrogen-bonding to the calix[4]pyrrole NH groups. In this aggregate, the two macrocyclic subunits approach each other with the *p*-nitrophenyl residues arranged in a "staggered" fashion shielding the included guest from the surrounding environment. 3-Hydroxybenzoic acid or 1,2-benzenedicarboxylic acid failed to induce capsule assembly because of a mismatch in the arrangement of the anionic binding sites in the deprotonated versions of these guests and the orientation of the two calix[4]pyrrole units in the capsule. These guests therefore form simple 1:1 complexes with **33** even if they are completely deprotonated.

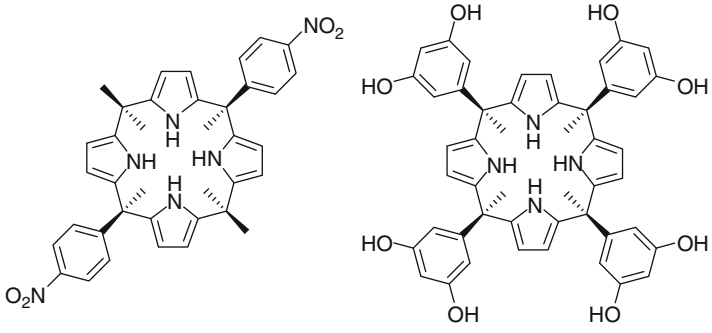

33 **34**

Crystallization of calix[4]pyrrole derivative **34** in the presence of tetramethylammonium chloride was shown to yield a hexameric capsular assembly in the solid state somewhat similar to that observed for **30a** [77]. In contrast to capsule $[(\mathbf{30a})_6(H_2O)_8]$, chloride anions bridging the different calix[4]pyrrole subunits are an important structural element in the capsule formed from **34**. Specifically, each subunit of **34** exhibits three intramolecular hydrogen bonds between the hydroxyl groups, which impart stability to the *cone* conformation. The side that does not show an intramolecular hydrogen bond directs the two hydroxyl groups toward a chloride anion. Each calix[4]pyrrole unit is intermolecularly hydrogen-bonded to only two of the four neighboring units through water molecules and through interactions with chloride anions. The hexameric capsule therefore comprises an assembly of two identical hemispheres, each made up of three units of **34**, water molecules, and three chloride anions along the seams. The two hemispheres are maintained together through electrostatic interactions between embedded cations and anions. This aggregate is spacious enough to accommodate 12 tetramethylammonium cations (six per hemisphere) and six chloride anions, each of which is hydrogen-bonded to the inwardly directed NH groups of the calix[4]pyrrole units. These NH groups therefore control the organization of the guest molecules inside the capsule as do the inwardly directed hydrogen bond donors in the capsule derived from **30c**.

Other types of molecular capsules with included anions have been described, but they do not involve directed hydrogen-bonding interactions between functional groups on the inside of the capsule and the guests [78, 79].

5 Cage-Type Receptors Containing Hydrogen Bond Acceptors and Donors

If it is already difficult to position either hydrogen bond acceptors or donors along the cavity of a molecular container or capsule that can interact with an included guest, it is even more so when acceptors and donors should be combined. Among the rare examples of these types of receptors is the bicyclic cage **35b** described by the Delgado group. The parent compound **35a** containing *m*-xylyl moieties exhibits the characteristic binding properties of polyaza cryptands [80]. Potentiometric measurements in 1:1 water/methanol (*v*/*v*) demonstrated, for example, that protonated host species are able to interact with anions such as Cl^-, I^-, NO_3^-, ClO_4^-, AcO^-, $H_2PO_4^-$, SO_4^{2-}, and SeO_4^{2-}. Noteworthy is the remarkable selectivity of **35a** for the dianionic tetrahedral anions of this guest series; association constants of the corresponding complexes range from 5.03 to 5.3 log units while those of the complexes with the monoanionic substrates are two to four orders of magnitude lower. Single crystal X-ray studies showed that one anion in the sulfate salt of hexaprotonated **35a** is encapsulated into the cage, establishing three NH···O hydrogen bonding interactions with two receptor NH groups. Additional hydrogen bonds are formed to six water molecules of which four are included into the cavity and also engage in hydrogen-bonding interactions with receptor NH groups projecting toward the inside.

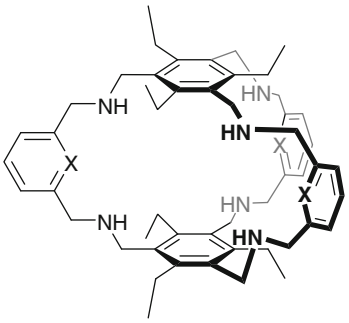

The importance of hydrogen bond formation in the interaction of **35a** with anions is evidenced by the fact that the fully protonated receptor, which lacks a hydrogen bond acceptor site, binds $H_2PO_4^-$ less efficiently than the pentaprotonated analog (log K_a of the $H_2PO_4^-$ complex of pentaprotonated **35a** amounts to 2.97 and for the hexaprotonated state to 2.12). In contrast, affinity for SO_4^{2-}, an anion which remains unprotonated even at low pH and therefore does not experience repulsive interactions inside the cavity of **35a**, increases from 3.74 for the pentaprotonated receptor to 5.03 for the hexaprotonated one.

In an attempt to reverse this selectivity receptor **35b** was synthesized that features ring nitrogens of 1,6-disubstituted pyridyl subunits as hydrogen bond acceptor sites even at the pH required for protonation of all six secondary amino groups [81]. Indeed, not only is $H_2PO_4^-$ affinity of **35b** larger than that of **35a** under the same conditions, $H_2PO_4^-$ affinity also increases when converting the pentaprotonated receptor into the fully protonated state (pentaprotonated **35b** has an $H_2PO_4^-$ affinity in terms of log K_a of 3.99 and hexaprotonated **35b** of 4.05). Both results clearly indicate that the hydrogen bond acceptor sites inside the cavity of **35b** provide additional attractive contacts with the dihydrogenphosphate anion, in turn causing an overall stabilization of the complex. Importantly, the characteristic binding mode of **35b** induces selectivity for $H_2PO_4^-$ over SO_4^{2-} at pH 7 despite the higher charge of the sulfate ion. Receptors **35a** and **35b** therefore nicely mimic the behavior of the sulfate-binding protein and the phosphate-binding protein, whose selectivity patterns also originate from the absence of a hydrogen bond acceptor site in the sulfate-binding protein and the presence of one in the phosphate-binding protein [82].

The second type of cage-type receptors presented in this section are the so-called calix[6]cryptureas or calix[6]cryptamides introduced by Jabin and coworkers. These receptors, an example of which is **36**, feature a TREN based cap that close the hydrophobic cavity of a calix[6]arene at the narrow rim and six *tert*-butyl groups controlling the size of the entrance to the cavity on the opposite side. Hydrogen bond acceptors in these receptors are positioned along the narrow calixarene rim in the form of ether oxygen atoms and hydrogen bond donors in the three urea moieties. This arrangement of different binding sites in close proximity allows **36** to interact strongly with suitable organic guest molecules and with ion pairs [83]. The complexation/decomplexation equilibrium of imidazolidin-2-one binding to **36** in $CDCl_3$ is, for example, slow on the NMR time-scale and associated with an association constant K_a of $>10^3$ M^{-1}. Protonation of the tertiary amino group in the cap increases the stability of this complex ($K_a > 5 \times 10^4$ M^{-1}). NMR binding studies demonstrated that complex formation

involves inclusion of the guest into the calixarene cavity, hydrogen-bonding interactions between the NH groups of the guest and two receptor oxygen atoms, and formation of bifurcated hydrogen bonds between the substrate's carbonyl group and those urea NH groups that are positioned closer to the cavity.

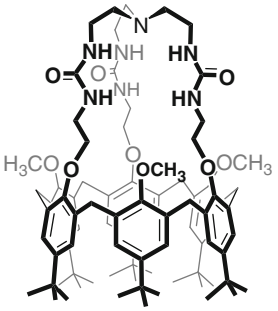

36

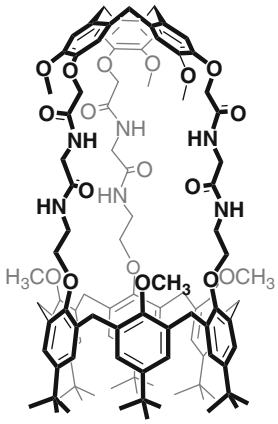

37

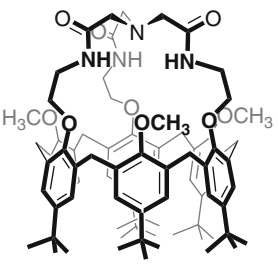

38

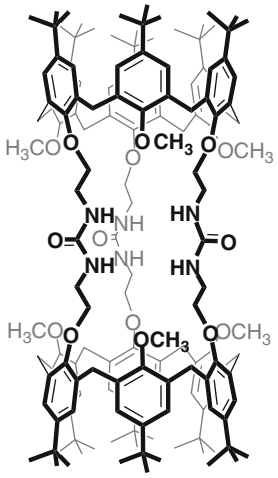

39

Ion pairs, specifically primary ammonium halides, interact with **36** by inclusion of the anion into the tris-urea derived cap where it interacts with the urea NH groups. The counterion is included into the calixarene cavity, as evidenced by significant upfield shifts of the alkyl signals in the ^{1}H NMR spectrum upon complex formation, with the headgroup protruding from the narrow opening to allow for hydrogen-bonding interactions between the ammonium protons and the ether oxygen atoms and for electrostatic interactions with the anion. Quaternary ammonium ions can also be bound inside the calixarene cavity but if halide salts are used whose cations are too large to be included into the cavity, e.g., tetrabutylammonium halides, only the anion is bound. Interestingly, protonation of the cap

does not reinforce anion binding, but causes the release of the anion from the cavity, an effect that was ascribed by the authors to a steric clash between the included anion and the proton on the introverted tertiary amino group.

The highly versatile pH dependent binding properties of **36** allowed the authors to switch reversibly between three complex species by addition of acid or base. This guest-switching cycle started from a mixture of protonated **36** and three competing guests, namely tetramethylammonium chloride, 1-propylammonium chloride, and imidazolidin-2-one in $CDCl_3/CD_3OD$ (98:2). The ^1H NMR spectrum of this mixture showed that only the imidazolidin-2-one complex was initially present. The addition of 2 equiv. of DBU gave rise, exclusively, to the complex with 1-propylammonium chloride through the deprotonation of the cap. The subsequent addition of a large excess of DBU led to the deprotonation of the ammonium ion and therefore to the quantitative formation of the tetramethylammonium chloride complex. The full reversibility of the switching processes was demonstrated through the progressive addition of picric acid restoring first the 1-propylammonium chloride complex and then the initial complex with the neutral substrate.

A number of other receptors structurally relating to **36** were described that possess overall similar binding properties although some characteristic differences were noted. Compound **37**, for example, containing a cyclotriveratrylene-derived cap instead of a TREN moiety, also binds imidazolidin-2-one or ammonium halides, but since this compound lacks the tertiary amino group it does not allow binding properties to be controlled by protonation [84].

Compound **38** is structurally more closely related to **36**, but the size of the cap is significantly smaller. This structural change increases affinity for imidazolidin-2-one, which is with a $K_a > 10^5\ M^{-1}$ at least one order of magnitude higher than that of **36** [85]. In marked contrast to **36**, where affinity for imidazolidin-2-one increases upon protonation of the host, protonation of **38** causes the guest to be expelled from the cavity, presumably because of a conformational reorganization induced by the formation of an intramolecular hydrogen bond between the protonated NH group and an introverted carbonyl group. Anion binding of **38** is restricted to fluoride, which is small enough to enter the cavity of the cap and to simultaneously interact with the three introverted NH groups. As a consequence, inclusion of alkyl ammonium cations into the calixarene cavity was only observed in the presence of fluoride ions. In the case of other ammonium halides, the energetically highly unfavorable dissociation of the ion pair, which is not compensated in the complex by ion-pairing with an anion bound at the level of the cap, prevented the ammonium ion from entering the calixarene cavity. As in the case of **36**, protonation of the TREN group causes release of the fluoride anion.

The tube-like receptor **39** was shown to bind two imidazolidin-2-one molecules inside the calixarene subunits or, more interestingly, ion triplets comprising an anion, which binds to the central urea moieties, and two ammonium ions, which are incorporated into the calixarene rings [86]. Particularly stable complexes are formed with ammonium sulfate salts even in relative polar media ($CD_3OD/CDCl_3$ 3:1), but chloride ions can also induce the formation of such complexes

albeit only in $CDCl_3$. In the absence of cations that can be bound inside the calixarene cavities, no interaction between anions and **39** was observed, demonstrating the importance of ion-pairing for complex stabilization.

A self-assembling molecular capsule with inwardly directed hydrogen bond acceptors and donors composed of two identical resorcarene derivatives with phenylalanine residues on each aromatic subunit, L-**40**, was recently reported by Kuberski and Szumna [87].

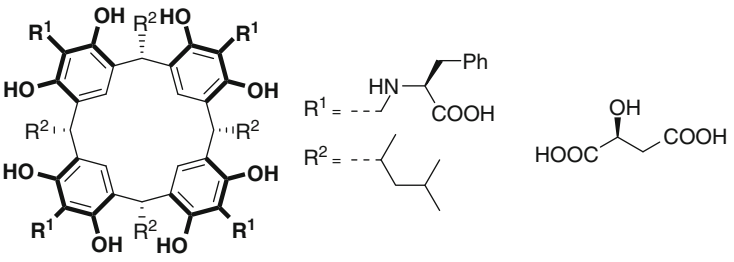

L-**40** *S*-**41**

This compound is well soluble in chloroform in spite of its polar nature, a result that was rationalized by the authors by the burial of the polar functionalities inside the interior of a capsule assembled from two molecules of L-**40**. X-ray crystallography confirmed this assumption. Capsules formed from L-**40** are sealed by two seams of salt bridges formed between the amino and carboxyl groups of the amino acid residues (Fig. 6). Owing to the numerous complementary hydrogen-bonding interactions the capsule core is tightly packed with almost no holes. All polar functionalities are isolated from the environment by the phenylalanine side chains. The interior of the capsule is filled with two nitromethane and four water molecules in the crystal. These solvent molecules form direct contact with the functional groups that stabilize the assembly. Specifically, the amino groups form hydrogen bonds to the nitromethane molecules, while the close proximity of the carboxyl groups to the water molecules suggests that the carboxylate groups serve as hydrogen bond acceptors.

Capsules deriving from **40** also exhibit high kinetic stability in solution which was demonstrated by mixing solutions of (L-**40**)$_2$ and (D-**40**)$_2$ in $CDCl_3$ and recording the ^{1}H NMR spectrum. This spectrum remained unchanged for more than 2 weeks. Only after addition of methanol, evaporation, and redissolution in $CDCl_3$ did clear changes occur. The resulting spectrum indicated the exclusive formation of the heterochiral capsule (L-**40**)(D-**40**), which not only demonstrated that the homochiral dimers are kinetically very stable in $CDCl_3$, but also that the heterochiral dimer is thermodynamically the more stable assembly.

Capsule (L-**40**)$_2$ easily incorporates small organic guest molecules such as alcohols, carboxylic acids, *N*-protected amino acids, and even inorganic salts of carboxylic acids. A pronounced preference was observed for hydroxy acids, which is the reason why most investigations concentrated on this type of guests. ^{1}H NMR spectroscopic binding studies in the absence (equilibration a solution of (L-**40**)$_2$ in toluene with solid guest) or in the presence of water (equilibration of a two phase mixture of solutions of

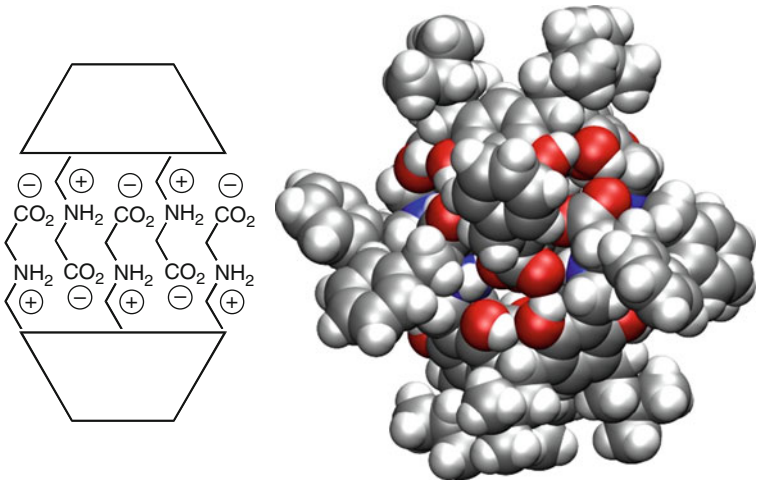

Fig. 6 Schematic representation of the arrangement of two subunits of L-**40** in the dimeric capsule (*left*) and space-filling model of the molecular structure of $[(\text{L-}\mathbf{40})_2{\cdot}(CH_3NO_2)_2{\cdot}(H_2O)_4]$ (*right*)

(L-**40**)$_2$ in toluene and of guest in water) revealed characteristic differences in the structures of the complex formed [88]. For example, with *S*-malic acid *S*-**41** as guest a capsule formed in the absence of water containing two guest molecules, while only one molecule of *S*-**41** is bound inside the cavity when complex formation was performed in the presence of water. This guest molecule resides in one hemisphere of the capsule; the other hemisphere most likely contains water molecules. The translational motion of the guest from one hemisphere to the other is slow on the NMR time-scale and associated with an energy barrier of 73.7 kJ mol^{-1} at 303 K. Investigations with other guests confirmed that water inside the cavity significantly affects the dynamics of the included guests. In general, the more hydrophilic the guest, the more pronounced the effect that water has on binding.

Binding studies in other solvents demonstrated that, for example, chloroform or acetone can also be coencapsulated inside (L-**40**)$_2$ allowing only one hydroxy acid to enter the cavity [89]. The hydrophobic toluene, on the other hand, is no good guest so that 2:1 guest/capsule complexes are usually observed. A comparison of the K_a values for a series of hydroxy acids in acetone-d_6 suggests that, as the guests become larger and more hydrophobic, the association constants become smaller. For guests of similar size but different polarity, more hydrophilic guests have higher affinities toward (L-**40**)$_2$, which is in agreement with the polar nature of the capsule's interior. The K_a of the 1:1 guest/capsule complex between *S*-malic acid and (L-**40**)$_2$ amounts to 506 M^{-1}, for example. The fact that the corresponding *R*-enantiomer of this guest is bound with a significantly smaller K_a of 157 M^{-1} shows that binding is moderately enantioselective. Moreover, experiments addressing the rate of complex formation demonstrated that although guest exchange is slow on the NMR time-scale it is much faster than rearrangement of the homochiral into heterochiral capsules, a result suggesting that guest exchange

proceeds via a gating mechanism and does not require the capsules to dissociate completely.

Information about the arrangement of the guest molecules inside (L-**40**)$_2$ was gained from the crystal structure of the capsule containing two *S*-malic acid molecules [89]. In the crystal, the two hemispheres are not identical because of steric interactions between the outwardly oriented phenylalanine side chains. As a consequence, the amino acid backbones are tilted in opposite directions, the hydrogen-bonding belts have opposing directionalities for complementary parts, and one hemisphere, denoted the *M* hemisphere, has fewer hydrogen bonds. Each hemisphere is filled with one guest molecule. In the *P* hemisphere, the carboxylic group of the guest acts both as a hydrogen bond donor and acceptor for interactions with ammonium cations and carboxylate anions along the capsule wall. The aliphatic CH_2 group is positioned in the hydrophobic part of the cavity, while the OH group interacts simultaneously as a donor and acceptor of hydrogen bonds. Although the second carboxylic group is positioned close to the central point of the capsule, and is most probably additionally disordered, it has the possibility of forming one hydrogen bond.

Similar types of hydrogen bonds are observed in the *M* hemisphere. The carboxylic group again interacts with both the ammonium and the carboxylate groups of the capsule, and the aliphatic CH_2 group is bound in the hydrophobic part of the cavity. However, due to the opposite tilt and chirality of the hydrogen-bonding system in this hemisphere, the hydroxy group at the stereogenic center has a different position. As a result, some hydrogen bonds are slightly longer and the guest molecule adopts a more crowded conformation. This crystal structure therefore clearly showed that the well defined pattern of functional groups along the seam of (L-**40**)$_2$ and not steric effects alone control the order of the guests inside the cavity.

6 Conclusions

This overview shows that molecular cages or capsules with inwardly oriented binding sites do not simply entrap guest molecules – they provide the guest with an electronically complementary environment in the interior. Complex formation is therefore not only a matter of filling the available space but complemented by directed interactions between the guest and the receptor walls. As a consequence, filling the receptor's internal space can be very efficient and packing coefficients of up to 70% have been observed [89], significantly larger than those of complexes of other molecular containers or capsules [90]. In addition, directionality of the interactions inside the receptor cavity induces an ordered arrangement of the included guest molecules, an effect that is probably not so important for smaller receptors where steric effects are usually sufficient to restrict the motion of the guests. In larger cavities, however, translational motions of the guests are often less difficult and an ordered arrangement of guest molecules can only be achieved when the guest finds positions on the inner cavity surface to which it can bind.

Increased kinetic stability in comparison to receptors with better accessible binding sites, caused by *constrictive binding*, is a common feature of all types of cage-type receptors, but combining constrictive binding with attractive interactions between the guest and the cage walls additionally increases thermodynamic stability, which can be low for receptors lacking suitable binding sites in the interior. The entropic component of complex stability, resulting from the release of solvent molecules upon incorporation of the guest into the receptor cavity, is thus complemented by a favorable enthalpic term. That this enthalpic term should not be taken for granted is demonstrated by the behavior of bis(cyclopeptide) **28**. Binding properties thus depend on subtle structural effects that are often not easy to predict for structurally relative complex receptors.

One of the more challenging aspects in the design of cages with functionalized interiors is the incorporation of converging binding sites along the concave inner surface of the cavity. A highly flexible and very promising approach relies on the use of coordinatively unsaturated metal centers, but other strategies can also be pursued. The examples described in Sect. 5 of this overview indicate that combining different binding sites into the cavity of receptors with confined cavities represents a particularly promising approach to develop potent and selective binders. Such systems might eventually be able to mimic the binding event inside the active center of a protein or, if at least two guests are included in a proper mutual arrangement, serve as molecular reaction vessels to induce the (stereoselective) transformation of suitable substrates. Further creative work is required to reach this ambitious goal.

References

1. Jasat A, Sherman JC (1999) Chem Rev 99:931
2. Sherman JC (1995) Tetrahedron 51:3395
3. Vougioukalakis GC, Roubelakis MM, Orfanopoulos M (2010) Chem Soc Rev 39:817
4. Thilgen C, Diederich F (2006) Chem Rev 106:5049
5. Cram DJ, Blanda MT, Paek K, Knobler CB (1992) J Am Chem Soc 114:7765
6. Cram DJ, Tanner ME, Knobler CB (1991) J Am Chem Soc 113:7717
7. Rudkevich DM, Hilmersson G, Rebek J Jr (1997) J Am Chem Soc 119:9911
8. Palmer LC, Rebek J Jr (2004) Org Biomol Chem 2:3051
9. Vysotsky MO, Pop A, Broda F, Thondorf I, Böhmer V (2001) Chem Eur J 7:4403
10. Dietrich B, Lehn J-M, Sauvage J-P (1969) Tetrahedron Lett 10:2889
11. Kang SO, Llinares JM, Day VW, Bowman-James K (2010) Chem Soc Rev 39:3980
12. García-España E, Díaz P, Llinares JM, Bianchi A (2006) Coord Chem Rev 250:2952
13. Park CH, Simmons HE (1968) J Am Chem Soc 90:2431
14. Leininger S, Olenyuk B, Stang PJ (2000) Chem Rev 100:853
15. Albrecht M, Janser I, Meyer S, Fröhlich R (2003) Chem Commun 2854
16. Fochi F, Jacopozzi P, Wegelius E, Rissanen K, Cozzini P, Marastoni E, Fisicaro E, Manini P, Fokkens R, Dalcanale E (2001) J Am Chem Soc 123:7539
17. Fujita M, Tominaga M, Hori A, Therrien B (2005) Acc Chem Res 38:369
18. Mal P, Breiner B, Rissanen K, Nitschke JR (2009) Science 324:1697
19. Pluth MD, Bergman RG, Raymond KN (2009) Acc Chem Res 42:1650
20. Saalfrank RW, Maid H, Scheurer A (2008) Angew Chem Int Ed 47:8794
21. Seidel SR, Stang PJ (2002) Acc Chem Res 35:972

22. Ward MD (2009) Chem Commun 4487
23. Glasson CRK, Meehan GV, Clegg JK, Lindoy LF, Turner P, Duriska MB, Willis R (2008) Chem Commun 1190
24. Tidmarsh IS, Taylor BF, Hardie MJ, Russo L, Clegg W, Ward MD (2009) New J Chem 33:366
25. Sgarlata C, Mugridge JS, Pluth MD, Tiedemann BEF, Zito V, Arena G, Raymond KN (2010) J Am Chem Soc 132:1005
26. Worm K, Schmidtchen FP, Schier A, Schäfer A, Hesse M (1994) Angew Chem Int Ed 33:327
27. Clever GH, Tashiro S, Shionoya M (2009) Angew Chem Int Ed 48:7010
28. Clever GH, Tashiro S, Shionoya M (2010) J Am Chem Soc 132:9973
29. Custelcean R, Bosano J, Bonnesen PV, Kertesz V, Hay BP (2009) Angew Chem Int Ed 48:4025
30. Hay BP, Firman TK (2002) Inorg Chem 41:5502
31. Amouri H, Mimassi L, Rager MN, Mann BE, Guyard-Duhayon C, Raehm L (2005) Angew Chem Int Ed 44:4543
32. Adarsh NN, Tocher DA, Ribas J, Dastidar P (2010) New J Chem 34:2458
33. Hiraoka S, Kiyokawa M, Hashida S, Shionoya M (2010) Angew Chem Int Ed 49:138
34. Motekaitis RJ, Martell AE, Dietrich B, Lehn J-M (1984) Inorg Chem 23:1588
35. Motekaitis RJ, Martell AE, Lehn J-M, Watanabe E (1982) Inorg Chem 21:4253
36. Fabbrizzi L, Pallavicini P, Parodi L, Taglietti A (1995) Inorg Chim Acta 238:5
37. O'Neil EJ, Smith BD (2006) Coord Chem Rev 250:3068
38. Beer PD, Hayes EJ (2003) Coord Chem Rev 240:167
39. Graf E, Lehn J-M (1975) J Am Chem Soc 97:5022
40. Graf E, Kintzinger JP, Lehn J-M, LeMoigne J (1982) J Am Chem Soc 104:1672
41. Barrett ES, Irwin JL, Edwards AJ, Sherburn MS (2004) J Am Chem Soc 126:16747
42. Rissanen K (2005) Angew Chem Int Ed 44:3652
43. Nguyen TV, Yoshida H, Sherburn MS (2010) Chem Commun 46:5921
44. Ebmeyer F, Vögtle F (1989) Angew Chem Int Ed 28:79
45. Haberhauer G, Oeser T, Rominger F (2005) Chem Eur J 11:6718
46. Sambasivan S, Kim S-G, Choi SM, Rhee YM, Ahn KH (2010) Org Lett 12:4228
47. Butterfield SM, Rebek J Jr (2006) J Am Chem Soc 128:15366
48. Renslo AR, Rebek J Jr (2000) Angew Chem Int Ed 39:3281
49. Graf E, Lehn J-M (1976) J Am Chem Soc 98:6403
50. Metz B, Rosalky JM, Weiss R (1976) J Chem Soc Chem Commun 533
51. Fujita T, Lehn J-M (1988) Tetrahedron Lett 29:1709
52. Kang SO, Day VW, Bowman-James K (2010) J Org Chem 75:277
53. Ballester P (2010) Chem Soc Rev 39:3810
54. Davis AP (2009) Org Biomol Chem 7:3629
55. Davis AP, Wareham RS (1998) Angew Chem Int Ed 37:2270
56. Klein E, Crump MP, Davis AP (2005) Angew Chem Int Ed 44:298
57. Ferrand Y, Klein E, Barwell NP, Crump MP, Jiménez-Barbero J, Vicent C, Boons G-J, Ingale S, Davis AP (2009) Angew Chem Int Ed 48:1775
58. Barwell NP, Crump MP, Davis AP (2009) Angew Chem Int Ed 48:7673
59. Lecollinet G, Dominey AP, Velasco T, Davis AP (2002) Angew Chem Int Ed 41:4093
60. Ferrand Y, Crump MP, Davis AP (2007) Science 318:619
61. Klein E, Ferrand Y, Barwell NP, Davis AP (2008) Angew Chem Int Ed 47:2693
62. Gale PA, Anzenbacher P Jr, Sessler JL (2001) Coord Chem Rev 222:57
63. Bucher C, Zimmerman RS, Lynch V, Sessler JL (2001) J Am Chem Soc 123:9716
64. Cafeo G, Colquhoun HM, Cuzzola A, Gattuso M, Kohnke FH, Valenti L, White AJP (2010) J Org Chem 75:6263
65. Kubik S, Goddard R, Kirchner R, Nolting D, Seidel J (2001) Angew Chem Int Ed 40:2648
66. Reyheller C, Hay BP, Kubik S (2007) New J Chem 31:2095
67. Otto S, Kubik S (2003) J Am Chem Soc 125:7804
68. Kubik S, Kirchner R, Nolting D, Seidel J (2002) J Am Chem Soc 124:12752

69. Fiehn T, Goddard R, Seidel RW, Kubik S (2010) Chem Eur J 16:7241
70. Atwood JL, Barbour LJ, Jerga A (2001) Chem Commun 2376
71. Gerkensmeier T, Iwanek W, Agena C, Fröhlich R, Kotila S, Näther C, Mattay J (1999) Eur J Org Chem 2257
72. MacGillivray LR, Atwood JL (1997) Nature 389:469
73. Atwood JL, Barbour LJ, Jerga A (2002) Proc Natl Acad Sci USA 99:4837
74. Ballester P, Gil-Ramírez G (2009) Proc Natl Acad Sci USA 106:10455
75. Rebek J Jr (2000) Chem Commun 637
76. Cafeo G, Kohnke FH, Valenti L, White AJP (2008) Chem Eur J 14:11593
77. Gil-Ramírez G, Benet-Buchholz J, Escudero-Adán EC, Ballester P (2007) J Am Chem Soc 129:3820
78. Park YS, Paek K (2008) Org Lett 10:4867
79. Hayashida O, Shivanyuk A, Rebek J Jr (2002) Angew Chem Int Ed 41:3423
80. Mateus P, Delgado R, Brandão P, Carvalho S, Félix V (2009) Org Biomol Chem 7:4661
81. Mateus P, Delgado R, Brandão P, Félix V (2009) J Org Chem 74:8638
82. Mangani S, Ferraroni M (1997) In: Bianchi A, Bowman-James K, García-España E (eds) Supramolecular chemistry of anions. Wiley, New York, p 63
83. Ménand M, Jabin I (2010) Chem Eur J 16:2159
84. Le Gac S, Jabin I (2008) Chem Eur J 14:548
85. Lascaux A, Le Gac S, Wouters J, Luhmer M, Jabin I (2010) Org Biomol Chem 8:4607
86. Moerkerke S, Ménand M, Jabin I (2010) Chem Eur J 16:11712
87. Kuberski B, Szumna A (2009) Chem Commun 1959
88. Szumna A (2009) Chem Commun 4191
89. Szumna A (2009) Chem Eur J 15:12381
90. Mecozzi S, Rebek J Jr (1998) Chem Eur J 4:1016

Top Curr Chem (2012) 319: 35–56
DOI: 10.1007/128_2011_272

Published online: 28 September 2011

Drug Delivery by Water-Soluble Organometallic Cages

Bruno Therrien

Abstract Until recently, organometallic derivatives were generally viewed as moisture- and air-sensitive compounds, and consequently very challenging to synthesise and very demanding in terms of laboratory requirements (Schlenk techniques, dried solvent, glove box). However, an increasing number of stable, water-soluble organometallic compounds are now available, and organometallic chemistry in aqueous phase is a flourishing area of research. As such, coordination-driven self-assemblies using organometallic building blocks are compatible with water, thus opening new perspectives in bio-organometallic chemistry.

This chapter gives a short history of coordination-driven self-assembly, with a special attention to organometallic metalla-cycles, especially those composed of half-sandwich complexes. These metalla-assemblies have been used as sensors, as anticancer agents, as well as drug carriers.

Keywords Bio-organometallic chemistry · Drug delivery · Half-sandwich complexes · Host–guest systems · Supramolecular chemistry

Contents

B. Therrien (✉)
Institut de chimie, Université de Neuchâtel, Av. de Bellevaux 51, CH-2000 Neuchâtel, Switzerland
e-mail: bruno.therrien@unine.ch

Abbreviations

bipy	4,4′-Bipyridine
bpe	1,2-Bis(4-pyridyl)ethylene
bpp	5,15-Bis(4-pyridyl)-10,20-diphenylporphyrin
bpy	2,2′-Bipyrimidine
Cp	Cyclopentadienyl
Cp*	Pentamethylcyclopentadienyl
DAniF	*N*,*N*′-Di(*p*-anisyl)formamidinate
dcbq	2,5-Dichloro-1,4-benzoquinone-3,6-diolato
dhbq	1,4-Benzoquinone-2,5-diolato
doaq	1,4-Anthraquinone-9,10-diolato
donq	1,4-Naphthoquinone-5,8-diolato
dotq	Tetracene-5,12-dione-6,11-diolato
en	Ethylenediamine
phen	4,7-Phenanthroline
tpp	5,10,15,20-Tetra(4-pyridyl)porphyrin
tppp	5,10,15-Tris(4-pyridyl)-20-phenylporphyrin
tpt	1,3,5-Tris(4-pyridyl)triazine

1 Introduction

The design of molecular hosts to encapsulate guest molecules in a confined environment is receiving considerable attention due to the analogy of these systems with the mode of action of enzymes. The "lock and key" model developed by Fischer [1] to explain the specificity between a substrate and the active site of an enzyme (Fig. 1) has been the bases for the development of host–guest chemistry [2]. Pioneered by Cram, Lehn and Pedersen [3], winners of the Nobel Prize in chemistry in 1987 for their contributions to the development and use of molecules with structure-specific interactions of high selectivity, synthetic molecular hosts were initially dominated by purely organic molecules: cyclodextrins, carcerands, cryptands, cucurbiturils and cavitands. However, the last 20 years have seen the emergence of discrete inorganic and organometallic metalla-hosts able to encapsulate, temporarily or permanently, various guest molecules in their cavity, thus opening new perspectives in coordination chemistry.

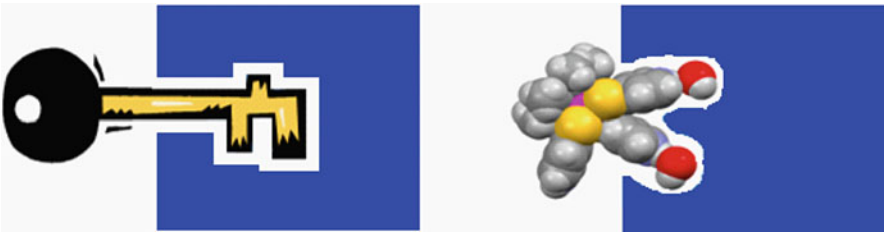

Fig. 1 Fischer's "lock and key" model

2 Inorganic Metalla-Assemblies

In the early 1990s, Fujita [4], Stang [5], and others [6] combined 90º coordination building blocks of square-planar metal ions with linear bidentate ligands to form triangular, square and rectangular architectures. For example, the combination of $Pt(PMe_3)_2$ corner units with 1,2-bis(4-pyridyl)ethylene (bpe) has generated a triangular structure, $[\{Pt(PMe_3)_2\}_3(bpe)_3]^{6+}$ (Fig. 2a) [7], while Pd(en) units (en = ethylenediamine) and 4,4′-bipyridine (bipy) gave a cationic square $[\{Pd(en)\}_4(bipy)_4]^{8+}$ (Fig. 2b) [8]. The same approach was used a few years later to generate three-dimensional metalla-assemblies by replacing linear bidentate ligands with multidentate connectors.

Some of the three-dimensional assemblies possess cavities large enough to accommodate guest molecules. Indeed, the $M_6(tpt)_4$ cage compounds [where M = Pd, Pt; tpt = 1,3,5-tris(4-pyridyl)triazine] developed by Fujita and coworkers in 1995 [9] remain some of the most studied host–guest systems (Fig. 3a). The cavity of the cationic $M_6(tpt)_4$ cages has been exploited in different ways, ranging from stabilisation of reactive species to microreactors. A tremendous number of other cage compounds using square-planar metal centres has been prepared in the last 15 years, such as the very large $Pt_{12}L'_4$ (where L′ = hexapyridyl ligand) cage compound (Fig. 3b) from Stang [10]. These examples illustrate the potential and versatility of using coordination chemistry to generate a multitude of two- and three-dimensional structures. Nowadays, transition metals with octahedral geometry are also commonly used to prepare two- and three-dimensional architectures [11].

A series of tetrahedral assemblies built from four metal ions (e.g., Ga^{3+}, Al^{3+}, In^{3+}, Fe^{3+}, Ti^{4+}, Ge^{4+}) and six bis-catechol ligands has been prepared by Raymond's group (Fig. 4a). These chiral hosts possess a small hydrophobic cavity

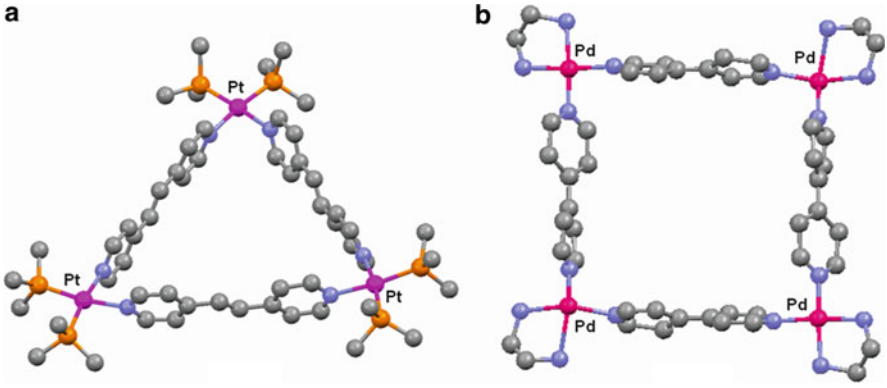

Fig. 2 Two-dimensional structures using square-planar metal ions, $[\{Pt(PMe_3)_2\}_3(bpe)_3]^{6+}$ (**a**) [7] and $[\{Pd(en)\}_4(bipy)_4]^{8+}$ (**b**) [8]

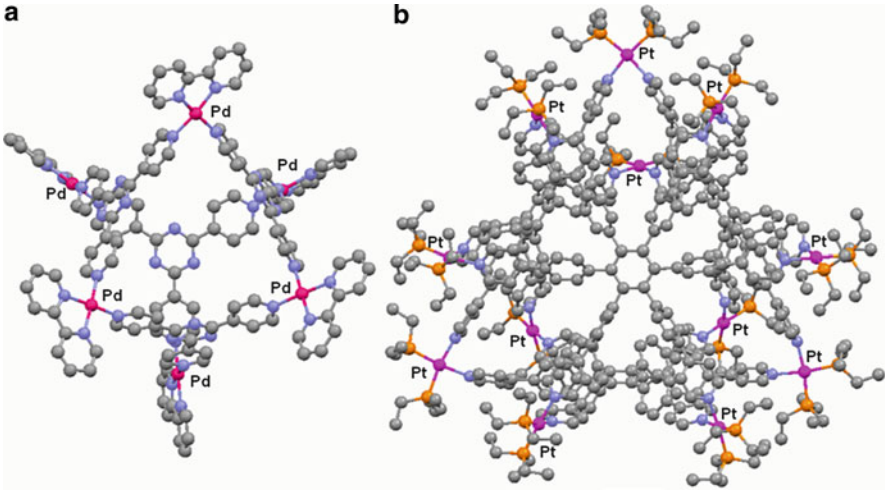

Fig. 3 Three-dimensional structures using square-planar metal ions, $[\{Pd(2,2'\text{-bipyridine})\}_6(tpt)_4]^{12+}$ (**a**) [9] and $[\{Pt(PEt_3)_2\}_{12}(L')_4]^{24+}$ (**b**) [10]

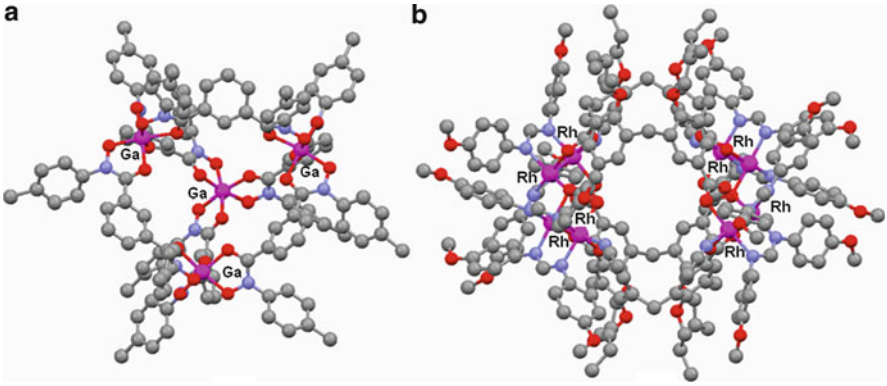

Fig. 4 Inorganic three-dimensional assemblies using octahedral metal ions, $[Ga_4\{\text{isophthal-di-}N\text{-(4-methylphenyl)hydroxamate}\}_6]$ (**a**) [12] and $[\{Rh_2(DAniF)_2(CH_3CN)\}_4(\text{calix[4]arenetetracarboxylinato})_2]$ (**b**) [13]

capable of accommodating cationic or neutral guest molecules [12]. Using metal–metal paddlewheel units, Cotton and Murillo have prepared several two- and three-dimensional inorganic assemblies [14]. For the largest assemblies, such as $[\{Rh_2(DAniF)_2(CH_3CN)\}_4(\text{calix[4]arenetetracarboxylinato})_2]$ [where DAniF = *N*, *N*′-di(*p*-anisyl)formamidinate] (Fig. 4b), guest molecules have been observed in the cavity [13].

Large polyhedral coordination cages using flexible bridging pyrazolyl–pyridine chelating ligands have been prepared by Ward and coworkers [15]. These large

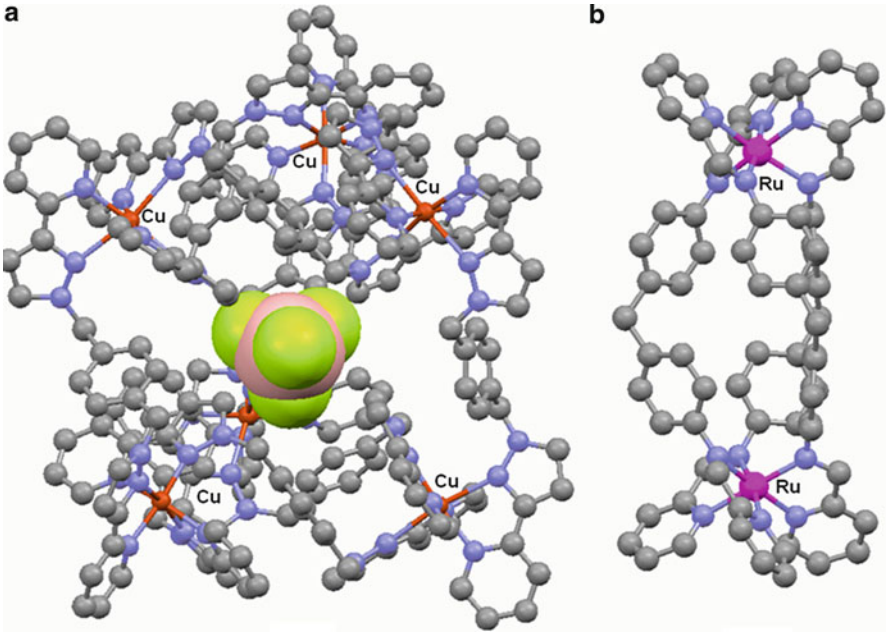

Fig. 5 Inorganic three-dimensional assemblies using octahedral metal ions, $[BF_4 \subset Cu_6\{1,4\text{-bis}((3\text{-}(2\text{-pyridyl})\text{-}1\text{-pyrazolyl})\text{methyl})\text{benzene}\}_9]^{12+}$ (**a**) (the BF_4 anion being represented by space-filling model) [15], and $[Ru_2\{\text{bis}(2\text{-pyridylmethylene})\text{benzene-}1,4\text{-diamine}\}_3]^{4+}$ (**b**) [16]

structures show dynamic behaviour in solution, thus generating M_6L_9, M_8L_{12} or $M_{16}L_{24}$ assemblies (where M = Ni^{2+}, Cu^{2+}, Zn^{2+}, Cd^{2+}) depending on the nature of the metal ions used (Fig. 5a). Triple-stranded helicates composed of three bis-pyridyl-imine ligands coordinated to two ruthenium centres have been synthesised by Hannon. These supramolecular cylinders (Fig. 5b) interact with DNA [17] and some of them exhibit anticancer activity [16].

So far, these inorganic metalla-cages have been used to generate a confined environment to not only encapsulate solvent molecules, but also to protect or stabilise sensitive compounds, to recognise and trap specific guest molecules, or to act as a microreactor for specific reactions [18]. Consequently, it is not surprising that the strategies developed to build up inorganic metalla-assemblies have been applied to organometallic chemistry.

3 Organometallic Metalla-Assemblies

Built on the experience gained from the synthesis of inorganic metalla-assemblies, both, two- and three-dimensional architectures have been obtained with organometallic building blocks. The *fac*-$Re(CO)_3$ corner unit was possibly the first

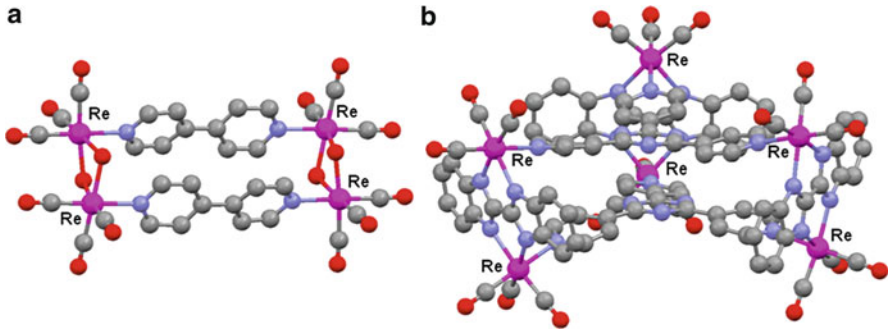

Fig. 6 Organometallic assemblies built with *fac*-$Re(CO)_3$ units, $\{Re(CO)_3\}_4(bipy)_2(\mu\text{-}O)_4$ (**a**) [20] and $\{Re(CO)_3\}_6(bpy)_3(tpt)_2$ (**b**) [21]

organometallic building block used for the rational design of metalla-cycles and three-dimensional metalla-assemblies [19]. The facial arrangement of the carbonyl groups controls the accessibility of the three remaining coordination sites of the octahedral rhenium centre, thus preventing the formation of polymeric species. Consequently, two- and three-dimensional architectures can be obtained from *fac*-$Re(CO)_3$ corners, if assembled with linear connectors and bidentate or tridentate ligands, thus forming metalla-assemblies such as the two-dimensional rectangle $[Re(CO)_3]_4(bipy)_2(\mu\text{-}O)_4$ (Fig. 6a) [20] or the triangular metalla-prism $\{Re(CO)_3\}_6(bpy)_3(tpt)_2$ (where bpy = 2,2′-bipyrimidine) [21] (Fig. 6b).

Among other metal carbonyl derivatives, the reaction of $Ru_3(CO)_{12}$ with dicarboxylic acid leads, after addition of axial ligands, to cage-like macrocycles, tetranuclear loops, hexanuclear triangles or octanuclear squares, depending on the nature of the dicarboxylato spacers [22]. Molecular triangles are obtained using terephthalic acid [23] or 4,4′-diphenyldicarboxylic acid [24], while squares are isolated with oxalic acid [25] (Fig. 7a). The hexanuclear macrocycle synthesised from 4,4′-diphenyldicarboxylic acid, $Ru_3(CO)_{12}$ and trimethylphosphine, $\{Ru_2(CO)_4\}_3(OOCC_6H_4COO)_3(PMe_3)_6$ [23], possesses a cavity of 11.1 × 11.1 × 11.1 $Å^3$, which can accommodate solvent molecules in the hydrophobic hollow space of its triangular structure (Fig. 7b).

Using a directional bonding approach, Stang and coworkers have prepared a series of dinuclear organometallic clips from platinum metal atoms coordinated to σ-bonded acetylene derivatives to generate, after addition of two tridentate ligands, organometallic metalla-prisms of different cavity sizes [26]. Similarly, dinuclear organometallic clips obtained from platinum σ-bonded acetylene were used to prepare two-dimensional assemblies of the type cyclotris[{2,9-bis(*trans*-$Pt(PEt_3)_2$)phenanthrene}(L″)] (where L″ = dicarboxylic acids) (Fig. 8a) [27]. On the other hand, three-dimensional assemblies using gold σ-bonded alkynyl ligands have been isolated after transformation of the alkynyl units into μ_4-methylydine ligands under basic conditions (Fig. 8b) [28].

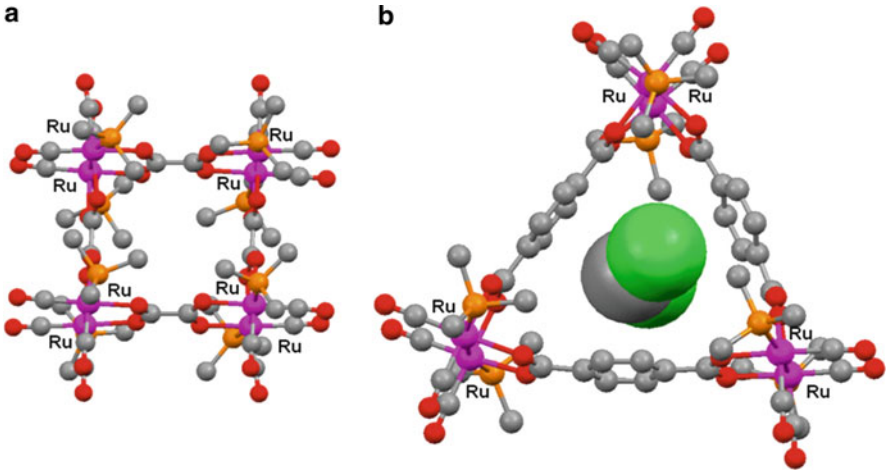

Fig. 7 Organometallic assemblies built with dinuclear ruthenium carbonyl building blocks, $\{Ru_2(CO)_4\}_4(OOCCOO)_4(PMe_3)_8$ (**a**) [25] and $[CH_2Cl_2 \subset \{Ru_2(CO)_4\}_3(OOCC_6H_4COO)_3(PMe_3)_6]$ (**b**) (CH_2Cl_2 being represented by space-filling model) [23]

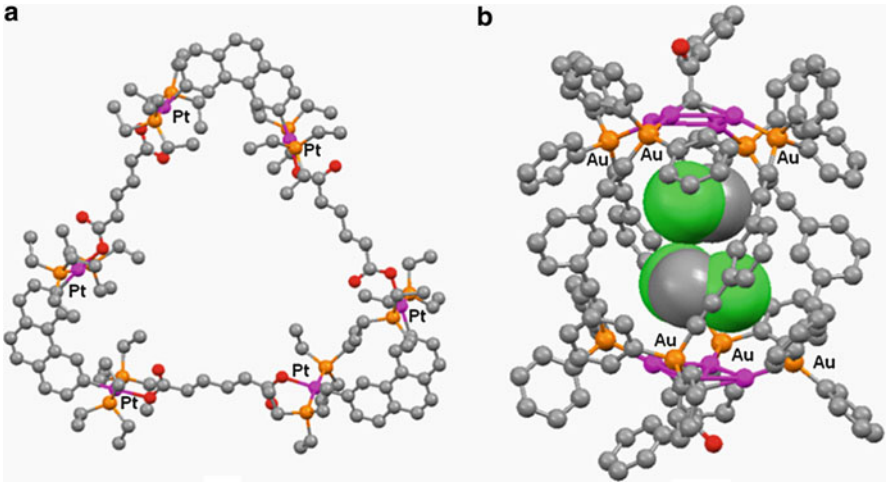

Fig. 8 Organometallic assemblies built from σ-bonded ligands, $[\{2,9\text{-bis}(Pt(PEt_3)_2)\text{phenanthrene}\}(OOCC_4H_8COO)]_3$ (**a**) [27] and $[(CH_2Cl_2)_2 \subset Au_8(CCOPh)_2(Ph_2PC_6H_4PPh_2)_4]^{2+}$ (**b**) (CH_2Cl_2 being represented by space-filling models) [28]

Nevertheless, among the large family of organometallic building blocks that can be used to prepare metalla-assemblies, half-sandwich complexes are certainly the most studied. Mainly employed in catalysis [29], half-sandwich complexes are now being extensively evaluated as anticancer agents [30], and they have also been used to generate metalla-assemblies [31].

4 Organometallic Metalla-Assemblies Composed of Half-Sandwich Complexes

In analogy to the three carbonyl groups in the *fac*-$Re(CO)_3$ unit, η^5-cyclopentadienyl and η^6-arene ligands can be used to control accessibility of the remaining coordination sites of an octahedral metal centre. The aromatic ligand occupies three of the six coordination sites at the metal centre, and the resulting coordination geometry is pseudo-tetrahedral, thus allowing better control of the synthesis of two- or three-dimensional assemblies. Indeed, CpM and Cp*M (where M = Rh, Ir, Ru; Cp = C_5H_5; Cp* = C_5Me_5) units have been extensively used to generate metalla-cycles, rectangles, trigonal prisms, hexagonal prisms and other supramolecular assemblies [31, 32]. Arene ruthenium and to a lesser extent arene osmium complexes (where arene = C_6H_6, C_6H_5Me, pPr^iC_6H_4Me, C_6Me_6) have been used to prepare similar two and three-dimensional assemblies [33].

Using tridentate ligands with various functionalities and coordinating abilities, a series of neutral and cationic tri-, tetra- and hexanuclear metalla-cycles have been synthesised [34]. Cyclic tetramers composed of Cp*Ir, Cp*Rh or (arene)Ru half-sandwich complexes and 6-purinethione derivatives have been isolated as triflate salts [35]. The cationic complex $[(Cp^*Ir)_4(L^1)_4]$ (where L^1 = 2-amino-6-purinethione), presented in Fig. 9a, forms in the solid state an infinite channel-like structure with S_4 symmetry. Replacing the 6-purinethione with pyridine-4-thiolato bridging ligands (L^2), the trinuclear metalla-cycle $[(Cp^*Ir)_3(L^2)_3]$ was obtained (Fig. 9b) [36].

In order to generate elongated structures, longer and more flexible spacers connecting two tri-functional ligands coordinated to six arene ruthenium units have been combined [37]. The $\{(p$Pr^i$C_6H_4Me)Ru\}_6(\mu$-$L^3)_2$ (where L^3 = 2,3-

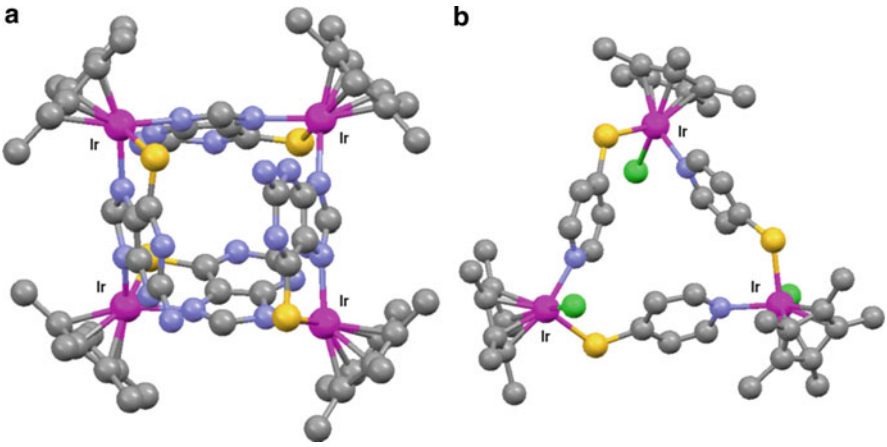

Fig. 9 Two-dimensional assemblies using half-sandwich complexes, $[(Cp^*Ir)_4$(2-amino-6-purinethione$)_4]$ (**a**) [35] and $[(Cp^*Ir)_3$(pyridine-4-thiolato$)_3]$ (**b**) [36]

dihydroxypyridine-based ligands) cylindrical structure is over 3 nm long. Coordinating tpt and the flexible dinuclear arene ruthenium clip, $[\{(p\mathrm{Pr^iC_6H_4Me})\mathrm{Ru}\}_2(\mu\text{-}\mathrm{L}^4)_2]$ (where L^4 = 3,6-dimethoxynaphthalene-2,7-dicarboxylato), a guest-adaptable trigonal prism was obtained [38]. In its empty form, the distance between the two tpt panels is 3.4 Å, whereas in the presence of two coronenes as guest molecules, the tpt–tpt distance reaches 10.9 Å (Fig. 10), and the host–guest system $[(\mathrm{coronene})_2 \subset \{(p\mathrm{Pr^iC_6H_4Me})\mathrm{Ru}\}_6(\mu\text{-}\mathrm{L}^4)_6(\mathrm{tpt})_2]^{6+}$ is observed.

Inspired by Prussian Blue, Rauchfuss group prepared anionic, cationic and neutral metalla-cages incorporating half-sandwich complexes [39]. Cationic derivatives such as $\{[\mathrm{CpCo(CN)_3}]_4[\mathrm{Cp^*Rh}]_4\}^{4+}$ [40] show no affinity for anions, whereas neutral and anionic cages interact strongly with small molecules. Indeed, the metalla-cage $\{[\mathrm{CpCo(CN)_3}]_4[\mathrm{Cp^*Ru}]_4\}$ reacts with monocations (where mc = $\mathrm{K^+}$, $\mathrm{Cs^+}$, $\mathrm{Rb^+}$, $\mathrm{Tl^+}$) to generate the corresponding host–guest systems $\{\mathrm{mc}\subset[\mathrm{CpCo(CN)_3}]_4[\mathrm{Cp^*Ru}]_4\}^+$ (Fig. 11a). Organometallic cryptands built from two Cp*M

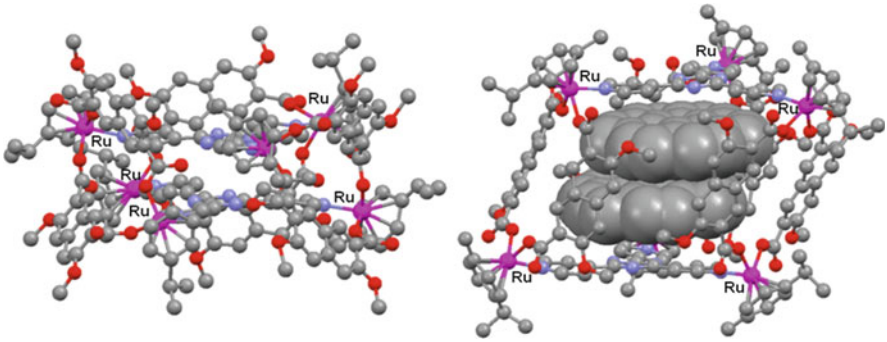

Fig. 10 Guest-adaptable metalla-cage $[\{(p\mathrm{Pr^iC_6H_4Me})\mathrm{Ru}\}_6(\mu\text{-}\mathrm{L}^4)_6(\mathrm{tpt})_2]$, empty (*left*) and encapsulating two coronene molecules (*right*) (coronene being represented by space-filling model) [38]

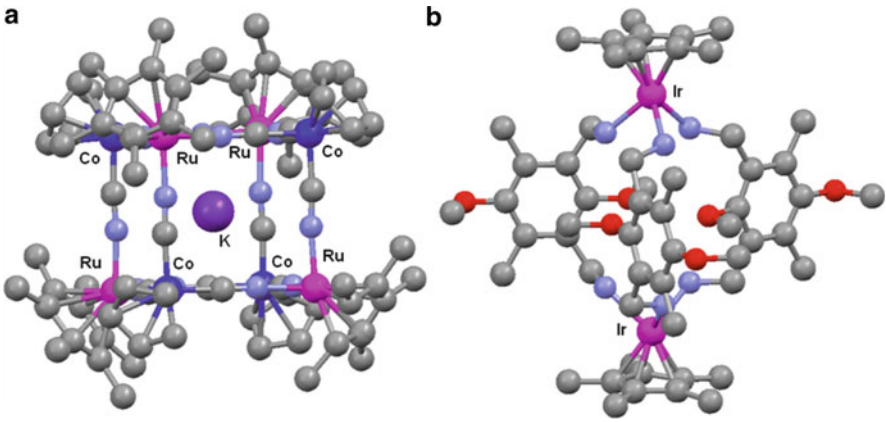

Fig. 11 Organometallic metalla-cages $\{\mathrm{K}\subset[\mathrm{CpCo(CN)_3}]_4[\mathrm{Cp^*Ru}]_4\}^+$ (**a**) [40] and $[(\mathrm{Cp^*Ir})_2(\mathrm{L}^5)_3]^{4+}$ (**b**) [41]

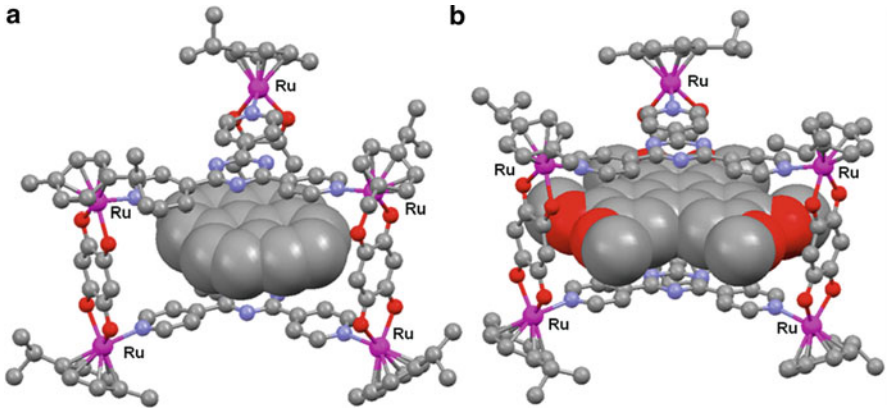

Fig. 12 Organometallic metalla-cages [pyrene⊂{(pPr^{i}C$_6$H$_4$Me)Ru}$_6$(μ-tpt)$_2$(μ-dhbq)$_3$]$^{6+}$ (**a**) [45] and [hexamethoxytriphenylene⊂{(pPr^{i}C$_6$H$_4$Me)Ru}$_6$(μ-tpt)$_2$(μ-dhbq)$_3$]$^{6+}$ (**b**) (guest molecules being represented by space-filling models) [46]

(where M = Rh, Ir) units and three diamino ligands have been found to encapsulate tetrafluoroborate anions in their cavities (Fig. 11b) [41]. The host–guest system [BF$_4$⊂(Cp*Ir)$_2$(L^5)$_3$]$^{3+}$ [where L^5 = 1,3-bis(aminomethyl)benzene] was confirmed by various NMR experiments.

Recently, we have shown the cationic metalla-prisms [{(pPr^{i}C$_6$H$_4$Me)Ru}$_6$(μ-tpt)$_2$(μ-C$_2$O$_4$)$_3$]$^{6+}$ [42] and [(Cp*Rh)$_6$(μ-tpt)$_2$(μ-C$_2$O$_4$)$_3$]$^{6+}$ [43] to possess "double-rosette"-type chirality with *P* or *M* configuration. Moreover, a concerted rotation of the aromatic rings of the tridentate tpt ligand was observed, creating additional three-bladed propeller chirality. In the more spacious 1,4-benzoquinone-2,5-diolato (dhbq) metalla-cage [{(pPr^{i}C$_6$H$_4$Me)Ru}$_6$(μ-tpt)$_2$(μ-dhbq)$_3$]$^{6+}$, planar aromatic molecules such as pyrene, triphenylene [44] or hexamethoxytriphenylene [45] were found to fit inside the cavity (Fig. 12). In these systems, which are called carceplexes, the guest molecules are permanently encapsulated in the cavity of the host.

These examples illustrate the versatility of half-sandwich complexes in the construction of two- and three-dimensional assemblies, thus providing a multitude of possibilities for producing new metalla-hosts for various applications.

5 Organometallic Assemblies Composed of Half-Sandwich Complexes for Biological Applications

Most macrocycles composed of half-sandwich complexes are positively charged and water soluble. The water solubility and stability of organometallic compounds are advantageous, and organometallic chemistry in aqueous-phase is growing rapidly [18]. The overall hydrophilicity of the metalla-cycles combined with potential inner hydrophobic interactions with guest molecules have been exploited previously.

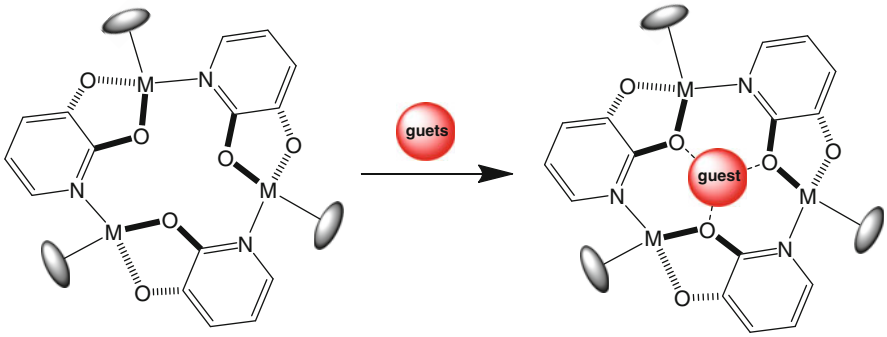

Scheme 1 Trinuclear metalla-cycles comprise of half-sandwich complexes, analogues of 12-crown-3, able to bind guest molecules in their inner cavity

The potential of using half-sandwich assemblies for sensing was first introduced by Fish in the early 1990s [46]. A series of metalla-cycles with specific interactions with small anions was described (Scheme 1). Molecular modelling suggested classic π–π interactions between the aromatic groups of various substituted aromatic carboxylic acids and the cavity of the trinuclear hosts. These trinuclear hosts are analogues to crown-ethers, thus offering alternatives to traditional cryptands [47]. Similar trinuclear metalla-cycles were recently evaluated on human cancer and fibroblast cells [48]. However, these compounds were found to be poorly cytotoxic towards ovarian (A2780 and A2780cisR) and fibroblast (VS79 and GS78) cancer cell lines.

Cationic tetranuclear metalla-cycles composed of arene ruthenium units bridged by tetradentate *OO*∩*OO* or *ON*∩*ON* chelating ligands and connected by bipyridyl linkers have been synthesised. The 4,7-phenanthroline (phen) and 4,4′-bipyridine linkers react with the dinuclear arene ruthenium complex $[\{(p\mathrm{Pr^iC_6H_4Me})\mathrm{Ru}\}_2(\mu\text{-LHoxo})(\mathrm{CF_3SO_3})_2]$ (where $\mathrm{LH_3oxo}$ = 4,6-dihydroxy-2-carboxy-1,3,5-triazine acid) to form the tetranuclear complexes $[\{(p\mathrm{Pr^iC_6H_4Me})\mathrm{Ru}\}_4(\mu\text{-LHoxo})_2(\mu\text{-phen})_2]^{4+}$ (Fig. 13a) and $[\{(p\mathrm{Pr^iC_6H_4Me})\mathrm{Ru}\}_4(\mu\text{-LHoxo})_2(\mu\text{-bipy})_2]^{4+}$, respectively [49]. These cationic metalla-cycles have been found to interact with DNA and to show good cytotoxicity on human ovarian cancer cell lines. Similarly, the dinuclear arene ruthenium complexes of the general formula $[\{(p\mathrm{Pr^iC_6H_4Me})\mathrm{Ru}\}_2(\mu\text{-}OO\cap OO)\mathrm{Cl_2}]$ [where *OO*∩*OO* = dhbq; 2,5-dichloro-1,4-benzoquinone-3,6-diolato (dcbq); 1,4-naphthoquinone-5,8-diolato (donq)] react with bipyridyl linkers (bpe, bipy, phen) in the presence of $\mathrm{AgCF_3SO_3}$ to generate the corresponding tetranuclear metalla-cycles $[\{(p\mathrm{Pr^iC_6H_4Me})\mathrm{Ru}\}_4(\mu\text{-}OO\cap OO)_2(\mu\text{-bipyridyl})_2]^{4+}$ [50, 51]. The molecular structure of $[\{(p\mathrm{Pr^iC_6H_4Me})\mathrm{Ru}\}_4(\mu\text{-dcbq})_2(\mu\text{-bipy})_2]^{4+}$ is presented in Fig. 13b. Accordingly, a series of tetranuclear osmium analogues have been synthesised recently [52]. Interestingly, they possess a lower general toxicity on A2780 and A2780cisR ovarian cancer cells than their ruthenium analogues

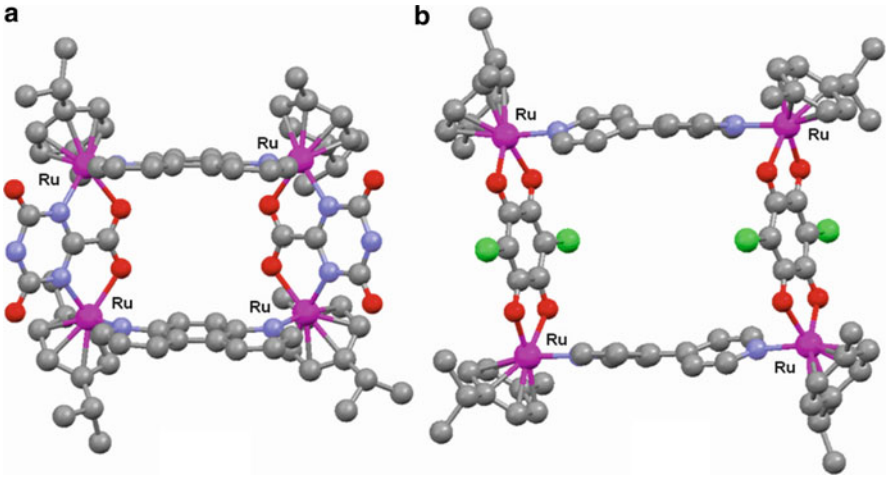

Fig. 13 Tetranuclear metalla-cycles, $[\{(p\text{Pr}^i\text{C}_6\text{H}_4\text{Me})\text{Ru}\}_4(\mu\text{-phen})_2(\mu\text{-LHoxo})_2]^{4+}$ (**a**) [49] and $[\{(p\text{Pr}^i\text{C}_6\text{H}_4\text{Me})\text{Ru}\}_4(\mu\text{-bipy})_2(\mu\text{-dcbq})_2]^{4+}$ (**b**) [50]

except for the tetranuclear complex, $[\{(p\text{Pr}^i\text{C}_6\text{H}_4\text{Me})\text{Os}\}_4(\mu\text{-dhbq})_2(\mu\text{-bipy})_2]^{4+}$, which is ten times more active than $[\{(p\text{Pr}^i\text{C}_6\text{H}_4\text{Me})\text{Ru}\}_4(\mu\text{-dhbq})_2(\mu\text{-bipy})_2]^{4+}$.

The supramolecular metalla-cubes $[\{(p\text{Pr}^i\text{C}_6\text{H}_4\text{Me})\text{Ru}\}_8(\mu\text{-tpp})_2(\mu\text{-}OO\cap OO)_4]^{8+}$, containing $OO\cap OO$ bridging ligands and 5,10,15,20-tetra(4-pyridyl)porphyrin (tpp) panels, interact strongly with duplex and human telomeric quadruplex DNA (Fig. 14). The interactions with duplex and human telomeric quadruplex DNA was studied by fluorescent intercalation displacement (FID) assay and surface plasmon resonance (SPR) experiments. These studies have shown the octacationic arene ruthenium metalla-boxes to be promising quadruplex DNA stabilisers and to possess a degree of selectivity for quadruplex over duplex DNA [53]. Moreover, all metalla-cubes have shown to be equally cytotoxic (IC_{50} = 7–15 μM) (IC_{50} being the drug concentration necessary for 50% inhibition of cell viability) against both A2870 and cisplatin-resistant A2780cisR cancer cells [54], thus clearly suggesting a mechanism of action different to that of cisplatin.

Cationic metalla-assemblies have been prepared using the same dinuclear arene ruthenium clips and 5,15-bis(4-pyridyl)-10,20-diphenylporphyrin (bpp) or 5,10,15-tris(4-pyridyl)-20-phenylporphyrin (tppp) instead of 5,10,15,20-tetra(4-pyridyl)porphyrin (tpp) (Fig. 15). The in vitro study showed that, despite having less ruthenium atoms per metalla-assemblies and a reduced overall charge as compared to the octanuclear arene ruthenium metalla-cubes, the cytotoxicity of these tetra- and hexanuclear metalla-assemblies was similar to those observed for the octanuclear metalla-cubes [55].

These large metalla-assemblies show several interesting features. They possess multiple metal centres, they are water soluble, and in some cases they can reach sizes approaching small enzymes. These features are quite valuable with a view to

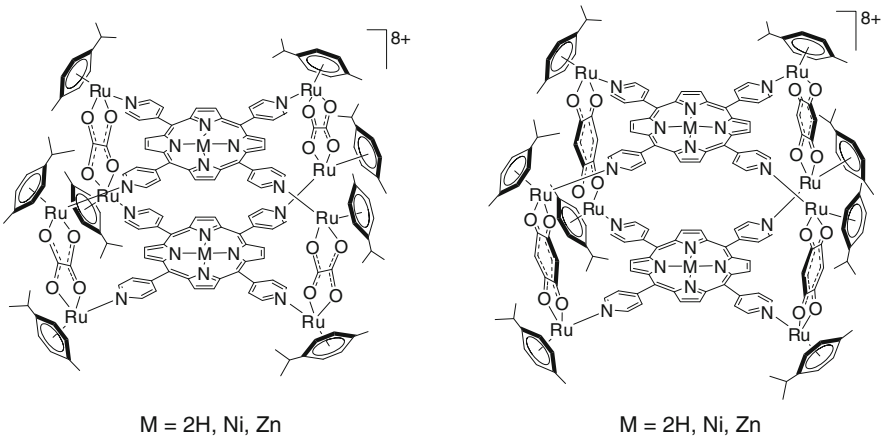

Fig. 14 Organometallic metalla-cubes, $[\{(p\mathrm{Pr^iC_6H_4Me})\mathrm{Ru}\}_8(\mu\text{-tpp-M})_2(\mu\text{-}OO\cap OO)_4]^{8+}$, able to interact with DNA and to inhibit cancer cell growth [53, 54]

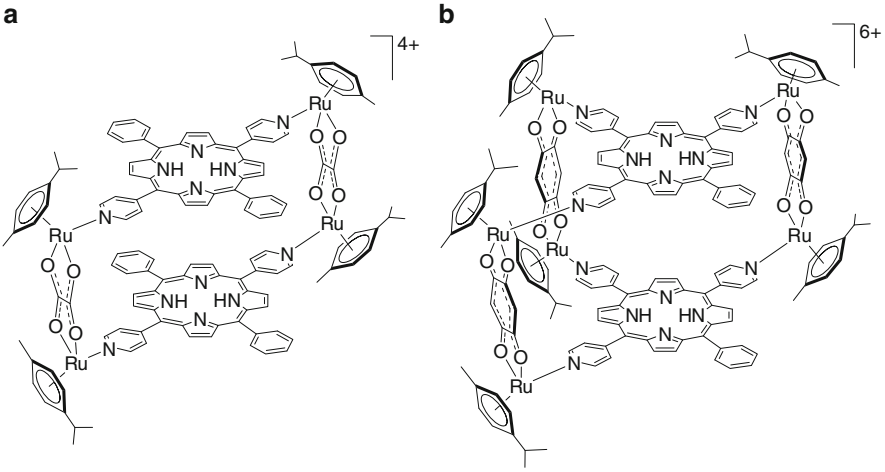

Fig. 15 Organometallic metalla-assemblies$[\{(p\mathrm{Pr^iC_6H_4Me})\mathrm{Ru}\}_4(\mu\text{-bpp-2H})_2(\mu\text{-}C_2O_4)_2]^{4+}$ (**a**) and $[\{(p\mathrm{Pr^iC_6H_4Me})\mathrm{Ru}\}_6(\mu\text{-tppp-2H})_2(\mu\text{-dhbq})_3]^{6+}$ (**b**) [55]

producing new anticancer agents. For instance, the multinuclear approach to improve the activity of anticancer metal-based drugs has been demonstrated [56], and large molecules are known to specifically target cancer cells by exploiting the enhanced permeability and retention (EPR) effect [57]. Consequently, the construction of large metalla-assemblies offers great potential for generating highly selective metal-based drugs for the treatment of cancer.

6 Organometallic Assemblies Composed of Half-Sandwich Complexes for Drug Delivery

Strategies to deliver drugs or prodrugs remain an active field of research. New drug delivery systems are essential to overcome drug resistance mechanisms, to better target cancers, and to regulate drug release. Therefore, it is quite common to find in the literature that the ultimate drug delivery system should possess high selectivity, be biodegradable, and be able to release the drug in a time-controlled manner [58]. However, we consider that if the carrier selectively targets cancer cells, having a cytotoxic drug delivery agent can be advantageous. Synergetic or at least additive effects can be envisaged if both the host and the guest are cytotoxic, and could consequently provide a multidrug therapy in a single host–guest compound.

This idea was first applied using an hexacationic arene ruthenium cage synthesised from the dinuclear complex $[\{(p\text{Pr}^{i}\text{C}_6\text{H}_4\text{Me})\text{Ru}\}_2(\mu\text{-dhbq})\text{Cl}_2]$ and tpt panels in the presence of silver triflate [59]. If the synthesis was performed in the presence of platinum or palladium bisacetylacetonate, the square-planar complex was encapsulated within the cage, thus giving rise to the carceplex systems $[\text{M(acac)}_2 \subset \{(p\text{-Pr}^{i}\text{C}_6\text{H}_4\text{Me})\text{Ru}\}_6(\mu\text{-dhbq})_3(\text{tpt})_2]^{6+}$ (where M = Pd, Pt). These systems are active against human ovarian cancer cells: The empty cage possesses an IC_{50} value of 23 μM; by using the platinum-containing cage the cytotoxicity doubles, and by using the palladium-containing cage the activity reaches 1 μM. The free M(acac)_2 complexes are inactive due to their insolubility in water. Based on these results, the "Trojan horse" concept for delivery of metal-containing guest molecules to cancer cells using a water-soluble organometallic host was proposed (Fig. 16).

This concept was further developed using pyrenyl derivatives with a dangling arm standing out of the cage [60]. The in vitro study revealed that the nature of the

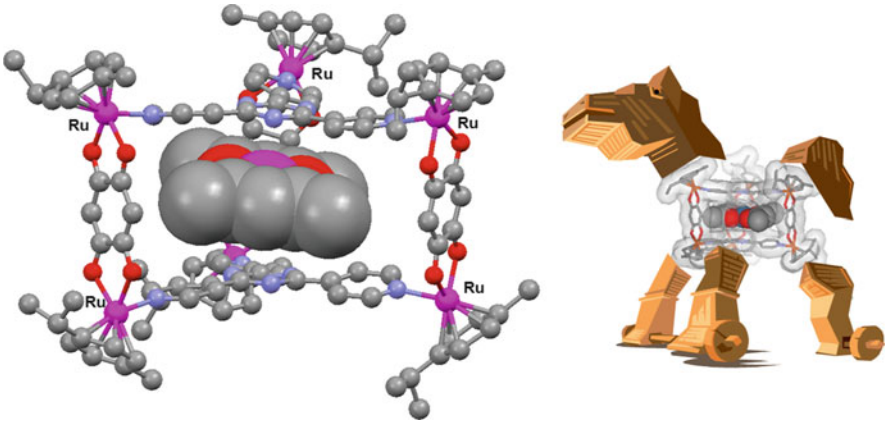

Fig. 16 "Trojan horse" concept illustrated by the platinum bisacetylacetonate complex being encapsulated in the metalla-cage, $[\text{Pt(acac)}_2 \subset \{(p\text{Pr}^{i}\text{C}_6\text{H}_4\text{Me})\text{Ru}\}_6(\mu\text{-dhbq})_3(\text{tpt})_2]^{6+}$ (Pt(acac)_2 being represented by space-filling model) [59]

functional group attached on the pyrenyl unit strongly influences the overall cytotoxicity of the host–guest systems. Therefore, this simple strategy of pyrenyl functionalisation offers the possibility to generate highly cytotoxic agents by fine tuning the nature of the functional group connected to the pyrenyl unit. Optimisation of this strategy is currently being investigated in our laboratory.

The encapsulation of a fluorescent pyrenyl derivative, 1-(4,6-dichloro-1,3,5-triazin-2-yl)pyrene (pyrene-R), has provided direct evidence for the release of a hydrophobic molecule from the metalla-cage $[\{(p\text{Pr}^i\text{C}_6\text{H}_4\text{Me})\text{Ru}\}_6(\mu\text{-dhbq})_3(\text{tpt})_2]^{6+}$, following uptake into cancer cells [61]. The fluorescence of pyrene-R has allowed monitoring of cellular uptake and accumulation, as well as an estimation of the efficiency of the $[\text{pyrene-R}\subset\{(p\text{Pr}^i\text{C}_6\text{H}_4\text{Me})\text{Ru}\}_6(\mu\text{-dhbq})_3(\text{tpt})_2]^{6+}$ system to transport and release its cargo (Fig. 17).

This fluorescent pyrenyl derivative (pyrene-R) was also encapsulated in the cavity of the more spacious metalla-cages $[\{(p\text{Pr}^i\text{C}_6\text{H}_4\text{Me})\text{Ru}\}_6(\mu\text{-donq})_3(\mu\text{-tpt})_2]^{6+}$, $[\{(p\text{Pr}^i\text{C}_6\text{H}_4\text{Me})\text{Ru}\}_6(\mu\text{-doaq})_3(\mu\text{-tpt})_2]^{6+}$ (where doaq = 1,4-anthraquinone-9,10-diolato) and $[\{(p\text{Pr}^i\text{C}_6\text{H}_4\text{Me})\text{Ru}\}_6(\mu\text{-dotq})_3(\mu\text{-tpt})_2]^{6+}$ (where dotq = tetracene-5,12-dione-6,11-diolato) [62]. In contrast to the carceplex $[\text{pyrene-R}\subset\{(p\text{Pr}^i\text{C}_6\text{H}_4\text{Me})\text{Ru}\}_6(\mu\text{-dhbq})_3(\text{tpt})_2]^{6+}$ system, the association constants (K_a) were determined for these three host–guest systems. Interestingly, a perfect correlation between the association constants and the fluorescence recorded by flow cytometry after incubation for 24 h on cancer cells was observed, thus paving the way for the rational design of organometallic metalla-cages that can function in a time-

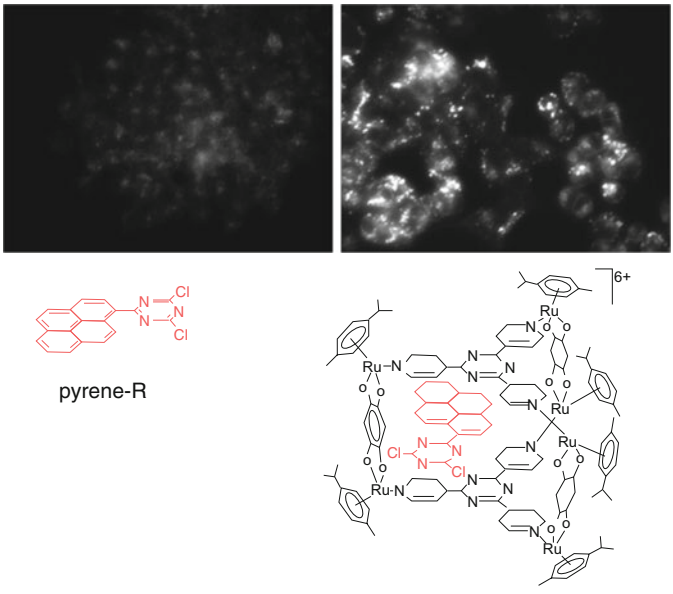

Fig. 17 Microscopy images (fluorescent light) of cancer cells incubated (2 μM, 24 h) with pyrene-R alone (*left*) and $[\text{pyreneR}\subset\{(p\text{Pr}^i\text{C}_6\text{H}_4\text{Me})\text{Ru}\}_6(\mu\text{-dhbq})_3(\text{tpt})_2]^{6+}$ (*right*) [61]

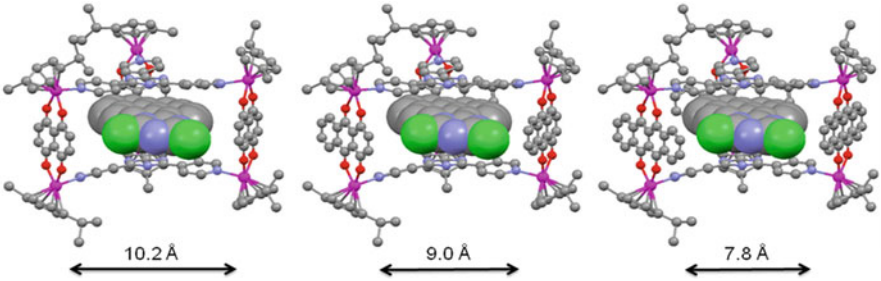

Fig. 18 Organometallic metalla-cages [pyrene-R⊂{(pPr^{i}C$_6$H$_4$Me)Ru}$_6$(μ-donq)$_3$(tpt)$_2$]$^{6+}$ (**a**), [pyrene-R⊂{(pPr^{i}C$_6$H$_4$Me)Ru}$_6$(μ-doaq)$_3$(tpt)$_2$]$^{6+}$ (**b**) and [pyrene-R⊂{(pPr^{i}C$_6$H$_4$Me)Ru}$_6$(μ-dotq)$_3$(tpt)$_2$]$^{6+}$ (**c**), showing the width of the portals (pyrene-R being represented by space-filling models) [62]

controlled manner. These metalla-cages possess similar cavity sizes but different portals (Fig. 18), thus controlling the release of the guest molecule after internalisation.

To better target cancer cells, pyrenyl-modified dendrimers have been encapsulated in the water-soluble metalla-cage [{(pPr^{i}C$_6$H$_4$Me)Ru}$_6$(μ-donq)$_3$(μ-tpt)$_2$]$^{6+}$ [63]. Three generations of pyrenyl-cyanobiphenyl dendrimers (P_0, P_1 and P_2) were synthesised, and the host–guest properties were studied after encapsulation using UV and NMR spectroscopy. A molecular simulation of the highest generation of pyrenyl-modified dendrimer (P_2) in the cavity of the metalla-cage is presented in Fig. 19. This study has shown that organometallic metalla-cages are able to deliver hydrophobic guest molecules with extremely large appendages into cancer cells.

The same strategy was recently applied to solubilise and evaluate the cytotoxicity of a well-known family of dendrimers composed of benzyloxy core with dodecanyloxy endgroups [64]. These kinds of dendrimers are lipophilic, and so far have never been evaluated in biological media. The pyrenyl-modified polybenzyloxy dendrimers (generations G_0 to G_2) encapsulated in the cavity of the metalla-cage [{(pPr^{i}C$_6$H$_4$Me)Ru}$_6$(μ-donq)$_3$(μ-tpt)$_2$]$^{6+}$ (Fig. 20) showed cytotoxicities comparable to those of cisplatin on human ovarian cancer cell lines, confirming the delivery ability of these organometallic metalla-cages.

We are now investigating the possibility of using pyrenyl derivatives with biological functions to tune up the properties of these systems to target specific diseases as well as to increase selectivity, activity and solubility. Recently, we have shown that organometallic-modified porphyrin compounds possess excellent chemotherapeutic and photodynamic properties at low concentration [65]. Therefore, the encapsulation of photosensitisers within [{(pPr^{i}C$_6$H$_4$Me)Ru}$_6$(μ-donq)$_3$ (μ-tpt)$_2$]$^{6+}$ and other cages has been performed in order to combine the cytotoxicity of half-sandwich complexes and photodynamic treatment. Porphyrins and phthalocyanines are the most common photosensitisers; being planar aromatic molecules and poorly soluble in water, they are the perfect candidates for encapsulation in organometallic metalla-cages. The in vitro activity and photo-activity of these [photosensitiser⊂cage] systems are under investigation and the results will be published soon.

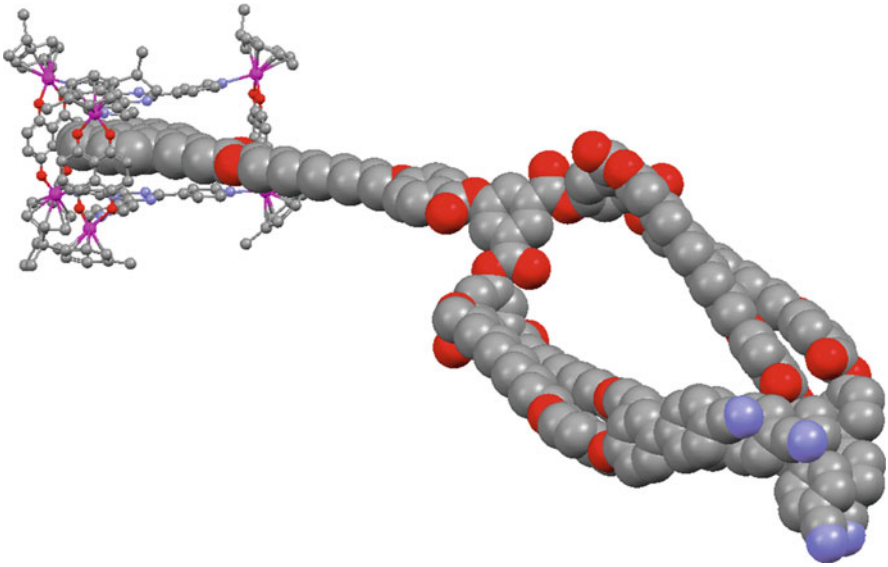

Fig. 19 Molecular structure of $[P_2 \subset \{(p\mathrm{Pr^iC_6H_4Me})\mathrm{Ru}\}_6(\mu\text{-donq})_3(\mathrm{tpt})_2]^{6+}$ showing the pyrenyl-modified dendrimer (P_2) (space-filling model) being encapsulated in the cavity of the metallacage [63]

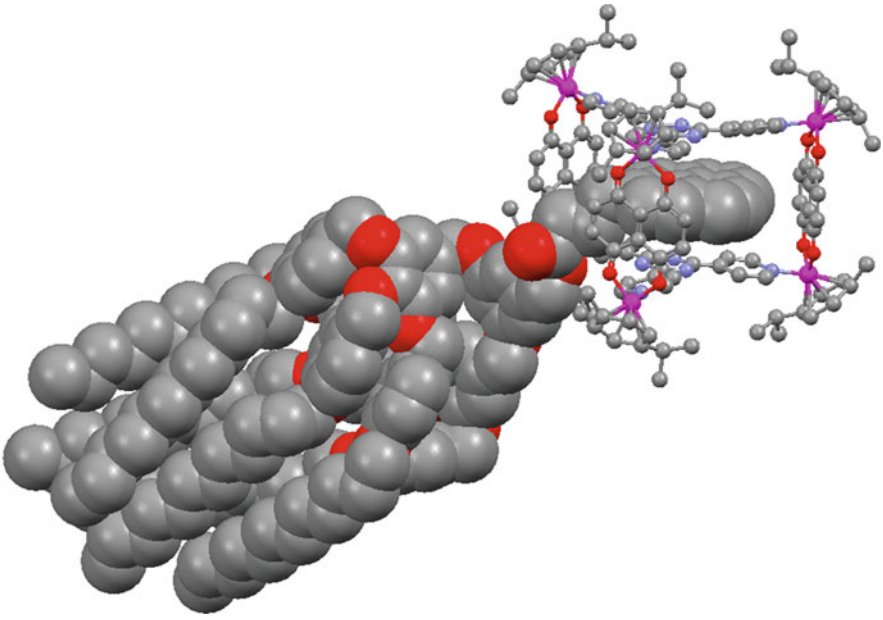

Fig. 20 Molecular structure of $[G_2 \subset \{(p\mathrm{Pr^iC_6H_4Me})\mathrm{Ru}\}_6(\mu\text{-donq})_3(\mathrm{tpt})_2]^{6+}$ (G_2 represented by space-filling model) [64]

7 Outlook

The use of water-soluble organometallic cages as drug carriers to deliver hydrophobic molecules offers great potential. The cage itself is cytotoxic, and selectivity can be achieved by exploiting the EPR effect. The cavity of the cage allows the transport to cancer cells of lipophilic molecules. Therefore, by judiciously selecting the guest molecule, targeting of a specific disease, adding selectivity, or increasing solubility can be achieved by these host–guest biological agents. Consequently, this multifunctional host and guest approach, in which both players possess distinct qualities and specificities, is certainly a winning strategy for the development of organometallic metalla-cages with synergistic effects, and will ultimately provide a new weapon in chemotherapy.

Acknowledgments The author would like to thank past and present members of his group, financial support from the Swiss National Science Foundation, and the Johnson Matthey Technology Centre for a generous loan of ruthenium trichloride hydrate.

References

1. Kunz H (2002) Emil Fischer–Unequalled classicist, master of organic chemistry research, and inspired trailblazer of biological chemistry. Angew Chem Int Ed Engl 41:4439–4451
2. Cram DJ, Cram JM (1974) Host-guest chemistry. Science 183:803–809
3. Lehn J-M (1988) Supramolecular chemistry – scope and perspectives. Molecules, supermolecules, and molecular devices (Nobel lecture). Angew Chem Int Ed Engl 27:89–112
4. Fujita M, Tominaga M, Hori A, Therrien B (2005) Coordination assemblies from a Pd(II)-cornered square complex. Acc Chem Res 38:371–380
5. Northrop BH, Zheng Y-R, Chi K-W, Stang PJ (2009) Self-organization in coordination-driven self-assembly. Acc Chem Res 42:1554–1563
6. Thanasekaran P, Liao R-T, Liu Y-H, Rajendran T, Rajagopal S, Lu K-L (2005) Metal-containing molecular rectangles: synthesis and photophysical properties. Coord Chem Rev 249:1085–1110
7. Schweiger M, Seidel SR, Arif AM, Stang PJ (2002) Solution and solid state studies of a triangle-square equilibrium: anion-induced selective crystallization in supramolecular self-assembly. Inorg Chem 41:2556–2559
8. Fujita M, Sasaki O, Mitsuhashi T, Fujita T, Yazaki J, Yamaguchi K, Ogura K (1996) On the structure of transition-metal-linked molecular squares. Chem Commun:1535–1536
9. Fujita M, Oguro D, Miyazawa M, Oka H, Yamaguchi K, Ogura K (1995) Self-assembly of ten molecules into a nanometer-sized organic host frameworks. Nature 378:469–471
10. Zheng Y-R, Zhao Z, Kim H, Wang M, Ghosh K, Pollock JB, Chi K-W, Stang PJ (2010) Coordination-driven self-assembly of truncated tetrahedral capable of encapsulating 1,3, 5-triphenylbenzene. Inorg Chem 49:10238–10240
11. Davis AV, Yeh RM, Raymond KN (2002) Supramolecular assembly dynamics. Proc Natl Acad Sci 99:4793–4796
12. Beissel T, Powers RE, Parac TN, Raymond KN (1999) Dynamic isomerisation of a supramolecular tetrahedral M_4L_6 cluster. J Am Chem Soc 121:4200–4206
13. Cotton FA, Lei P, Lin C, Murillo CA, Wang X, Yu S-Y, Zhang Z-X (2004) A calyx[4]arene carceplex with four Rh_2^{4+} fasteners. J Am Chem Soc 126:1518–1525

14. Cotton FA, Lin C, Murillo CA (2002) The use of dimetal building blocks in convergent syntheses of large arrays. Proc Natl Acad Sci 99:4810–4813
15. Stephenson A, Argent SP, Riis-Johannessen T, Tidmarsh IS, Ward MD (2011) Structures and dynamic behaviour of large polyhedral coordination cages: an unusual cage-to-cage interconversion. J Am Chem Soc. doi:10.1021/ja107403p
16. Pascu GI, Hotze ACG, Sanchez-Cano C, Kariuki BM, Hannon MJ (2007) Dinuclear ruthenium (II) triple-stranded helicates: luminescent supramolecular cylinders that bind and coil DNA and exhibit activity against cancer cell lines. Angew Chem Int Ed Engl 46:4374–4378
17. Malina J, Hannon MJ, Brabec V (2008) Interaction of dinuclear ruthenium(II) supramolecular cylinders with DNA: sequence-specific binding, unwinding, and photocleavage. Chem Eur J 14:10408–10414
18. Laughrey Z, Gibb BC (2011) Water-soluble, self-assembling container molecules: an update. Chem Soc Rev 40:363–386
19. Casanova M, Zangrando E, Munini F, Iengo E, Alessio E (2006) *fac*-$[Re(CO)_3(dmso\text{-}O)_3](CF_3SO_3)$: a new versatile and efficient Re(I) precursor for the preparation of mono and polynuclear compounds containing *fac*-$[Re(CO)_3]^+$ fragments. Dalton Trans:5033–5045
20. Liao R-T, Yang W-C, Thanasekaran P, Tsai C-C, Sathiyendiran M, Liu Y-H, Rajendran T, Lin H-M, Tseng T-W, Lu K-L (2008) Rhenium-based molecular rectangular boxes with large inner cavity and high shape selectivity towards benzene molecule. Chem Commun:3175–3177
21. Dinolfo PH, Coropceanu V, Brédas J-L, Hupp JT (2006) A new class of mixed-valence systems with orbitally degenerate organic redox centers examples based on hexa-rhenium molecular prisms. J Am Chem Soc 128:12592–12593
22. Therrien B, Süss-Fink G (2009) Sawhorse-type diruthenium tetracarbonyl complexes. Coord Chem Rev 253:2639–2664
23. Auzias M, Therrien B, Süss-Fink G (2007) Tetra- and hexanuclear cage molecules based on diruthenium tetracarbonyl sawhorse units: synthesis and molecular structure of $[\{Ru_2(CO)_4(PPh_3)_2\}_2(O_2CCH_2CO_2)_2]$ and $[\{Ru_2(CO)_4(PMe_3)_2\}_3(O_2CC_6H_4CO_2)_3]$. Inorg Chem Commun 10:1420–1424
24. Byerley JJ, Rempel GL, Takebe N, James BR (1971) Catalytic carbonylation of amines using ruthenium complexes under mild conditions. J Chem Soc D: Chem Commun:1482–1483
25. Shiu K-B, Lee H-C, Lee G-H, Wang Y (2002) Synthesis, structures, and solvent-occlusion properties of a molecular loop and a molecular square using tetracarbonyl- and diphosphine-ligated diruthenium(I) as building blocks and dicarboxylates as linkers. Organometallics 21: 4013–4016
26. Seidel SR, Stang PJ (2002) High-symmetry coordination cages via self-assembly. Acc Chem Res 35:972–983
27. Mukherjee PS, Das N, Kryschenko YK, Arif AM, Stang PJ (2004) Design, synthesis, and crystallographic studies of neutral platinum-based macrocycles formed via self-assembly. J Am Chem Soc 126:2464–2473
28. Koshevoy IO, Haukka M, Selivanov SI, Tunik SP, Pakkanen TA (2010) Assembly of the Au-diphosphine helical cage molecules *via* alkynyl-μ_4-methylydine ligand transformation. Chem Commun 46:8926–8928
29. Therrien B (2009) Functionalised η^6-arene ruthenium complexes. Coord Chem Rev 253: 493–519
30. Gasser G, Ott I, Metzler-Nolte N (2011) Organometallic anticancer compounds. J Med Chem 54:3–25
31. Rauchfuss TB, Severin K (2008) Supramolecular architectures based on organometallic half-sandwich complexes. In: Atwood JL, Steed JW (eds) Organic nanostructures. Wiley-VCH, Weinheim
32. Han Y-F, Jia W-G, Yu W-B, Jin G-X (2009) Stepwise formation of organometallic macrocycles, prisms and boxes from Ir, Rh and Ru-based half-sandwich units. Chem Soc Rev 38: 3419–3434

33. Therrien B (2009) Arene ruthenium cages: Boxes full of surprises. Eur J Inorg Chem: 2445–2453
34. Severin K (2006) Supramolecular chemistry with organometallic half-sandwich complexes. Chem Commun:3859–3867
35. Yamanari K, Ito R, Yamamoto S, Konno T, Fuyuhiro A, Fujioka K, Arakawa R (2002) Cyclic tetramers composed of rhodium(III), iridium(III), or ruthenium(II) half-sandwich and 6-purinethiones. Inorg Chem 41:6824–6830
36. Han Y-F, Lin Y-J, Jia W-G, Jin G-X (2009) Half-sandwich Ir-based neutral organometallic macrocycles containing pyridine-4-thiolato ligands. Dalton Trans:2077–2080
37. Olivier C, Scopelliti R, Severin K (2009) Expanding the size of organometallic nanostructures: A hexanuclear (cymene)Ru cylinder with a length of more than 3 nm. Eur J Inorg Chem: 207–210
38. Mirtschin S, Slabon-Turski A, Scopelliti R, Velders AH, Severin K (2010) A coordination cage with an adaptable cavity size. J Am Chem Soc 132:14004–14005
39. Boyer JL, Kuhlman ML, Rauchfuss TB (2007) Evolution of organo-cyanometallate cages: supramolecular architectures and new Cs^+-specific receptors. Acc Chem Res 40:233–242
40. Ramesh M, Rauchfuss TB (2004) Structural and mechanistic studies on ion insertion into the molecular box $\{[CpCo(CN)_3]_4[Cp^*Ru]_4\}$. J Organomet Chem 689:1425–1430
41. Amouri H, Rager MN, Cagnol F, Vaissermann J (2001) Rational design and X-ray molecular structure of the first irido-cryptand and encapsulation of a tetrafluoroborate anion. Angew Chem Int Ed Engl 40:3636–3638
42. Govindaswamy P, Linder D, Lacour J, Süss-Fink G, Therrien B (2006) Self-assembled hexanuclear arene ruthenium metallo-prisms with unexpected double helical chirality. Chem Commun:4691–4693
43. Govindaswamy P, Linder D, Lacour J, Süss-Fink G, Therrien B (2007) Chiral or not chiral? A case study of the hexanuclear metalloprisms $[Cp^*_6M_6(\mu_3\text{-tpt})\text{-}\kappa N)_2(\mu\text{-}C_2O_4\text{-}\kappa O)_3]^{6+}$ (M = Rh, Ir). Dalton Trans:4457–4463
44. Mattsson J, Govindaswamy P, Furrer J, See Y, Yamaguchi K, Süss-Fink G, Therrien B (2008) Encapsulation of aromatic molecules in hexanuclear arene ruthenium cages: a strategy to build up organometallic carceplex prisms with a dangling arm standing out. Organometallics 27:4346–4356
45. Govindaswamy P, Furrer J, Süss-Fink G, Therrien B (2008) Encapsulation of triphenylene derivatives in the hexanuclear arene ruthenium metallo-prismatic cage $[Ru_6(p\text{-}Pr^iC_6H_4Me)_6(tpt)_2(dhbq)_3]^{6+}$ (dhbq = 2,5-dihydroxy-1,4-benzoquinonato). Z Anorg Allg Chem 634: 1349–1352
46. Smith DP, Baralt E, Morales B, Olmstead MM, Maestre MF, Fish RH (1992) Bioorganometallic chemistry. 1. Synthetic and structural studies in the reactions of a nucleobase and several nucleosides with a (η^5-pentamethylcyclopentadienyl)rhodium aqua complex. J Am Chem Soc 114:10647–10649
47. Fish RH (2010) A bioorganometallic chemistry overview: from Cytochrome P450 enzyme metabolism of organotin compounds to organorhodium-hydroxytamoxifen complexes with potential anti-cancer properties; a 37 year perspective at the interface of organometallic chemistry and biology. Aust J Chem 63:1505–1513
48. Ang WH, Grote Z, Scopelliti R, Juillerat-Jeanneret L, Severin K, Dyson PJ (2009) Organometallic complexes that interconvert between trimeric and monomeric structures as a function of pH and their effect on human cancer and fibroblast cells. J Organomet Chem 694:968–972
49. Linares F, Galindo MA, Galli S, Angustias Romero M, Navarro JAR, Barea E (2009) Tetranuclear coordination assemblies based on half-sandwich ruthenium(II) complexes: noncovalent binding to DNA and cytotoxicity. Inorg Chem 48:7413–7420
50. Mattsson J, Govindaswamy P, Renfrew AK, Dyson PJ, Štěpnička P, Süss-Fink G, Therrien B (2009) Synthesis, molecular structure, and anticancer activity of cationic arene ruthenium metallarectangles. Organometallics 28:4350–4357

51. Linares F, Quartapelle Procopio E, Galindo MA, Angustias Romero M, Navarro JAR, Barea E (2010) Molecular architecture of redox-active half-sandwich Ru(II) cyclic assemblies. Interactions with biomolecules and anticancer activity. Cryst Eng Comm 12:2343–2346
52. Barry NPE, Edafe F, Dyson PJ, Therrien B (2010) Anticancer activity of osmium metallarectangles. Dalton Trans 39:2816–2820
53. Barry NPE, Abd Karim NH, Vilar R, Therrien B (2009) Interactions of ruthenium coordination cubes with DNA. Dalton Trans:10717–10719
54. Barry NPE, Zava O, Dyson PJ, Therrien B (2010) Synthesis, characterization and anticancer activity of porphyrin-containing organometallic cubes. Aust J Chem 63:1529–1537
55. Barry NPE, Zava O, Furrer J, Dyson PJ, Therrien B (2010) Anticancer activity of opened arene ruthenium metalla-assemblies. Dalton Trans 39:5272–5277
56. Cossa G, Gatti L, Zunino F, Perego P (2009) Strategies to improve the efficacy of platinum compounds. Curr Med Chem 16:2355–2365
57. Maeda H, Bharate GY, Daruwalla J (2009) Polymeric drugs for efficient tumor-targeted drug delivery based on EPR-effect. Eur J Pharm Biopharm 71:409–419
58. Langer R, Tirrell DA (2004) Designing materials for biology and medicine. Nature 428: 487–492
59. Therrien B, Süss-Fink G, Govindaswamy P, Renfrew AK, Dyson PJ (2008) The "complex-in-a-complex" cations $[(acac)_2M\subset Ru_6(p\text{-}iPrC_6H_4Me)_6(tpt)(dhbq)_3]^{6+}$: a trojan horse for cancer cells. Angew Chem Int Ed Engl 47:3773–3776
60. Mattsson J, Zava O, Renfrew AK, Sei Y, Yamaguchi K, Dyson PJ, Therrien B (2010) Drug delivery of lipophilic pyrenyl derivatives by encapsulation in a water soluble metalla-cage. Dalton Trans 39:8248–8255
61. Zava O, Mattsson J, Therrien B, Dyson PJ (2010) Evidence for drug release from a metalla-cage delivery vector following cellular internalisation. Chem Eur J 16:1428–1431
62. Barry NPE, Zava O, Dyson PJ, Therrien B (2011) Excellent correlation between drug release and portal size in metalla-cage drug delivery systems. Chem Eur J 17:9669–9677
63. Pitto-Barry A, Barry NPE, Zava O, Deschenaux R, Dyson PJ, Therrien B (2011) Double targeting of tumours with pyrenyl-modified dendrimers encapsulated in an arene-ruthenium metallaprism. Chem Eur J 17:1966–1971
64. Pitto-Barry A, Barry NPE, Zava O, Deschenaux R, Dyson PJ, Therrien B (2011) Encapsulation of pyrene-functionalized poly(benzyl ether) dendrons into a water-soluble organometallic cage. Chem Asian J 6:1595–1603
65. Schmitt F, Govindaswamy P, Zava O, Süss-Fink G, Juillerat-Jeanneret L, Therrien B (2009) Combined arene ruthenium porphyrins as chemotherapeutics and photosensitizers for cancer therapy. J Biol Inorg Chem 14:101–109

Top Curr Chem (2012) 319: 57–78
DOI: 10.1007/128_2011_290

Published online: 3 November 2011

Reversibly Expanded Encapsulation Complexes

Dariush Ajami and Julius Rebek

Abstract Synthetic receptors that surround their target molecules – self assembled capsules and deep cavitands – have emerged as the most realistic models of enzymes active sites. They were introduced to study the behaviour of molecules isolated in small spaces and it has become increasingly clear that the behavior of molecules in dilute aqueous solution does not reflect their behavior in confimed spaces. The synthetic receptors fold around their target guests, isolate them from the bulk solvent, provide a hydrophobic environment and present the guests with each other in a limited space. These features combine to show high binding selectivity, large rate from the ground up; they are designed, synthesized then tested. In recent years, we have found a short-cut to total synthesis; some capsules readily insert spacer elements in the presence of suitable guests that fill the enlarged spaces. This expands the repertoire of containers and the present review describes their structures, the nature of the spaces inside, the exchange dynamics, and the rules that govern their formation.

Keywords Compression • Encapsulation • Filling space • Guest exchange • Spacers

Contents

D. Ajami and J. Rebek (✉)
Department of Chemical Biology and Chemistry, The Scripps Research Institute, 10550 North Torrey Pines Road, La Jolla, CA 92037, USA
e-mail: jrebek@scripps.edu

1 Introduction

Reversible encapsulation isolates molecules in very small spaces and allows their characterization by routine spectroscopic methods. These host guest complexes are self-assembled in the solution phase, but they generally exclude bulk solvent [1]. Instead, the capsule walls provide the solvation for the guests, and simultaneously act as mechanical barriers that isolate and stabilize the guests. Unlike cleft-like receptors used in molecular recognition studies [2], the capsules completely surround the guests and many short-lived reactive intermediates can be isolated, stabilized, and characterized in capsules: phosphine carbonyl adducts [3], labile siloxanes [4], organometallics [5], delicate heterocycles [6], and white phosphorus [7]. Even species that are unknown in solution can be observed in the protective space of a capsule, whether covalently bonded [8, 9], self-assembled with hydrogen bonds [10–19], metal/ligand interactions [20, 21], or hydrophobic effects [22]. In a recent review we described the assembly of resorcinarene hexamers, the largest of hydrogen-bonded hosts [23] and their encapsulation behavior. Here we report an alternative access to larger spaces through reversible expansion of a cylindrical capsule.

The cylindrical capsule host **1.1** (Fig. 1) spontaneously assembles in apolar organic solvents when appropriate guests are present. The guest role can be played in an uninspired way simply by solvent molecules. For example, three molecules of $CHCl_3$, two molecules of toluene, or one molecule of *n*-undecane are nicely

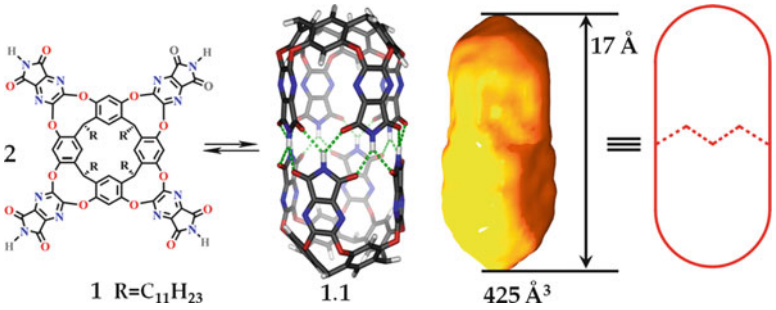

Fig. 1 *From left*: line drawing of the tetraimide cavitand **1**, model of the dimeric capsule **1.1**, the size and shape of the space inside, and the cartoon representation of capsule (some groups omitted for clarity)

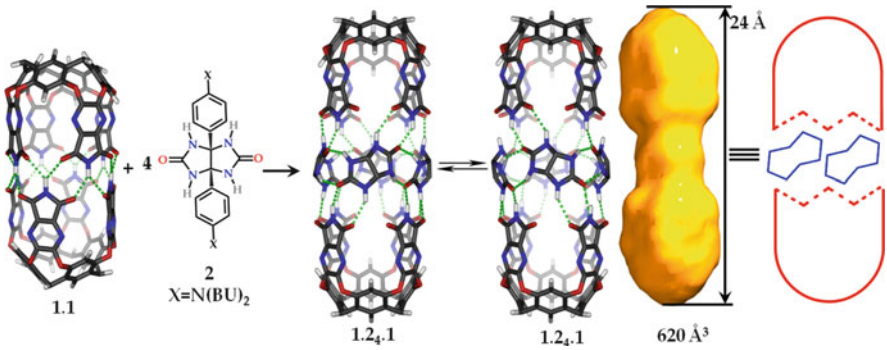

Fig. 2 Expansion of the capsule with glycoluril spacers creates extended capsule **1.2$_4$.1** in racemic form (the peripheral alkyl and aryl groups have been removed for viewing clarity). The cartoon representation used elsewhere in this work is also shown

accommodated inside. But the concentrations of these solvents as neat liquids are ~10 M, and forcing them out of the capsule by a guest of even higher concentration is hard to arrange. Instead, we use deuterated mesitylene as the solvent of choice: it is the largest commercially available medium for Nuclear Magnetic Resonance (NMR) studies and is inconveniently shaped for the space inside; it does not compete well with intended guests of appropriate size, shape, and chemical surface [24]. The capsule is held together through a seam of bifurcated hydrogen bonds and solvents that compete for these bonds to prevent capsule formation, even when strong attractive forces exist between guest and host.

From the moment capsule **1.1** was introduced, we found it irresistible to tamper with it – enhance its solubility and enlarge its capacity. Attempts to expand the resocinarene base or extension of the walls by, say, covalently incorporating naphthalene units [25] met with no success [26]. Noncovalent insertion fared no better as the intended spacers such as the two-dimensional durene bisimides proved too insoluble in the mesitylene medium. Desultory work delayed the solution to the expansion problem; it took 8 years to find and involved the three-dimensional glycoluril module (Fig. 2). This structure, bent in shape and rich in hydrogen bonding possibilities, was outfitted with peripheral aliphatic groups (octyloxyphenyl, dodecylphenyl, or dibutylaniline) to enhance its solubility. The patterns of the donors and acceptors on glycolurils complement the adjacent walls of the cavitand, even if the angles of the former (113°) do not match those of the latter (90°). Moreover, the arrangement makes for the strongest hydrogen bonds: the ureido carbonyls are superior hydrogen bond acceptors and the acidic N-Hs of the imides are the best donors. Our previous experience with this strong acid/strong base driving force for assembly [27] made us confident that insertion would occur. And it did – but neither in the expected geometry nor in the obvious stoichiometry [28]. Instead, a "belt" of *four* glycolurils integrated into the middle of the capsule in an arrangement that resulted in a chiral assembly **1.2$_4$.1**.

2 The Steric Environment

The encapsulation of *trans*-7-tetradecene in both **1.1** and the new assembly illustrates these features through the NMR spectra (Fig. 3) [29]. Integration of proton signals shows that four molecules of glycoluril are present and the changes in chemical shifts of the guest indicates a longer space in the modified capsule. The aromatic panels with polarizable π surfaces impart a strong magnetic anisotropy to the cavity and result in upfield shifts in the NMR signals of encapsulated species. The furthest upfield shifts correspond to nuclei closest to the resorcinarene ends and to the capsule's aromatic walls. For example, *trans*-7-tetradecene is some 4 Å longer in a fully extended conformation than the space inside capsule **1.1**. But a coiled shape with 8 *gauche* conformations compresses the alkene to a shorter and thicker shape. The coiled alkane is stabilized through attractive CH-π interactions with the cavity's polarizable aromatic lining. Comparison of the signals of *trans*-7-tetradecene in the two capsules (Fig. 3) shows that the hydrogens on C_2/C_{13}, C_3/C_{12}, and C_4/C_{11} of this guest have shifted downfield in the new capsule. Accordingly, these hydrogens have moved away from the capsule's walls and ends, indicating a relaxed, extended conformation. The doubling of the proton signals on C_2/C_{13} and C_4/C_{11} in the longer capsule indicates that these hydrogens are diastereotopic because they are in an asymmetric magnetic environment.

The NMR evidence reveals further details of the hydrogen bonding patterns. The four added glycolurils form hydrogen bonds with each half of the original capsule and with each other. In the model proposed in Fig. 2, each glycoluril has four hydrogen bonds with cavitands. The strong hydrogen bonds between the imide N–H of the cavitand and the ureido oxygen of the glycoluril results in a 3 ppm

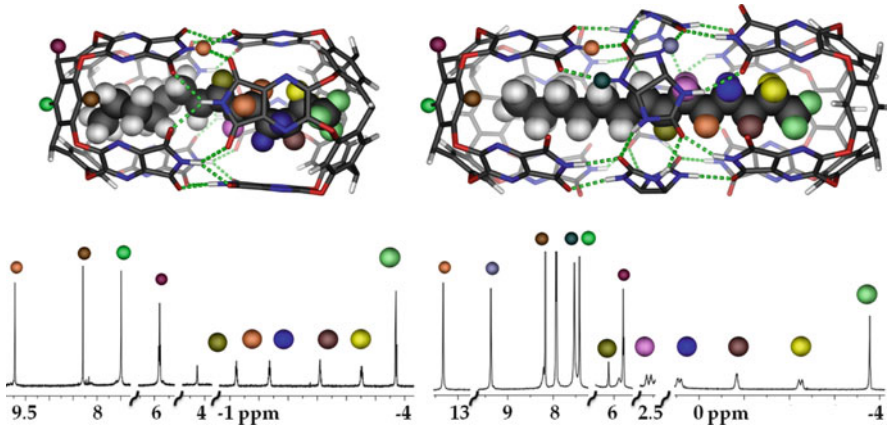

Fig. 3 (*Top*) Calculated structure of *trans*-7-tetradecene in capsule **1.1** (*left*) and the expanded **1.2$_4$.1** (*right*). The peripheral groups have been removed for viewing clarity. (*Bottom*) The ^{1}H NMR spectra (600 MHz, mesitylene-d_{12}) of *trans*-7-tetradecene (5 mM) in **1.1** (1 mM) or **1.2$_4$.1** (1 mM). The assignments are color-coded

downfield shift of the imide hydrogen to 13 ppm. The other two hydrogen bonds between spacer and cavitand appears around 7 ppm. These involve the ureido NH of the glycoluril (a good donor) and the imide carbonyl of the cavitand (a weak acceptor). The signals at ~ 9 ppm represent four good hydrogen bonds between adjacent spacers. A total of 24 hydrogen bonds hold the new assembly together, but 1 carbonyl oxygen of each imide wall is left without a hydrogen bond donor. These unpaired carbonyl groups clash with the adjacent imide panels; the clashes can be relieved by "twisting" the array of the imide walls as shown in Fig. 4. The twist changes the symmetry of the cavitands from C_{4v} to C_4, and the arrangement of the spacer elements produces a chiral structure, as shown. Surprisingly, the chiral assembly emerges from achiral subunits but, of course, the assembly is racemic [30].

The tapered ends of the capsule can select between various functional groups on guests inside. For example, the terminal methyl "knob" of an alkane can approach the resorcinarene end, but it cannot penetrate deeply. On the other hand, the narrower terminal acetylene can access this space quite nicely. A model of the C_{16} acetylene is shown in Fig. 4 [31]. The acetylenic hydrogen is deep in the tapered

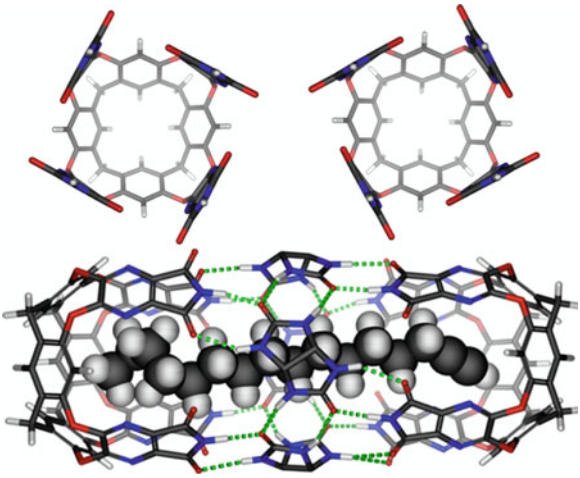

Fig. 4 (*Top*) The walls of the capsule are twisted and create an asymmetric magnetic environment. (*Bottom*) Calculated complex with 1-hexadecyne

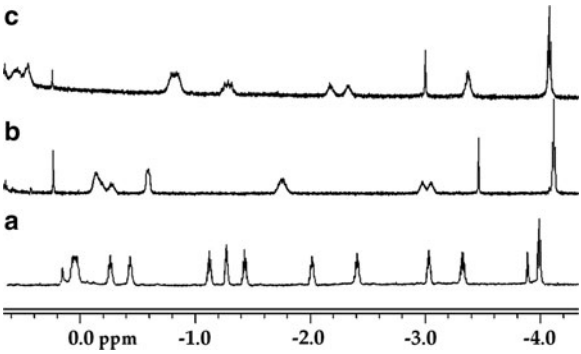

Fig. 5 Encapsulation18 of terminal alkynes in **1.1** and **1.2$_4$.1**. Upfield regions of the ^{1}H NMR spectra (600 MHz, mesitylene *d*12) of **1.1** (2 mM) and terminal alkynes (15 mM): (**a**) 1-pentadecyne, (**b**) 1-pentadecyne and **2** (4 mM), (**c**) 1-hexadecyne and **2** (4 mM)

end and, if the constricted center of the assembly requires an extended alkane conformation, the remote end of the alkane must coil to be accommodated. This indeed appears to be the case: the methylene NMR signals near that end shift upfield (Fig. 5) as they move physically closer to the walls of the capsule.

3 The Magnetic Environment

Insertion of the spacer elements as shown increases the length of the assembly by 7 Å and its inner space by 200 $Å^3$, and the accommodation of *n*-alkanes from C_{14} to C_{19} is possible [32, 33]. The longer guests must undergo compression to fit within **1.2$_4$.1**. As the alkane coils, the number of methylene groups in the shielding zone increases and the *gauche* conformations force the hydrogens near the twisted walls. We used computational methods to map the magnetic shielding/deshielding through nucleus independent chemical shift (NICS) [34] calculations at the B3LYP/6–31 G* level of density functional theory [35]. A cartoon of the map is shown in Fig. 6 along the central axis of **1.2$_4$.1** with spacing distances of 1 Å. The calculated values are in good agreement with the experimental observables and the map can be used to predict the location of a guest nucleus inside the cavity.

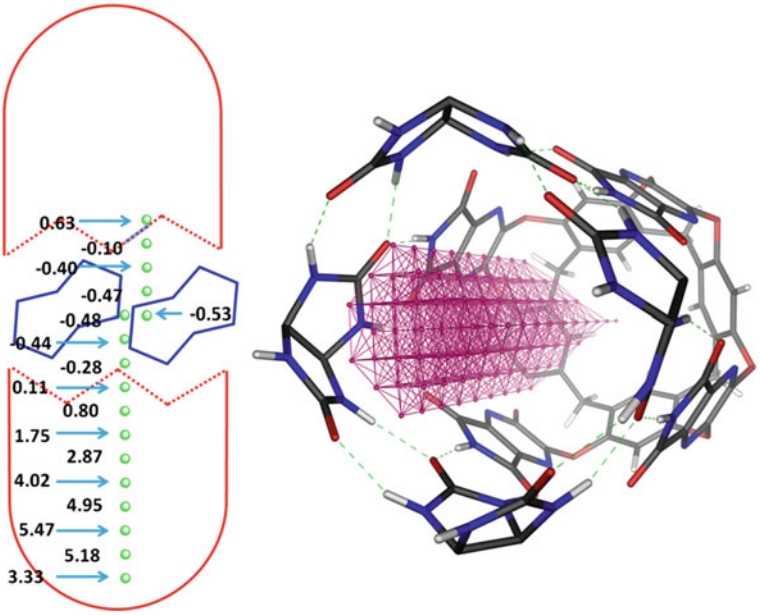

Fig. 6 Mapping the inner space: (*left*) DFT calculated NICS values for the space inside **1.2$_4$.1**, (*right*) dummy atoms placed throughout the entire space of extended capsule with 1 Å separations. The symmetry of capsule reduces the number of required coordinates

For example, encapsulated *n*-nonadecane shows six upfield shifted signals and their methylene geminal hydrogens are all diastereotopic. The tapered spaces at the ends of the capsule lead to some anomalies in "effective sizes" of guests. A centrally located methyl group (e.g., tolyl) is well positioned to access the tapered end; an ethyl group cannot penetrate as deeply and the rest of the molecule is pushed off the capsule's central axis. The penultimate methylene is then near the twisted walls and experiences the chiral environment. Only one methyl of an isopropyl group can be in the tapered space at a given time, and these functions also show diastereotopic doublets in their spectra. A *tert*-butyl group cannot access the tapered space at all. The upshot is that while the *p*-ethyl, *p*-isopropyl, and *p-tert*-butyl guests have (by any external measure) the same length, they show different positions – and apparent lengths – in these capsules.

Nuclei positioned in the middle of capsule experience a moderate deshielding. The aromatic units on the outer surfaces of the four glycolurils present their edges to guests of the capsule. These effects were seen earlier with aromatic glycoluril-based capsules [36], and the magnetic anisotropy imparted to guests by asymmetric elements *outside* capsules has also been encountered [37]. For *trans*-7-tetradecene, the signals for the vinyl hydrogens located near the center of the cavity are shifted *downfield* by a $\Delta\delta$ of 0.72 ppm and the methyl groups positioned at the tapered ends of the capsule are shifted *upfield* by a $\Delta\delta$ of -4.7 ppm.

4 Compression of Guests

A coiled alkane applies stress to the inside of capsule **1.2$_4$.1** and this force must be resisted or the capsule would explode. An alternative statement is that the capsule squeezes guests but structural features of the guest limit their compression. How are these forces detected and evaluated? We will look at the problem from both the host and guest perspectives through perturbations in their behavior. The capsule **1.2$_4$.1** racemizes and this is apparent from the coalescence of the diastereotopic NMR signals of the germinal hydrogens. The racemization rates are obtained by EXSY spectra taken at different temperatures and free energies of activation $\Delta G^{\ddagger}$ are readily calculated from these measurements and the Eyring equation. A reasonable – but unproven – mechanism involves the concerted rotation of all glycolurils ~ 30° in one direction (Fig. 7). This process creates new hydrogen bonds as the old ones are broken and results an achiral intermediate [38]. This intermediate is slightly longer than either enantiomer. Accordingly, we proposed that the racemization rates would increase with increased length of the guests: the longer, more compressed guests rates should apply more pressure to the interior of the capsule and coax the assembly toward the longer, achiral transition structure. This proved to be the case: we found $\Delta G^{\ddagger} = 17.2$, 16.7, and 15.7 kcal/mol for C_{17}, C_{18}, and C_{19}, respectively; the longer guests have lower activation barriers. For C_{16} encapsulated in **1.2$_4$.1** no evidence of racemization was observed, even on heating, and the activation barrier is at least 22 kcal/mol. This alkane can fit inside with a fully extended conformation.

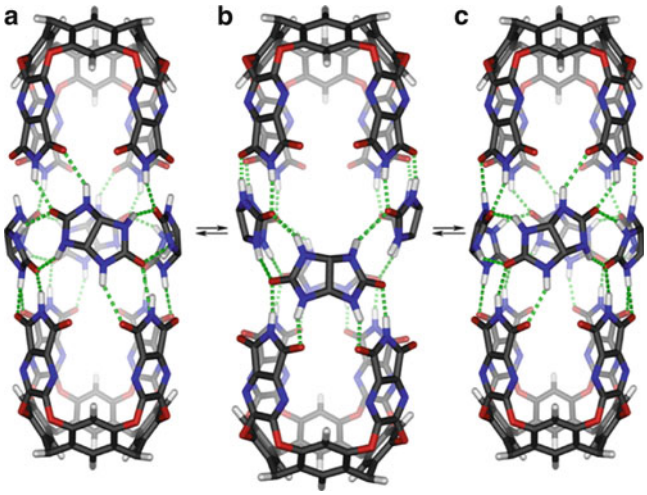

Fig. 7 Proposed racemization mechanism for the assembly: the spacer units are rotated in a concerted manner until the symmetric intermediate b is reached

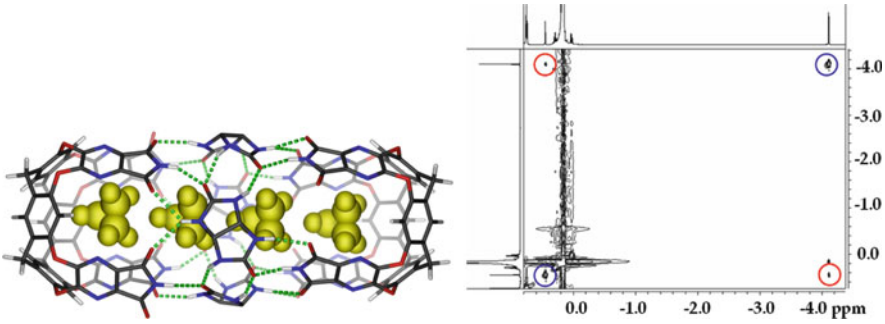

Fig. 8 Encapsulation of cyclopropane in **1.2$_4$.1**. Crosspeaks (*circled in red*) indicate exchange of guest positions within the capsule

The smaller cyclopropane is also encapsulated but four molecules are involved (Fig. 8). Together they fill about 36% of the capsules space and 2D ROESY spectroscopy showed that the encapsulated cyclopropanes can exchange their position inside the capsule on the NMR time scale. Integration of the cross-peaks gave an activation barrier of 18.5 kcal/mol for this exchange of positions. The application of ideal gas laws to the encapsulation gives very high pressures; several hundred atmospheres are calculated *even though the gases are applied at ambient pressure*. This reflects just how far the system is from an ideal gas. The guests are not point masses and their collisions with the walls are hardly elastic, rather they are "sticky" in nature. The attractive CH/π interactions between the guests and the aromatic walls stabilize the system and allow these high "pressures" to be achieved.

5 Isolated Hydrogen Bonds

Evidence of compression of the guests in the isolated environment of the host was revealed by a study of hydrogen-bonded carboxylic acid dimers in these same capsules. The chemical shifts of the O—H···O signals moved downfield as the effective lengths of the dimers increased from 14.59 ppm for *p*-toluic acid, 14.77 ppm for *p*-ethyl-benzoic acid, 15.98 ppm for *p*-*tert*-butyl-benzoic acid, and 16.72 ppm for *p*-methyl-cinnamic acid (Fig. 9) [39]. Good correlations exist for ^{1}H NMR chemical shifts, O...O distances, and hydrogen positions using solid state NMR, X-ray diffraction, and neutron scattering [40–45]. Encapsulation of the carboxylic acid dimers results in slow H-bonded proton exchange, and spectra measured at intermediate deuterium fractions showed separate signals for the HH dimer and the HD dimer. The difference, defined as $\Delta\delta = \delta_{HD} - \delta_{HH}$, serves as a sensitive probe for H-bond geometries [46–48] (hydrogen bond isotope effects studied by NMR [49]). The encapsulated carboxylic acid dimers behave as if they experienced an external pressure from the inner walls of the capsule. The extrapolated pressures are 4–10 kbar, and while these figures appear high, the trend is in agreement with the amplification of intermolecular forces, particularly equilibrium isotope effects [50, 51], seen during the temporary isolation of species in capsules.

There are many kinds of capsules but few have the capacity to position co-guests in predictable orientations. We used the ability of **1.2$_4$.1** to do so, and applied it to evaluate hydrogen-bonding interactions between boronic acids, carboxylic acids, and primary amides [52]. The phenyl boronic acids are useful as components of covalently self-assembled systems [53], and we found that the *p*-methyl, methoxy, ethyl, and isopropyl derivatives all fit as symmetrical dimers inside **1.2$_4$.1**. The structure of the boronic acid dimer has been debated but a recent theoretical study found the doubly hydrogen-bonded exo/endo conformer (Fig. 10) to be lowest in

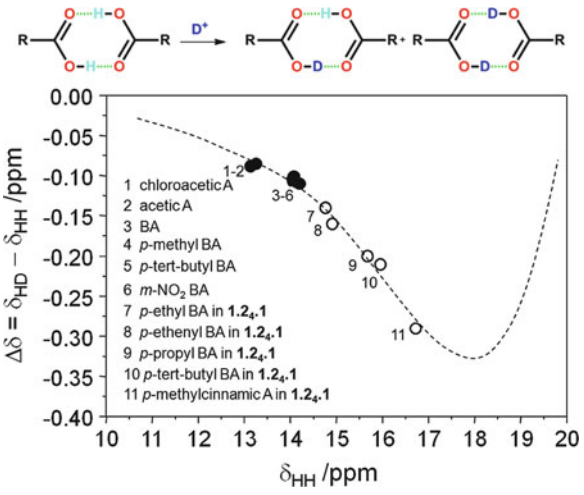

Fig. 9 H/D isotope effects on the hydrogen bond geometries: H/D isotope effects, $\Delta\delta = \delta_{HD} - \delta_{HH}$, for the encapsulated benzoic acid (BA) derivatives (d_{12} mesitylene, *open circles*) and non-encapsulated (CDF3/CDF2Cl; *filled circles*) dimers of carboxylic acids as a function of the bridging proton chemical shift δ_{HH}

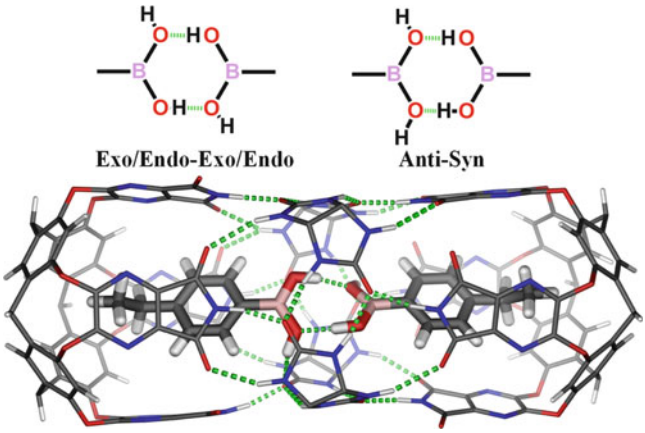

Fig. 10 The structures of the *exo-endo* and *anti-syn* isomers of the H-B(OH)$_2$ hydrogen-bonded dimer. The energy-minimized structure (HF/6-31 g*) of the *exo–endo* isomer of *p*-ethyl-phenyl boronic acid dimer in **1.2$_4$.1**

energy [54]. The structure has planar (C_{2h}) symmetry with both involved and spectator hydrogens. The alternate syn/anti dimer was computed to be accessible in more polar media.

The spectator acidic hydrogens provide another means of accelerating the racemization of the capsule. Guests that present hydrogen bond donor and acceptor groups to the middle of the assembly can catalyze the rotation of the glycolurils and interconversion of the capsule enantiomers through acid/base catalysis. The spectrum for *p*-Me-phenyl boronic acid shows broadened NH signals of the glycoluril spacer, and for *p*-isopropyl-phenyl boronic acid, the diastereotopic methyl signals of the isopropyl group appeared as a broad doublet, indicating fairly rapid racemization of the capsule on the NMR timescale. The signals for the spectator hydrogens of the *p*-ethyl and *i*-propyl derivatives appeared at 7.72 and 8.12 ppm, respectively.

We compared combinations of encapsulated carboxylic acids, boronic acids, and carboxamides to determine the strongest interactions – at least in the context of the capsule [55]. Direct competition experiments between guests of the same size (the *p*-ethyl derivatives) were used to eliminate the effects of "fit".

The boronic acid (B), carboxylic acid (C), and primary amide (A) were first used in pairwise competitions with 1 equiv. of each guest (relative to the extended capsule). Separate signals are seen for the N–H resonances of the benzamide and phenyl boronic acid co-encapsulated with corresponding carboxylic acids (Fig. 11). All three combinations and their respective homodimers were observed. The symmetrical homodimers are half as probable as the heterodimers with distributions of 25% and 50%, respectively. The carboxylic acid (C) and amide (A) formed a heterodimer (BC = 53%) but its concentration is 4.8 times that of the underrepresented amide dimer (AA = 11%) and 1.5 times that of the carboxyl dimer (CC = 36%). The BC heterodimer matches the best donor with the best acceptor but its concentration is merely what is statistically expected. The real difference is

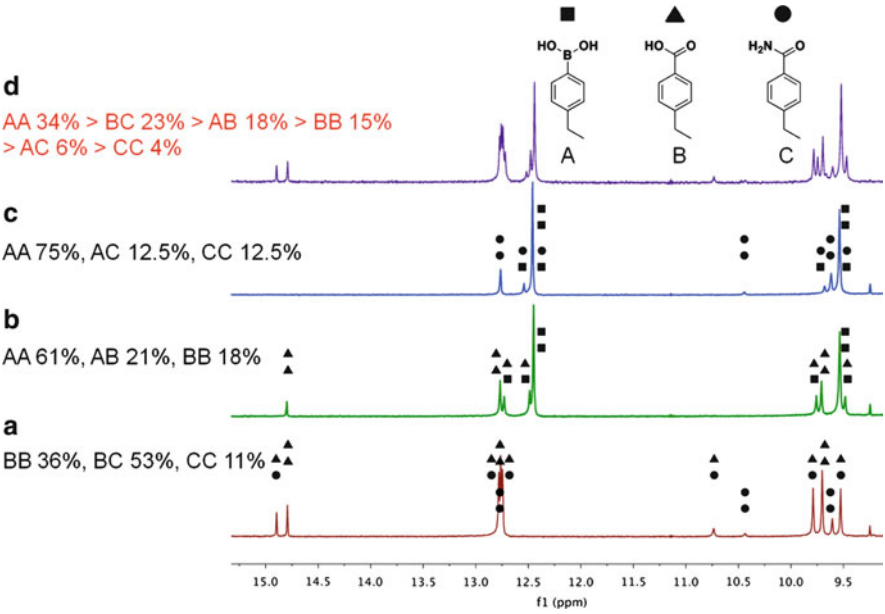

Fig. 11 The downfield region of ^{1}H NMR spectra (600 MHz, mesitylene-d_{12}) of **1.2$_4$.1** with equimolar mixture of: (**a**) *p*-ethyl benzamide and *p*-ethyl benzoic acid, (**b**) *p*-ethyl phenyl boronic acid and *p*-ethyl benzoic acid, (**c**) *p*-ethyl phenyl boronic acid and *p*-ethyl benzamide, and (**d**) *p*-ethyl phenyl boronic acid, *p*-ethyl benzoic acid and *p*-ethyl benzamide

between symmetrical acid carboxylic dimer, which is 3.3 times more favored than the amide dimer. The boronic acid homodimer BB is always favored, whether it competes with an acid or amide function, making this the best hydrogen bonding pair in this series. The heterodimer of carboxylic acid and boronic acid (BC, 21%) is favored over the homodimer of the carboxylic acid (CC, 18%).

When all three hydrogen bonding partners are competed against each other, the same trend is seen: the best pair is the boronic acid dimer with 34%, followed by the acid amide heterodimer with 23%, acid boronic acid heterodimer with 18%, acid acid homodimer with 15%, the boronic acid amide heterodimer with 6%, and the amide homodimer is the least stable with 4% as shown in Fig. 11.

At first glance, the dominance of the boronic acid-containing complexes would indicate its superiority as a partner for hydrogen bonding. But the exo/endo boronic acid dimer has twice as many ways to form than does a carboxylic acid dimer (there are four times as many if syn/anti arrangements are included). The low concentrations of heterodimers with boron shows it underperforms as a partner for carboxylic acids and amides: it is neither a superior donor nor acceptor. Instead, the high concentration of boronic acid dimers must reflect its statistical advantages, but could also suggest a balanced self-complementarity of average donor and acceptor. The carboxylic acid/amide pair is overrepresented as it matches the best donor and acceptor. While the weak amide dimer is no surprise, the carboxylic acid dimer appears more robust

than intuition would suggest. The rapid exchange of partners in solution and the average signals that result would not allow the dissection of these equilibria. The simultaneous characterization of all the species through reversible encapsulation showcases the power of this technique applied to physical organic chemistry.

6 Arrangements of Guests

The extended capsule has enough space to allow two long molecules to fit inside. If these molecules, for example, *p*-disubstituted benzenes, are unsymmetrical, then a number of different arrangements can be expected. We introduced the term "social isomerism" to describe this situation [56]. Social isomers are diastereomers but, unlike the situation in organic chemistry – where covalent connectedness determines the relationship between diastereomers – it is the restricted space of the capsule that enforces and maintains the arrangements in space. Specifically, the molecules inside are too large to slip past one another and, in the case of *p*-disubstituted benzenes, the molecules are too long to tumble freely inside the space, at least on the NMR time scale. For examples, *p*-cymene, *p*-ethyl-toluene, and *p*-methyl-styrene show social isomerism in the extended capsule (Fig. 12) [57]. Surprisingly, for the *p*-cymene case only two of the three possible isomers are observed.

The isomer with isopropyl groups in the narrower center of the assembly appears energetically inaccessible. But with *p*-ethyl-toluene the most favored isomer places the ethyl groups in the center and, unaccountably, the unsymmetrical isomer represents only a few percent of the mixture as shown in Fig. 12, although it is statistically favored. In contrast, *p*-methylstyrene is well behaved and shows exactly what is expected from a statistical distribution of social isomers. Simple

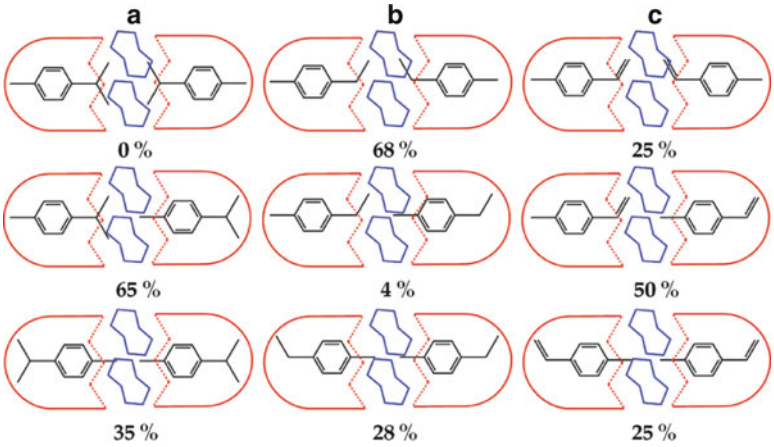

Fig. 12 Cartoon representation of the social isomers of (**a**) *p*-cymene, (**b**) *p*-ethyl-toluene, and (**c**) *p*-methyl-styrene in **1.2$_4$.1**

monosubstituted phenyl groups, ethyl, propyl, or butyl benzenes, likewise show little evidence of social isomerism. Instead, these guests always present the thinner alkyl groups toward the center of the assembly. Apparently this region cannot accommodate two benzene rings.

7 Control of Guest Exchange

7.1 Light

Switching devices that are reversible and work on the molecular level are essential features of nanomachinery. Control of the access to capsules, the transport of molecules in and out of the cavities, is desirable and we examined a well-established system that uses light as a switching device: the *cis-trans* photoisomerization of azobenzenes [58, 59]. The azobenzenes have been applied in the supramolecular chemistry of crown ethers [60–62], cyclodextrins [63, 64], and even proteins [65, 66]. The photoisomerization changes the shape in a predictable way and we used azobenzene photoisomerization in an indirect sense to control reversible encapsulation.

The encapsulation of benzanilides [67] and stilbenes [68] in **1.1** guaranteed that the isosteric *trans*-azobenzene would also be an ideal fit [69]. Direct competition of *n*-tridecane with *trans*-azobenzene showed the latter to be a much better guest for the capsule. Only a methyl singlet is seen in the ^{1}H NMR spectrum and no *n*-tridecane is observed inside (Fig. 13). Irradiation at 365 nm for 30 min causes the encapsulation of *n*-tridecane. This is apparent from its NMR signals (Fig. 13). Photoexcitation of the azobenzene forces its folding to *cis*-azobenzene which is too thick to fit in the capsule. Accordingly, as it folds it clashes with the capsule walls and disrupts hydrogen bonds [70]. This facilitates the entry of other guests and avoids creation of an empty capsule. The NMR shows signals corresponding to *cis*-**1** in the free solution at 6.59 ppm and 6.67 ppm. Kinetic studies confirmed that the isomerization of *trans*-**1** takes place inside the capsule. Brief heating of this sample to 160°C reconverts *cis*-**1** to its *trans* conformation, which rapidly replaces *n*-tridecane in the capsule. The irradiation/heating cycle can be repeated many times without deterioration of the spectra.

The forcing out of *trans*-azobenzene on irradiation by light allows the encapsulation of any other potential guest. For entropic reasons, a single large guest generally replaces two smaller occupants [71], but the forced photoisomerization can reverse the trend. For example, competition of hydrogen-bonded homodimers of benzoic acid or benzamide with 3 equiv. of *trans*-azobenzene shows only the azo compound is encapsulated in **1.1**. However, irradiation causes the azo compound to be replaced by the respective dimers. Again, brief heating restores the initial state (Fig. 13). This cycle can also be repeated many times.

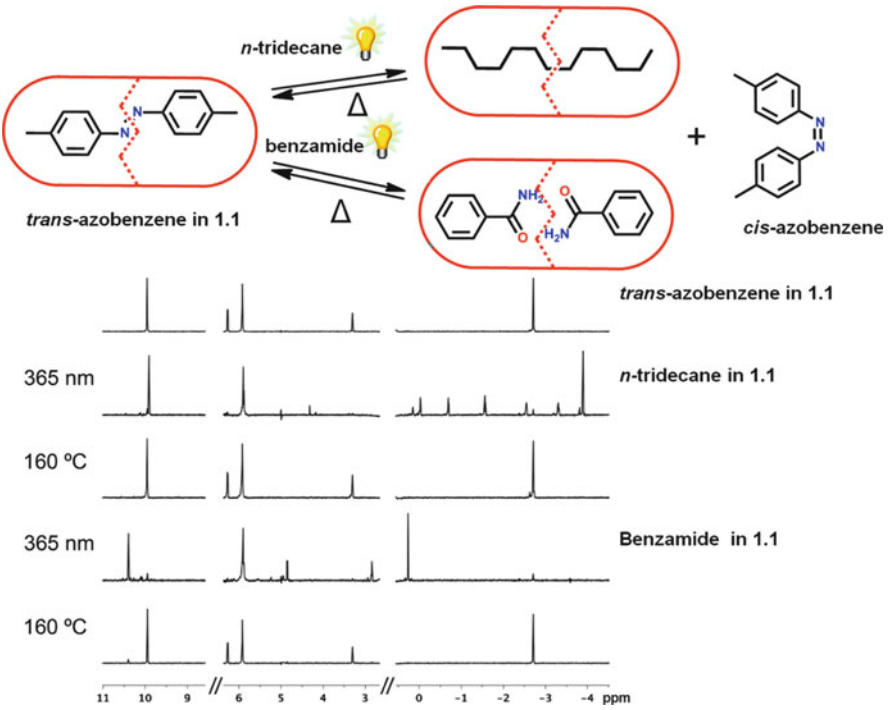

Fig. 13 Light induced replacement of *trans*-4,4-dimethyl azobenzene by *n*-tridecane or benzamide dimer in **2**·**2** (*top*). Appropriate regions of the ^{1}H NMR spectra (mesitylene-d_{12}, 20°C) are shown before irradiation (when *trans*-azobenzene is the only guest) and after irradiation at 365 nm wavelength for 50 min at 20°C (either *n*-tridecane or benzamide dimer is the only guest). After heating the sample to 160°C for 2 min, the initial state is reversibly restored (*bottom*)

Guest exchange in deep cavitands [72] involves related vase-to-kite conformational changes of the walls and Diederich et al. have shown that only two walls need undergo this motion to enable guest exchange [73]. We determined the exchange rate of encapsulated azobenzene with *n*-tridecane as an incoming guest without irradiation. Even when 30 equiv. of *n*-tridecane compete with *trans*-4,4-dimethyl-azobenzene for the capsule, only 19% of *trans*-azobenzene is replaced at equilibrium. This point is reached only after a day, showing that the exchange is very slow. The exchange rates determined by fluorescence methods are consistent with these findings [74, 75].

Parallel experiments were performed with the extended capsule **1.2$_4$.1** (Fig. 14, top), using a longer azobenzene *trans*-4-methyl-4'-hexyl-azobenzene [76] as the light-responsive guest in the assembly. The relevant signals of the ^{1}H NMR spectrum are shown in Fig. 14 (bottom). The loss of symmetry makes for separate sets of signals for the two cavitand ends and the hydrogens on the edges of the glycolurils. Competition of 10 equiv. of *trans*-4-methyl-4'-hexyl-azobenzene with 2 equiv. of 4-ethylbenzamide shows only the encapsulated azo compound. After irradiation at 365 nm, the hydrogen-bonded homodimer of 4-ethylbenzamide replaced the azo compound as the guest. This new assembly is symmetric as reflected in its simplified

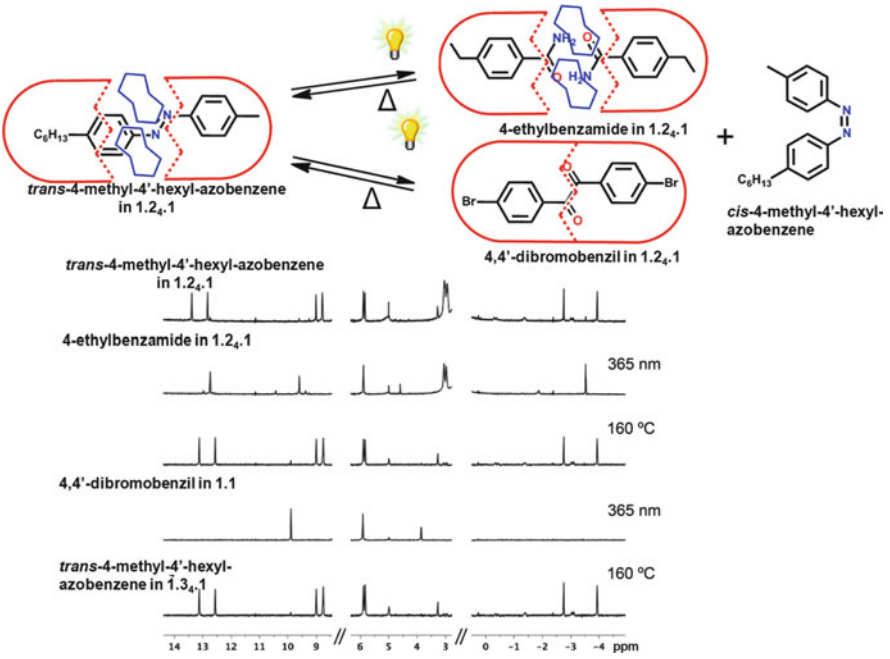

Fig. 14 Light induced guest exchange and assembly rearrangement. Replacement of *trans*-**4** by dimeric 4-ethylbenzamide maintains the extended assembly **1.2$_4$.1**. With *4,4'*-dibromobenzil, light induces guest exchange with formation of **1.1** (*top*). Relevant regions of the ^{1}H NMR spectra (mesitylene-d_{12}, 20°C) before irradiation (*trans*-4-methyl-4'-hexyl-azobenzene is the only guest) and after irradiation at 365 nm wavelength for 50 min at 20°C (the homodimer of 4-ethylbenzamide is the only guest in **1.2$_4$.1** and 4,4'-dibromobenzil is the only guest in **1.1**). After heating the sample to 160°C for 2 min, the initial state is quantitatively restored (*bottom*)

NMR spectrum. Heating the sample to 160°C for 2 min restores the initial state; again, the cycle was repeated many times (Fig. 14).

We also used photoisomerization as a means of switching between assemblies **1.1** and **1.3$_4$.1**. Here, we took advantage of the low solubility 4-dodecanephenyl glycoluril **3** in deuterated mesitylene. The glycoluril dissolves well only when it is incorporated into the capsular assembly. When a mixture of **1**, glycoluril **3,** and 3 equiv. of *trans*-4-methyl-4'-hexyl-azobenzene is heated, the extended assembly **1.3$_4$.1** is formed with the azo compound as the only guest. Likewise, in the presence of added 4,4'-dibromobenzil the same assembly is formed, since the benzyl is a poor guest for **1.1**. But after irradiation for 50 min at 365 nm, only the capsule assembly **1.1** is obtained with 4,4'-dibromobenzil as guest. The disproportionation process is apparently aided by the precipitation of **3** from solution. The original extended assembly **1.3$_4$.1** with *trans*-4-methyl-4'-hexyl-azobenzene reappearing as the only encapsulated species can be restored on heating the turbid solution for 2 min to 160°C (Fig. 14). Again, this cycle was repeated many times to establish the photochemical control of expanded capsule assembly.

7.2 Acid/Base

We also devised a system that uses acid/base control of expansion and contraction of the capsules and their guests. A number of studies with the cylindrical capsule defined its application as a reaction vessel [77, 78] but the conformational flexibility [79] of normal alkanes as guests (which adopt shapes complementary to their hosts) offered an opportunity to create what we termed a "spring-loaded" device.

Alkanes as long as tetradecane (*n*-C_{14}) are encapsulated in **1** but longer alkanes, such as *n*-C_{15}, do not fit inside. Even C_{14} cannot fit in an extended conformation; like the longer alkanes in the expanded capsule it must adopt a compressed conformation that applies stress to the capsule [80]. Coiling into a helical shape reduces its length by about 5 Å, enough to be accommodated and results in attractive CH-π interactions between guest and the capsule (Fig. 15). This coiling increases the potential energy because in the liquid phase [81] each *gauche* interaction incurs some 0.55 kcal/mol. The helical conformation was deduced from 2D NMR crosspeaks that show the proximity of hydrogens on C_1 to C_5, C_2 to C_6, etc. (Fig. 15) [82].

As previously mentioned, the belt of glycolurils that inserts into the capsule increases the length by some 7 Å and the volume by nearly 50% [83]. In the expanded capsule tetradecane relaxes into an extended conformation and this is evident from changes in the ^{1}H NMR spectrum. The NMR signals move downfield as the methylenes of the alkane move away from the walls and toward the center of the structure. The different NMR spectra of tetradecane in the original vs the expanded capsule is shown in Fig. 16.

The insertion of four glycolurils constricts the center of the cavity and creates a chiral nanoenvironment that is apparent in the diastereotopic proton signals at C_2. Benzanilide, which is an ideal guest for **1.1**, can displace the alkane and return the system to the original capsule. To control the coiling and extension of the alkane by addition of acids and bases, we prepared glycoluril bearing peripheral basic

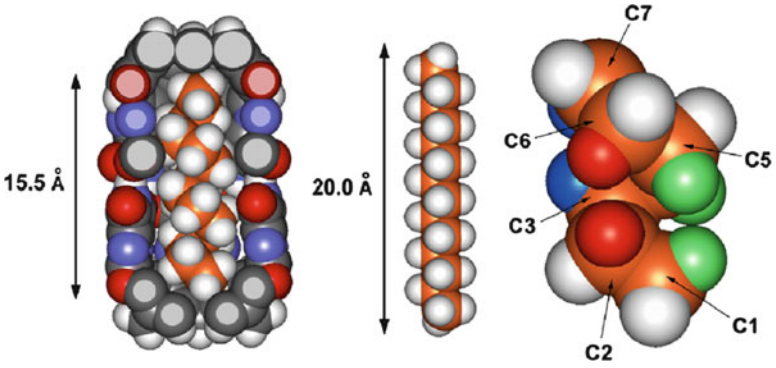

Fig. 15 Dimensions of encapsulated *n*-C_{14} (*left*) and in an extended conformation (*center*). The crosspeaks observed in the 2D NMR spectra are color coded on the model of the helically coiled conformation (*right*)

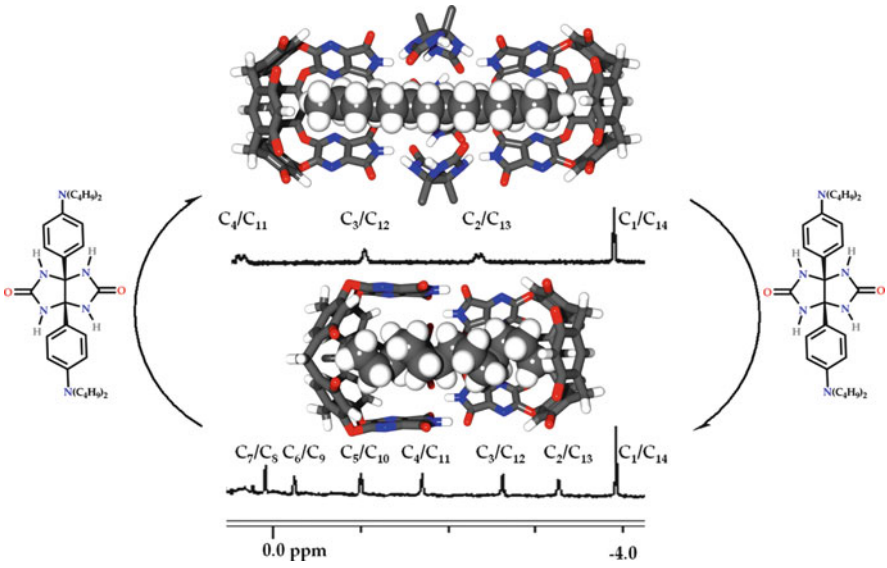

Fig. 16 The reversible compression and expansion of encapsulated *n*-tetradecane. The conformation of the *n*-tetradecane was deduced from the upfield regions of the ^{1}H NMR spectra which are shown together with the respective host guest complexes. In the expanded capsule **1.2$_4$.1** the signals move downfield as the methylenes move away from the capsule's walls and toward its center. The chiral space of the expanded assembly is reflected by the diastereotopic signals for the methylenes. The glycolurils insert under basic conditions; acidic conditions precipitate the glycouril and regenerate the capsule **1.1** with coiled tetradecane inside

sites [84]. The addition of this glycoluril allows the coiled alkane to extend in the longer capsule **1.2$_4$.1**. This is the expansion step. Then HCl gas is bubbled into the NMR sample which protonates the basic sites on the glycoluril and causes precipitation of the HCl salt. This treatment regenerates the original capsule **1.1** with the coiled alkane inside. This is the compression step. To continue to the expansion step, trimethylamine was introduced to the sample: it deprotonates the salt and allows the glycoluril to re-enter the solution and assemble the expanded capsule. Then acid was added to regenerate **1.1** (Fig. 16). Some six cycles of expansion and compression of *n*-tetradecane were possible in a single NMR sample before the buildup of trimethylamine hydrochloride deteriorated the ^{1}H NMR spectra.

As previously described, the expanded capsule could accommodate normal C_{15}, C_{16}, C_{17}, C_{18}, and C_{19}, but the appearance of a new capsule in the presence of C_{19} was unexpected. This capsule incorporated *two* belts of glycolurils [85]. This hyperextended capsule **1.2$_8$.1** (Fig. 17) also accommodated appropriately lengthy fatty acid derivatives such as anandamide, which is the naturally-occurring ligand for the cannabanoid receptor of the brain [86]. Even longer hydrocarbons such as C_{24} to C_{29} induced the formation of another encapsulation complex involving *three* glycoluril belts. A total of 15 molecules make up this assembly, and we have reason to believe that even longer capsules can be made with the simple recipe of **1**, glycoluril **2**, and ever-longer alkanes. These results are reported in Fig. 18.

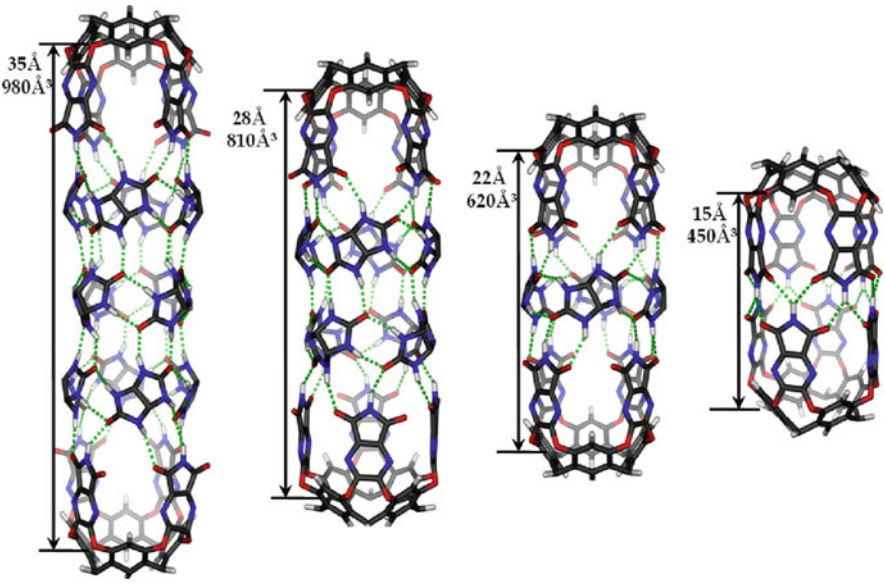

Fig. 17 Energy minimized structures and approximate dimensions of capsules extended by glycolurils. The length refers to the accessibility of methyl groups in the inner space. Peripheral groups have been removed for viewing clarity

Guest	Volume(Å³)	PC(%) in 1.1	PC(%) in $1.2_4.1$	PC(%) in $1.2_8.1$	PC(%) in $1.2_{12}.1$
n-$C_{13}H_{28}$	230	54	37		
n-$C_{14}H_{30}$	247	58	40		
n-$C_{15}H_{32}$	264	62	42		
n-$C_{16}H_{34}$	281		45		
n-$C_{17}H_{36}$	297		48		
n-$C_{18}H_{38}$	314		51	39	
n-$C_{19}H_{40}$	331		53	41	
n-$C_{20}H_{42}$	348		56	43	
n-$C_{21}H_{44}$	364			45	
n-$C_{22}H_{46}$	381			47	
n-$C_{23}H_{48}$	399			49	41
n-$C_{24}H_{50}$	417			51	43
n-$C_{25}H_{52}$	434			54	44
n-$C_{26}H_{54}$	450				46

Fig. 18 Relevant data for alkane dimensions and their packing coefficients (PCs) are given. Alkanes that occupy two different capsules are shown in *red*

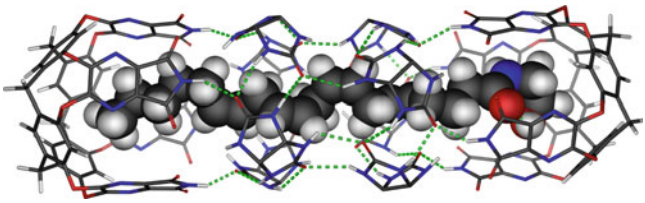

Fig. 19 The energy-minimized (AM1) structure of encapsulated anandamide inside doubly-expanded capsule $\mathbf{1.2_8.1}$

We used our experience with reversible encapsulation to arrive at a rule regarding the proper filling of space, the 55% solution [87]. The filling of space probably drives other recognition phenomena, even in those synthetic receptors that do not completely surround their targets [88]. Some of the earliest, finite self-assemblies in solution based on melamine/cyanuric acid recognition [89] had no other function than to fill space. However unconventional, the departure from mainstream physical organic chemistry [90] is familiar to us and may offer rewards.

The hyperextended capsule provides the required tool to encapsulate more complex and even bioactive compounds. The adaptability of the larger assembly with a number of natural products having long and narrow shapes has been probed and it has been found that they are readily encapsulated by the cavitand/glycoluril system. These include arachidonic acid, the substrate for the biosynthesis of the prostaglandins, and several of its derivatives including capsaicin and anandamide (Fig. 19), the endogenous ligand for the cannabinoid receptor [91]. Oleamide, one of the fatty acid amides involved in sleep induction [92], and its ethyl ester derivative were also encapsulated. The release of these natural products from the capsules can be accomplished through the changes in the polarity of the medium or, in special cases, acid/base chemistry. We intend to screen these and other bioactive compounds with these capsules inside micelles to study their uptake and release characteristics. For realistic applications in medicine, we would have to overcome the 1:1 stoichiometry problem that makes these assemblies too expensive. The first step in this process is establishing the application of these capsules as (recyclable) transporters across membranes, but this aspect is outside the scope of this chapter.

Acknowledgements We are grateful to the Skaggs Institute for Research and the National Institutes of Health (GM 27932) for financial support.

References

1. Rebek J Jr (2009) Accounts Chem Res 42:1660–1668
2. Galán A, de Mendoza J, Toiron C, Bruix M, Deslongchamps G, Rebek J Jr (1991) J Am Chem Soc 113:9424–9425
3. Parac TN, Caulder DL, Raymond KN (1998) J Am Chem Soc 120:8003–8004
4. Yoshizawa M, Kuskawa T, Fujita M, Yamaguchi K (2000) J Am Chem Soc 122:6311–6312

5. Fiedler D, Bergman RG, Raymond KN (2006) Angew Chem Int Ed Engl 45:745–748
6. Iwasawa T, Mann E, Rebek J Jr (2006) J Am Chem Soc 128:9308–9309
7. Mal P, Breiner B, Rissanen K, Nitschke JR (2009) Science 324:1697–1699
8. Sherman JC (1995) Tetrahedron 51:3395–3422
9. Brody MS, Schalley CA, Rudkevich DM, Rebek J Jr (1999) Angew Chem Int Ed Engl 38:1640–1644
10. Avram L, Cohen Y (2004) J Am Chem Soc 126:11556–11563
11. Shivanyuk A, Rebek J Jr (2001) Chem Commun 2424–2425
12. Hof F, Nuckolls C, Rebek J Jr (2000) J Am Chem Soc 122:4251–4252
13. Kerckhoffs JMCA, ten Cate MGJ, Mateos-Timoneda MA, van Leeuwen FWB, Snellink-Ruël B, Spek AL, Kooijman H, Crego-Calama M, Reinhoudt DN (2005) J Am Chem Soc 127: 12697–12708
14. MacGillivary LR, Atwood JL (1997) Nature 389:469–472
15. Gerkensmeier T, Iwanek W, Agena C, Fröhlich R, Kotila S, Näther C, Mattay J (1999) Eur J Org Chem 1999:2257–2262
16. Shivanyuk A, Rebek J Jr (2003) J Am Chem Soc 125:3432–3433
17. Kobayashi K, Ishii K, Sakamoto S, Shirasaka T, Yamaguchi K (2003) J Am Chem Soc 125:10615–10624
18. González JJ, Ferdani R, Albertini E, Blasco JM, Arduini A, Pochini A, Prados P, de Mendoza J (2000) Chem Eur J 6:73–80
19. Scarso A, Pellizzaro L, De Lucchi O, Linden A, Fabris F (2007) Angew Chem Int Ed Engl 46:4972–4975
20. Yoshizawa M, Tamura M, Fujita M (2006) Science 312:251–254
21. Ziegler M, Brumaghim JL, Raymond KN (2000) Angew Chem Int Ed Engl 39:4119–4121
22. Kaanumalle LS, Gibb CLD, Gibb BC, Ramamurthy V (2005) J Am Chem Soc 127:3674–3675
23. Avram L, Cohen Y, Rebek J Jr (2011) Chem Commun 47:5368–5375
24. Heinz T, Rudkevich DM, Rebek J (1998) Nature 394:764–766
25. Tucci FC, Rudkevich DM, Rebek J Jr (1999) J Org Chem 64:4555–4559
26. Tucci FC, Rudkevich DM, Rebek J Jr (2000) Chemistry (A Eur J) 6:1007–1016
27. Martin T, Obst U, Rebek J Jr (1998) Science 281:1842–1845
28. Ajami D, Rebek J (2006) J Am Chem Soc 128:5314–5315. doi:10.1021/ja060095q
29. Ajami D, Rebek J Jr (2006) J Am Chem Soc 128:5314–5315
30. Rivera JM, Craig SL, Martín T, Rebek J Jr (2000) Angew Chem Int Ed Engl 39:2130–2132
31. Ajami D, Rebek J Jr (2008) Heterocycles 76:169–176
32. Ajami D, Rebek J Jr (2006) J Am Chem Soc 128:5314–5315
33. Ajami D, Rebek J Jr (2007) Proc Natl Acad Sci USA 104:16000–16003
34. Schleyer PVR, Maerker C, Dransfeld A, Jiao H, Hommes NJRV (1996) J Am Chem Soc 118:6317–6318
35. Frisher MJ et al (2002) Gaussian 03. Guassian Inc, Pittsburgh, PA
36. Lützen A, Renslo AR, Schalley CA, O'Leary BM, Rebek J Jr (1999) J Am Chem Soc 121: 7455–7456
37. Amaya T, Rebek J Jr (2004) J Am Chem Soc 126:6216–6217
38. Ajami D, Rebek J Jr (2009) Nat Chem 1:87–90
39. Ajami D, Tolstoy P, Dube H, Odermatt S, Koeppe B, Guo J, Limbach H-H, Rebek J Jr (2011) Angew Chem Int Ed Engl 50:528–531
40. Harris RK, Jackson P, Merwin LH, Say BJ, Hägele GS (1988) J Chem Soc Faraday Trans I 84:3649–3672
41. Sternberg U, Brunner EL (1994) J Magn Res A 108:142–150
42. Brunner E, Sternberg U (1998) J Progr NMR Spect 32:21–57
43. Mildvan TK, Harris AS (1999) Proteins Struct Funct Genet 35:275–282
44. McDermott A, Ridenour CF (1996) Proton chemical shift measurements in biological solids. In: Encyclopedia of NMR. Wiley, Sussex, UK, pp 3820–3825
45. Emmler T, Gieschler S, Limbach HH, Buntkowsky G (2004) Mol Struct 700:29–38

46. Detering C, Tolstoy PM, Golubev NS, Denisov GS, Limbach HH (2001) Dokl Phys Chem 379:1–4
47. Shenderovich IG, Limbach HH, Smirnov SN, Tolstoy PM, Denisov GS, Golubev NS (2002) Phys Chem Chem Phys 4:5488–5497
48. Tolstoy PM, Schah-Mohammedi P, Smirnov SN, Golubev NS, Denisov GS, Limbach HH (2004) J Am Chem Soc 126:5621–5634
49. Limbach HH, Denisov GS, Golubev NS (2005) Isotope effects in chemistry and biology In: Kohen A, Limbach HH (eds) Taylor & Francis, Boca Raton FL, pp 193–230
50. Rechavi D, Scarso A, Rebek J Jr (2004) J Am Chem Soc 126:7738–7739
51. Zhao YL, Houk KN, Rechavi D, Scarso A, Rebek J Jr (2004) J Am Chem Soc 126: 11428–11429
52. Ajami D, Dube H, Rebek J Jr (2011 J Am Chem Soc 133:9689–9691
53. Nishimura N, Kobayashi K (2008) Angew Chem Int Ed Engl 47:6255–6258
54. Larkin JD, Bhat KL, Markham GD, Brooks BR, Schaefer HFIII, Bock CW (2006) J Phys Chem A 110:10633–10642
55. Ajami D, Dube H, Rebek J Jr (2011) J Am Chem Soc 133:9689–9691
56. Shivanyuk A, Rebek J Jr (2002) J Am Chem Soc 124:12074–12075
57. Ajami D, Rebek J Jr (2009) J Org Chem 74:6584–6591
58. Balzani V, Credi A, Venturi M (eds) Molecular devices and machines a journey into the nanoworld. Wiley-VCH, pp 288–328
59. Kay ER, Leigh DA, Zerbetto F (2007) Angew Chem Int Ed Engl 46:72–191
60. Shinkai S, Ogawa T, Nakaji T, Kusano Y, Manabe O (1979) Tetrahedron Lett 20:4569–4572
61. Shinkai S, Nakaji T, Nishida Y, Ogawa T, Manabe O (1980) J Am Chem Soc 102:5860–5865
62. Shinkai S, Nakaji T, Ogawa T, Shigematsu K, Manabe O (1981) J Am Chem Soc 103:111–115
63. Gloe K (ed) (2005) Macrocyclic chemistry current trends and future perspectives. Springer, Netherlands, pp 203–218
64. Wang Y, Ma N, Wang Z, Zhang X (2007) Angew Chem Int Ed Engl 46:2823–2826
65. Deal WJ Jr, Erlanger BF, Nachmansohn D (1969) Proc Natl Acad Sci USA 64:1230–1234
66. Banghart MR, Mourot A, Fortin DL, Yao JZ, Kramer RH, Trauner D (2009) Angew Chem Int Ed Engl 48:9097–9101
67. Heinz T, Rudkevich DM, Rebek J Jr (1999) Angew Chem Int Ed Engl 38:1136–1139
68. Körner SK, Tucci FC, Rudkevich DM, Heinz T, Rebek J Jr (2000) Chem Eur J 6:187–195
69. Heinz T, Rudkevich D, Rebek J Jr (1998) Nature 394:764–766
70. Dube H, Ajami D, Rebek J Jr (2010) Angew Chem Int Ed 49: 3192–3195
71. Kang J, Rebek J Jr (1996) Nature 382:239–241
72. Cram DJ, Choi H-J, Bryant JA, Knobler CB (1992) J Am Chem Soc 114:7748–7765
73. Gottschalk T, Jaun B, Diederich F (2007) Angew Chem Int Ed Engl 46:260–264
74. Barrett ES, Dale TJ, Rebek J Jr (2007) J Am Chem Soc 129:8818–8824
75. Castellano RK, Craig SL, Nuckolls C, Rebek J Jr (2000) J Am Chem Soc 122:7822–7876
76. Dabrowski R, Kenig K, Raszewski Z, Kedzierski J, Sadowska K (1980) Mol Cryst Liq Cryst 61:61–78
77. Rebek J Jr (2005) Angew Chem Int Ed Engl 44:2068–2078
78. Chen J, Rebek J Jr (2002) Org Lett 4:327–329
79. Schramm MP, Rebek J Jr (2006) Chem Eur J 12:5924–5933
80. Scarso A, Trembleau L, Rebek J Jr (2003) Angew Chem Int Ed Engl 42:5499–5502
81. Eliel E, Wilen SH (1994) Stereochemistry of organic compounds. Conformation of acyclic molecules. Wiley, New York, pp 597–664, chap 10
82. Scarso A, Trembleau L, Rebek J Jr (2004) J Am Chem Soc 126:13512–13518
83. Ajami D, Rebek J Jr (2006) J Am Chem Soc 128:5314–5315
84. Ajami D, Rebek J Jr (2006) J Am Chem Soc 128:15038–15039
85. Ajami D, Rebek J Jr (2007) Angew Chem Int Ed Engl 46:9283–9286
86. Ajami D, Rebek J Jr (2007) Proc Natl Acad Sci USA 104:16000–16003
87. Mecozzi S, Rebek J Jr (1998) Chemistry (A Eur J) 4:1016–1022

88. Palmer LC, Rebek J Jr (2004) Org Biomol Chem 2:3051–3059
89. Whitesides GM, Mathias JP, Seto CT (1991) Science 254:1312
90. Rebek J (1979) Tetrahedron 35:723
91. Devane WA, Hanus L, Breuer A, Pertwee RG, Stevenson LA, Griffin G, Gibson D, Mandelbaum A, Etinger A, Mechoulam R (1992) Science 258:1946–1949
92. Cravatt BF, Lerner RA, Boger DL (1996) J Am Chem Soc 118:580–590

Top Curr Chem (2012) 319: 79–98
DOI: 10.1007/128_2011_245

Published online: 11 November 2011

Container Molecules Based on Imine Type Ligands

A. Carina Schulze and Iris M. Oppel

Abstract This chapter will give a short overview about container molecules, their synthesis and possible applications. The main focus is on those which are based on imine type ligands. These containers can be used for example for guest exchange, gas separation, as chemical sensors or for the stabilisation of white phosphorus under water. The described cages have wide openings or tightly closed ones. For one cage the reversible opening and closing is also described.

Keywords Cage compounds · Coordination · Encapsulation · SCHIFF base reaction · Supramolecular chemistry

Contents

1 Introduction

The large field of supramolecular coordination chemistry could be divided into polymers [1–5] and discrete compounds [6–10]. Coordination polymers or metal organic frameworks (MOF) are not only described in the literature but are also

A.C. Schulze and I.M. Oppel (✉)
RWTH Aachen, Institute for Inorganic Chemistry, Landoltweg 1, 52074 Aachen, Germany
e-mail: Iris.Oppel@ac.rwth-aachen.de

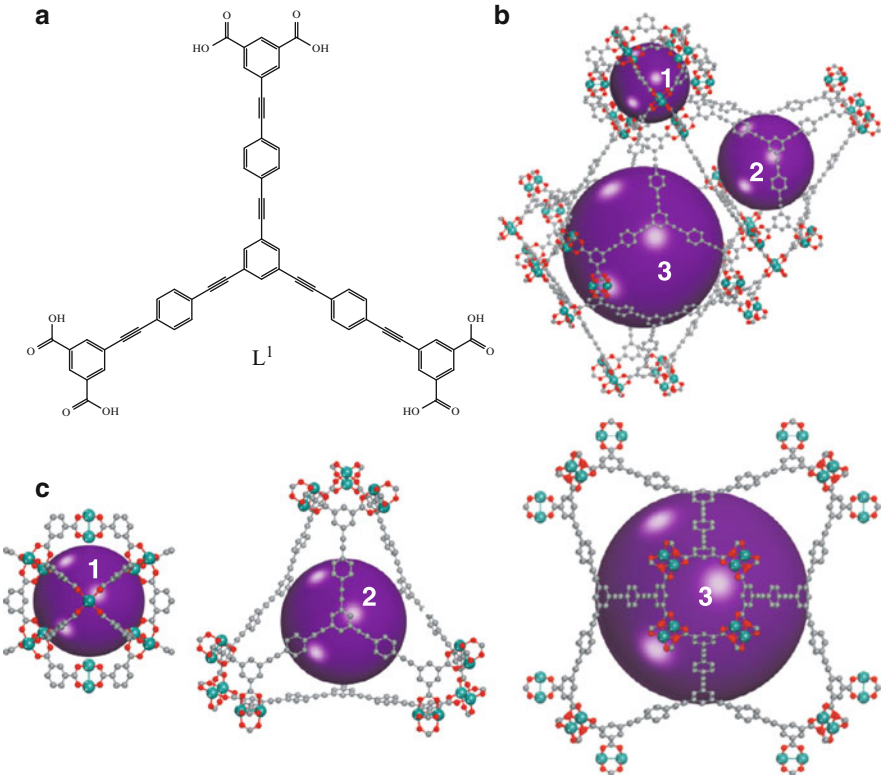

Fig. 1 (**a**) Ligand $\mathbf{L^1}$. (**b**) MOF for gas storage synthesised by J. T. Hupp et al. (**c**) The three parts of the MOF [11]

already used for industrial applications like gas storage, molecular separation, chemical catalysis, sensing, ion exchange and drug delivery [11–25]. For example, one MOF with gas storage capacity is $[Cu_3(\mathbf{L^1})(H_2O)_3]_n$ ($\mathbf{L^1}$ see Fig. 1a) synthesised by J. T. Hupp and coworkers. The compound consists of three different types of cage structures (Fig. 1b, c) with different diameters (13.4, 15.4 and 27.4 Å) of the cavity within the framework. The resulting polymer shows a surface area of 6.143 $m^2\ g^{-1}$, measured by BET. The excess H_2 uptake of the polymer is 18.2 mg g^{-1} at 1 bar and 99.5 mg g^{-1} at 56 bar and an excess CO_2 uptake of 2.043 mg g^{-1} at 40 bar [11].

However, herein we focus on the discrete compounds, especially the three-dimensional cages or container molecules [6–10], formed mainly by coordination of metal ions with organic ligands. On the other hand, there also exist three-dimensional compounds where the stability is partly due to hydrogen bonds, π–π interactions, Van der Waals forces or dipole–dipole interactions. Beside those three-dimensional compounds, one-dimensional structures like, for instance, helicates [26–30] and two-dimensional ones, the polygons, are also known [31–36].

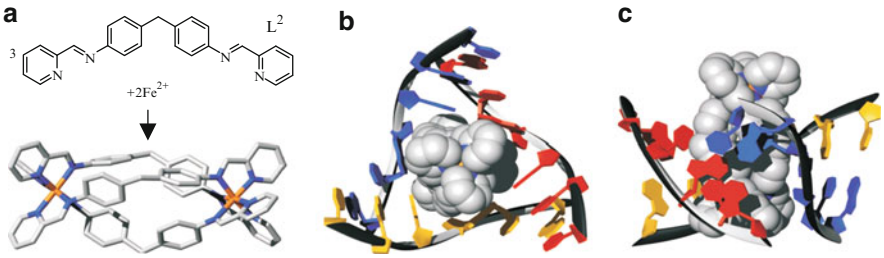

Fig. 2 Helicate which bind on three-way junction on DNA [37]. (**a**) Synthesis, (**b**) *top* and (**c**) *side view* of DNA and helicate

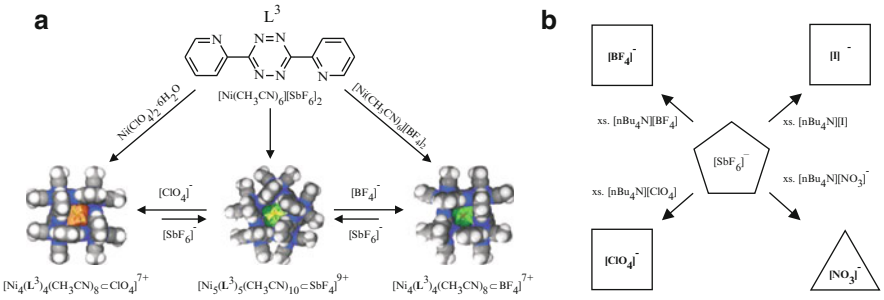

Fig. 3 Converting two-dimensional structures into each other [36]

One example for a helicate ($[Fe_2(\mathbf{L^2})_3]Cl_4$) was described by the group of A. Rodger et al. It is formed by reacting a bis(pyridylimine) ligand ($\mathbf{L^2}$) with $FeCl_2$. The helicate is described to have a preference for binding a three-way junction on DNA with a central TA sequence. This observation shows a possible way of drug binding to DNA (Fig. 2) [37–41].

Many two-dimensional polygons are described in the literature [31–36]. They exhibit shapes like triangles, squares, pentagons and so on, whose formation can be influenced by the used counterion as demonstrated in the following example. In Fig. 3a the ligand 3,6-bis(2-pyridyl)-1,2,4,5-tetrazine ($\mathbf{L^3}$) forms either a square or a pentagon depending on the counterion of the employed nickel salt. Starting with the pentagon, the shape of the polygon can be converted into either a triangle or a square by using a counterion with the right geometry (Fig. 3b) [36].

Beside these examples of one- and two-dimensional structures, many others are known in the literature. Many three-dimensional structures have also been described. These container molecules could be designed by following the molecular library method from P. Stang and coworkers. The combination of different building blocks leads to different shaped complexes (Fig. 4) [42].

This principle can be explained in detail by the example of a tetrahedron, which can be built by using different building blocks in the four illustrated ways (Fig. 5).

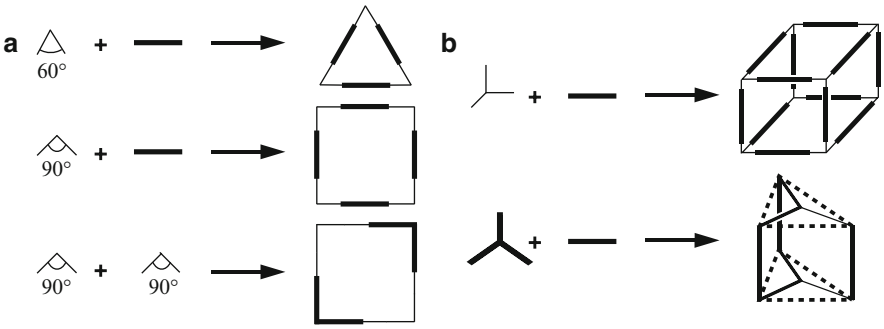

Fig. 4 Molecular library method from P. Stang. (**a**) 2D and (**b**) 3D [42]

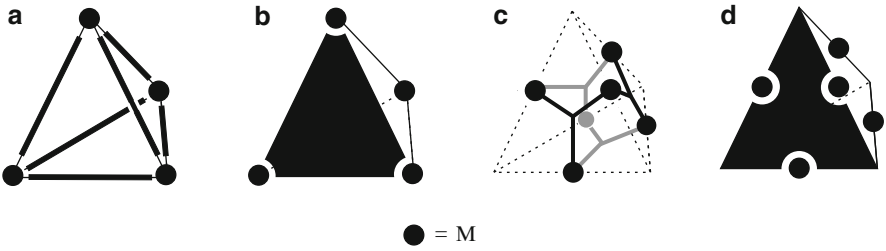

Fig. 5 Different types of tetrahedra: (**a**) M_4L_6, (**b**) M_4L_4, (**c**) M_6L_4 and (**d**) M_6L_4

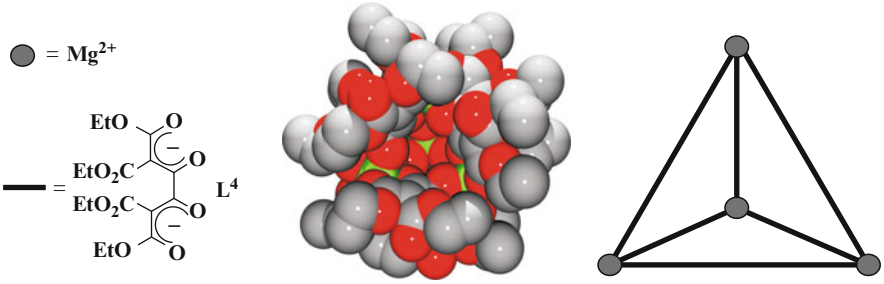

Fig. 6 First M_4L_6 tetrahedron [43]

The first way (Fig. 5a) is by using four metal ions with at least three free coordination sites and six bridging ligands. The resulting tetrahedron exhibits the M_4L_6 topology, where the metal ions are located at the corners of the cage while the ligands represent the edges.

An example of this type of cage is the tetrahedron of the group of R. W. Saalfrank. It was designed in 1988 and was the first example of a coordination cage described in the literature. It was synthesised with $\mathbf{L^4}$ (Fig. 6) and MeMgI in THF [43].

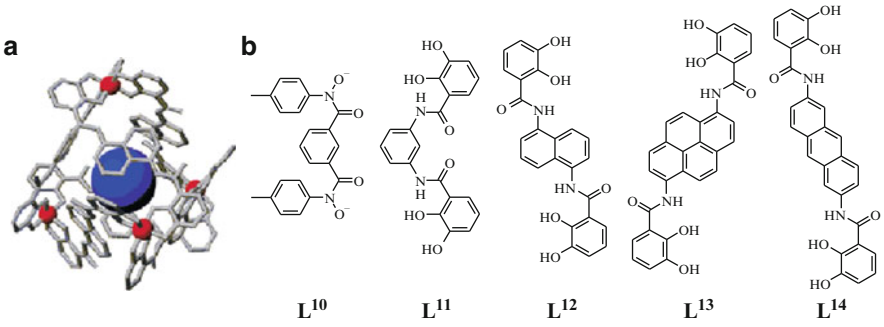

Fig. 7 (**a**) M_4L_6 tetrahedron by K.N. Raymond and co-workers. (**b**) Possible ligands [44–51]

Another example of this connection type is the tetrahedra of K. N. Raymond and coworkers. These could be synthesised with the ligands shown in Fig. 7b ($\mathbf{L^5}$–$\mathbf{L^9}$) and different metal ions like Ga^{3+}, Al^{3+}, Fe^{3+}, In^{3+}, Ge^{4+}, Ti^{4+} and Sn^{4+} [44–51].

These container molecules exhibit large openings on each triangle face. That is why different exchange processes can potentially take place. In the literature various applications are described such as encapsulation of neutral molecules or cations [44–74]. Reactive or unstable species could also be stabilised [63, 67, 75–78]. The cages can serve as a catalyst, e.g. for the Aza Cope rearrangement [54, 66, 79–81] and for the hydrolysis of several compounds [82–85]. They have also been used for C–H bond activation [54, 57, 61, 66, 69] or Nazarov cyclisation [86].

The second example of how a tetrahedron could be built demonstrates once again that four metal ions with the same requirements as in the first one are needed. However, in this case the six linear ligands are replaced by four C_3 symmetric ligands (covering the faces) which can connect a metal at each corner. The resulting structure exhibits M_4L_4 topology.

This type of tetrahedron was first synthesised by M. D. Ward et al. in 1995. It is obtained from the reaction of [3-(2′-pyridyl)pyrazol-1-yl]hydroborate ($\mathbf{L^{15}}$) and Mn^{2+}. Beside Mn^{2+}, analogous tetrahedra could be made with Fe^{2+}, Co^{2+}, Ni^{2+} and Zn^{2+}. The resulting cages are all nearly completely closed ones (Fig. 8) [87].

The third way leads to an adamantane with M_6L_4 topology, which is sometimes described in the literature as an octahedron with every second face empty. To build such a cage, again four C_3 symmetric ligands are needed to connect metal centres. However the six metal ions are no longer located at the corners of the cage but now in the middle of each edge instead.

The group of M. Fujita synthesised coordination cages of this shape while reacting a triazin ligand ($\mathbf{L^{16}}$–$\mathbf{L^{18}}$) with different Pd^{2+} or Pt^{2+} compounds. Two of the coordination sites in the square planar environment of these metal atoms are blocked by a coligand, like ethylene diamine, *N*,*N*,*N*′,*N*′-tetramethylethylene diamine or 2,2′-bipyridine, while the other two sites are used for coordination bonds to the C_3 symmetric ligand. In the resulting tetrahedra, compounds could be

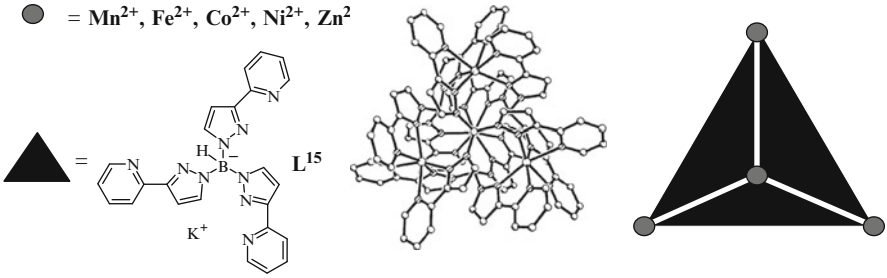

Fig. 8 M_4L_4 tetrahedron by M.D. Ward et al. [87]

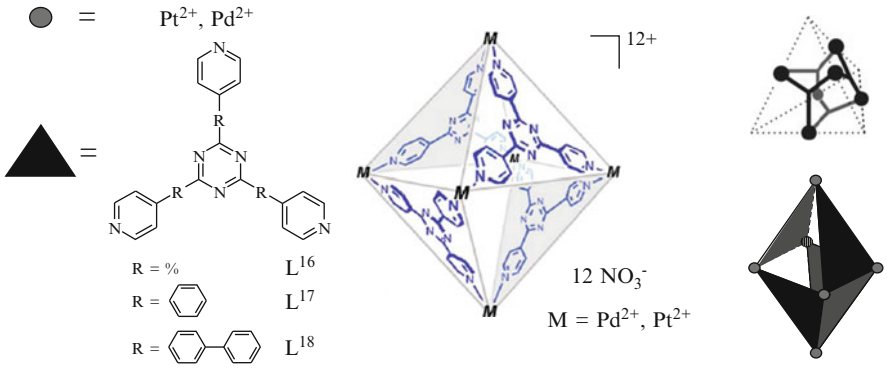

Fig. 9 Adamantane like tetrahedron by the group of M. Fujita [88–111]

encapsulated and unstable species could be stabilised [88–111] (Fig. 9). Furthermore, the cage could be used as a reaction vessel for various reactions like the Diels Alder reaction [112–116], photodimerisation [101, 107, 112, 115–120], photochemical 1,4-radical addition [121], photo oxidation [107, 122], Wacker oxidation [123, 124] or photochemical cyclisation [125].

The last type of tetrahedron once again exhibits the M_6L_4 topology, but the resulting cage is now more tightly closed. It is built again by four C_3 symmetric ligands which are much larger and able to connect metal ions on the edges of the cage (Fig. 10) [126, 127].

This type of cage molecules are synthesised by us and will be discussed in more detail in the corresponding paragraph.

In total, many different container molecules of various shapes like tetrahedra, octahedra, cubes, triangular bipyramids, dodecahedra, icosahedra, cuboctahedra or various shaped prisms or antiprisms have been described in the literature up to now [6–10]. Altogether they are far too many to be described in detail. Therefore this chapter focuses only on container molecules based on imine type ligands.

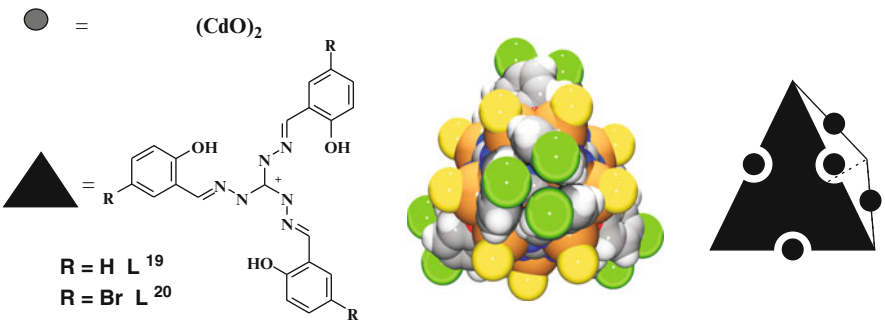

Fig. 10 M_6L_4 tetrahedra by the group of Iris M. Oppel [126, 127]

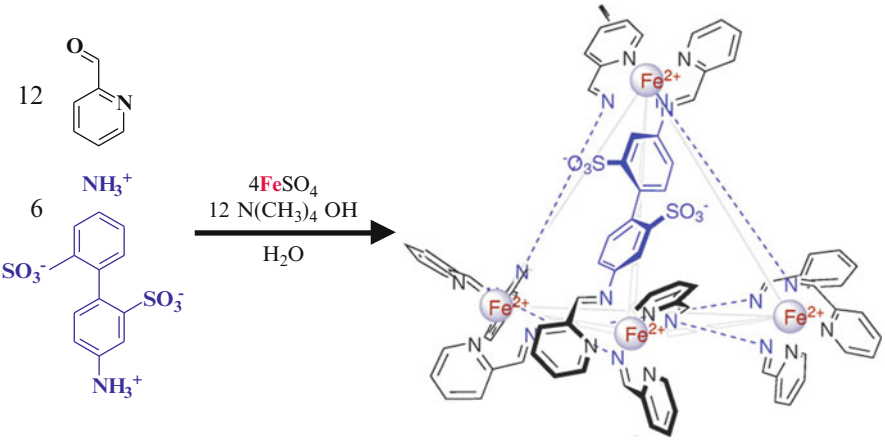

Fig. 11 Formation of the tetrahedron shaped cage by Jonathan R. Nitschke et al. [128]

2 M_4L_6 Tetrahedron for the Stabilisation of White Phosphorus and Gas Separation

The group of Jonathan R. Nitschke synthesised an anionic cage with the outer shape of a tetrahedron (M_4L_6 topology). This cage is capable of binding hydrophobic guests in aqueous solution and in the solid state. Known guest molecules are cyclopentane [128], cyclohexane [128], white phosphorus (P_4) [129, 130] and SF_6 [131].

The cage is formed as the unique product of the reaction of 4,4′-diaminobiphenyl-2,2′-disulfonic acid with 2-formylpyridine, iron(II) sulphate and tetramethylammonium hydroxide in an aqueous solution (Fig. 11). These compounds are all commercially available and inexpensive [128].

As iron atoms are exclusively in a low-spin state, the resulting diamagnetic compound is suitable for NMR spectroscopy. The solubility of the cage in H_2O with

34 g L^{-1} is probably caused by the sulfonate groups, which are arranged towards the exterior. The inner cavity of the cage is approximately 141 $Å^3$ in volume, as determined by X-ray diffraction. Molecules such as cyclopentane or cyclohexane fit in this void. Due to their size these molecules fill the cavity by 51% and 61% respectively, which is closed to the optimal 55% provided by the Rebek rule [132]. Due to the effect that cyclohexane is the favoured guest, the tetrahedron could be used for the separation of both hydrocarbons (Fig. 12) [128].

The cage, carrying cyclohexane inside, could be opened in two different ways. The first irreversible way is by adding tris(2-ethylamino)amine, so an imine exchange takes place and a new iron complex is formed (Fig. 13a). The other reversible way is by changing the pH value of the solution by adding *p*-toluenesulfonic acid (opening) or sodium bicarbonate (closing) [128, 132].

Beside the cyclic hydrocarbons, white phosphorus (P_4) could also be encapsulated. P_4 is an allotrope which is highly pyrophoric in an oxygen atmosphere. By means of this encapsulation the P_4 molecules became water-soluble and air-stable. This stability was confirmed by ^1H NMR spectra, which remained unchanged for over 4 months. The reason for the stability is not that the openings of the tetrahedron faces are too small for O_2 molecules to reach the interior. Instead, the proposed reason is that the first product built by the reaction of P_4 with O_2 is too big to fit inside the cavity of the cage any more. By adding benzene to an aqueous solution of the P_4-containing tetrahedron, a guest exchange takes place. This means the phosphorus is released, while the benzene is encapsulated, so the cage is

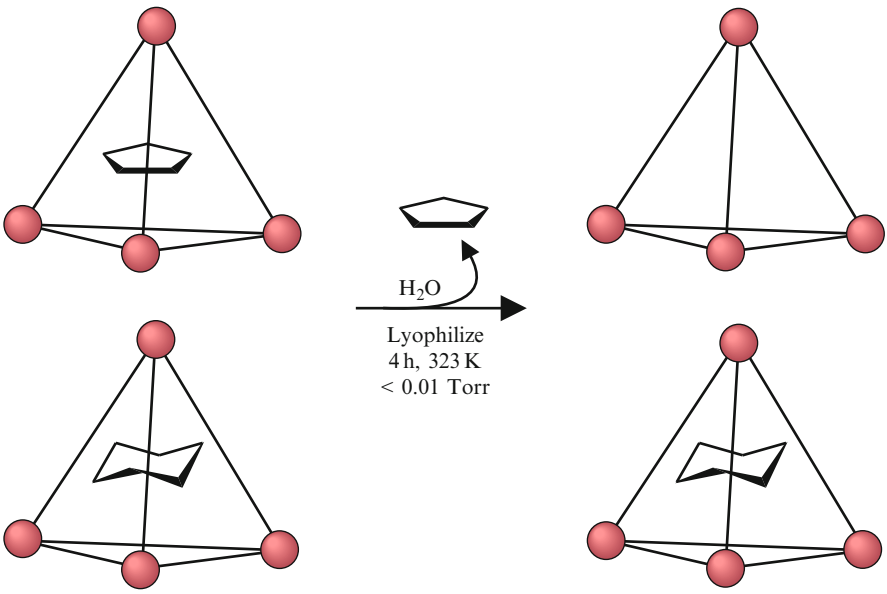

Fig. 12 Separation of cyclopentane and cyclohexane by the cage [128]

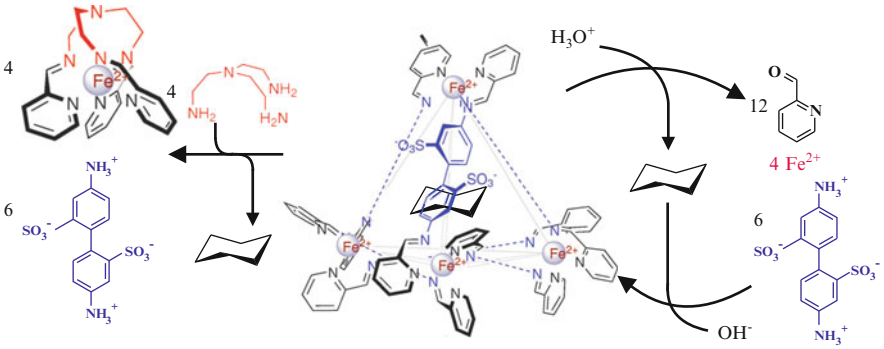

Fig. 13 Irreversible (*left*) and reversible (*right*) opening of the cage [128, 132]

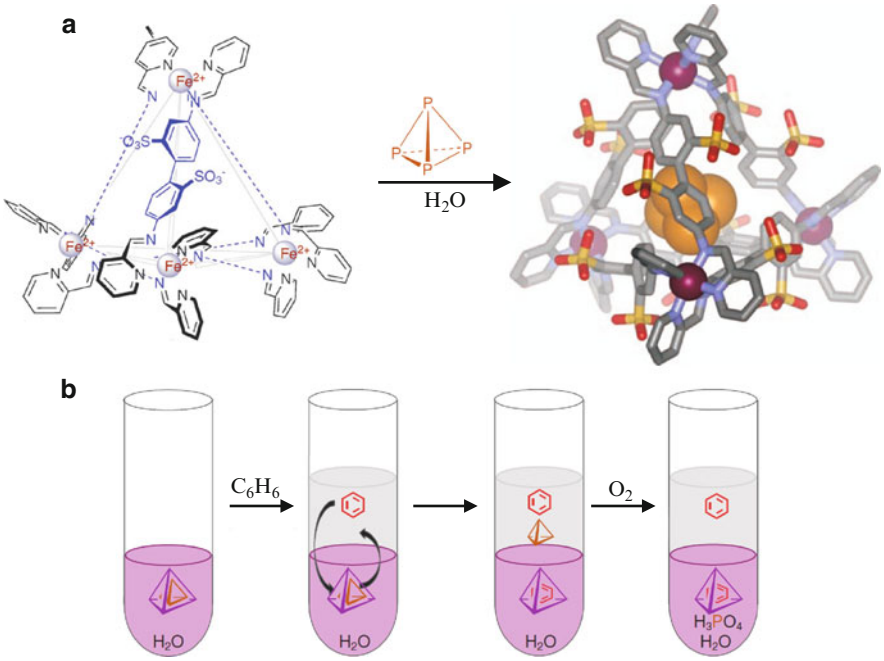

Fig. 14 (**a**) P_4 encapsulated in cage. (**b**) Release of P_4 [129, 130]

reusable. The released P_4 loses its stability and is oxidised by air forming H_3PO_4 (Fig. 14) [129, 130].

Another possible guest molecule is the chemically inert gas SF_6. This gas is known to be the most potent and long living greenhouse gas; 1 g is climatically equivalent to 24 kg of CO_2 [133, 134]. The gas could be bound within the cage not only in the solid state but also in solution. So it is one of the first examples of gas binding within a discrete coordination cage in solution. By trapping the gas inside

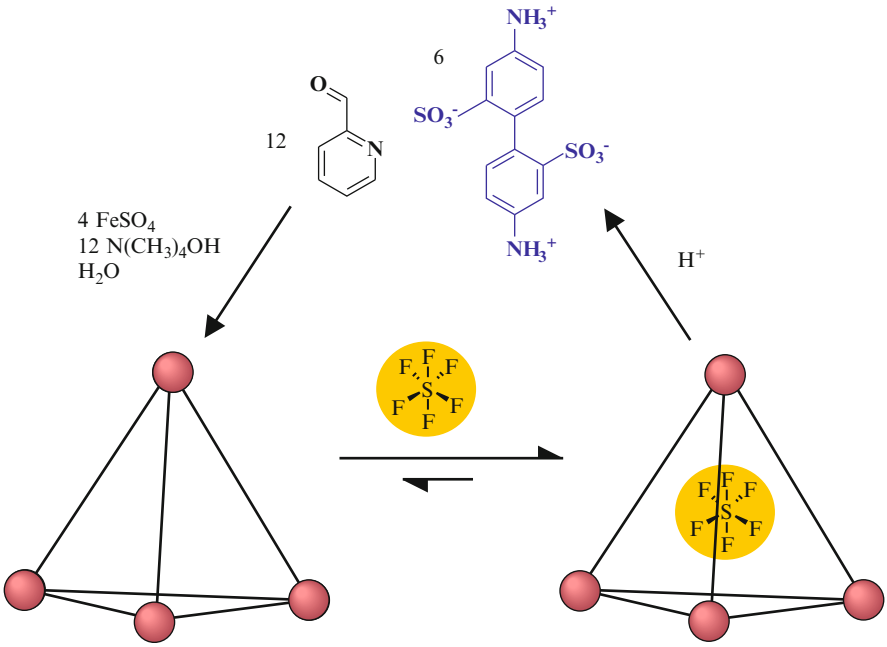

Fig. 15 Encapsulation of SF_6 [131]

the cage, its solubility in water could be increased about 30 times. The cage could also be used for the gas separation of SF_6 from Xe, Ar, N_2, O_2, C_2H_4, CO_2 or N_2O, because only SF_6 is encapsulated within the cage. This effect could be useful for the recycling of the gas (Fig. 15) [131].

3 M_4L_4 Tetrahedra with Successive Guest Exchange

Markus Albrecht and co-workers synthesised three M_4L_4 tetrahedra based on different C_3-symmetric imine type ligands. The ligands are shown in Fig. 16. For the formation of these ligands, 2,3-dihydroxybenzaldehyde was reacted with the product of the reduction of the corresponding trinitro derivative ($\mathbf{L^{21}}$) or with a tris-amine derivative ($\mathbf{L^{22}}$, $\mathbf{L^{23}}$) [30, 135–141].

The discrete coordination cages of the type $M_8[Ti_4(\mathbf{L^{21–23}})_4]$ ($M = Li^+$, Na^+ or K^+) are all formed by the reaction of the ligands with $TiO(acac)_2$ in the presence of M_2CO_3 ($M = Li^+$, Na^+ or K^+) in DMF (Fig. 17) [30, 135–141].

The resulting tetrahedra $[Ti_4(\mathbf{L^{21}})_4]^{8+}$ and $[Ti_4(\mathbf{L^{23}})_4]^{8+}$ differ in their outer size, as can be gauged by the Ti–Ti distances of 17 Å for $[Ti_4(\mathbf{L^{21}})_4]^{8+}$ and 23.5 Å for $[Ti_4(\mathbf{L^{23}})_4]^{8+}$. The larger cage also possesses wider openings on its faces but, in

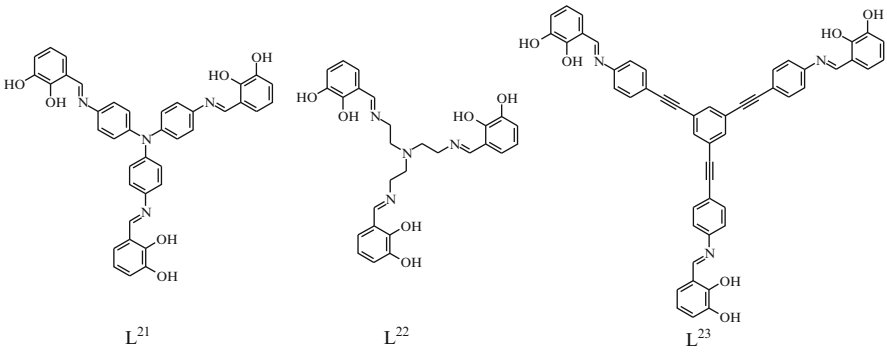

Fig. 16 Different C_3 symmetric ligands [30, 135–141]

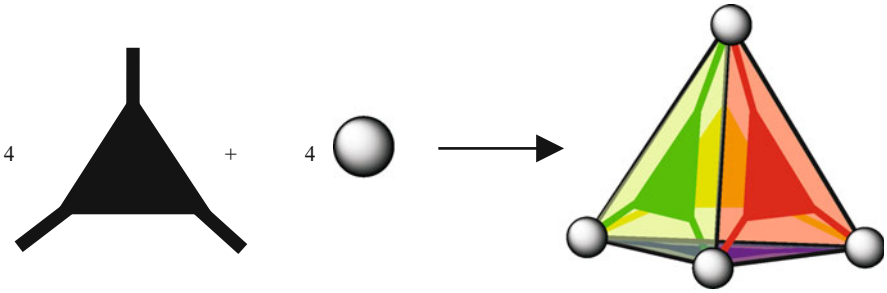

Fig. 17 Formation of the tetrahedra of Markus Albrecht et al. [30, 135–141]

contrast, the cavities of both cages are quite similar in size due to a twist in the spacer of $\mathbf{L^{23}}$ [139].

Earlier synthesised M_4L_4 cages have smaller cavities with no guest molecules inside [87, 142, 143]. In contrast, the interiors of the cages described by M. Albrecht are big enough to accommodate guest molecules and one example is now described in more detail.

Within the cage $M_8[Ti_4(\mathbf{L^{21}})_4]$ ($M = Li^+$, Na^+ or K^+) four counterions are bound to the internal oxygen atoms of the titanium tris(catecholate) units together with three DMF molecules per cation. Those counterions could be exchanged successively with primary ammonium ions as shown in Fig. 18. This exchange could be monitored by ^{1}H NMR spectroscopy, e.g. for the $Li_8[Ti_4(\mathbf{L^{21}})_4]$ complex [139].

4 M_4L_6 Tetrahedra as a Chemical Sensors

Chunhua Yan and coworkers designed "metal-tuneable" M_4L_6 tetrahedra. For the synthesis of these cages the group uses two different C_3-symmetric facial ligands. Both could be synthesised via a Schiff base reaction. The first is made by the

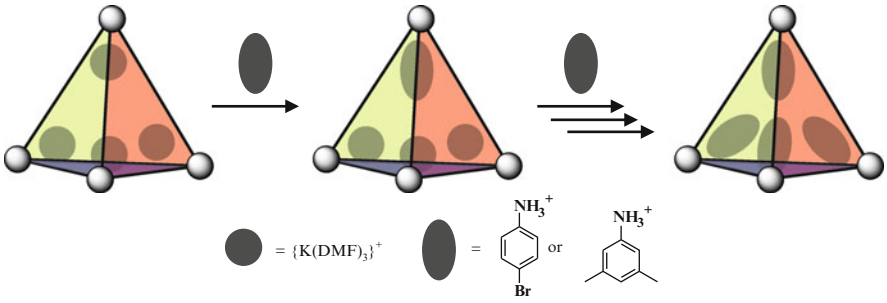

Fig. 18 Successive exchange of $\{K(DMF)_3\}^+$ against primary ammonium ions [139]

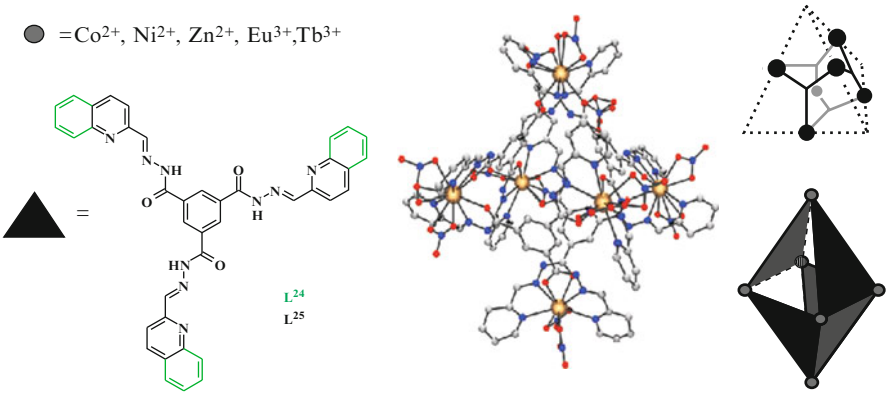

Fig. 19 Adamantane tetrahedra by Chunhua Yan and coworkers [144]

reaction of 2-quinoline carboxaldehyde with 1,3,5-tricarbohydrazine benzene in ethanol ($\mathbf{L^{24}}$). For the other ligand the quinoline function was replaced by a pyridine one ($\mathbf{L^{25}}$). In total, five similar coordination cages with five different metal ions were synthesised, two with $\mathbf{L^{24}}$ while using cobalt(II) or zinc(II) ions and three while reacting $\mathbf{L^{25}}$ with nickel(II), europium(III) or terbium(III) ions (Fig. 19) [144].

In the first ligand ($\mathbf{L^{24}}$), the three quinoline groups act as chromophores and fluorophores, so that host–guest interaction could lead to changes in the optical properties. Such changes can be measured by adding glucosamine (NH_2-Glu) to $[M_4(H_9(\mathbf{L^{24}}))_6]^{9+}$ ($M = Co^{2+}$, Zn^{2+}). The UV/Vis spectra for both cages show ligand-based charge-transfer bands in an acetonitrile solution (Fig. 20a). By adding NH_2-Glu a significant increase and decrease of the absorbance at about 345 and 420 nm, respectively, is observed. In addition to this effect the $[Zn_4(H_9(\mathbf{L^{24}}))_6]^{9+}$ cage also shows an increasing emission signal at 510 nm in its fluorescence spectra when NH_2-Glu is added (Fig. 20b) [144].

In contrast to these optical effects, the addition of glucose leads to no change in the spectra. This means that the synthesised cages $[M_4(H_9(\mathbf{L^{24}}))_6]^{9+}$

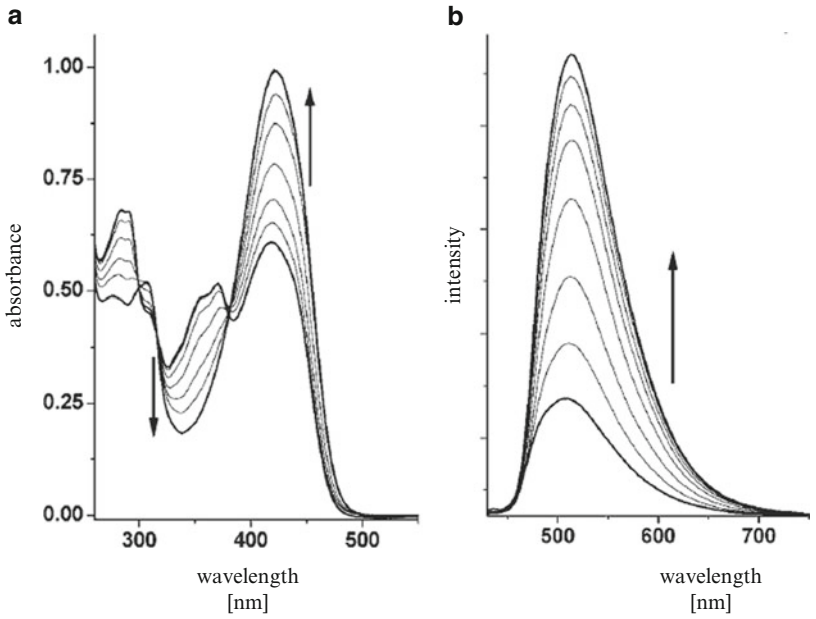

Fig. 20 (**a**) UV/Vis spectra and (**b**) fluorescence spectra (excitation at 380 nm) of $[Zn_4(H_9(\mathbf{L}^{\mathbf{24}}))_6]^{9+}$ [144]

Fig. 21 **a**) Glucose.
b) Glucoseamine (NH_2-Glu)

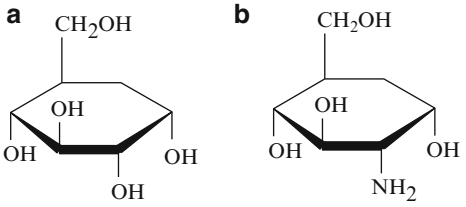

($M = Co^{2+}$, Zn^{2+}) could be used as optical sensors for the selective recognition of NH_2-Glu (Fig. 21) [144].

Modification of the ligand by replacing the quinoline with a pyridine group allows the introduction of lanthanoid ions (Eu^{3+}, Tb^{3+}) into the cage and luminescence properties [144].

5 Various Nearly Closed Coordination Cages

In our group we are interested in the formation of various shaped container molecules with different derivatives of tris(2-hydroxybenzylidene)triaminoguanidinium chloride ligand. These ligands could all be synthesised via a Schiff base

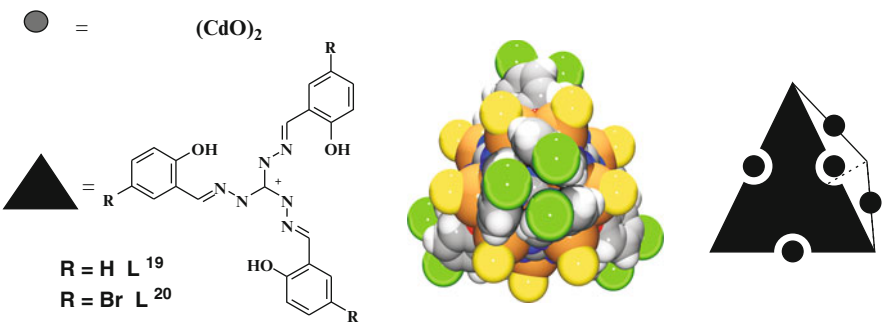

Fig. 22 M_6L_4 tetrahedra by the group of Iris M. Oppel [126, 127]

reaction in which triaminoguanidinium chloride is reacted with the corresponding benzaldehyde derivative. In the following figures (Figs. 22–25), each cage is shown together with the used derivative of the ligand [126, 127, 145–150].

By reacting the $\mathbf{L^{19}}$ or $\mathbf{L^{20}}$ with $CdCl_2{\cdot}2H_2O$ in the presence of Et_3N, a nearly closed coordination cage with the outer shape of a tetrahedron could be obtained. Each ligand coordinates three (CdCl)-units, and the triangular faces thus formed are linked by the phenolate oxygen bridging two neighbouring Cd atoms. In this way four membered $(CdO)_2$-rings are formed. The cavity size of the cages is approximately 180 $Å^3$. The interior is filled with Et_4N^+ or Et_3NH^+ and water respectively, as shown by X-ray diffraction (Fig. 22) [126, 127].

The cage $[Cd_6(\mathbf{L^{20}})_4]$ was also analysed via ESI mass spectroscopy, which confirmed that the guest molecules are Et_3NH^+ and H_2O. In addition, the analysis shows that the tetrahedron is also stable in the gas phase [127].

Another cage which could be designed with ligand $\mathbf{L^{19}}$ features the shape of an octahedron. For this synthesis the principle of the molecular library method was used. This means that a planar C_3 symmetric ligand was reacted with the square planar metal ion Pd^{2+}. The ligand system is known to bind the metal ions in a tris chelating manner. So only one coordination site of the Pd^{2+} ion is left. To connect the generated triangular faces, a coligand which provides the right connection angle of 109.5° is required. In this case the used coligand is sodium 5,5-diethylbarbiturate, whose binding angle for this compound is known to be about 108–117°. All three components react together with Et_4NCl and Et_3N in a mixture of acetonitrile and water to build a tightly closed octahedron of M_6L_8 topology, $Na_4[Et_3NH]_{12}[\{Pd_3(\mathbf{L^{19}})\}_8\{\mu\text{-}(bar)\}_{12}]{\cdot}xH_2O$ (Fig. 23). The inner cavity is about 1,600 $Å^3$, filled with four Na^+ ions and approximately 20 water molecules. The octahedron is again tightly closed with H···H-distances of 2.5 Å observed at the corners [147].

Such an octahedron could not be synthesised with $\mathbf{L^{20}}$ in contrast to the tetrahedron, because the additional bromine atoms would point towards each other at unacceptably short distances at each of the corners. The only way to connect these larger triangles as faces of a capsule together is to form a trigonal

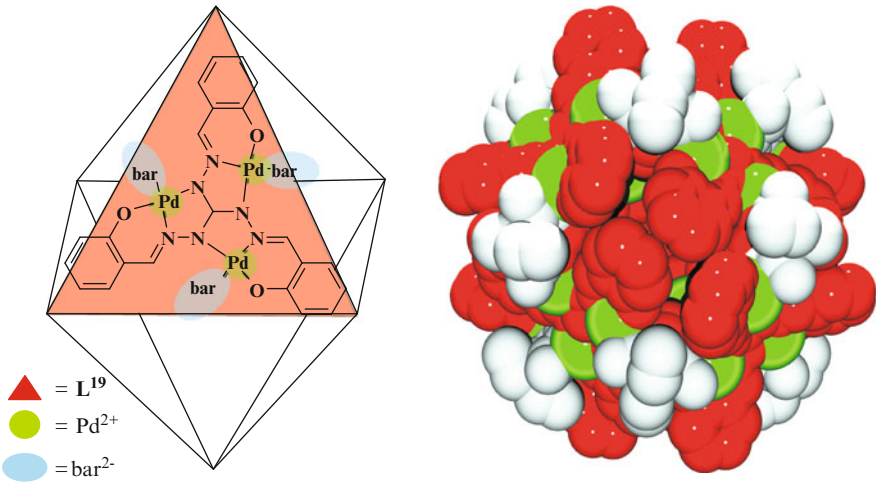

Fig. 23 Tightly closed M_6L_8 octahedron [147]

bipyramid, which requires the linkage of only six faces instead of eight. That is exactly what was observed in the reaction of $\mathbf{L^{20}}$, Pd(II), NaHbar, Et_4NCl and Et_3N. The resulting trigonal bipyramid, $(Et_3NH)_6(Et_4N)_6[\{Pd_3(\mathbf{L^{20}})\}_6(\mu\text{-bar})_9\text{–}(Hbar)_9]$ is depicted in Fig. 24. The influence of the bromine atoms can be illustrated by comparing the Br–Br distances of the corners. The axial corners of the cage show Br–Br distances of 6.20(8)–6.24(8) Å while the equatorial ones are more open (5.15(8)–12.4(2) Å). The inner volume of the cage is again about 1600 $Å^3$, and its cavity is time occupied by four Et_3NH^+ and one Et_4N^+ counter cations [148].

Parallel to the formation of the trigonal bipyramid an open tetrahedron of the composition $(Et_3NH)(Et_4N)_4[\{Pd_3(\mathbf{L^{20}})\}_4(\mu\text{-bar})_4(Hbar)_4]$ is always formed in the same synthesis. The cavity is approximately 800 $Å^3$ in size. This cage can also be described as an incomplete triangular bipyramid, with two faces missing. These two compounds show clearly the influence of the counter cations. Within the trigonal bipyramid four Et_3NH^+ and one Et_4N^+ are encapsulated while within the open tetrahedron one can find no Et_3NH^+ but three Et_4N^+ ions [148].

If a mixture of $\mathbf{L^{20}}$ and $\mathbf{L^{25}}$ is reacted with the smaller metal ion Zn^{2+} in the presence of Et_3N in MeOH, another type of cage is formed. Previously zinc complexes synthesised with the derivatives of $\mathbf{L^{19}}$ show that the zinc ion does not fit as well as Cd^{2+} into the plane of the ligand. The ions are screwed out of the plane. That means it should be possible to connect them more easily with the phenolate oxygen of another ligand or a coligand. In fact two $Zn_3(\mathbf{L^{19}})$-building blocks can be connected by three methanolate coligands. Both ligands are connected via a methoxy group and in this way they form a kind of triangular double layer face. If these building blocks are made asymmetrical by the use of one small and one large derivative of $\mathbf{L^{19}}$, they can form a tetrahedron with the outer shape of a double

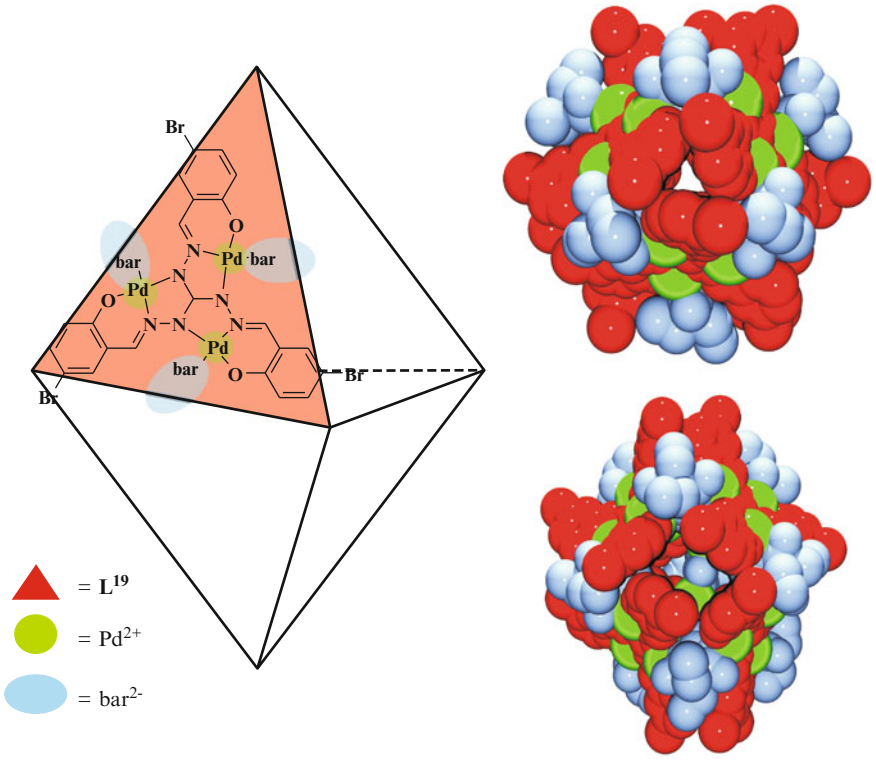

Fig. 24 Trigonal bipyramid [148]

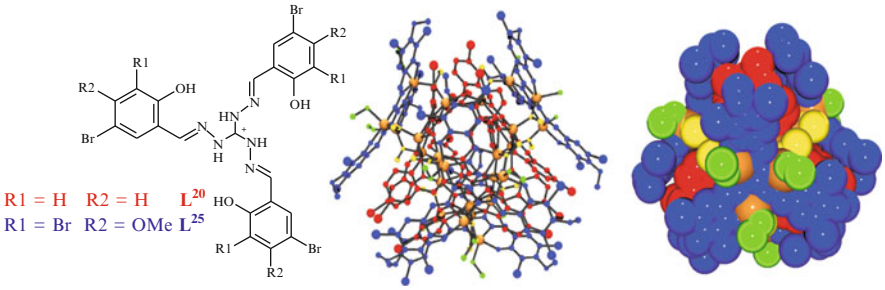

Fig. 25 Double walled tetrahedron [149]

walled tetrahedron $((Et_3NH)_4(H_2O)[\{Zn_3(\{\mu\text{-}(OCH_3)\}_3\{Zn_3(solvent)_3(\mathbf{L^{25}})\})(\mathbf{L^{20}})\}_4]$, solvent = MeOH, H_2O). This cage is additionally stabilised by weak $OCH_3\cdots$Br interactions (3.1 Å) at each corner. The cavity (~180 Å^3) is occupied by one Et_4N^+ cation (Fig. 25) [149].

6 Conclusion

Container molecules in general show an increasing number of applications and so do the container molecules based on imine type ligands. Many different shapes of open or nearly closed ones could already be synthesised. Those cages are known to encapsulate different types of guest molecules. This encapsulation can be selective and permanent or reversible. The container molecules described are also used for stabilisation of different compounds such as the allotrope P_4. They can be used as gas or optical sensors. One of the described cages can also be opened and closed selectively.

In summary, container molecules open a wide field of unknown opportunities in chemistry, with more and more interesting and useful applications to be expected.

References

1. Zhao D, Timmons DJ, Yuan D, Zhou H-C (2011) Acc Chem Res. doi:10.1021/ar100112y
2. Bordiga S, Bonino F, Lillerud KP, Lamberti C (2010) Chem Soc Rev 12:39
3. Meilikhov M, Yusenko K, Esken D, Turner S, Van Tendeloo G, Fischer RA (2010) Eur J Inorg Chem 24:3701
4. Guo M, Cai H-L, Xiong R-G (2010) Inorg Chem Commun 13:1590
5. Silva CG, Corma A, Garcia H (2010) J Mater Chem 20:3141
6. Stephenson A, Argent SP, Riis-Johannessen T, Tidmarsh IS, Ward MD (2011) J Am Chem Soc 133:858
7. Breiner B, Clegg JK, Nitschke JR (2011) Chem Sci 2:51
8. Yoshizawa M, Fujita M (2010) Bull Chem Soc Jpn 83:609
9. Ward MD (2009) Chem Commun 4487
10. Perry JJ, Perman JA, Zaworotko MJ (2009) Chem Soc Rev 38:1400
11. Farha OK, Yazaydin AÖ, Eryazici I, Malliakas CD, Hauser BG, Kanatzidis MG, Nguyen S, Snurr RQ, Hupp JT (2010) Nat Chem 2:944
12. Sava DF, Kravtsov VC, Eckert J, Eubank JF, Nouar F, Eddaoudi M (2009) J Am Chem Soc 131:10394
13. Lin X, Telepeni I, Blake AJ, Dailly A, Brown CM, Simmons JM, Zoppi M, Walker GS, Thomas KM, Mays TJ, Hubberstey P, Champness NR, Schröder M (2009) J Am Chem Soc 131:2159
14. Murray LJ, Dinca M, Long JR (2009) Chem Soc Rev 38:1294
15. Kaye SS, Dailly A, Yaghi OM, Long JR (2007) J Am Chem Soc 129:14176
16. Furukawa H, Yaghi OM (2009) J Am Chem Soc 131:8875
17. Koh K, Wong-Foy AG, Matzger AJ (2009) J Am Chem Soc 131:4184
18. Rosi NL, Eckert J, Eddaoudi M, Vodak DT, Kim J, O'Keeffe M, Yaghi OM (2003) Science 300:1127
19. Eddaoudi M, Kim J, Rosi N, Vodak D, Wachter J, O'Keeffe M, Yaghi OM (2002) Science 295:469
20. Li J-R, Kuppler RJ, Zhou H-C (2009) Chem Soc Rev 38:1477
21. Ma L, Abney C, Lin W (2009) Chem Soc Rev 38:1248
22. Lee J, Farha OK, Roberts J, Scheidt KA, Nguyen ST, Hupp JT (2009) Chem Soc Rev 38:1450
23. Allendorf MD, Bauer CA, Bhakta RK, Houk RJT (2009) Chem Soc Rev 38:1330
24. Min KS, Suh PM (2000) J Am Chem Soc 122:6834
25. An J, Geib JS, Rosi NL (2009) J Am Chem Soc 131:8376

26. Albrecht M (2010) Z Anorg Allg Chem 636:2198
27. Zheng X-D, Lu T-B (2010) Cryst Eng Commun 12:324
28. Hiratani K, Albrecht M (2008) Chem Soc Rev 37:2413
29. He C, Zhao Y, Guo D, Lin Z, Duan C (2007) Eur J Inorg Chem 3451
30. Albrecht M, Janser I, Fröhlich R (2005) Chem Commun 157
31. Ning G-H, Yao L-Y, Liu L-X, Xie T-Z, Li Y-Z, Qin Y, Pan Y-J, Yu S-Y (2010) Inorg Chem 49:7783
32. North BH, Zheng Y-R, Chi K-W, Stang PJ (2009) Acc Chem Res 42:1554
33. Li S-S, Northrop BH, Yuan Q-H, Wan L-J, Stang PJ (2009) Acc Chem Res 42:249
34. Kumar A, Sun S-S, Lees AJ (2008) Coord Chem Rev 252:922
35. Lee SJ, Lin W (2008) Acc Chem Res 41:521
36. Campos-Fernández CS, Schottel BL, Chifotides HT, Bera JK, Bacsa J, Koomen JM, Russell DH, Dunbar KR (2005) J Am Chem Soc 127:12909
37. Müller J, Lippert B (2006) Angew Chem Int Ed 45:2503
38. Oleksi A, Blanco AG, Boer R, Usón I, Aymamí J, Rodger A, Hannon MJ, Coll M (2006) Angew Chem Int Ed 45:1227
39. Hannon MJ, Moreno V, Prieto MJ, Moldrheim E, Sletten E, Meistermann I, Isaac CJ, Sanders KJ, Rodger A (2001) Angew Chem Int Ed 40:879
40. Hannon MJ, Painting CL, Jackson A, Hamblin J, Errington W (1997) Chem Commun 1807
41. Meistermann I, Moreno V, Prieto MJ, Moldrheim E, Sletten E, Khalid S, Mark Rodger P, Peberdy JC, Isaac CJ, Rodger A, Hannon MJ (2002) Proc Natl Acad Sci USA 99:5069
42. Stang PJ (1998) Chem Eur J 4:19
43. Saalfrank RW, Stark A, Peters K, von Schnering HG (1988) Angew Chem 100:878
44. Caulder DL, Raymond KN (1999) Acc Chem Res 32:975
45. Leung DH, Bergman RG, Raymond KN (2007) J Am Chem Soc 129:2746
46. Andersen UN, Seeber G, Fiedler D, Raymond KN, Lin D, Harris D (2006) J Am Soc Mass Spectrom 17:292
47. Ziegler M, Davis AV, Johnson DW, Raymond KN (2003) Angew Chem 115:689
48. Davis AV, Yeh RM, Raymond KN (2002) Proc Natl Acad Sci USA 99:4793
49. Ziegler M, Miranda JJ, Andersen UN, Johnson DW, Leary JA, Raymond KN (2001) Angew Chem 113:755
50. Terpin AJ, Ziegler M, Johnson DW, Raymond KN (2001) Angew Chem 113:161
51. Caulder DL, Raymond KN (1999) Dalton Trans 1185
52. Pluth MD, Bergman RG, Raymond KN (2008) J Org Chem 73:7132
53. Biros SM, Bergman RG, Raymond KN (2007) J Am Chem Soc 129:12094
54. Pluth MD, Raymond KN (2007) Chem Soc Rev 36:161
55. Pluth MD, Johnson DW, Szigethy G, Davis AV, Teat SJ, Oliver AG, Bergman RG, Raymond KN (2009) Inorg Chem 48:111
56. Pluth MD, Bergman RG, Raymond KN (2008) J Am Chem Soc 130:6362
57. Leung DH, Bergman RG, Raymond KN (2008) J Am Chem Soc 130:2798
58. Pluth MD, Tiedemann BEF, van Halbeek H, Nunlist R, Raymond KN (2008) Inorg Chem 47:1411
59. Davis AV, Fiedler D, Ziegler M, Terpin AJ, Raymond KN (2007) J Am Chem Soc 129:15354
60. Tiedemann BEF, Raymond KN (2007) Angew Chem 119:5064
61. Leung DH, Bergman RG, Raymond KN (2006) J Am Chem Soc 128:9781
62. Davis AV, Fiedler D, Seeber G, Zahl A, van Eldik R, Raymond KN (2006) J Am Chem Soc 128:1324
63. Fiedler D, Bergman RG, Raymond KN (2006) Angew Chem 118:759
64. Tiedemann BEF, Raymond KN (2006) Angew Chem 118:89
65. Davis AV, Raymond KN (2005) J Am Chem Soc 127:7912
66. Fiedler D, Leung DH, Bergman RG, Raymond KN (2005) Acc Chem Res 38:349
67. Brumaghim JL, Michels M, Raymond KN (2004) Eur J Org Chem 4552
68. Fiedler D, Leung DH, Bergman RG, Raymond KN (2004) J Am Chem Soc 126:3674

69. Leung DH, Fiedler D, Bergman RG, Raymond KN (2004) Angew Chem 116:981
70. Fiedler D, Pagliero D, Brumaghim JL, Bergman RG, Raymond KN (2004) Inorg Chem 43:846
71. Parac TN, Scherer M, Raymond KN (2000) Angew Chem 112:1288
72. Sgarlata C, Mugridge JS, Pluth MD, Tiedemann BEF, Zito V, Arena G, Raymond KN (2010) J Am Chem Soc 132:1005
73. Mugridge JS, Bergman RG, Raymond KN (2010) J Am Chem Soc 132:1182
74. Mugridge JS, Bergman RG, Raymond KN (2010) Angew Chem Int Ed 49:3635
75. Pluth MD, Bergman RG, Raymond KN (2007) J Am Chem Soc 129:11459
76. Dong VM, Fiedler D, Carl B, Bergman RG, Raymond KN (2006) J Am Chem Soc 128:14464
77. Brumaghim JL, Michels M, Pagliero D, Raymond KN (2004) Eur J Org Chem 5115
78. Ziegler M, Brumaghim JL, Raymond KN (2000) Angew Chem 112:4285
79. Hastings CJ, Fiedler D, Bergman RG, Raymond KN (2008) J Am Chem Soc 130:10977
80. Fiedler D, van Halbeek H, Bergman RG, Raymond KN (2006) J Am Chem Soc 128:10240
81. Fiedler D, Bergman RG, Raymond KN (2004) Angew Chem 116:6916
82. Pluth MD, Bergman RG, Raymond KN (2009) J Org Chem 74:58
83. Pluth MD, Bergman RG, Raymond KN (2008) J Am Chem Soc 130:11423
84. Pluth MD, Bergman RG, Raymond KN (2007) Angew Chem 119:8741
85. Pluth MD, Bergman RG, Raymond KN (2007) Science 316:85
86. Hastings CJ, Pluth MD, Bergman RG, Raymond KN (2010) J Am Chem Soc 132:6938
87. Amoroso AJ, Jefferey JC, Jones PL, McCleverty JA, Thornton P, Ward MD (1995) Angew Chem Int Ed Engl 34:1443
88. Fujita M, Umemoto K, Yoshizawa M, Fujita N, Kusukawa T, Biradha K (2001) Chem Commun 509
89. Yamashita K, Kawano M, Fujita M (2007) Chem Commun 4102
90. Tashiro S, Fujita M (2006) Bull Chem Soc Jpn 79:833
91. Tashiro S, Tominaga M, Kawano M, Therrien B, Ozeki T, Fujita M (2005) J Am Chem Soc 127:4546
92. Yoshizawa M, Kusukawa T, Kawano M, Ohhara T, Tanaka I, Kurihara K, Niimura N, Fujita M (2005) J Am Chem Soc 127:2798
93. Kumazawa K, Yoshizawa M, Liu H-B, Kamikawa Y, Moriyama M, Kato T, Fujita M (2005) Chem Eur J 11:2519
94. Yoshizawa M, Tamura M, Fujita M (2004) J Am Chem Soc 126:6846
95. Kusukawa T, Fujita M (2002) J Am Chem Soc 124:13576
96. Sun W-Y, Kusukawa T, Fujita M (2002) J Am Chem Soc 124:11570
97. Kusukawa T, Yoshizawa M, Fujita M (2001) Angew Chem 113:1931
98. Sakamoto S, Yoshizawa M, Kusukawa T, Fujita M, Yamaguchi K (2001) Org Lett 3:1601
99. Ibukuro F, Kusukawa T, Fujita M (1998) J Am Chem Soc 120:8561
100. Kusukawa T, Fujita M (1998) Angew Chem 110:3327
101. Sun W-Y, Yoshizawa M, Kusukawa T, Fujita M (2002) Curr Opin Chem Biol 6:757
102. Maurizot V, Yoshizawa M, Kawano M, Fujita M (2006) Dalton Trans 2750
103. Nakabayashi K, Kawano M, Kato T, Furukawa K, Ohkoshi S, Hozumi T, Fujita M (2007) Chem Asian J 2:164
104. Kawano M, Kobayashi Y, Ozeki T, Fujita M (2006) J Am Chem Soc 128:6558
105. Kobayashi Y, Kawano M, Fujita M (2006) Chem Commun 4377
106. Nakabayashi K, Kawano M, Fujita M (2005) Angew Chem 117:5456
107. Yoshizawa M, Fujita M (2005) Pure Appl Chem 77:1107
108. Nakabayashi K, Kawano M, Yoshizawa M, Ohkoshi S, Fujita M (2004) J Am Chem Soc 126:16694
109. Yoshizawa M, Kusukawa T, Fujita M, Sakamoto S, Yamaguchi K (2001) J Am Chem Soc 123:10454
110. Yoshizawa M, Kusukawa T, Fujita M, Yamaguchi K (2000) J Am Chem Soc 122:6311
111. Kusukawa T, Fujita M (1999) J Am Chem Soc 121:1397

112. Nishioka Y, Yamaguchi T, Yoshizawa M, Fujita M (2007) J Am Chem Soc 129:7000
113. Yoshizawa M, Tamura M, Fujita M (2006) Science 312:251
114. Kusukawa T, Nakai T, Okano T, Fujita M (2003) Chem Lett 32:284
115. Murase T, Horiuchi S, Fujita M (2010) J Am Chem Soc 132:2866
116. Horiuchi S, Nishioka Y, Murase T, Fujita M (2010) Chem Commun 46:3460
117. Nishioka Y, Yamaguchi T, Yoshizawa M, Fujita M (2008) J Am Chem Soc 130:8160
118. Takaoka K, Kawano M, Ozeki T, Fujita M (2006) Chem Commun 1625
119. Yoshizawa M, Takeyama Y, Okano T, Fujita M (2003) J Am Chem Soc 125:3243
120. Yoshizawa M, Takeyama Y, Kusukawa T, Fujita M (2002) Angew Chem 114:1403
121. Yamaguchi T, Fujita M (2008) Angew Chem 120:2097
122. Yoshizawa M, Miyagi S, Kawano M, Ishiguro K, Fujita M (2004) J Am Chem Soc 126:9172
123. Yoshizawa M, Sato N, Fujita M (2005) Chem Lett 34:1392
124. Ito A, Kusukawa T, Fujita M (2000) Chem Lett 29:598
125. Furusawa T, Kawano M, Fujita M (2007) Angew Chem 119:5819
126. Müller IM, Robson R, Separovic F (2001) Angew Chem Int Ed 40:4385
127. Müller IM, Möller D, Schalley CA (2005) Angew Chem Int Ed 44:480
128. Mal P, Schultz D, Beyeh K, Rissanen K, Nitschke JR (2008) Angew Chem Int Ed 47:8297
129. Mal P, Breiner B, Rissanen K, Nitschke JR (2009) Science 324:1697
130. Raymond KN (2009) Nature 460:585
131. Riddell IA, Smulders MMJ, Clegg JK, Nitschke JR (2011) Chem Commun 47:457
132. Mal P, Nitschke JR (2010) Chem Commun 46:2417
133. Maiss M, Brenninkmeijer CAM (1998) Environ Sci Technol 32:3077
134. Lindley AA, McCulloch A (2005) J Flour Chem 126:1457
135. Aguiari A, Bullita E, Casellato U, Guerriero P, Tamburini S, Vigato PA, Russo U (1994) Inorg Chim Acta 219:135
136. Aguiari A, Bullita E, Casellato U, Guerriero P, Tamburini S, Vigato PA (1992) Inorg Chim Acta 202:157
137. Albrecht M, Janser I, Meyer S, Weis P, Fröhlich R (2003) Chem Commun 2854
138. Albrecht M, Janser I, Runink J, Raabe G, Weis P, Fröhlich R (2004) Angew Chem 116:6832
139. Albrecht M, Janser I, Burk S, Weis P (2006) Dalton Trans 2875
140. Albrecht M, Burk S, Weis P, Schalley CA, Kogej M (2007) Synthesis 23:3736
141. Albrecht M, Janser I, Fröhlich R (2004) Synthesis 12:1977
142. Brückner C, Powers RE, Raymond KN (1998) Angew Chem Int Ed 37:1837
143. Saalfrank RW, Glaser H, Demleitner B, Hampel F, Chowdhry MM, Schünemann V, Trautwein AX, Vaughan GBM, Yeh R, Davis AV, Raymond KN (2002) Chem Eur J 8:493
144. He C, Lin Z, He Z, Duan C, Xu C, Wang Z, Yan C (2008) Angew Chem 120:891
145. Müller IM, Robson R (2000) Angew Chem Int Ed 39:4357
146. Müller IM, Möller D (2005) Eur J Inorg Chem 257
147. Müller IM, Spillmann S, Franck H, Pietschnig R (2004) Chem Eur J 10:2207
148. Müller IM, Möller D (2005) Angew Chem Int Ed 44:2969
149. Oppel (neé Müller) IM, Föcker K (2008) Angew Chem Int Ed 47:402
150. Müller IM, Möller D, Föcker K (2005) Chem Eur J 11:3318

Top Curr Chem (2012) 319: 99–124
DOI: 10.1007/128_2011_279

Published online: 8 December 2011

Molecular Capsules Derived from Resorcin[4]arenes by Metal-Coordination

Tobias Schröder, Satya Narayan Sahu, and Jochen Mattay

Abstract A short introduction to the fundamental features and recent developments of supramolecular chemistry is presented besides defining scope and limitation of this review article. A brief overview about calix[n]arenes and especially resorcin[4]arenes and their conformationally rigid cavitands is given. Selected examples are presented to demonstrate the dependence of self-assembly of cavitands exhibiting different flexibility either due to their basic macrocycle or due to flexible receptor units commonly located at the *o,o′*-position of the resorcinarene ring. In addition, the process of self-assembly is also controlled by metal coordination geometry as shown by one example. The receptor units may also be connected at the methylene group of the cavitand as shown by one example. Examples of supramolecular architectures are presented utilizing the special features of 2,2′:6′,2″-terpyridine (terpy) metal-binding ligand. The synthesis and characterization of a metallo-supramolecular Zn-coordination cage with a diameter of 4–5 nm based on a cavitand-terpy building block is presented in detail.

Keywords Cavitand · Metal coordination · Resorcin[4]arene · Self-assembly · Supramolecular chemistry · Terpyridine ligand

Contents

T. Schröder, S.N. Sahu, and J. Mattay (✉)
Organic Chemistry I, Faculty of Chemistry, Bielefeld University, Bielefeld, Germany
e-mail: tobias.schroeder4@t-online.de; mattay@uni-bielefeld.de

1 Introduction

1.1 General

Concepts of supramolecular chemistry have changed the way scientists perceive chemical structures: not as independent entities but as interacting structures. The "chemistry beyond the molecule" has opened the view to understand, design, and use assemblies of molecules [1, 2]. Starting with the development of ligand-receptor systems to explore the basic principles of molecular recognition, the increasing systematization of supramolecular binding motifs and building blocks has facilitated self-assembly by design, yielding impressive architectures, and stimulating chemistry, biology, physics, and material sciences [3]. The wide implementation is reflected in the research areas, such as supramolecular catalysis [4], supramolecular polymers [5], and supramolecular electronics [6]. Adaptive chemical systems, which can be obtained by taking advantage of the weakness of supramolecular bonds and the reversibility of the formation of supramolecular structures, are subjects of current research interest.[7] Besides exploring the prospects offered by supramolecular chemistry in various fields, a deeper understanding of its principles remains a basic challenge. Two important aspects are generally governed during the formation of a supramolecular capsule which are the controlled self-assembly of hollow architectures and the dynamic strength of interactions between building blocks.

Moreover, the inner cavity of supramolecular capsules provides a discrete, well-defined environment ideally suited to investigate effects of compartmentalization and processes in confined spaces [8]. To realize technical applications as detection and stabilization of encapsulated molecules or their use as nano-sized reaction vessels, precise control of important factors such as size, stability, porosity of the walls, and functionalization of the inner surface have to be achieved [9–18]. Several capsules have been synthesized and a proof of principle for several applications has been provided, but in most cases their use is restricted to small guest molecules. The development of spacious architectures which are able to encapsulate several bulky molecules and are amenable for decoration of the inner surface with functional groups will constitute an important step on the way to functional systems.

The stability of supramolecular binding motifs defines the degree of reversibility during self-assembly and therefore the ability for self-correction, ensures the integrity of the structure, and controls the adaptability to environmental changes [3]. Connecting building blocks via multiple hydrogen bonds is one of the most

frequently used strategies to obtain dynamic structures. The combination of predictable orientation and fast equilibration accounts for the increasing interest in employing hydrogen bonds in supramolecular design principles [19–21]. On the other hand, metal-coordination-driven self-assembly has become another tool for creating a variety of multicomponent self-assemblies due to the possibility of a large number of combinations of coordination motifs and ligands. Therefore metal-coordinated self-assembly is being intensely developed as a promising approach to design supramolecular cage architectures possessing nanoscale cavities [22–25]. Moreover, the directional bonding nature facilitated by the metal ion defines a higher structural control over the coordination geometries while the thermodynamic properties of metal-ligand bonding regulate the overall stability of the giant coordination cages.

1.2 Scope

This chapter concentrates on a special type of monomeric building block, namely the cavitands (derived from resorcin[4]arenes), and is restricted to capsules formed by metal coordination rather than H-bonding. Beside reviewing some selected examples of metal-coordination cages from the literature (Sect. 3) emphasis is laid on molecular architectures involving terpyridine (tpy) ligands as connecting units (Sect. 4) and on results from our own laboratory (Sect. 5) rather than to give a comprehensive overview about molecular capsules derived from calix[n]arenes in general [26]. Such a comprehensive review article covering aspects of covalent as well as supramolecular capsules involving all types of non-covalent interactions is currently in production [27]. Readers interested in the modern analytical methods used in supramolecular chemistry and especially in a new method of studying the complexation dynamics by Single Molecule Force Spectroscopy are referred to [28, 29].

2 Cavitands and Calix[n]arenes: Building Blocks for Supramolecular Capsules

The synthesis of hollow architectures based on cavitands started in 1985, when Cram et al. reported on the inclusion of solvent molecules in a carcerand obtained by covalent linkage of two cavitands [30]. Since then, molecular and supramolecular capsules have been prepared from cavitands and calix[n]arenes due to two important properties: the bowl-shaped form and the various functionalizations which can be introduced at the *upper rim* of the cavitands or the *wider rim* of the calix[n]arenes (Fig. 1).

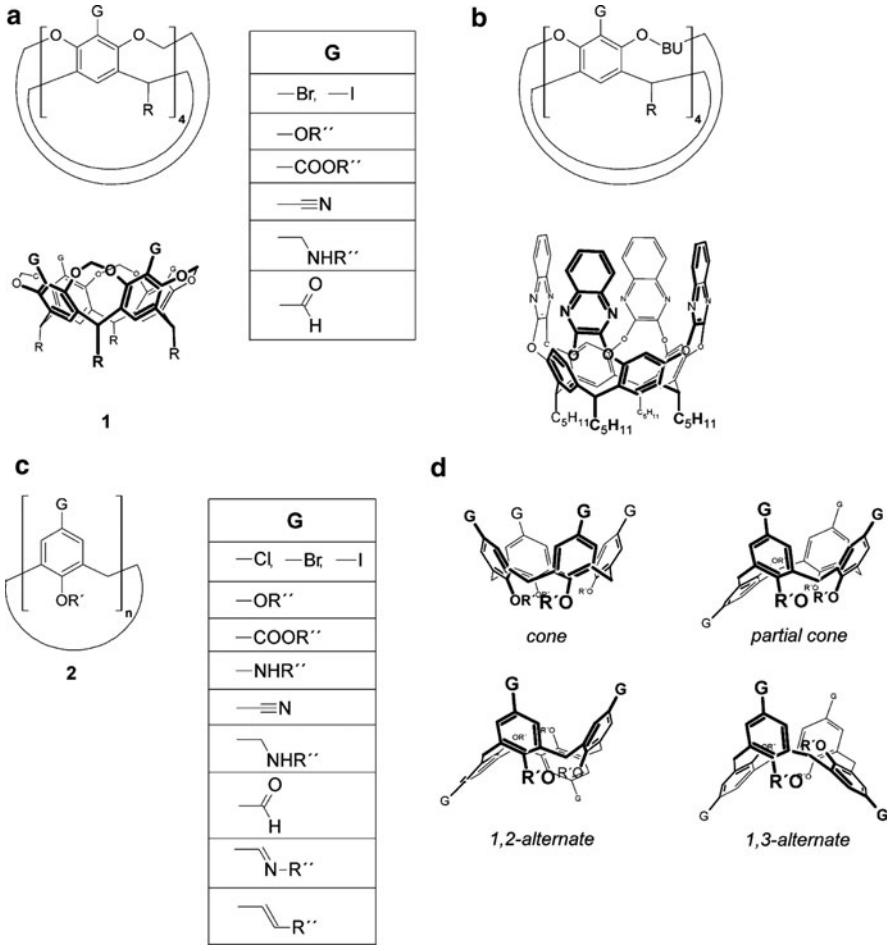

Fig. 1 **(a)** Structure of a methylene-bridged cavitand **1** substituted with functional groups (G) at the *upper rim*. **(b)** General structure of cavitands with different bridging units (BU) and one example of an aryl-bridged cavitand [38]. **(c)** Structure of calix[n]arenes **2** with functional groups (G) at the *wider rim*. **(d)** Conformations of calix[4]arenes

While the conformation of the methylene-bridged cavitands **1** is fixed (Fig. 1a), a number of more flexible cavitands with other bridging units (BU) have been prepared (Fig. 1b) [31, 32]. Depending on the substituent R′ at phenolic oxygen and the group (G) attached to the *wider rim*, the calix[n]arenes **2** can adopt different conformations (Fig. 1c, d) [33, 34]. The calix[n]arenes with more than four phenol units in the cyclophane basis are particularly flexible.

Because cavitands and calix[n]arenes with various functional groups (G) can be synthesized, a range of reactions can be applied to obtain substituted derivatives. Some of these molecules can be used as receptors for neutral molecules and ions, for the synthesis of stationary phases for chromatography and as catalysts for

organic reactions [34–37]. In the following sections it will be shown that cavitands which can be easily synthesized from resorcin[4]arenes (a subgroup of calix[n] arenes) are valuable building blocks for complex structures such as supramolecular capsules due to the unique combination of shape and functional groups that can be attached to the cyclophane basis. Cavitands are especially suitable as building blocks for higher and defined structures due to their conformational rigidity.

3 Coordination Cages from Cavitands: Influence of Ligand Design on Metal-Directed Self-Assembly

3.1 Receptor Units at the o,o′ *Position of the Cavitand*

Several metallo-supramolecular cages with different geometries have been synthesized from cavitands functionalized with metal-coordinating groups at the *upper rim* [18]. The successful self-assembly of such building blocks is a complex reaction that yields the most thermodynamically stable product [39]. A reversible formation of the coordinative bonds is necessary to allow "error correction" by partial disassembly of less stable intermediates to form the final more stable assembly. On the other hand, a stable connection of the cage subunits has to be realized to ensure the integrity of the structure and allow the characterization of the assembly in solution. The development of rigid ligands with a high preference to self-assemble to only one aggregate with defined geometry is of major importance for the synthesis of coordination cages. The degree of preorganization of building blocks derived from cavitands is controlled by the shape and conformational freedom of the cavitand basis and the flexibility of the attachment of the metal-coordinating group. To illustrate the impact of the ligand properties on the geometry of the obtained structures, selected examples of coordination cages based on cavitands are presented in this section.

The self-assembly of the tetra(cyano)cavitands **3** and **4** with a different flexibility of the cavitand basis was investigated by Dalcanale et al. (Fig. 2) [40, 41]. Compared to the methylene-bridged cavitand **4**, the ethylene-bridged cavitand **3** is conformationally less rigid. The higher flexibility of **3** accounts for the lower tendency to aggregate to discrete coordination cages. While **4** forms dimeric coordination cages in the presence of $Pd(dppp)(CF_3SO_3)_2$, no successful capsule self-assembly was observed for the flexible cavitand **3**.

Kobayashi and co-workers have further extended the work of Dalcanale et al. [40, 41] to achieve selective self-assembly of a homo- or hetero-cavitand cage via metal coordination based on ligand tuning (Fig. 3) [42–45]. The authors reported a series of tetra(4-pyridyl)-cavitand (**6**), tetrakis(4-pyridylethynyl)-cavitand (**7**), and tetrakis(4-cyanophenyl)-cavitand (**8**) molecules and demonstrated that addition of square-planar $Pd(dppp)(OTf)_2$ complex (**9**) to cavitand **6–8** in 4:2 ratios respectively resulted in the formation of homo cavitand cages $\{(\mathbf{7})_2\,[Pd(dppp)]_4\}^{8+}\cdot 8(TfO^-)$ (**10**)

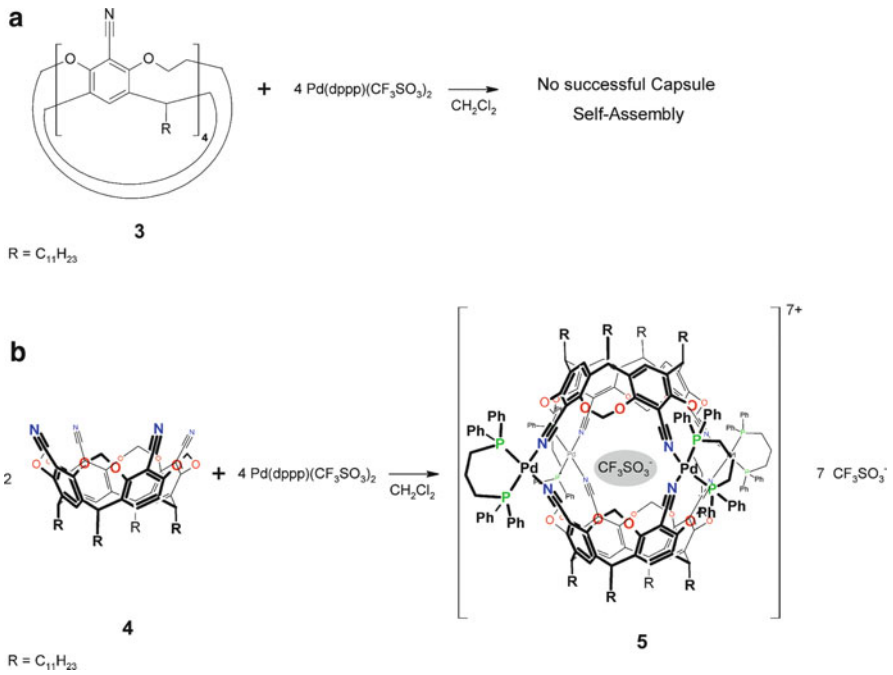

Fig. 2 **(a)** The ethylene-bridged cavitand **3** is not suited for capsule self-assembly with Pd(dppp)$(CF_3SO_3)_2$. **(b)** Self-assembly of the methylene-bridged cavitand **4** to the dimeric capsule **5**

and $\{(\mathbf{8})_2[Pd(dppp)]_4\}^{8+}\cdot 8(TfO^-)$ (**11**) while the cavitand **6** gave various species of aggregates as evidenced from its broad and complicated ^{1}H NMR signals. On the other hand a 1:1:4 mixture of **6**, **8**, and **9** exclusively self-assembled into a highly symmetrical hetero-cavitand metal coordination cage **12** as evidenced from its ^{1}H NMR signals which suggested a C_{4V} symmetry for the coordination cage while a similar cavitands-metal molar ratio of **6**, **7** and **9**, and **7**, **8** and **9** did not result in any hetero-cavitand cages. The authors proposed that the observed selectivity during the self-assembly of the homo or hetero-cavitand cages **10–12** via metal coordination could be attributed to the differences of the inherent coordination ability of cavitand ligands (**6** $\geq$ **7** $>$ **8**), the flexibility of dihedral angle between ligand moiety and the cavitand scaffold (**7** $>$ **8** $\approx$ **6**), and the steric hindrance between dppp and the cavitand metal coordination sites (**6** $>$ **7** $>$ **8**). Moreover, the selective formation of hetero-cavitand cages **12** could be achieved by controlling the addition order of cavitand ligand **6** to the homo cavitand cage **11** through dynamic self-assembly based on kinetic control [45].

Haino and co-workers have reported the synthesis of a self-assembling dimeric capsule via metal-coordination utilizing two octadentate resorcin[4]arene cavitands possessing four bipyridyl groups (**13**) which complex four silver cations (Ag^+) in a tetrahedral fashion (Fig. 4) [46, 47]. A detailed computational study of the dimeric metallo-capsule **14** revealed a large and elaborate three-dimensional inner capsular

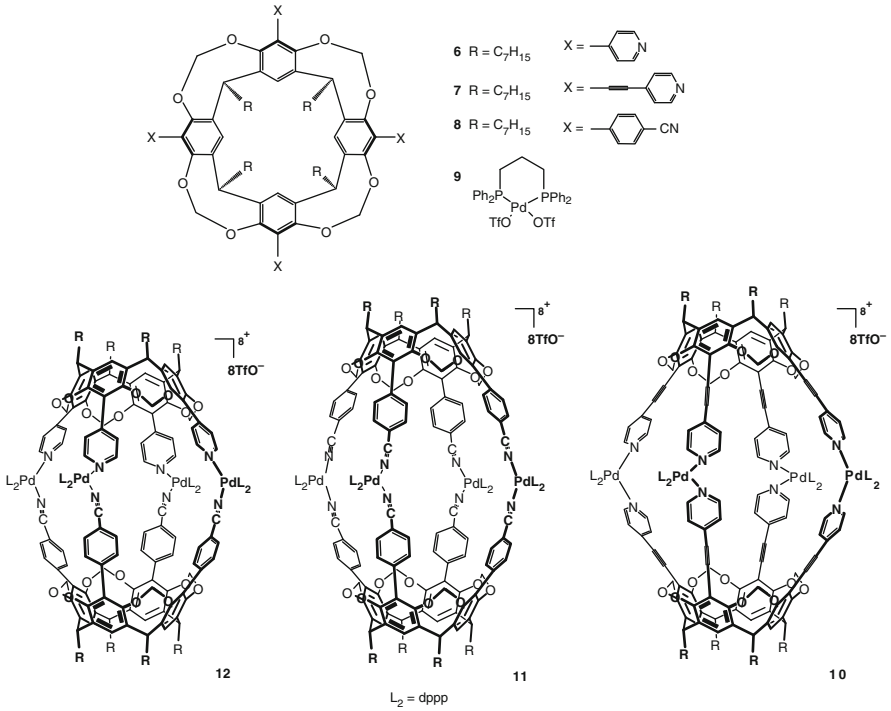

Fig. 3 Homo- and hetero capsules **10–12** from monomers **6–8** via Pd-coordination with **9**

cavity which might be able to distinguish slight structural differences in flexible alkyl-diacetate guests as well as rigid aromatic guests. The thermodynamic studies on the binding characteristic of the capsule demonstrated that not only the CH-π interactions between the methyl groups on the guest termini and the aromatic cavity walls but also desolvation of the inner cavity play a significant role in the guest encapsulation. Moreover the cavity can preferentially select hydrogen-bonded heterodimers over homodimers of a mixture of two or three carboxylic acids [47].

The kind of attachment of the metal coordinating groups to the cavitand is an important structure-defining parameter. Hong et al. studied the self-assembly of a cavitand **15** functionalized with pyridyl groups via flexible ether linkages (Fig. 5) [48, 49]. Due to the conformational freedom of the connection, intramolecular coordination of the metal (Pt^{2+} and Pd^{2+}) centers is observed in competition with intermolecular complexation leading to the supramolecular capsules **16a**–**b**. While the capsules **16a**–**b** and the half-capsules **17a**–**b** are in dynamic equilibrium in nitromethane, the dimeric capsule is formed exclusively in chloroform/methanol mixtures.

Further examples for structural diversity induced by non-rigid linkage of the metal coordinating groups to the cavitand basis have been provided by Beer et al. (Fig. 6) [50]. In the presence of different metal ions, the cavitand **19** with four

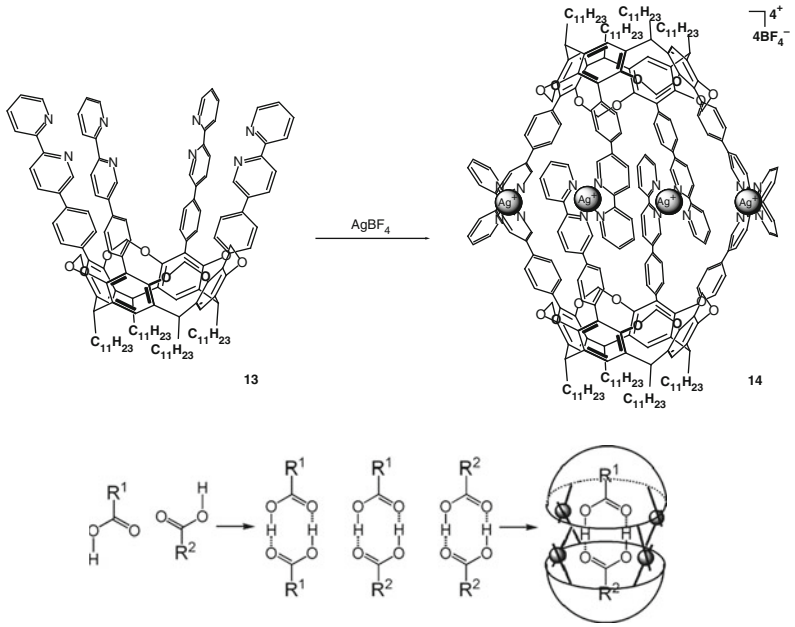

Fig. 4 Schematic representation of the selective encapsulation of various guest molecules in the hydrogen-bonded heterodimer **14**

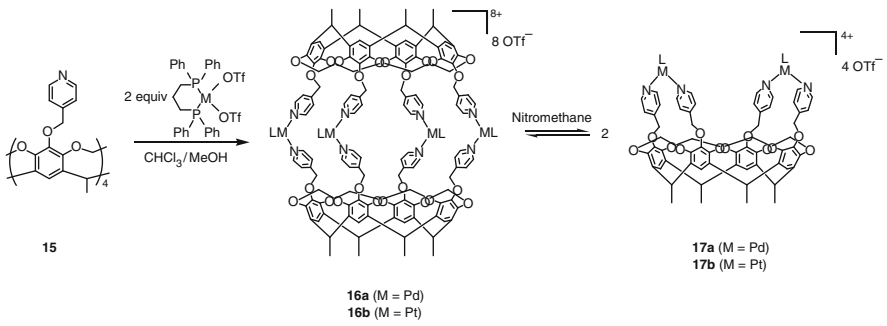

Fig. 5 Self-assembly of **15** and equilibrium between capsules **16a–b** and interclipped bowls **17a–b**

thiocarbamate units attached via methylene groups to the cyclophane aggregates to trimeric or tetrameric species. Reaction of **19** with Zn^{2+} yields the trimeric aggregate **20** with the cavitands located at the corners of an equilateral triangle [51]. All edges of the triangle are doubly spanned by two zinc ions coordinated to the same cavitands. In the presence of Cu^{2+} ions, tetrameric species **21** are formed [52]. Determination of the molecular structure by X-ray diffraction analysis showed that the cavitands lie at the apices of a flattened tetrahedron with two edges doubly spanned by two copper ions coordinated to the same cavitands.

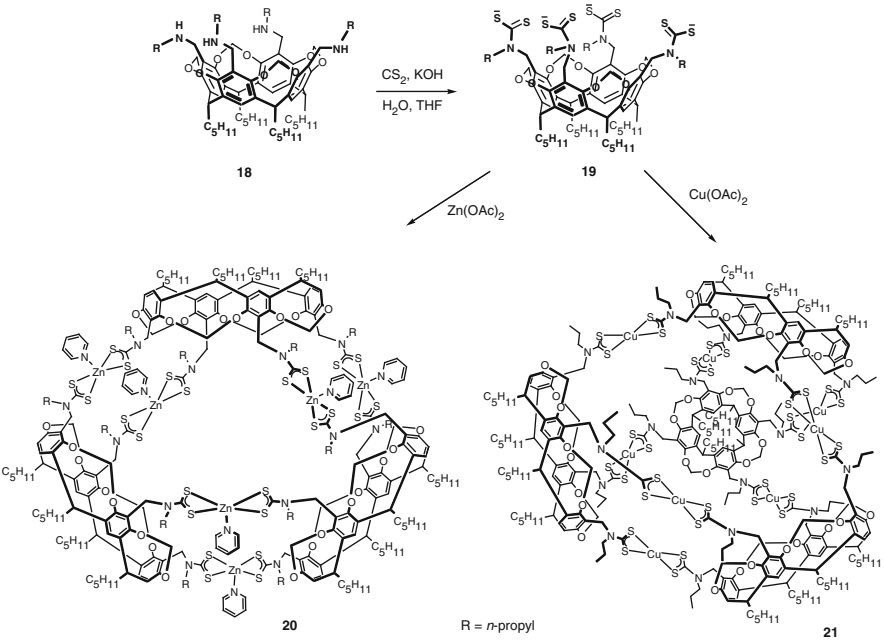

Fig. 6 Synthesis of the tetra(thiocarbamate)cavitand **19** and self-assembly of **19** in the presence of Zn^{2+} or Cu^{2+} ions

To ensure the integrity of the assemblies in solution, stable connections between the building blocks of the cages are required. Figure 7 shows an example of an aggregate that has been characterized in the solid state by X-ray diffraction analysis, while no evidence for intact coordination cages in solution were obtained [53]. The assembly **23** contains six tetra(carboxyl)cavitands **22** that are stitched together by Zn^{2+} ions coordinated to the carboxylate groups. In the solid state, one-dimensional coordination polymers of the coordination cages **23** are formed by aggregation through linear μ-hydroxy- or μ-oxo-linkages. Attempts to provide evidence for discrete hexameric species in solution by ESI-MS or NMR spectroscopy have not been successful. The insufficient stability of the aggregates can be attributed to the weak connection of the cavitands via the carboxylate groups at the *upper rim* coordinated to zinc ions.

The laboratories of Sherburn et al. and Stang et al. have synthesized selectively functionalized bispyridyl cavitand molecules (**26**, **27**) through the incorporation of two pyridine units at the A,C-distal positions of the upper rim of resorcin[4]arene cavitand and demonstrated that the cavitands readily self-assemble to form the supramolecular triangle metal complexes (**28a–b**, **29a–b**) in the presence of linear bis-platinum complex **25** (Fig. 8) [54]. The NMR spectra of these assemblies are very simple (e.g., a single ^{31}P NMR resonance for all complexes) suggesting thereby that the assemblies are either highly symmetrical or rapidly equilibrating at room temperature. On the other hand, treatment of cavitands (**26**, **27**) with

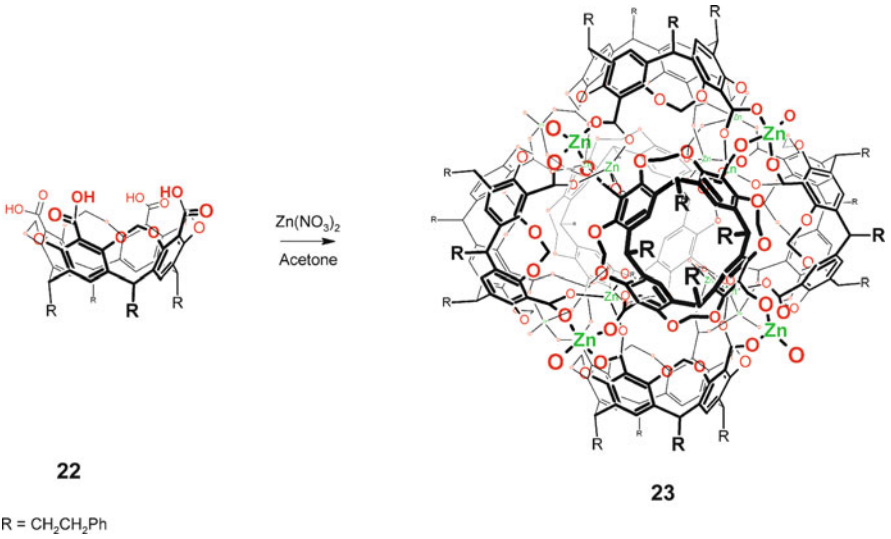

Fig. 7 Formation of the hexameric assembly **23** contained in the coordination polymer (which is not shown for clarity)

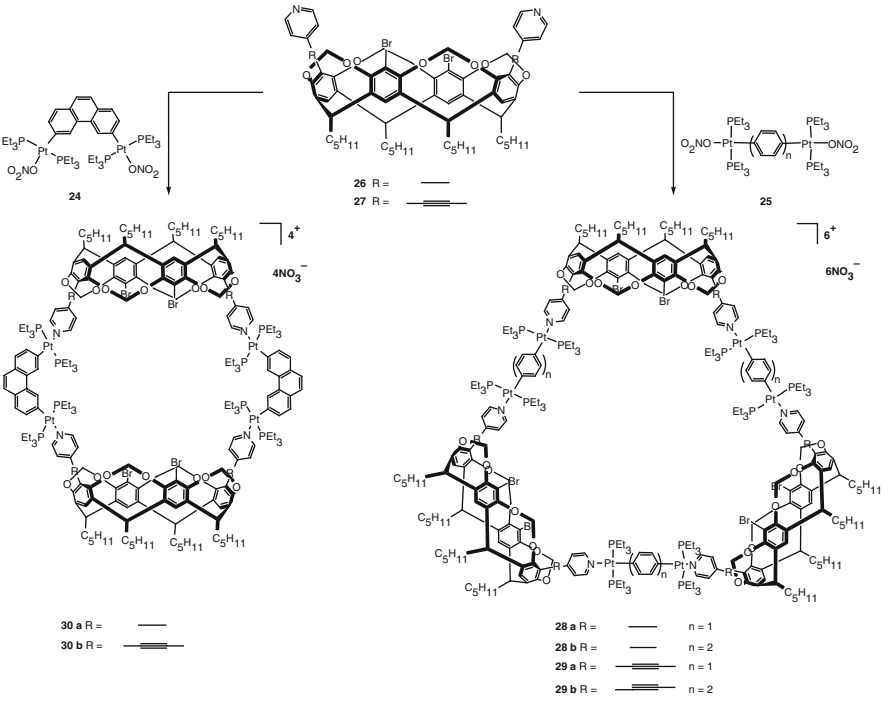

Fig. 8 Synthesis of supramolecular metallo complexes **28–30**

2,9-(*trans*-$Pt(PEt_3)_2NO_3)_2$-phenanthrene (**24**) leads to the formation of dimeric cavitand metal complexes (**30a–b**).

3.2 *Receptor Units at the Bridging Methylene Position of the Cavitand*

Dalcanale and co-workers have reported the synthesis of deep-cavity coordination cages (**32a–h**) through cage self-assembly (CSA) of two tetrapyridyl-substituted deep-cavity cavitand ligands (**31**) connected through four square-planar palladium or platinum complexes (Fig. 9) [55]. The authors show that the capsule internal cavity resembles an ellipsoid with a calculated volume of 840 Å and possesses four lateral portals having a diameter of about 6 Å which is large enough to allow the fast entry–exit of counter ions in solution. Stability studies of these metallo-cages revealed that the platinum cages are kinetically more stable at room temperature and cannot be disassembled even by competitive triethylamine ligands whereas the palladium cages are kinetically labile and can be disassembled under similar conditions. In another report the same research group used the phenyl units as spacers to extend the cavity size (**33**) to form deeper cavity metal-coordination cages (**34a–f**) while retaining at the same time the relative orientation of the pyridine moieties and the rigidity of the cavitand framework both pivotal for CSA [56].

4 Terpyridines as Building Blocks for Coordination Cages

2,2′:6′,2″-Terpyridine is a common metal-binding domain which has been increasingly used as a supramolecular motif in the past 20 years [57, 58]. Due to the *meridional* orientation of this tridentate ligand, its *bis*-complexes with metal centers, preferring an octahedral coordination geometry, can be used as linear connecting units (Fig. 10). As the metal center determines the dynamic properties of the complexes, highly directional linkages that are kinetically inert ($M = Co^{3+}$, Cr^{3+}, Fe^{2+}, Ru^{2+}) or kinetically labile ($M = Zn^{2+}$, Cd^{2+}) can be realized.

Besides metallocycles, metallodendrimers, and metallo-supramolecular polymers [58], few examples of hollow supramolecular architectures have been obtained from polytopic ligands containing terpyridine units. Lehn et al. used heteroaromatic ligands with terpyridine type coordination sites to obtain cylindrical self-assembled architectures (Fig. 11) [60]. For synthesis of the cage **37**, tris-2,4,6-(2-pyrimidyl)-1,3,5-triazine (**35**) was mixed with lead triflate in

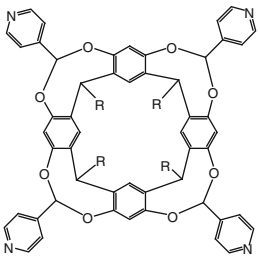

31a R = $C_{11}H_{23}$
31b R = CH_2CH_2Ph

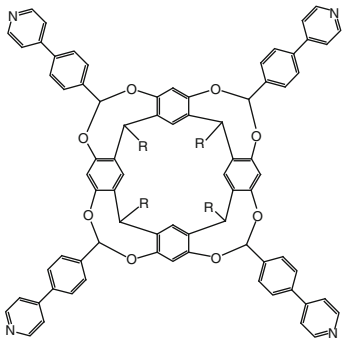

33 a R = $C_{11}H_{23}$
33 b R = C_6H_{13}

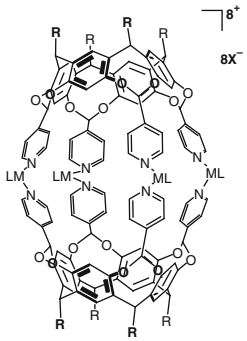

32a R = $C_{11}H_{23}$ M = Pt L = dppp X = CF_3SO_3
32b R = $C_{11}H_{23}$ M = Pd L = dppp X = CF_3SO_3
32c R = $C_{11}H_{23}$ M = Pd L = en X = CF_3SO_3
32d R = $C_{11}H_{23}$ M = Pd L = en X = NO_3
32e R = C_2H_4Ph M = Pt L = dppp X = CF_3SO_3
32f R = C_2H_4Ph M = Pd L = dppp X = CF_3SO_3
32g R = C_2H_4Ph M = Pd L = en X = CF_3SO_3
32h R = C_2H_4Ph M = Pd L = en X = NO_3

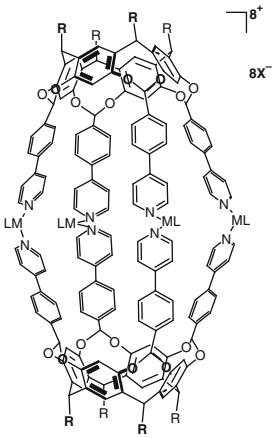

34a R = $C_{11}H_{23}$ M = Pt L = dppp X = CF_3SO_3
34b R = $C_{11}H_{23}$ M = Pd L = dppp X = CF_3SO_3
34c R = $C_{11}H_{23}$ M = Pt L = $(PEt_3)_2$ X = CF_3SO_3
34d R = C_6H_{13} M = Pt L = dppp X = CF_3SO_3
34e R = C_6H_{13} M = Pd L = dppp X = CF_3SO_3
34f R = C_6H_{13} M = Pd L = en X = CF_3SO_3

Fig. 9 Design of cavitand ligands **31a–b** and **33a–b** and the self-assembly of cavitands to form metallo-supramolecular cages **32a–h** and **34a–f**

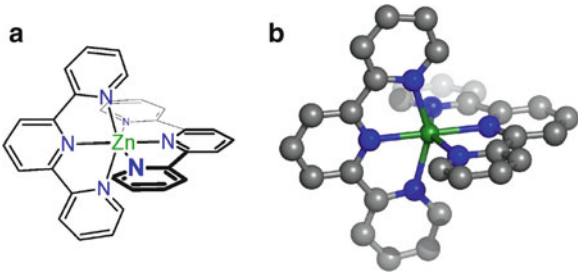

Fig. 10 **(a)** Structure of 2,2′:6′,2″-terpyridine and $[Zn(tpy)_2]^{2+}$. **(b)** Molecular structure of $[Zn(tpy)_2]^{2+}$ as determined by X-ray diffraction analysis [59]

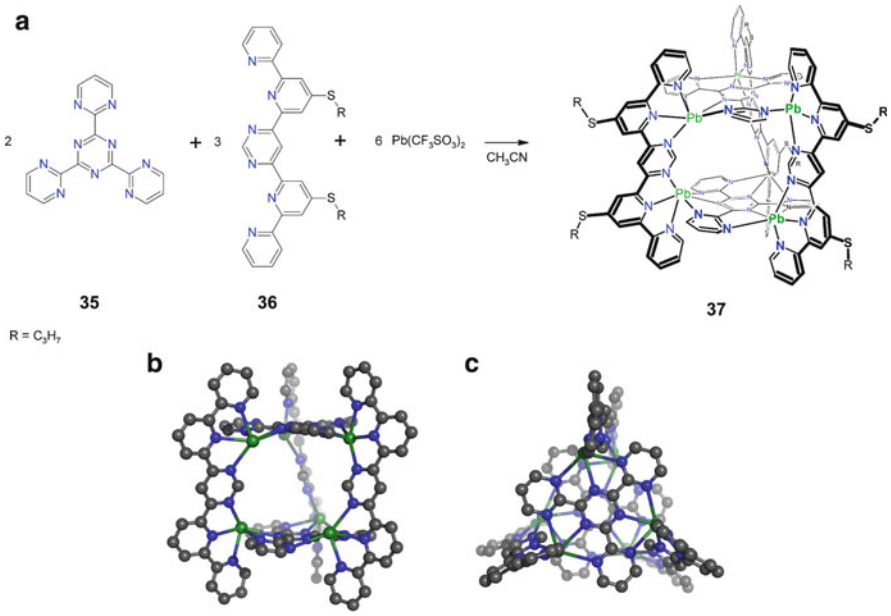

Fig. 11 **(a)** Formation of the cylindrical cage **37** by self-assembly. **(b,c)** Structure of **37** as determined by X-ray diffraction analysis ((**b**) side view, (**c**) top view, substituents and coordinated triflate ions omitted)

acetonitrile. After 2 h at room temperature, ligand **36** was added and the solution stirred overnight at room temperature. In the assembly **37**, the lead ions are coordinated by six nitrogens of the chelating heterocycles and two triflate ions (which are omitted in Fig. 11 for clarity). The highly symmetrical structure is reflected in the ^{1}H NMR spectrum, which contains only two sets of signals for the ligands **35** and **36**.

The extended scaffolding ligand **39** is also suited to yield a cylindrical coordination cage (Fig. 12). The assembly **40** was characterized by ESI-MS and NMR spectroscopy. The ^{1}H NMR spectrum of the highly symmetrical aggregate shows one set of signals for the ligands **39** and two sets of signals for the ligands **38**, which were attributed to the cap ligands at the top and the bottom of the assembly and the ligand in the interior.

Schmittel et al. prepared nanoprisms by heteroleptic aggregation of terpyridine and phenanthroline containing ligands in the presence of Zn^{2+} ions (Fig. 13) [61]. In the ditopic ligand **42**, the phenanthroline moieties are substituted by bulky aryl groups. These substituents prevent the formation of homoleptic $[Zn(phenanthroline)_2]^{2+}$ complexes. Thus, heteroleptic zinc complexes can be selectively prepared by coordination of the bis-phenanthroline ligand **41** to Zn^{2+} and subsequent addition of the tris-terpyridine ligand **41** (HETTAP approach, *HET*eroleptic *T*erpyridine *A*nd *P*henanthroline aggregation) [62]. When the tritopic terpyridine ligand **42** is added to a solution of the ditopic phenanthroline ligand **41**

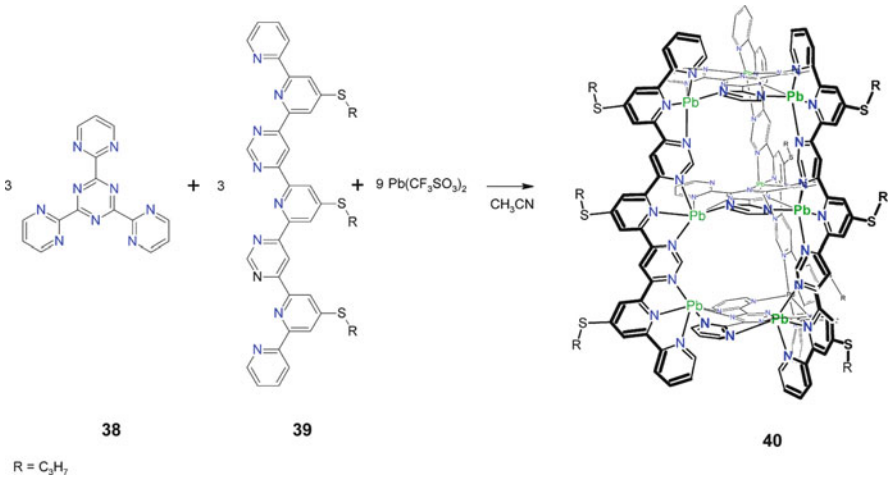

Fig. 12 Association of **38** and **39** to the cylindrical cage **40**

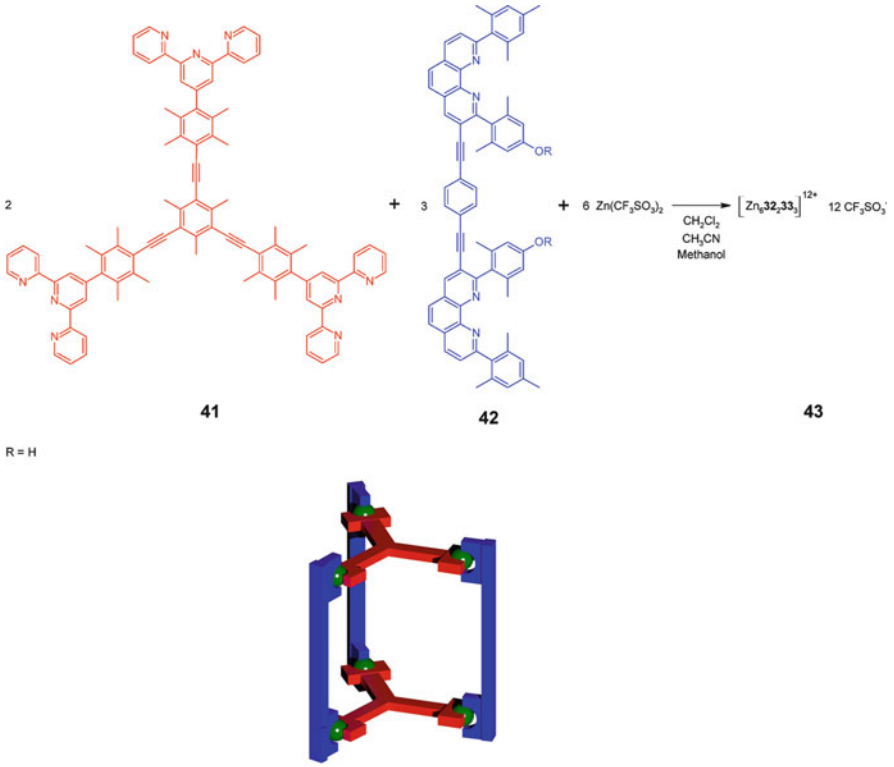

Fig. 13 Formation of the nanoprism **43** by heteroleptic aggregation and schematic representation of the proposed structure

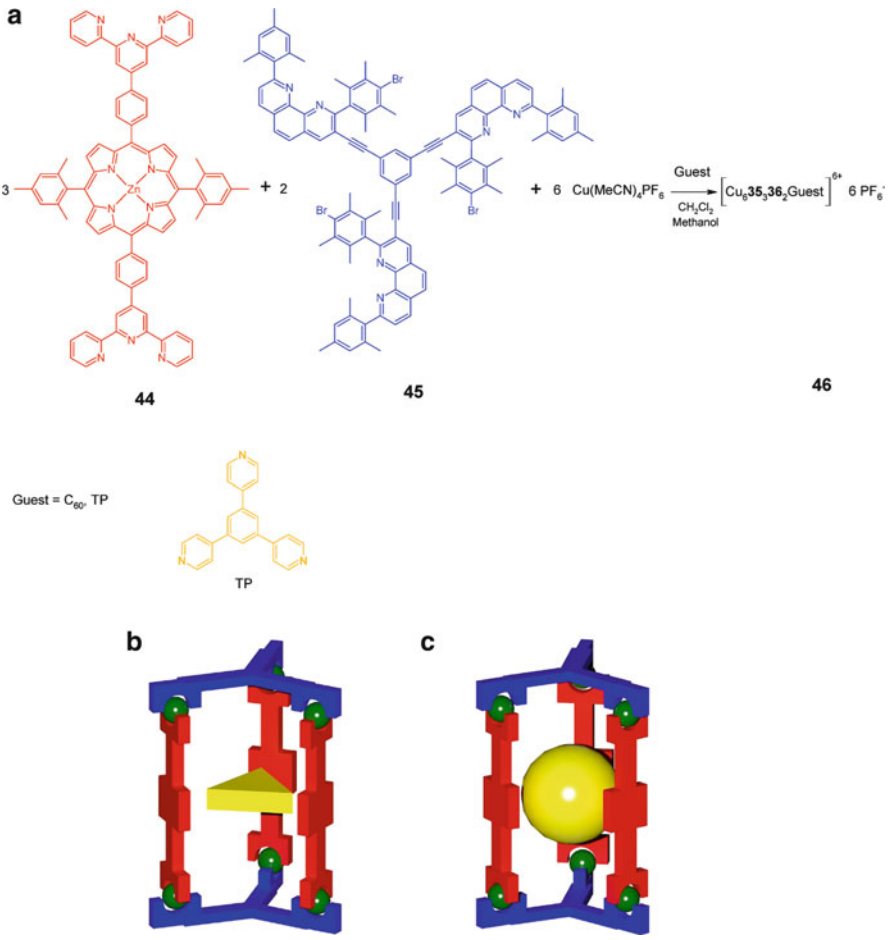

Fig. 14 **(a)** Self-assembly of filled nanoprisms **46**. **(b**,**c)** Schematic representation of the proposed structures

and Zn^{2+}, self-assembly yields discrete nanoprisms **43**. In agreement with the proposed structure, the ^{1}H NMR spectrum showed only one set of signals for the (panelling) ligand **41** and one set of signals for the (scaffolding) ligand **42** that spans the edges of the prism.

The sensitivity of the self-assembly process towards the ligand design is reflected in the association of the ligands **44** and **45** in the presence of copper ions (Fig. 14) [63]. In contrast to **41** and **42**, ditopic terpyridyl ligands and tritopic phenanthroline ligands were used. Reaction of **45** with Cu^{1+} ions and subsequent addition of the bis-terpyridyl ligand **44** yielded a product mixture with the expected metallo-supramolecular cage as a minor component. A templating effect was

successfully used to realize quantitative formation of the prismatic structure. In the presence of appropriate guest molecules as C_{60} or a trispyridine (TP), the self-assembly of the cages proceeded smoothly.

5 Synthesis of a Large Metallo-Supramolecular Cage from a Cavitand-Terpy Building Block [64]

For the synthesis of a cavitand functionalized with terpyridyl groups via rigid linkages, transition metal catalyzed cross-coupling reactions are especially well suited. Starting with the boronic acid ester **48** [65], attachment of the terpyridyl groups to the cavitand was realized by Suzuki–Miyaura reaction with the tetraiodo-cavitand **47** (Fig. 15).

Initial attempts to prepare a self-assembled spheroidal cage using zinc triflate yielded a colorless solid which was insoluble in organic solvents.

To increase the solubility of the aggregates formed, the large lipophilic TFPB anions (TFPB = tetrakis-(3,5-bis-(trifluoromethyl)-phenyl)-borate) were used instead of the triflate anions [66–68]. The zinc salt $[Zn(NCMe)_6][TFPB]_2$ **50** was obtained by reaction of zinc bromide with Ag(TFBP) in acetonitrile under exclusion of light. Addition of tetrahydrofuran-d_8 to a mixture of the cavitand **49** and the zinc salt **50** gave the coordination cage **51** after keeping the reaction mixture at 60 °C for 1 h (Fig. 16).

The product, which was readily soluble in organic solvents including acetone, tetrahydrofuran, and methylene chloride, was characterized by ESI-MS, ^{1}H, and ^{13}C NMR spectroscopy, diffusion NMR spectroscopy, SAXS measurements and elementary analysis. In the ESI-MS, multiply charged ions [**51**-n TFPB]$^{n+}$ with $n = 7-11$ containing the intact coordination cage were observed exclusively

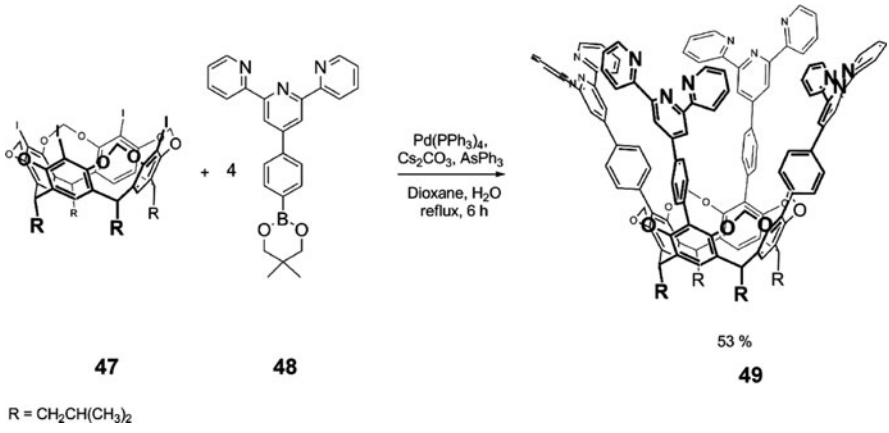

Fig. 15 Preparation of a tetra-(4-(2,2′:6′,2″-terpyridyl)-phenyl)-cavitand **49**

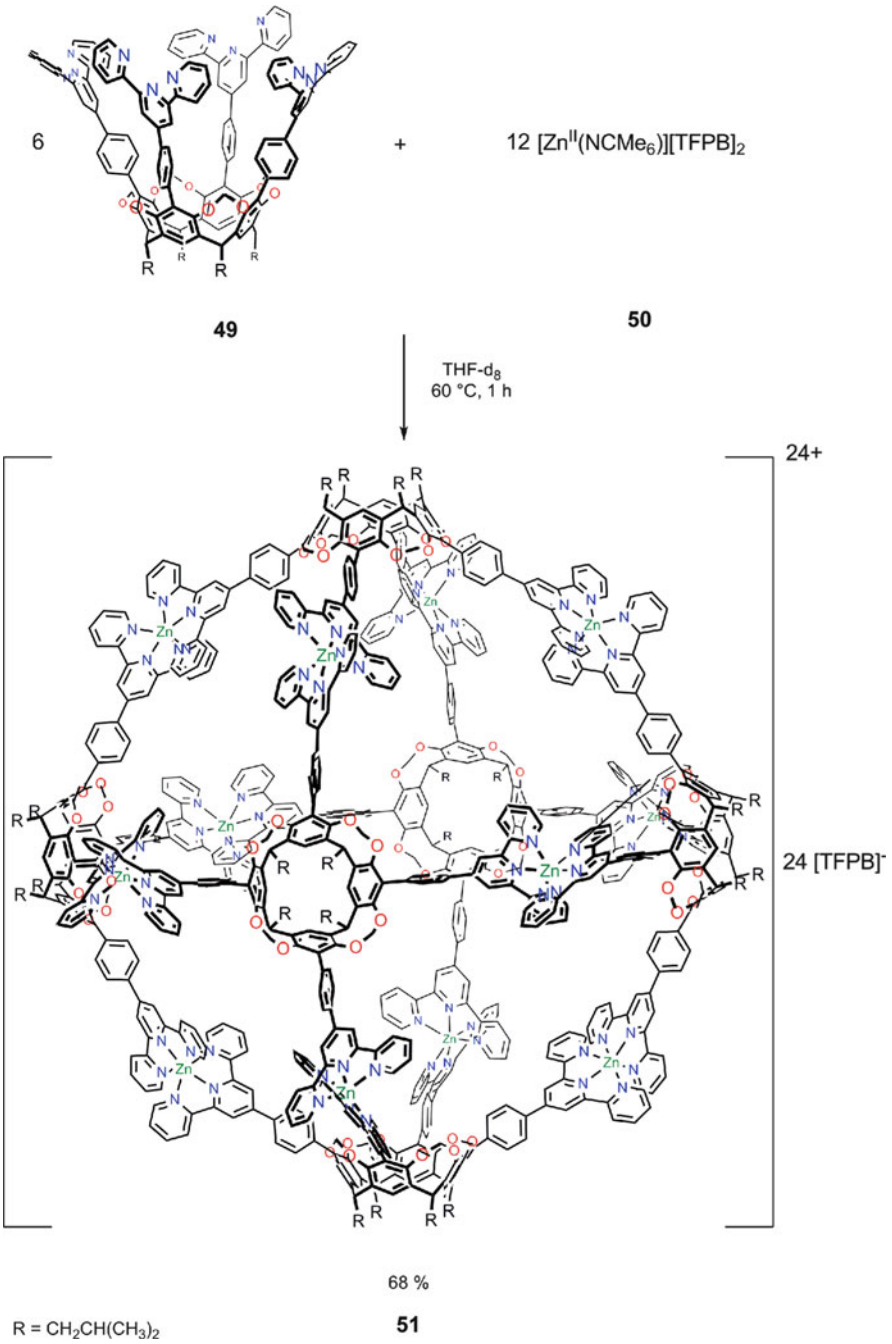

Fig. 16 Synthesis of the hexameric assembly **51**

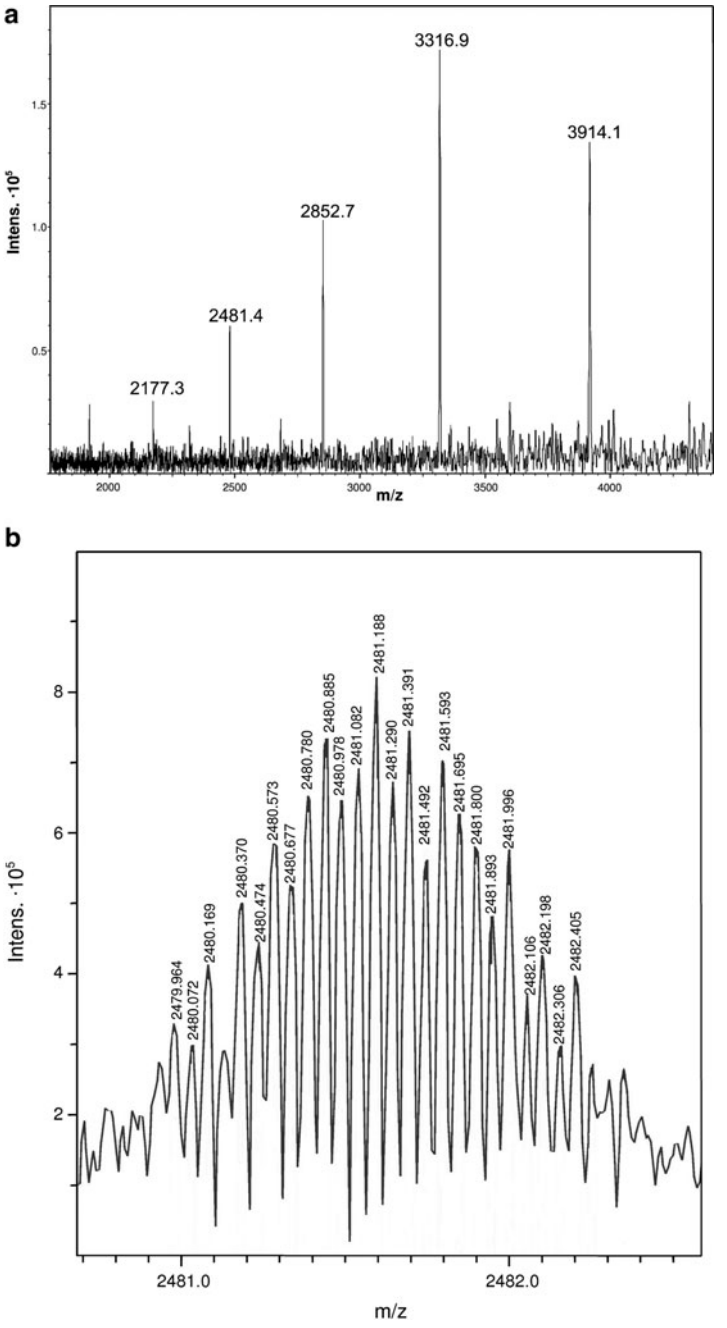

Fig. 17 **(a)** ESI-MS of **51**. **(b)** Isotopically resolved pattern observed for [**51**-10 TFPB]$^{10+}$

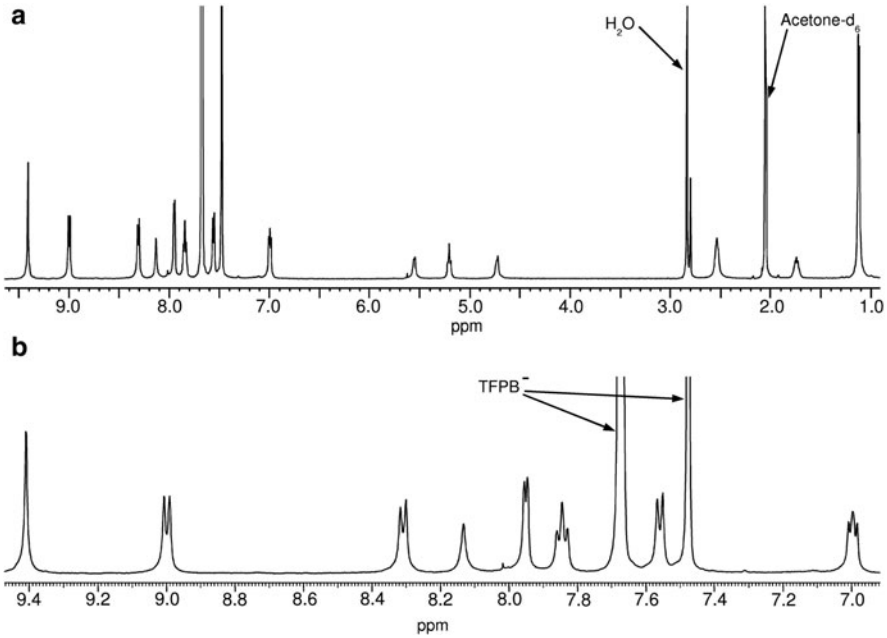

Fig. 18 **(a)** ^{1}H NMR spectrum (500 MHz) of **51** in acetone-d_6. **(b)** Zoom into the aromatic region

(Fig. 17). The isotope patterns prove the charge states of the ions and confirm the hexameric nature of the aggregate.

The ^{1}H and ^{13}C NMR spectra indicate a highly symmetrical structure of **51** (Fig. 18). For all six cavitands in the assembly, only one set of signals is observed. Furthermore, even for the 2,2′:6′,2″-(terpyridyl)phenyl groups only five different resonances are detected, which can be explained with a rotation of the terpyridyl groups resulting in a fast exchange at the NMR timescale at room temperature. The characteristic shift of the signals of the hydrogen atoms in *meta*- and *ortho*-positions to the nitrogen atoms compared to the resonances of free cavitand **49** signifies the coordination of the Zn^{2+}ions by the terpyridyl groups.

Diffusion NMR spectroscopy experiments were carried out to determine the diffusion coefficient D of the cavitand **49** and the coordination cage **51** [69]. While for the free cavitand **49** a diffusion coefficient of $D = (4.91 \pm 0.04) \times 10^{-10}$ m^2 s^{-1} was obtained, a significantly slower diffusion ($D = 2.06 \pm 0.05) \times 10^{-10}$ m^2 s^{-1} was observed for the large assembly **51** in tetrahydrofuran-d_8 at 20 °C. Assuming a nearly spheroidal form, the diameter of **51** was estimated to be 4 nm.

SAXS (Small Angle X-ray Scattering) measurements provided further insight into the structure of the assembly in solution [70]. Using the GNOMN/DAMMIN software packages, the SAXS data were used to reconstruct a low resolution three-dimensional particle shape (yellow semitransparent spheres in Fig. 19) [71–74].

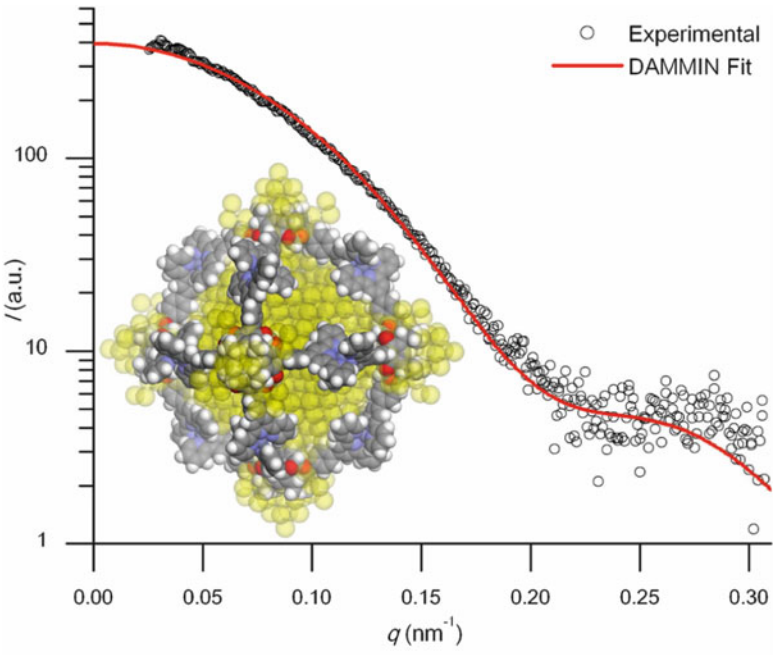

Fig. 19 Main plot: SAXS intensity (I) vs momentum transfer for a solution of **51** in acetonitrile (5.1 g L^{-1}). The *symbols* and the *solid line* correspond to the experimental data points and the numerical fit using GNOM/DAMMIN simulated annealing, constraining the symmetry to the point group P432 ($\chi = 1.397$). *Inset*: reconstructed low resolution particle shape for **51** obtained by the GNOM/DAMMIN fit (*semitransparent spheres*) superimposed onto the PM3 stationary point (space-filling model, *iso*-butyl groups substituted by methyl groups)

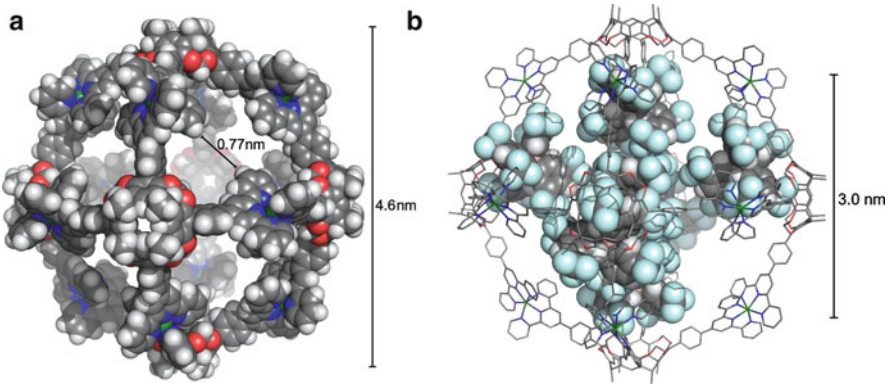

Fig. 20 **(a)** Space-filling representation of the *O*-symmetric stationary point of the methyl derivative of **51** on the PM3 hypersurface. **(b)** Representation of the energy minimized structure of the methyl derivative **51** containing seven TFPB anions obtained from a force field calculation

The radius of gyration obtained as well as the reconstructed shape is in very good agreement with the expected dimensions of the coordination cage **42** (Fig. 20).

Attempts to grow single crystals suitable for X-ray diffraction analysis of **51** failed. Therefore, the structure of the assembly **51** (*iso*-butyl groups substituted by methyl groups) was optimized under the constraint of *O* symmetry using the semiempirical PM3 method (Fig. 20) [75]. In the modeled structure, the cavitands lie at the apices of an octahedron. The edges of the platonic solid are defined by the zinc ions coordinated to the terpyridyl groups. While the largest distance of the zinc ions at opposite edges is approximately 3.9 nm, the largest distance between the methyl groups are 4.6 nm. According to the calculations, openings with a minimal diameter of 0.77 nm exist between adjacent bis-terpyridyl zinc complexes. Based on the modeled structure, the size of the inner cavity was evaluated with the program CARVER [76]. The largest sphere that fits into the capsule has a diameter of approximately 3 nm, which corresponds to a volume of about 14 nm^3. A force field calculation of the gas phase energy minimized structure demonstrates that up to seven TFPB anions could be encapsulated, illustrating the dimensions of the inner cavity.

In cooperation with the group of Dirk Volkmer (Ulm University), the synthetic procedure established for the preparation of the tetra-(4-(2,2′:6′,2″-terpyridyl)-phenyl)-cavitand **49** was adapted for the synthesis of terpyridyl-substituted calix[n]arenes [77]. The tetra-(4-(2,2′:6′,2″-terpyridyl)-phenyl) calix[4]arenes **54a**,**b** and the penta-(4-(2, 2′:6′, 2″-terpyridyl)-phenyl)calix[5]arene **55** can be prepared from the boronic acid ester **48** and tetrabromocalix[4]arene **52a** or **b** and pentabromocalix[5]arene **53**, respectively (Fig. 21).

The flexibility of the calix[4]arene basis is reflected in the molecular structure of **54a** as determined by X-ray diffraction analysis (Fig. 22). The calix[4]arene adopts a *flattened cone* conformation with intramolecular π-stacking of two terpyridyl

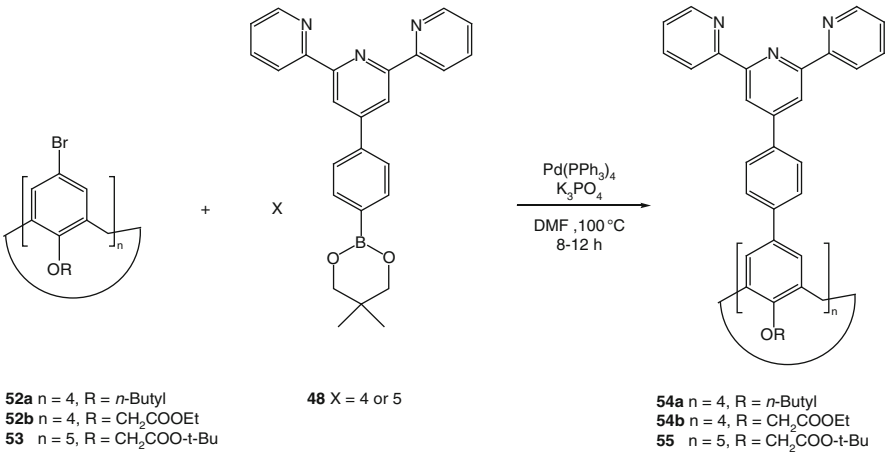

52a n = 4, R = *n*-Butyl
52b n = 4, R = CH_2COOEt
53 n = 5, R = CH_2COO-t-Bu

48 X = 4 or 5

54a n = 4, R = *n*-Butyl
54b n = 4, R = CH_2COOEt
55 n = 5, R = CH_2COO-t-Bu

Fig. 21 Synthesis of terpyridyl-substituted calix[n]arenes

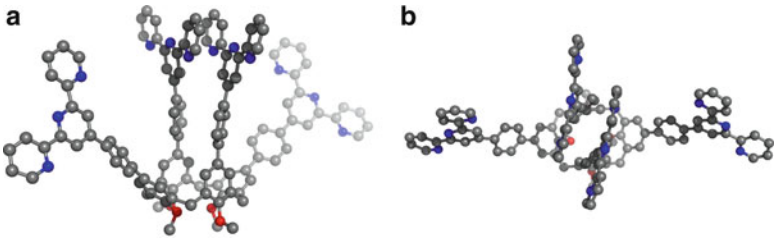

Fig. 22 Structure of **54a** as determined by X-ray diffraction analysis

units. While the hexameric coordination cage **51** has been obtained from the rigid terpyridine-substituted cavitand **49**, the lower degree of preorganization of the calix [n]arenes leads to a significantly different self-assembly in the presence of Zn^{2+} ions with a variety of species formed as determined by ESI-MS and ^{1}H NMR spectroscopy.

In conclusion, a large metallo-supramolecular capsule **51** based on a terpyridyl-substituted cavitand has successfully been synthesized. The low flexibility of the methylene-bridged cavitand units and the rigid attachment of the terpyridyl groups to the cavitand basis yield the highly preorganized tetratopic ligand **49**. The relative orientation of the metal coordinating sites is suited for the self-assembly of **49** in the presence of zinc ions to the stable, highly symmetrical coordination cage **51**. To prevent irreversible formation of insoluble precipitates during self-assembly, the use of lipophilic anions as tetrakis-(3,5-bis-(trifluoromethyl)-phenyl)-borate (TFPB) is essential. The structure of the hexameric assembly has been modeled using semiempirical PM3 method. According to the calculated structure, and in agreement with experimental data from diffusion NMR and SAXS measurements, the diameter is approximately 4.5 nm. The size of the inner cavity of the aggregate is characterized by the diameter ($d = 3$ nm) of the largest sphere that fits into the capsule and is large enough to encapsulate several bulky molecules. Therefore, this coordination cage is an example for a large molecular flask, which can be used for the stabilization of reactive species or as nanoscale reaction chambers [17]. To realize such advanced applications, the encapsulation of guest molecules in the cage **51** will be investigated in further studies.

The synthetic route to the cavitand **49** can with minor changes be applied to synthesize terpyridyl-substituted calix[4]arenes **54a** and **54b** and the calix[5]arene **55**. Due to the higher flexibility of the cyclophane basis, the self-assembly behavior of these ligands is significantly different, yielding product mixtures upon addition of zinc ions. Besides templating effects of appropriate guest molecules, the introduction of substituents at the *narrow rim* of the calix[n]arene basis might be a possibility to rigidify the ligand and gain enhanced control over the self-assembly process.

6 Summary

In this chapter we have summarized selected examples of supramolecular capsules starting from resorcin[4]arene derivatives. Self-assembling is initiated only by metal-coordination rather than by other types of non-covalent interaction such as H-bonding, etc., and covalent bond formation. Ligand design, coordination geometry, and flexibility of the monomeric units strongly influence the architecture of the new-formed coordination capsules. In addition, reversible formation of the coordinative bonds is necessary to allow "error correction" by partial disassembly of less stable intermediates to form the final more stable assembly. Using terpyridine (tpy) ligands and linear linkers as connecting units, giant supramolecular capsules are accessible as shown for the Zn-coordination cage discussed in Sect. 5 of this review. Applications such as controlled encapsulation and release of guest molecules (for transport processes) as well as controlled reactions in the confined cavity of these supramolecular capsules (for catalysis) will be the subject of future activities.

Acknowledgments Financial Support by the *Deutsche Forschungsgemeinschaft* (SFB 613) is gratefully acknowledged. TS is grateful for a predoctoral scholarship of the University of Bielefeld and SNS for a BOYSCAST fellowship 2009–2010 by the Department of Science and Technology (DST), Government of India. Part of this contribution was taken from the Ph.D. thesis of TS (Bielefeld University 2010).

References

1. Lehn JM (2002) Toward complex matter: supramolecular chemistry and self organisation. Proc Natl Acad Sci USA 99:4763
2. Lehn JM (1988) Supramolecular chemistry-scope and perspectives molecules, supermolecules, and molecular devices. Angew Chem Int Ed 27:89
3. Steed JW, Atwood JL (2009) Supramolecular chemistry, 2nd edn. Wiley, Chichester
4. Uraguchi D, Ueki Y, Ooi T (2009) Chiral organic ion pair catalysts assembled through a hydrogen-bonding network. Science 326:120
5. Cordier P, Tournilhac F, Soulie-Ziakovic C, Leibler L (2008) Self-healing and thermoreversible rubber from supramolecular assembly. Nature 451:977
6. Schenning APHJ, Meijer EW (2005) Supramolecular electronics; nanowires from self-assembled π-conjugated systems. Chem Commun 3245
7. Lehn JM (2007) From supramolecular chemistry towards constitutional dynamic chemistry and adaptive chemistry. Chem Soc Rev 36:151
8. Rebek J (2005) Simultaneous encapsulation: molecules held at close range. Angew Chem Int Ed 44:2068
9. Hof F, Craig SL, Nuckolls C, Rebek J (2002) Molecular encapsulation. Angew Chem Int Ed 41:1488
10. Yoshizawa M, Tamura M, Fujita M (2006) Diels–Alder in aqueous molecular hosts: unusual regioselectivity and efficient catalysis. Science 312:251
11. Fiedler D, Leung DH, Bergman RG, Raymond KN (2005) Selective molecular recognition, C–H bond activation, and catalysis in nanoscale reaction vessels. Acc Chem Res 38:349
12. Mal P, Breiner B, Rissanen K, Nitschke JR (2009) White phosphorus is air-stable within a self-assembled tetrahedral capsule. Science 324:1697

13. Pluth MD, Bergman RG, Raymond KN (2007) Acid catalysis in basic solution: a supramolecular host promotes orthoformate hydrolysis. Science 316:85
14. Koblenz TS, Wassenaar J, Reek JNH (2008) Reactivity within a confined self-assembled nanospace. Chem Soc Rev 37:247
15. Fujita M, Tominaga M, Hori A, Therrien B (2005) Coordination assemblies from a Pd(II)-cornered square complex. Acc Chem Res 38:369
16. Vriezema DM, Aragones MC, Elemans JAAW, Cornelissen JJLM, Rowan AE, Nolte RJM (2005) Self-assembled nanoreactors. Chem Rev 105:1445
17. Yoshizawa M, Klosterman JK, Fujita M (2009) Functional molecular flasks: new properties and reactions within discrete, self-assembled hosts. Angew Chem Int Ed 48:3418
18. Dalgarno SJ, Power NP, Atwood JL (2008) Metallo-supramolecular capsules. Coord Chem Rev 252:825
19. Gianneschi NC, Masar MS, Mirkin CA (2005) Development of a coordination chemistry-based approach for functional supramolecular structures. Acc Chem Res 38:825
20. Schneider HJ (2009) Binding mechanism in supramolecular complexes. Angew Chem Int Ed 121:3924
21. Prins LJ, Reinhoudt DN, Timmerman P (2001) Noncovalent synthesis using hydrogen bonding. Angew Chem Int Ed 40:2382
22. Seidel SR, Stang PJ (2002) High-symmetry coordination cages via self-assembly. Acc Chem Res 35:972
23. Caulder DL, Powers RE, Parac TN, Raymond KN (1998) The self-assembly of a predesigned tetrahedral M_4L_6 supramolecular cluster. Angew Chem Int Ed 37:1840
24. Ikeda A, Yoshimura M, Udzu H, Fukuhara C, Shinkai S (1999) Inclusion of [60]fullerene in a homooxacalix[3]arene-based dimeric capsule cross-linked by a PdII-pyridine interaction. J Am Chem Soc 121:4296
25. Fujita M, Oguro D, Miyazawa M, Oka H, Yamaguchi K, Ogura K (1995) Self-assembly of ten molecules into nanometre-sized organic host frameworks. Nature 378:469
26. Schröder T (2010) Synthesis and single-molecule force spectroscopy of supramolecular capsules. PhD Thesis, Bielefeld University, Bielefeld
27. Sahu SN, Mattay J et al (2011) Calixarene based molecular capsules. Chem Rev (submitted)
28. Schröder T, Walhorn V, Mattay J, Anselmetti D (2011) Single molecule force spectroscopy of supramolecular complexes. In: Schalley C (ed) Analytical methods in supramolecular chemistry. Wiley-VCH, Weinheim (in press)
29. Schröder T, Sahu SN, Anselmetti D, Mattay J (2011) Supramolecular capsules derived from resorcin[4]arenes by H-bonding and metal coordination. Synthesis, characterization and single-molecule force spectroscopy. Isr J Chem 51:725
30. Cram DJ, Karbach S, Kim YH, Baczynskyj L, Kallemeyn GW (1985) Shell closure of two cavitands forms carcerand complexes with components of the medium as permanent guests. J Am Chem Soc 107:2575
31. Botta B, Cassani M, D'Acquarica I, Subissati D, Zappia G, Monache GD (2005) Resorcarenes: hollow building blocks for the host-guest chemistry. Curr Org Chem 9:1167
32. Timmerman P, Verboom W, Reinhoudt DN (1996) Resorcinarenes. Tetrahedron 52:2663
33. Böhmer V (1995) Calixarenes, macrocycles with (almost) unlimited possibilities. Angew Chem Int Ed 34:713
34. Asfari Z, Böhmer V, Harrowfield J, Vicens J (2001) Calixarenes 2001,1st edn. Kluwer, Dordrecht
35. Crisóstomo FRP, Lledó A, Shenoy SR, Iwasawa T, Rebek J (2009) Recognition and organocatalysis with a synthetic cavitand receptor. J Am Chem Soc 131:7402
36. Ruderisch A, Iwanek W, Pfeiffer J, Fischer G, Albert K, Schurig V (2005) Synthesis and characterization of a novel resorcinarene-based stationary phase bearing polar headgroups for use in reversed-phase high-performance liquid chromatography. J Chromatogr A 1095:40
37. Baldini L, Casnati A, Sansone F, Ungaro R (2007) Calixarene-based multivalent ligands. Chem Soc Rev 36:254

38. Moran JR, Ericson JL, Dalcanale E, Bryant JA, Knobler CB, Cram DJ (1991) Vases and kites as cavitands. J Am Chem Soc 113:5707
39. Steed JW, Turner DR, Wallace KJ (2007) Core concepts in supramolecular chemistry and nanochemistry, 1st edn. Wiley, Chichester, pp 107–170
40. Fochi F, Jacopozzi P, Wegelius E, Rissanen K, Cozzini P, Marastoni E, Fisicaro E, Manini P, Fokkens R, Dalcanale E (2001) Self-assembly and anion encapsulation properties of cavitand-based coordination cages. J Am Chem Soc 123:7539
41. Jacopozzi P, Dalcanale E (1997) Metal-induced self-assembly of cavitand-based cage molecules. Angew Chem Int Ed 36:613
42. Kobayashi K, Ishii K, Sakamoto S, Shirasaka T, Yamaguchi K (2003) Guest-induced assembly of tetracarboxyl-cavitand and tetra(3-pyridyl)-cavitand into a heterodimeric capsule via hydrogen bonds and CH-halogen and/or CH-π interaction: control of the orientation of the encapsulated guest. J Am Chem Soc 125:10615
43. Kobayashi K, Ishii K, Yamanaka M (2005) Orientational isomerism and binding ability of nonsymmetrical guests encapsulated in a self-assembling heterodimeric capsule. Chem Eur J 11:4725
44. Kobayashi K, Yamada Y, Yamanaka M, Sei Y, Yamaguchi K (2004) Complete selection of a self-assembling homo- or hetero-cavitand cage via metal coordination based on ligand tuning. J Am Chem Soc 126:13896
45. Yamanaka M, Yamada Y, Sei Y, Yamaguchi K, Kobayashi K (2006) Selective formation of a self-assembling homo or hetero cavitand cage via metal coordination based on thermodynamic or kinetic control. J Am Chem Soc 128:1531
46. Haino T, Kobayashi M, Chikaraishi M, Fukazawa Y (2005) A new self-assembling capsule via metal coordination. Chem Commun 2321
47. Haino T, Kobayashi M, Fukazawa Y (2006) Guest encapsulation and self-assembly of a cavitand-based coordination capsule. Chem Eur J 12:3310
48. Park SJ, Shin DM, Sakamoto S, Yamaguchi K, Chung YK, Lah MS, Hong JI (2005) Dynamic equilibrium between a supramolecular capsule and bowl generated by inter- and intramolecular metal clipping. Chem Eur J 11:235
49. Park SJ, Hong JI (2001) Self-assembled nanoscale capsules between resorcin[4]arene derivatives and Pd(II) or Pt(II) complexes. Chem Commun 1554
50. Fox OD, Cookson J, Wilkinson EJS, Drew MGB, MacLean EJ, Teat SJ, Beer PD (2006) Nanosized polymetallic resorcinarene-based host assemblies that strongly bind fullerenes. J Am Chem Soc 128:6990
51. Fox OD, Drew MGB, Wilkinson EJS, Beer PD (2000) Cadmium- and zinc-directed assembly of nano-sized, resorcarene-based host architectures which strongly bind C_{60}. Chem Commun 391
52. Fox DO, Drew MGB, Beer PD (2000) Resorcarene-based nanoarchitectures: metal-directed assembly of a molecular loop and tetrahedron. Angew Chem Int Ed 112:135
53. Ugono O, Moran JP, Holman KT (2008) Closed-surface hexameric metal-organic nanocapsules derived from cavitand ligands. Chem Commun 1404
54. Jude H, Sinclair DJ, Das N, Sherburn MS, Stang PJ (2006) Self-assembly of supramolecular platimun complexes with bis-4-pyridyl cavitands. J Org Chem 71:4155
55. Pirondini L, Bertolini F, Cantadori B, Ugozzoli F, Massera C, Dalcanale E (2002) Design and self-assembly of wide and robust coordination cages. Proc Natl Acad Sci USA 99:4911
56. Pinalli R, Cristini V, Sottili V, Geremia S, Campagnolo M, Caneschi A, Dalcanale E (2004) Cavitand-based nanoscale coordination cages. J Am Chem Soc 126:6516
57. Constable EC (2007) 2,2′:6′,2″-terpyridines: from chemical obscurity to common supramolecular motifs. Chem Soc Rev 36:246
58. Schubert US, Hofmeier H, Newkome GR (2006) Modern terpyridine chemistry, 1st edn. Wiley-VCH, Weinheim
59. Dumitru F, Petit E, Lee A, Barboiu M (2005) Homo- and heteroduplex complexes containing terpyridine-type ligands and Zn^{2+}. Eur J Inorg Chem 4255

60. Garcia AM, Bassani DM, Lehn JM, Baum G, Fenske D (1999) Self-assembly of multicomponent multimetallic lead(II) complexes of cylindrical architecture. Chem Eur J 5:1234
61. Schmittel M, He B (2008) Void and filled supramolecular nanoprisms-notable differences between seemingly identical construction principles. Chem Commun 4723
62. Schmittel M, Kalsani V, Mal P, Bats JW (2006) The HETTAP approach: self-assembly and metal ion sensing of dumbbell-shaped molecules and clip molecules. Inorg Chem 45:6370
63. Schmittel M, He B, Mal P (2008) Supramolecular multicomponent self-assembly of shape-adaptive nanoprisms: wrapping up C_{60} with three porphyrin units. Org Lett 10:2513
64. Schröder T, Brodbeck R, Letzel M, Mix A, Schnatwinkel B, Tonigold M, Volkmer D, Mattay J (2008) A self-assembling metallosupramolecular cage based on cavitand-terpyridine subunits. Tetrahedron Lett 49:5939
65. Aspley CJ, Williams JAG (2001) Palladium-catalysed cross-coupling reactions of ruthenium bis-terpyridyl complexes: strategies for the incorporation and exploitation of boronic acid functionality. New J Chem 25:1136
66. Buschmann WE, Miller JS (1998) Sources of naked divalent first-row metal ions: synthesis and characterization of $[M^{II}(NCMe)_6]^{2+}$ (M = V, Cr, Mn, Fe, Co, Ni) salts of tetrakis[3,5-bis (trifluoromethyl)phenyl]borate. Chem Eur J 4:1731
67. Brookhart M, Grant B, Volpe AF (1992) $[(3,5\text{-}(CF_3)_2C_6H_3)_4B]^-[H(OEt_2)_2]^+$: a convenient reagent for generation and stabilization of cationic, highly electrophilic organometallic complexes. Organometallics 11:3920
68. Nishida H, Tadaka N, Yoshimura M, Sonoda T, Kobayashi H (1984) Tetrakis[3,5-bis (trifluoromethyl)phenyl]borate. Highly lipophilic stable anionic agent for solvent-extraction of cations. Bull Chem Soc Jpn 57:2600
69. Cohen Y, Avram L, Frish L (2005) Diffusion NMR spectroscopy in supramolecular and combinatorial chemistry: an old parameter–new insights. Angew Chem Int Ed 44:520
70. Glatter O (1979) The interpretation of real-space information from small angle scattering experiments. J Appl Crystallogr 12:166
71. Svergun DI (1992) Determination of the regularization parameter in indirect-transform methods using perceptual criteria. J Appl Crystallogr 25:495
72. Svergun DI (1999) Restoring low resolution structure of biological macromolecules from solution scattering using simulated annealing. Biophys J 76:2879
73. Svergun DI (1991) Mathematical methods in small-angle scattering data analysis. J Appl Crystallogr 24:485
74. Semenyuk AV, Svergun DI (1991) GNOM-a program pachage for small-angle scattering data processing. J Appl Crystallogr 24:537
75. Stewart JJP (1989) J Comp Chem 13:157
76. Damborsky J, Petřek P, Banáš P, Otyepka M (2007) Identification of tunnels in proteins, nucleic acids, inorganic materials and molecular ensembles. Biotechnol J 2:62
77. Liu JM, Tonigold M, Bredenkötter B, Schröder T, Mattay J, Volkmer D (2009) Synthesis of terpyridine-substituted calix[n]arenes. Tetrahedron Lett 50:1303

Top Curr Chem (2012) 319: 125–170
DOI: 10.1007/128_2011_280

Published online: 9 December 2011

Coronates, Spherical Containers, Bowl-Shaped Surfaces, Porous 1D-, 2D-, 3D-Metallo-Coordination Polymers, and Metallodendrimers

Rolf W. Saalfrank and Andreas Scheurer

Abstract Supramolecular coordination cages and polymers bear exceptional advantages over their organic counterparts. They are available in one-pot reactions and in high yields and display physical properties that are generally inaccessible with organic species. Moreover, their weak, reversible, noncovalent bonding interactions facilitate error checking and self-correction. This review emphasizes the achievements in supramolecular coordination container as well as polymer chemistry initiated by serendipity and their materialization based on rational design. The recognition of similarities in the synthesis of different supramolecular assemblies allows prediction of potential structures in related cases. The combination of detailed symmetry considerations with the basic rules of coordination chemistry has only recently allowed for the design of rational strategies for the construction of a variety of nanosized spherical containers, bowls, 1D-, 2D-, and 3D-coordination polymers with specified size and shape.

Keywords 1D-coordination polymers · 2D-coordination polymers · 3D-coordination polymers · Coronates · Host–guest chemistry · Metallodendrimers · Self-assembly · Spherates · Supramolecular chemistry

Contents

Progress is linked to the past

R.W. Saalfrank (✉) and A. Scheurer
Department Chemie und Pharmazie, Anorganische Chemie, Universität Erlangen-Nürnberg, Egerlandstr. 1, 91058 Erlangen, Germany
e-mail: rolf.saalfrank@chemie.uni-erlangen.de; andreas.scheurer@chemie.uni-erlangen.de

1 Introduction

Biology provides striking illustrations of thermodynamically stable architectures, such as the tobacco mosaic virus, DNA, and numerous protein complexes, generated via self-assembly [1–3]. Though the conceptual origins of self-assembly are rooted in biology, self-assembly is by no means restricted to biology [4–8]. In synthetic chemistry self-assembly leads basically to discrete nanoscale molecular devices and has therefore been proposed as a strategy for the development of new materials. To achieve the high degree of selectivity that we are used to from natural processes, synthetic chemists must improve conventional multistep reactions. For that reason, tailor-made templates, which recognize matching reaction partners and

bring them sufficiently close together to promote intermolecular reactions, are needed. In the past, numerous recognition motifs mimicking nature were offered in which metal ions often play an important role.

Lehn has described supramolecular chemistry as an information science in which molecular subunits that contain the necessary information self-assemble into large specific structures [9–15]. Consequently, self-assembly has been recognized as a powerful tool for the construction of supramolecular scaffolds, as demonstrated by numerous excellent contributions [16–66].

As the systems discussed in this review gradually became more and more complex, their presentation became more and more difficult. Therefore, to enhance understanding without loss of information, we have put much effort into the design of self-explanatory cartoons. The importance of abstraction and minimization for rapid recognition of complex pictures is especially useful in the case of nanosized 1D-, 2D-, and 3D-coordination polymers. All structural motives presented in this review are based on single crystal X-ray structure analyses and displayed as POVRAY stereoviews (red-blue: if necessary for didactic reasons). Unless stated otherwise, protons, disorder, and solvent molecules are omitted for clarity. We recommend the reader viewing the figures take the time sometimes necessary for the brain to adapt in order to experience the 3D world. The additional information the 3D pictures reveal is well worth this effort. The breadth of supramolecular coordination polymer chemistry has become progressively more apparent. Recent years have seen an explosive growth, as documented by the increasing number of laboratories joining the field whose work has been reported in an immense number of publications. It is therefore impossible to provide an exhaustive account of this field. We do not claim to give a complete overview, and examples are selected and highlighted according to their originality and are taken mainly from our own work. This review provides a personal account of how new synthetic tools were developed and put to use in our current work.

2 Coronates, Spherical Containers, Bowl-Shaped Surfaces Bis- and Tris-Bidentate Chelators as Endoreceptors: Cation-Mediated Formation of Metallocoronates and {2}-Metallocryptates and their One-Dimensional Coordination Polymers

2.1 Coronates and Sandwich Complexes

Previously, we pointed out the structural analogy between coronates and {2}- and {3}-cryptates and their topologically equivalent metallocoronates and

metallocryptates [67]. If the principles of organic crown ether chemistry are applied to the chemistry of metallocrown ethers (MCs), the complexation of differently sized cations by MCs should lead to metallocoronates of varying structures. As the ionic radii of alkali- and alkaline-earth-metal cations differ significantly, while the diameter of the MCs does not change substantially, the inclusion of small cations, such as Na^+ or Ca^{2+}, should lead to a complex with an Na^+ or Ca^{2+}/MC = 1:1 stoichiometry. In contrast, encapsulation of the larger K^+ ion should lead to an MC ether sandwich complex with a K^+/MC = 1:2 stoichiometry. Consequently, reaction of diethyl ketipinate H_2L^1 (**1**) with copper(II) acetate in the presence of calcium nitrate led to green crystals of the neutral trinuclear metallocoronate $[(Ca\subset\{Cu_3(L^1)_3\})(NO_3)_2]$ (**2**; Scheme 1, Fig. 1) [68]. The guest Ca^{2+} ion, whose charge is compensated by the two axially coordinated nitrate ions, is located in the center of the metallocoronand host.

Whereas encapsulation of the small cation Ca^{2+} ion led to host-guest system **2** with an M/MC = 1:1 stoichiometry, double deprotonation of di-*tert*-butyl ketipinate H_2L^2 (**1**) with 2 N potassium hydroxide and reaction of the dianion $(L^2)^{2-}$ with copper(II) chloride in methanol afforded the MC ether sandwich complex $[(K\subset\{Cu_3(L^2)_3\}_2)OMe]$ (**3**) with a K/MC = 1:2 stoichiometry (Scheme 1, Fig. 1) [68, 69].

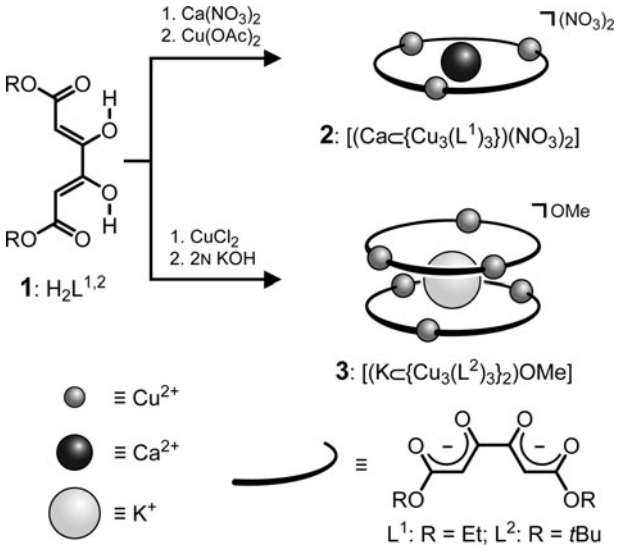

Scheme 1 Formation and schematic representation of $[(Ca\subset\{Cu_3(L^1)_3\})(NO_3)_2]$ (**2**) and $[(K\subset\{Cu_3(L^2)_3\}_2)OMe]$ (**3**)

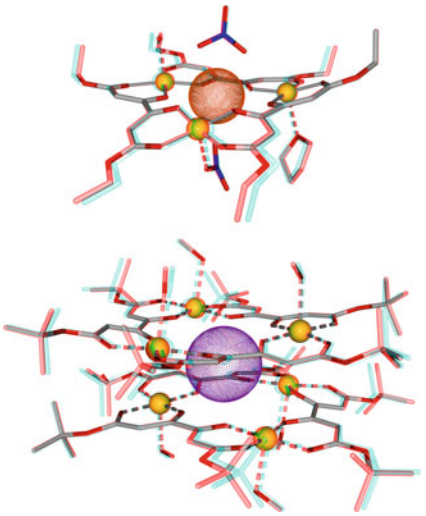

Fig. 1 Stereo representation of $[(Ca\subset\{Cu_3(L^1)_3\})(NO_3)_2]$ (**2**) (*top*) and cation $[K\subset\{Cu_3(L^2)_3\}_2]^+$ $(\mathbf{3})^+$ (*bottom*; the disordered counterion MeO^- is omitted for clarity)

2.2 *One-Dimensional Coordination Polymers from Metallocoronates: Threading Cesium Ions*

Further studies on the supramolecular coordination chemistry of copper(II) focused on the synthesis of oligonuclear complexes by self-assembly with the pentadentate ligand $(L^3)^{2-}$ with 2,6-pyridinyl-spacer [70]. To this end, H_2L^3 (**4**) was treated with calcium hydride and copper(II) acetate to give the metallocoronate $[(Ca\subset\{Cu_2(L^3)_2\})(OAc)_2]$ (**5**; Scheme 2). In the crystal, **5** is present as a dinuclear copper(II) coronate in which a calcium ion is encapsulated in the center; two acetates act as counterions.

In contrast, treatment of a solution of H_2L^3 (**4**) with copper(II) acetate and cesium carbonate does not yield a metallocoronate similar to **5**. Instead, the larger cesium ion, which prefers a higher coordination number, functions as a template for the formation of the one-dimensional coordination polymer $^1_\infty[(\{Cs_2\subset(\{Cu_2(L^3)_2\}_2\{OAc\}_2)\}Cs)_2(OAc)_2]$ (**6**; Scheme 2). The individual modules of **6** are composed of two concave $\{Cu_2(L^3)_2\}$ metallocoronands linked by two bidentate acetate ions. Endohedral encapsulation of two cesium ions and two acetate ions together with two molecules of ethanol in the container $(\{Cu_2(L^3)_2\}_2\{OAc\}_2)$ gives the cryptate $\{(Cs{\cdot}EtOH)_2\subset(\{Cu_2(L^3)_2\}_2\{OAc\}_2)\}$. Exohedral coordination of a further cesium ion to the cryptate generates the self-complementary unit $(\{(Cs{\cdot}EtOH)_2\subset(\{Cu_2(L^3)_2\}_2\{OAc\}_2)\}Cs)^+$. Linkage of two of these building blocks, alternately rotated by 90°, finally affords the dicationic monomer $[(\{(Cs{\cdot}EtOH)_2\subset(\{Cu_2(L^3)_2\}_2\{OAc\}_2)\}Cs)_2]^{2+}$ of the one-dimensional coordination polymer **6**. Charge compensation is achieved by acetate ions. To the best of our knowledge, the interatomic distances of the threaded cesium cations in **6** are the shortest measured to date (Fig. 2).

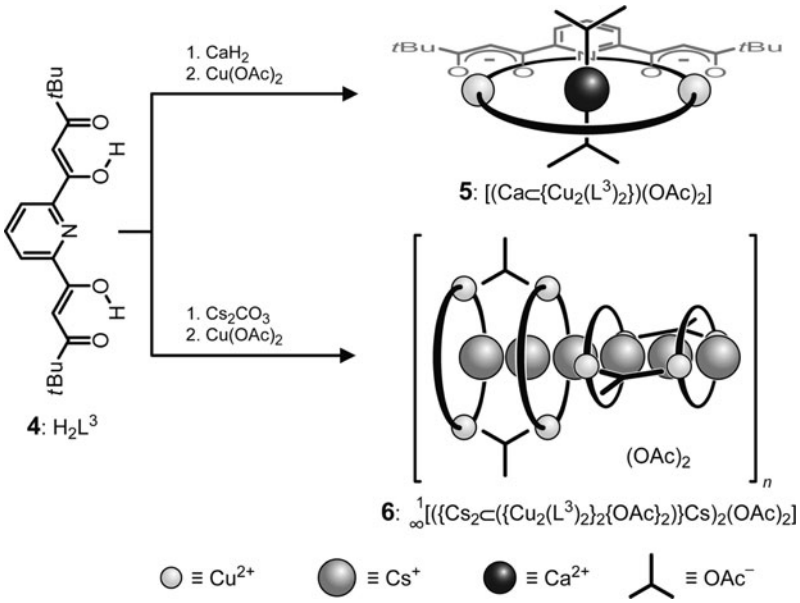

Scheme 2 Formation and schematic representation of $[(Ca\subset\{Cu_2(L^3)_2\})(OAc)_2]$ (**5**) and $_{\infty}^{1}[(\{Cs_2\subset(\{Cu_2(L^3)_2\}_2\{OAc\}_2)\}Cs)_2(OAc)_2]$ (**6**)

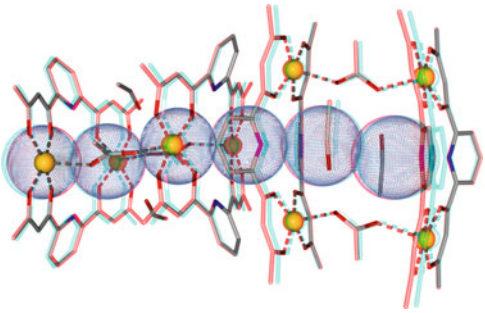

Fig. 2 Stereo representation of the dicationic repeating unit $[(\{(Cs{\cdot}EtOH)_2\text{-}\subset(\{Cu_2(L^3)_2\}_2\{OAc\}_2)\}Cs)_2]^{2+}$ of **6**, highlighting the close contact of the cesium ions (for clarity the *t*Bu groups are represented by Me)

2.3 {2}-Metallocryptates of Iron(III)

To synthesize the {2}-ironcryptates $[M\subset\{Fe_2(L^3)_3\}][X]_n$ (**7**–**9**, $n = 1$–3), 2,6-pyridinyl-spacered H_2L^3 (**4**) was treated with potassium hydride, strontium hydride, or lanthanum(III) chloride and subsequently with iron(III) chloride (Scheme 3) [71–75]. For instance, an X-ray analysis revealed that the cavity of {2}-metallocryptate $[K\subset\{Fe_2(L^3)_3\}]PF_6$ (**7**) is occupied by a potassium ion, with ninefold coordination to six ligand oxygen atoms and to three pyridine nitrogen

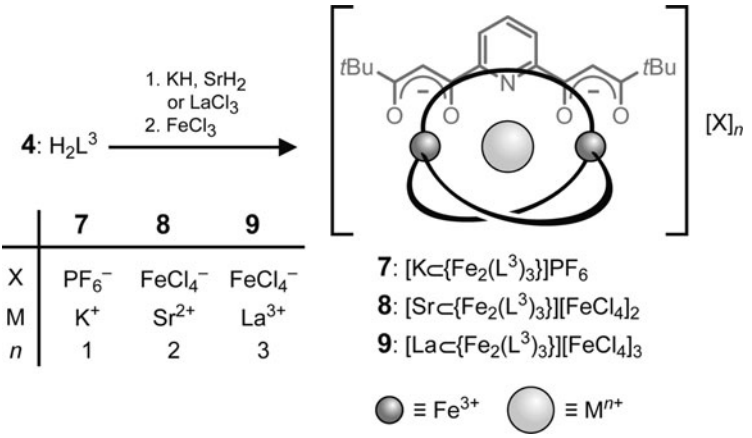

	7	8	9
X	PF_6^-	$FeCl_4^-$	$FeCl_4^-$
M	K^+	Sr^{2+}	La^{3+}
n	1	2	3

Scheme 3 Formation and schematic representation of $[M\subset\{Fe_2(L^3)_3\}][X]_n$ (**7–9**, $n = 1$–3)

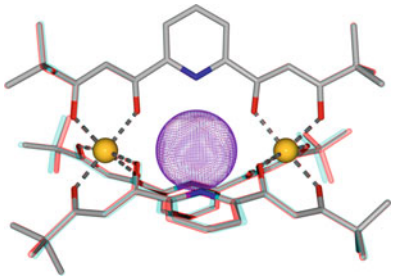

Fig. 3 Stereo representation of the cation *meso*-(Δ/Λ)-*fac*-$[K\subset\{Fe_2(L^3)_3\}]^+$ of **7**

donors (Fig. 3). There is a hexafluorophosphate counterion, and the two iron bridgeheads of the {2}-metallocryptate are octahedrally surrounded by six oxygen donors. In contrast to racemic homochiral {2}-ironcryptates **8** and **9**, the two iron centers in *meso*-(Δ/Λ)-*fac*-**7** have opposite configurations.

2.4 One-Dimensional Coordination Polymers from {2}-Metallocryptates of Metal(II) Ions

2.4.1 One-Dimensional Linear Strings

For further developments in the field of supramolecular coordination chemistry, it is of great interest to investigate how nature copes with electronically mismatched metal/ligand combinations. In other words, this type of approach transfers the intellectual responsibility for design to the molecules themselves [76, 77].

To expand the void in complexes derived from ligands mentioned so far, a catecholate ether spacer was adapted to the bis-1,3-diketo ligand system, as for instance in H_2L^4 (**10**). Consequently, reaction of six-coordinate nickel(II) and **10** in the presence of cesium carbonate yielded the neutral one dimensional polymer $_{\infty}^{1}$[{(Cs⊂{(Δ,Δ)-$Ni_2(L^4)_3$})Cs}{(Cs⊂{(Λ,Λ)-$Ni_2(L^4)_3$})Cs}] *meso*-(**11**) (Scheme 4) [78]. The fundamental building block is the {2}-metallocryptand $\{Ni_2(L^4)_3\}^{2-}$ core which is composed of two nickel centers linked through three bis-1,3-diketo dianions $(L^4)^{2-}$ with catecholate functionality (Fig. 4). The resulting {2}-metallocryptands are homochiral with either (Δ,Δ)-*fac* or (Λ,Λ)-*fac* stereochemistry at the nickel centers

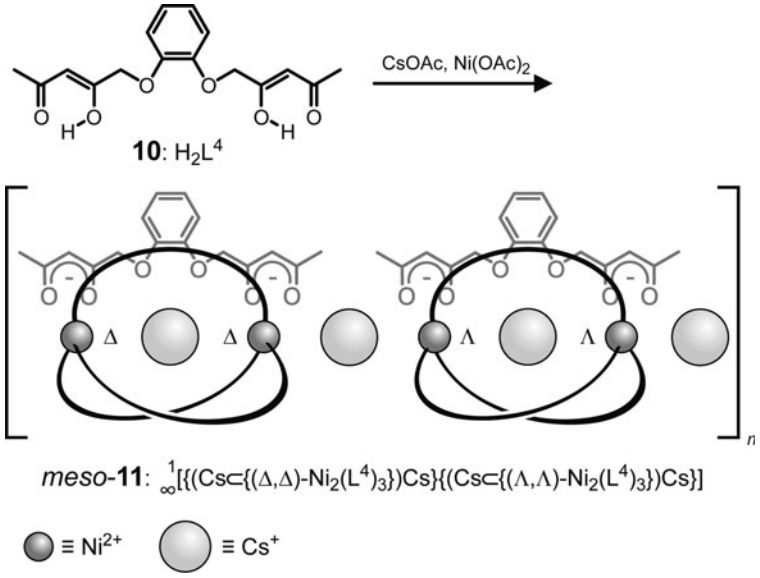

Scheme 4 Formation and schematic representation of $_{\infty}^{1}$[{(Cs⊂{(Δ,Δ)-$Ni_2(L^4)_3$})Cs}{(Cs⊂-{(Λ,Λ)-$Ni_2(L^4)_3$})Cs}] *meso*-(**11**)

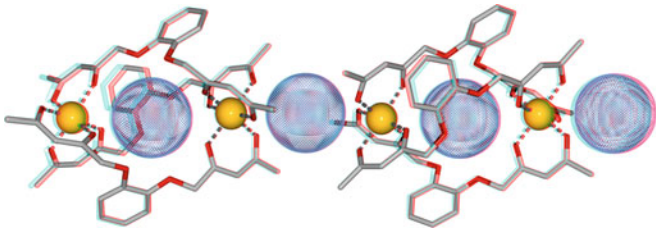

Fig. 4 Stereo representation of the repeating unit of one dimensional polymer $_{\infty}^{1}$[{(Cs⊂{(Δ,Δ)-$Ni_2(L^4)_3$})Cs}{(Cs⊂{(Λ,Λ)-$Ni_2(L^4)_3$})Cs}] *meso*-(**11**)

and can host a cesium ion in the cavity, which is coordinated by six carbonyl and six catecholate oxygen donors. Charge compensation of the thus formed enantiomers $[Cs\subset\{(\Delta,\Delta)/(\Lambda,\Lambda)\text{-}Ni_2(L^4)_3\}]^-$ is achieved through extra external cesium ions to give the neutral self-complementary building blocks $[Cs\subset\{(\Delta,\Delta)/(\Lambda,\Lambda)\text{-}Ni_2(L^4)_3\}Cs]$. These self-complementary building blocks aggregate alternately end-on through the external cesium ions to yield the one-dimensional coordination polymer *meso*-**11**.

When H_2L^4 (**10**) was treated with magnesium(II) acetate in the presence of cesium acetate, the cesium ions again function as templates. However, in contrast to the nickel case, which afforded *meso*-**11**, with magnesium(II) ions $_\infty^1[(Cs\subset\{(\Delta,\Delta)/(\Lambda,\Lambda)\text{-}Mg_2(L^4)_3\})Cs]$ *rac*-(**12**) was formed. Homochiral building blocks $[(Cs\subset\{(\Delta,\Delta)\text{-}Mg_2(L^4)_3\})Cs]$ and $[(Cs\subset\{(\Lambda,\Lambda)\text{-}Mg_2(L^4)_3\})Cs]$aggregate end-on across the external cesium ions to give the one-dimensional homochiral strings $_\infty^1[(Cs\subset\{(\Delta,\Delta)\text{-}Mg_2(L^4)_3\})Cs]$ Δ-(**12**) and $_\infty^1[(Cs\subset\{(\Lambda,\Lambda)\text{-}Mg_2(L^4)_3\})Cs]$ Λ-(**12**), which are packed in the crystal in alternating homochiral layers to give *rac*-**12** (Scheme 5, Fig. 5) [79]. Therefore, in the solid state the metal centers (Ni^{II} vs Mg^{II}) are controlling the sequence of chiral {2}-metallocryptates, leading to the formation of meso and homochiral 1D-coordination polymers *meso*-**11** and *rac*-**12**, respectively.

2.4.2 Meandering One-Dimensional Strings

To suppress the formation of self-complementary monomers and their polymerization by making the external pockets of the cryptates too small to host the external cesium ions, H_2L^5 (**13**) with bulkier phenyl groups was used. To that end, stoichiometric amounts of H_2L^5, alkali acetates, and divalent hexacoordinate metal acetates were reacted (Scheme 6). Since the polymers *meso*-**14** are isostructural, only the structure of *meso*-**14e** is discussed in detail. In *meso*-**14e**, two {2}-metallocryptate

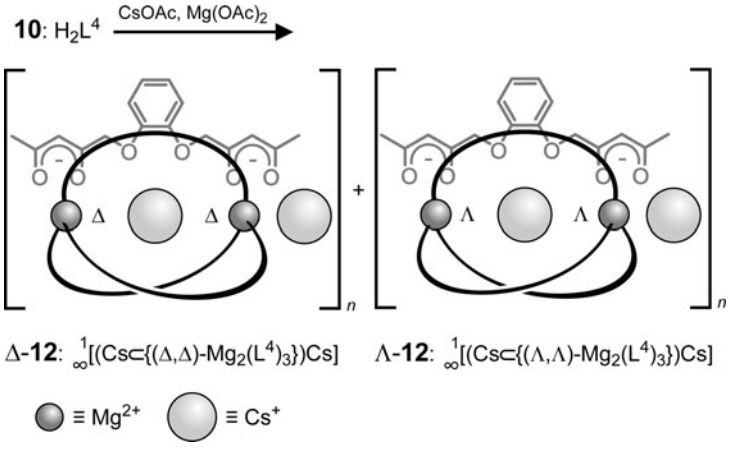

Scheme 5 Formation and schematic representation of homochiral $_\infty^1[(Cs\subset\{(\Delta,\Delta)\text{-}Mg_2(L^4)_3\})Cs]$ Δ-(**12**) and $_\infty^1[(Cs\subset\{(\Lambda,\Lambda)\text{-}Mg_2(L^4)_3\})Cs]$ Λ-(**12**) of *rac*-**12**

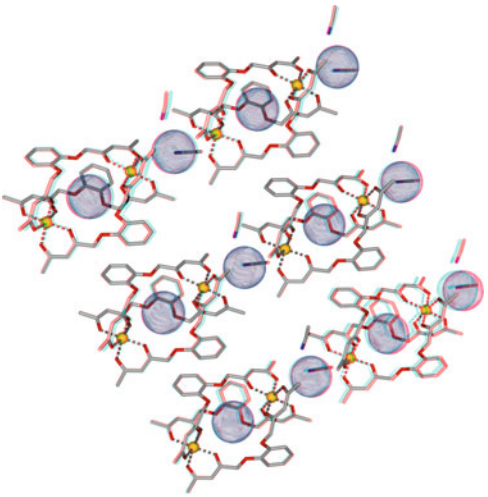

Fig. 5 Stereo representation of part of a homochiral layer of *rac*-**12** built-up by six homochiral repeating units $[(Cs\subset\{(\Lambda,\Lambda)\text{-}Mg_2(L^4)_3\})Cs]$, together with coordinating acetonitrile solvent molecules

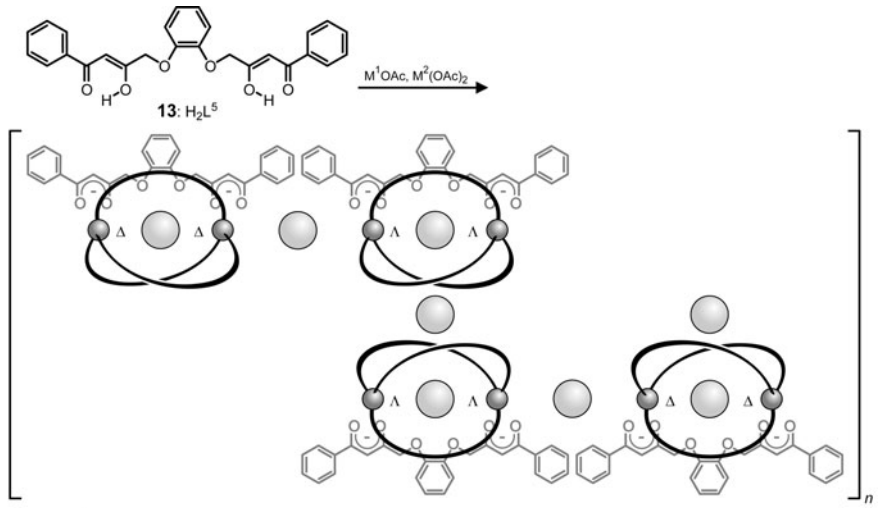

Scheme 6 Formation and schematic representation of meandering $_{\infty}^{1}[(\{(Cs\subset\{(\Delta,\Delta)\text{-}Co_2(L^5)_3\})\text{-}Cs_{end}(Cs\subset\{(\Lambda,\Lambda)\text{-}Co_2(L^5)_3\})\}Cs_{side})(\{(Cs\subset\{(\Lambda,\Lambda)\text{-}Co_2(L^5)_3\})Cs_{end}(Cs\subset\{(\Delta,\Delta)\text{-}Co_2(L^5)_3\})\}Cs_{side})]$ *meso*-(**14e**)

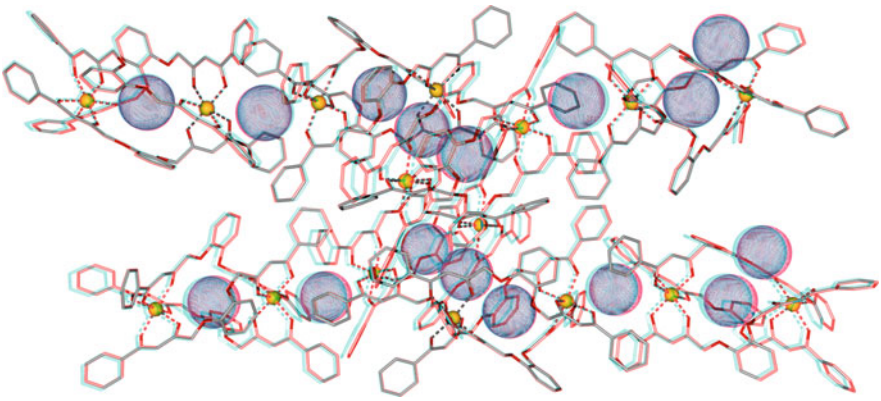

Fig. 6 Stereo representation of two repeating units of meandering $_{\infty}^{1}$[({Cs⊂{(Δ,Δ)-$Co_2(L^5)_3$}})-Cs_{end}(Cs⊂{(Λ,Λ)-$Co_2(L^5)_3$}})Cs_{side})({Cs⊂{(Λ,Λ)-$Co_2(L^5)_3$})Cs_{end}(Cs⊂{(Δ,Δ)-$Co_2(L^5)_3$}})Cs_{side})] *meso*-(**14e**) in the solid state

enantiomers are linked end-on by only one cesium ion to give a *meso*-fragment, and a second fragment is coordinated side-on to these units, giving meandering polymer *meso*-**14e**. Therefore, Cs_{end} links the enantiomers (Cs⊂{(Δ,Δ)/(Λ,Λ)-$Co_2(L^5)_3$})$^-$ to give *meso*-{(Cs⊂{(Δ,Δ)-$Co_2(L^5)_3$})Cs_{end}(Cs⊂{(Λ,Λ)-$Co_2(L^5)_3$})}$^-$, while Cs_{side} links the *meso*-fragments across their homochiral {2}-metallocryptate halves to give $_{\infty}^{1}$[({Cs⊂{(Δ,Δ)-$Co_2(L^5)_3$})Cs_{end}(Cs⊂{(Λ,Λ)-$Co_2(L^5)_3$})}Cs_{side})({Cs⊂-{(Λ,Λ)-$Co_2(L^5)_3$})Cs_{end}(Cs⊂{(Δ,Δ)-$Co_2(L^5)_3$})}Cs_{side})] *meso*-(**14e**). The meandering strands of the isostructural *meso*-**14e** polymers are packed in parallel in the crystal (Fig. 6) [79].

3 Bis-Bidentate Chelators: Mixed-Valent Tetranuclear Chelate Complexes of Iron [M⊂{$Fe_{4-n}^{II}Fe_n^{III}(L^6)_6$}]$^{0\pm}$ with Endohedral Guests

The neutral mixed-valent tetranuclear iron chelate complexes [M⊂{$Fe^{II}Fe_3^{III}(L^6)_6$}] (**16**) are available according to the direct method in a one-pot reaction from dialkyl malonates **15** with methyllithium, iron(II) chloride, and oxalyl chloride with subsequent aerobic aqueous ammonium chloride or alkali metal chloride work up [80].

However, when aqueous solutions of tetramethylammonium chloride, lithium chloride, or alkaline-earth-metal chlorides were used, aerobic workup afforded the all-iron(III) complexes [H_2O⊂{$Fe_4^{III}(L^6)_6$}] (**17**). Accordingly, [NH_4⊂{$Fe_4^{III}(L^6)_6$}]$^+$ (NH_4-**18**) was synthesized directly, starting with iron(III) chloride and followed by workup with an aqueous solution of ammonium acetate instead of tetramethylammonium chloride. Furthermore, the all-iron(III) complex

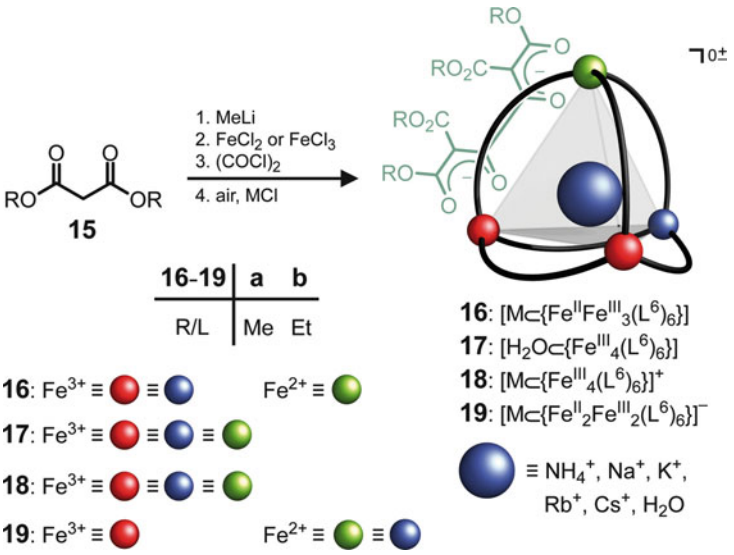

Scheme 7 Formation and schematic representation of $[M\subset\{Fe^{II}Fe_3^{III}(L^6)_6\}]$ (**16**), $[H_2O\subset\{Fe_4^{III}(L^6)_6\}]$ (**17**), $[NH_4\subset\{Fe_4^{III}(L^6)_6\}]^+$ (NH_4-**18**) and $[NH_4\subset\{Fe_2^{II}Fe_2^{III}(L^6)_6\}]^-$ (NH_4-**19**)

cations $[K\subset\{Fe_4^{III}(L^6)_6\}]^+$ (K-**18**) and $[Cs\subset\{Fe_4^{III}(L^6)_6\}]^+$ (Cs-**18**) are accessible from **17** by simple exchange of the encapsulated water molecule for the corresponding alkali metal ions. Finally, the mixed-valent complex anion $[NH_4\subset\{Fe_2^{II}Fe_2^{III}(L^6)_6\}]^-$ (NH_4-**19**) is available from dialkyl malonates **15** with methyllithium, iron(II) chloride, and oxalyl chloride after rapid aerobic workup with an aqueous ammonium chloride solution (Scheme 7) [80]. The mixed-valent or all-iron(III) nature of Cs-16**b**, Cs-**18b**, K-**18b**, and NH_4-**19b** was determined by Mössbauer spectroscopy [81]. The complexes **16**–**19** are formed as racemic mixtures and are basically isostructural, with (Δ,Δ,Δ,Δ)/(Λ,Λ,Λ,Λ)-configuration at the octahedrally coordinated iron centers; the complexes have approximately *T*-molecular symmetry. The four iron centers are located in the apices of a tetrahedron with water or cations encapsulated in the center, and the six edges are bridged by the doubly negatively charged, ditopic, tetradentate chelate ligands. Figure 7 displays the X-ray structure of $[NH_4\subset\{Fe^{II}Fe_3^{III}(L^6)_6\}]$ (NH_4-**16a**).

To enlarge the size of the cavity of the tetrahedral complexes mentioned so far, 4,4'-phenylene and 4,4'-biphenylene spacers were introduced. For instance, when tetramethyl terephthaloyldimalonate was deprotonated with sodium hydride and the doubly negatively charged ditopic, tetradentate ligand $(L^{phen})^{2-}$ treated with iron (III) chloride, complex $[Fe_4(L^{phen})_6]$ with an empty cavity was isolated (not shown). In contrast to racemic (Δ,Δ,Δ,Δ)/(Λ,Λ,Λ,Λ)-(**16**–**19**), complex (Δ,Δ,Λ,Λ)-$[Fe_4(L^{phen})_6]$ is achiral (*meso*-form) and has S_4-molecular symmetry in the crystal [82–85].

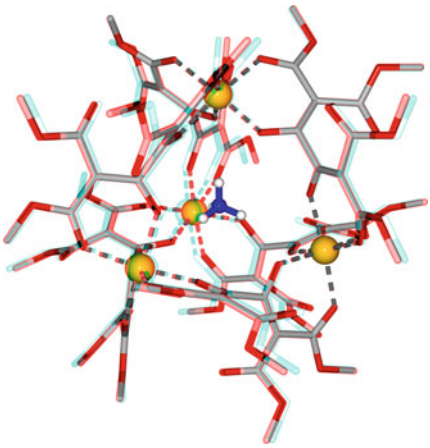

Fig. 7 Stereo representation of (Δ,Δ,Δ,Δ)-$[NH_4\subset\{Fe^{II}Fe_3{}^{III}(L^6)_6\}]$ (NH_4-**16a**)

4 Tris-Bidentate Chelators

4.1 Unoccupied Tetranuclear Chelate Complexes $[Fe_4(L^7)_4]$ and $[Fe_6(L^8)_6]$ from 1,3,5-Substituted Phenyl Centered Tripodal Tris-Bidentate Chelators

Compared with the *T*-symmetric edge-bridged complexes described in Sect. 3, there are far fewer examples of *T*-symmetric complexes in which the octahedrally coordinated metal centers in the vertices of a tetrahedron are linked by tripodal tris-(bidentate) ligands that occupy the tetrahedral faces. In a one-pot reaction, the tetranuclear iron(III) chelate complex $[Fe_4(L^7)_4]$ (**22**) was generated from benzene-1,3,5-tricarboxylic acid trichloride **20** and bis-*tert*-butyl malonate **21** ($R^1 = t$Bu). Alternatively, hexanuclear trigonal antiprismatic iron chelate complex $[Fe_6(L^8)_6]$ (**23**) was formed starting from bis-*para*-tolyl malonate **21** ($R^2 = p$Tol) by employing the same reaction conditions as for the synthesis of **22** (Scheme 8) [86–90].

The all-iron(III) nature of **22** and **23** was determined by Mössbauer spectroscopy. In $[Fe_4(L^7)_4]$ (**22**), four octahedrally coordinated iron centers constitute the apices of a tetrahedron, and the four tripodal, tris(bidentate) ligands $(L^7)^{3-}$ are centered above the triangular faces of the tetrahedron [86]. Hence, **22** has nearly *T*-molecular symmetry, and the crystals are composed as racemic mixtures of homoconfigurational (Δ,Δ,Δ,Δ)/(Λ,Λ,Λ,Λ)-*fac* stereoisomers. There is no evidence that the cavity of the tetrahedron hosts a guest (Fig. 8, top) [49, 62, 91–99].

Complex $[Fe_6(L^8)_6]$ (**23**) can be described as having idealized D_3-molecular symmetry. The iron centers define the apices of a distorted trigonal antiprism in which six tripodal, tris(bidentate) ligands $(L^8)^{3-}$ make up the equatorial faces, leaving the top and bottom triangles unoccupied. All six iron(III) ions are

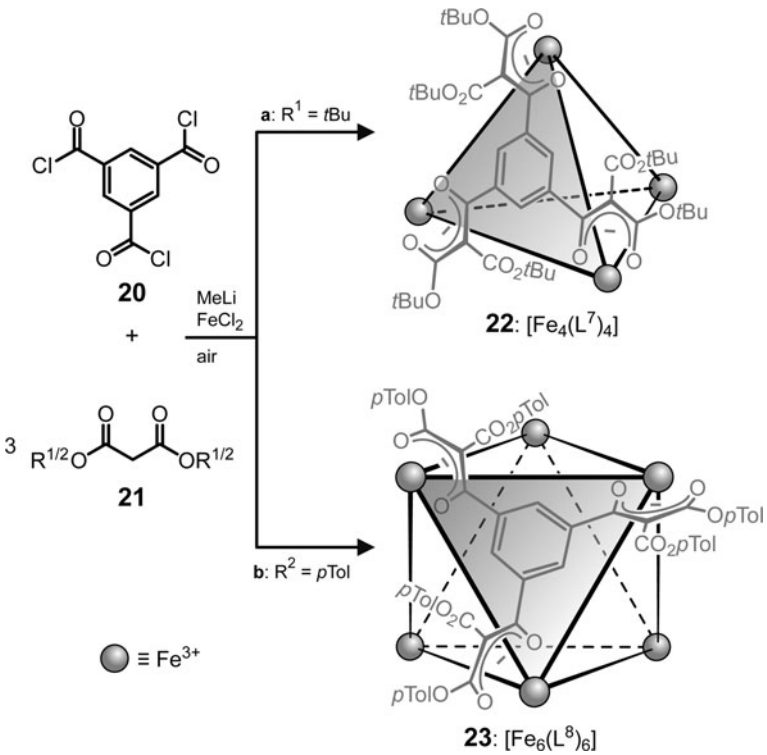

Scheme 8 Formation and schematic representation of $[Fe_4(L^7)_4]$ (**22**) and $[Fe_6(L^8)_6]$ (**23**)

identically octahedrally coordinated, and **23** exists as a racemic mixture of homoconfigurational (Δ,Δ,Δ,Δ,Δ,Δ)/(Λ,Λ,Λ,Λ,Λ,Λ)-*fac* stereoisomers (Fig. 8, bottom).

4.2 Occupied Tetranuclear Chelate Complexes $[M\subset\{In_4^{III}(L^9)_4\}]$ from an N-Centered Tripodal Heptadentate Chelator

Since there is no evidence that the electron deficient cavity of the tetrahedron **22** (Sect. 4.1) hosts a guest, in general N-centered tripodal heptadentate ligands $(L)^{3-}$ should be suitable to complex and bridge appropriate metal ions, leading to oligonuclear cages appropriate to host cationic guests. Therefore, when H_3L^9 (**24**) was treated with cesium carbonate and indium(III) perchlorate, pentanuclear host–guest complex $[Cs\subset\{In_4(L^9)_4\}]ClO_4$ (**25**) was isolated. However, when the experiment was repeated in absence of an alkali base, endohedral N-protonated tetranuclear $[In_4(H^NL^9)_4](ClO_4)_4$ (**26**) was isolated. On the other hand, reaction of indium(III) perchlorate and H_3L^9 (**24**) with subsequent addition of triethylamine

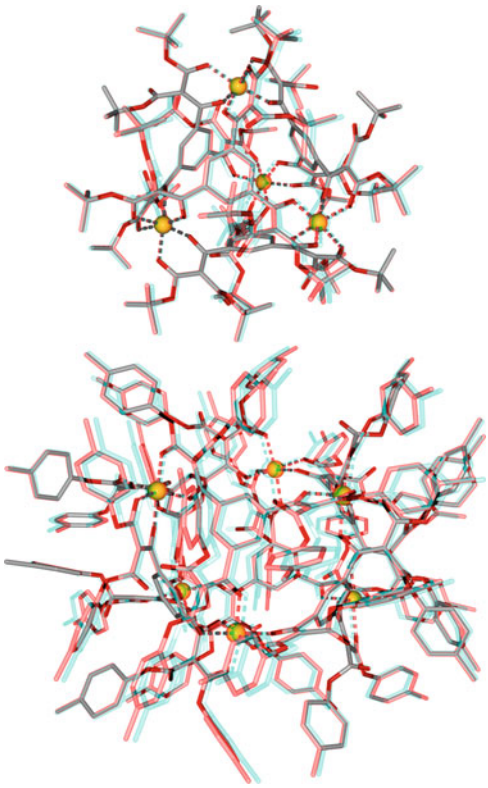

Fig. 8 Stereo representation of (Δ,Δ,Δ,Δ)-*fac*-$[Fe_4(L^7)_4]$ (**22**) (*top*), and (Δ,Δ,Δ,Δ,Δ,Δ)-*fac*-$[Fe_6(L^8)_6]$ (**23**) (*bottom*)

afforded the neutral tetranuclear complex $[In_4(L^9)_4]$ (**27**) (Scheme 9) [49, 62, 91–100].

The structure determination of **25**–**27** was accomplished by ^1H and ^{13}C NMR spectroscopy. In racemic, homochiral (Δ,Δ,Δ,Δ)/(Λ,Λ,Λ,Λ)-*fac* **25** and **26**, four indium ions constitute the apices of a tetrahedron, and the four tripodal ligands $(L^9)^{3-}$ are centered above the triangular faces of the tetrahedron. Hence, **25** and **26** have nearly *T* symmetry. There are a cesium ion or four protons linked to the nitrogen lone pairs directed to the cavity center of the tetrahedron (Fig. 9) [100]. Whereas in the complexes **25** and **26** with *T*-molecular symmetry all four ligands are equivalent, a tripling of the signals was observed in both the ^1H and ^{13}C NMR spectra of **27**. According to the X-ray structure, (Δ,Δ,Λ,Λ)-$[In_4(L^9)_4]$ (**27**) has idealized S_4-molecular symmetry, and the indium ions have a distorted octahedral coordination sphere with alternative Δ or Λ configuration. In addition, the X-ray data imply that the C_3 symmetry of the ligands $(L^9)^{3-}$ in **27** is broken during complexation to the indium ions and that the lone pairs at nitrogen are displaced with respect of the interior in **25** and **26** to the surface in **27**. However, despite the desymmetrized C_1-symmetric ligands $(L^9)^{3-}$, **27** is intrinsically achiral. This is due

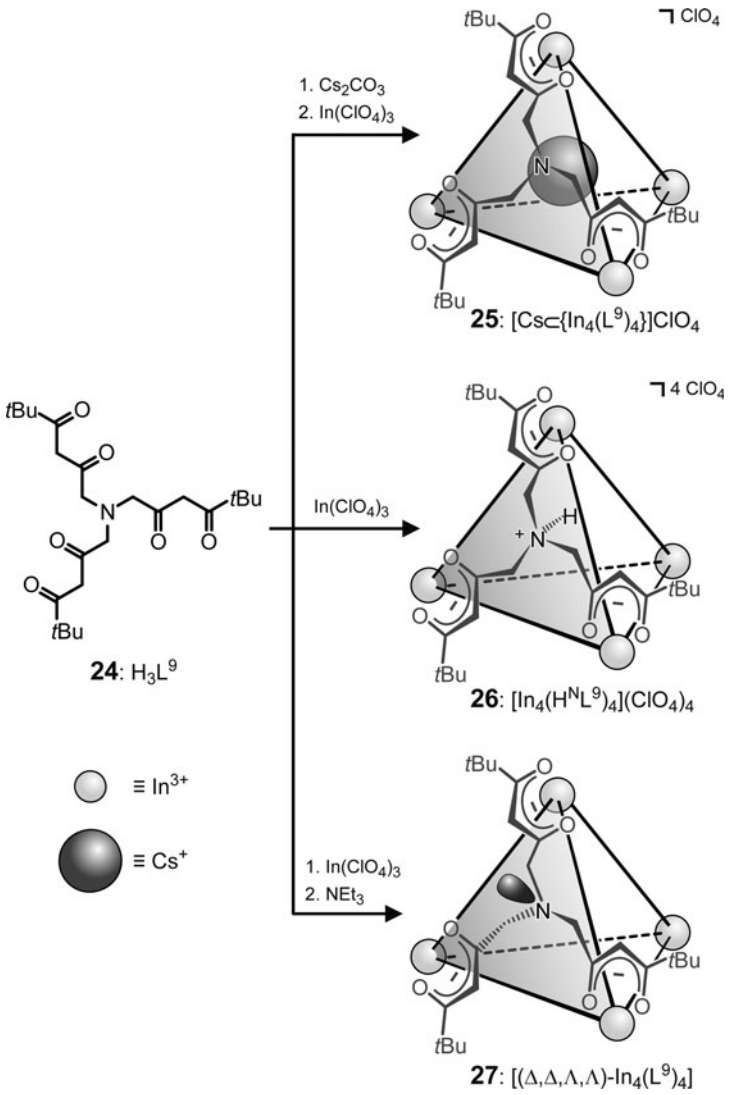

Scheme 9 Formation and schematic representation of $[Cs\subset\{In_4(L^9)_4\}]ClO_4$ (**25**), $[In_4(H^NL^9)_4](ClO_4)_4$ (**26**), and *meso*-(Δ,Δ,Λ,Λ)-$[In_4(L^9)_4]$ (**27**)

to the (*P*)/(*M*) helicity of the ligands $(L^9)^{3-}$ resulting in an overall S_4 molecule symmetry of *meso*-(Δ,Δ,Λ,Λ)-(*P*,*P*,*M*,*M*)-$[In_4(L^9)_4]$ (**27**) (Fig. 9) [100].

In total agreement with the X-ray data, the ^{1}H NMR spectrum of **27** in $[D_8]$toluene at 20 °C displays two sets of three signals for the olefinic protons and *t*Bu groups. The diastereotopic CH_2 protons appear as three simple, but different, AB systems. This proves **27** to be kinetically stable on the NMR timescale. Most interestingly, the ^{1}H NMR spectrum of *meso*-(Δ,Δ,Λ,Λ)(*P*,*P*,*M*,*M*)-$[In_4(L^9)_4]$ (**27**) revealed

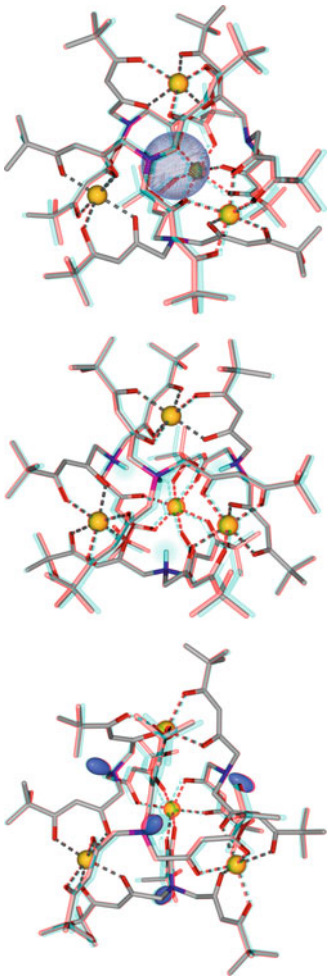

Fig. 9 Stereo representation of monocation of (Δ,Δ,Δ,Δ)-$[Cs\subset\{In_4(L^9)_4\}]^+$ (**25**)$^+$ (*top*), tetracation (Λ,Λ,Λ,Λ)-$[In_4(H^NL^9)_4]^{4+}$ (**26**)$^{4+}$ (*center*), and neutral *meso*-(Δ,Δ,Λ,Λ)-(*P*,*P*,*M*,*M*)-$[In_4(L^9)_4]$ (**27**) (*bottom*)

temperature dependence. In the range of 20–105 °C the signals of the olefinic protons (blue), the *t*Bu groups (red), and the diastereotopic CH_2 protons (green) become broader and finally coalesce (Fig. 10) [101]. The unique dynamic temperature-dependent ^{1}H NMR spectroscopic behavior of *meso*-**27** can be explained by an unprecedented mesomerization of the identical twins (Δ,Δ,Λ,Λ)(*P*,*P*,*M*,*M*)-**27** ⇄ (Λ,Λ,Δ,Δ)(*M*,*M*,*P*,*P*)-**27'** (Fig. 10). This mesomerization process is the first of this type and requires *four* tandem Bailar twists, which result in the inversion of the chirality at the indium centers together with the (*P*)/(*M*) inversion of the *four* coordinated C_1-symmetric helical ligands $(L^9)^{3-}$. This mesomerization process is reversible and occurs non-dissociative without the formation of diastereomers. Furthermore, it is worth noting that **27** and **27'** are identical and would only be distinguishable in the case of two pairs of different metal ions.

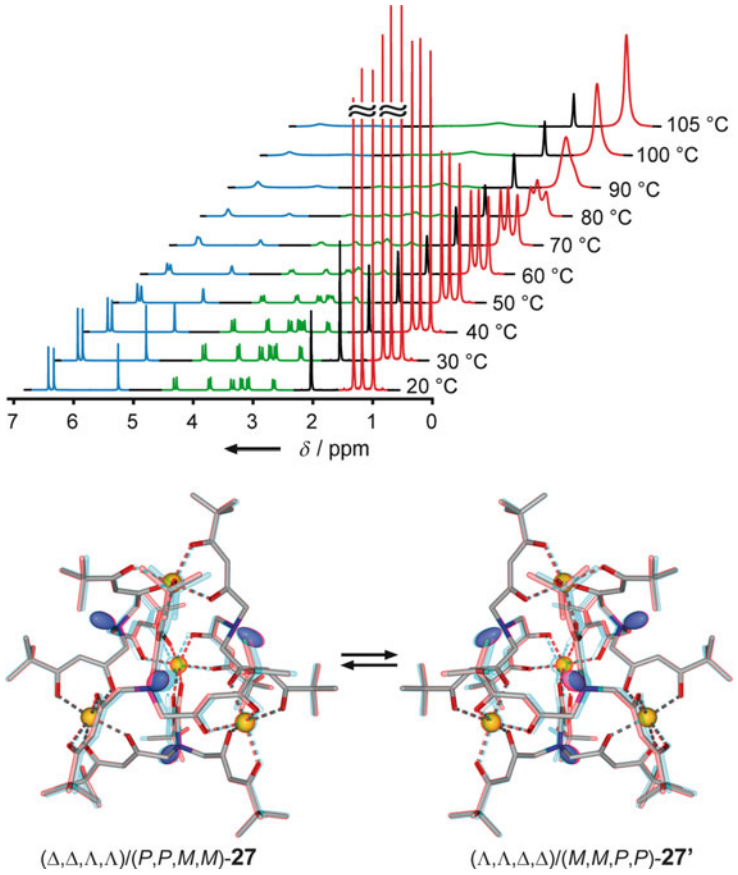

Fig. 10 *Top*: Variable-temperature (VT) ^{1}H NMR spectrum of *meso*-(Δ,Δ,Λ,Λ)-(*P*,*P*,*M*,*M*)-[$In_4(L^9)_4$] (**27**). *Bottom*: 3D presentation of the mesomerization (Δ,Δ,Λ,Λ)(*P*,*P*,*M*,*M*)-**27** ⇄ (Λ,Λ,Δ,Δ)(*M*,*M*,*P*,*P*)-**27'**

5 Bis-Bidentate Chelators: Tetranuclear Chelate Complexes of Metal(II) Ions $[(R^2NH_3)_4 \cap \{M_4^{II}(L^{10,11})_6\}]$ with Exohedral Guests

The tetranuclear magnesium chelate complexes $[(NH_4)_4 \cap \{Mg_4(L^{10,11})_6\}]$ (**29a,b**) were first synthesized by reaction of dialkyl malonate **28**, methylmagnesium iodide, and oxalyl chloride, followed by workup in aqueous ammonium chloride solution [102–105]. Now methyllithium/magnesium chloride instead of methylmagnesium iodide (direct method) is used, which by mere replacement of magnesium chloride by the chlorides of manganese, cobalt, and nickel also allows the synthesis of the corresponding tetranuclear complexes **29** (with $M^{II} = Mn^{2+}$, Co^{2+}, Ni^{2+}) [103, 105].

The doubly bidentate bridging ligands $(L^{10,11})^{2-}$ are formally obtained by *template coupling* of two dialkyl malonate monoanions with oxalyl chloride and spontaneous double deprotonation of the bis(enol) intermediates (Scheme 10).

To tune the physical and chemical properties of $[(NH_4)_4 \cap \{Mg_4(L^{10})_6\}]$ (**29a**), the direct method was extended by the exchange method (Scheme 11) [104]. Addition of an excess of *n*-alkylamines R^3-NH_2 leads to replacement of the

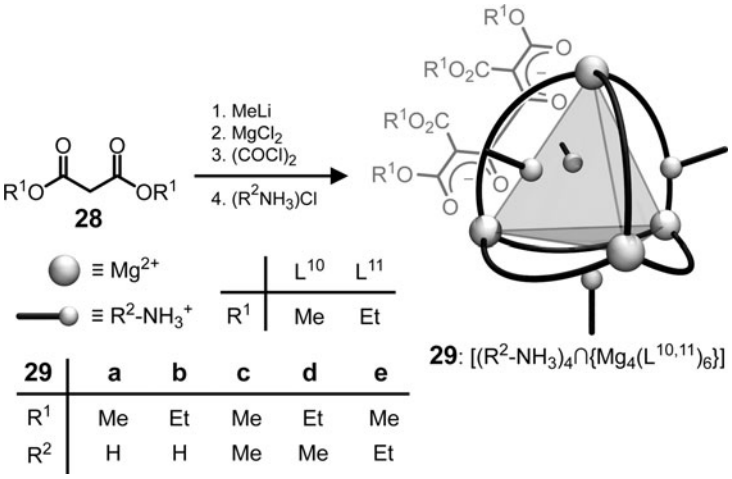

Scheme 10 Formation and schematic representation of $[(R^2NH_3)_4 \cap \{Mg_4(L^{10,11})_6\}]$ (**29**)

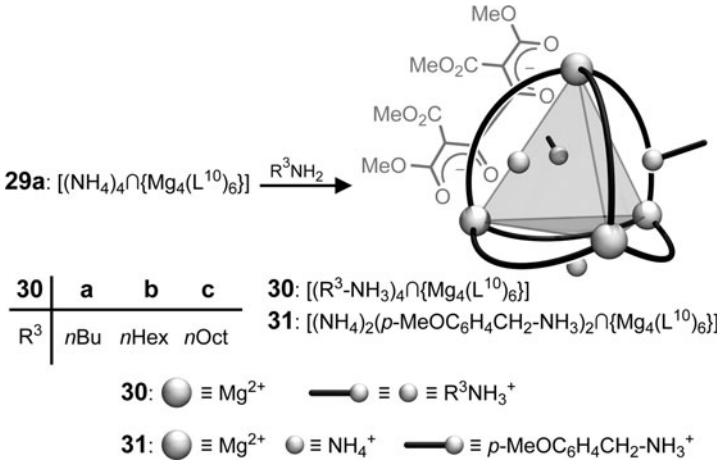

Scheme 11 Formation and schematic representation of $[(R^3NH_3)_4 \cap \{Mg_4(L^{10})_6\}]$ (**30**) and $[(NH_4)_2(p\text{-}MeOC_6H_4CH_2NH_3)_2 \cap \{Mg_4(L^{10})_6\}]$ (**31**)

ammonium ions in **29a** with *n*-alkylammonium ions to form the tetrakis-(*n*-alkylammonium)tetrahemispheraplexes $[(R^3NH_3)_4 \cap \{Mg_4(L^{10})_6\}]$ (**30**) or $[(NH_4)_2$-$(p\text{-}MeOC_6H_4CH_2NH_3)_2 \cap \{Mg_4(L^{10})_6\}]$ (**31**). Exchange of the four ammonium ions in $[(NH_4)_4 \cap \{Mg_4(L^{11})_6\}]$ (**29b**) by alkali-metal cations is achieved by stirring a solution of **29b** with potassium or cesium hydroxide to give the tetra-alkali-metal tetramagnesium chelate complexes $[M_4^I \cap (H_2O \subset \{Mg_4(L^{11})_6\})]$ ($M^I = K^+$, Cs^+) with an extra endohedrally encapsulated water molecule (not presented in Scheme 11) [104]. Similarly, when **29b** is stirred in solution with an excess of cobalt(II) chloride for several hours, the magnesium(II) ions are exchanged for cobalt(II) ions.

Furthermore, the study reveals that the space available at the surface of the tetrahedral, tetraanionic cores $\{Mg_4(L^{10,11})_6\}^{4-}$ depends on the steric demand of the ligands $(L^{10,11})^{2-}$, forcing the formation of $[(NH_4)_2(p\text{-}MeOC_6H_4CH_2NH_3)_2 \cap$-$\{Mg_4(L^{10})_6\}]$ (**31**) or of $[Na(EtNH_3)_3 \cap \{Mg_4(L^{11})_6\}]$ (not presented in Scheme 11) [104]. All the tetrahedral complexes are formed as racemic mixtures with either (Δ,Δ,Δ,Δ)-*fac* or (Λ,Λ,Λ,Λ)-*fac* configurations at the stereogenic metal centers. Since the complexes **29–31** are basically isostructural, only the solid-state structure of **31** is discussed as an example (Fig. 11). The $\{Mg_4(L^{10})_6\}^{4-}$ core of **31** is a distorted tetrahedron composed of four magnesium(II) ions, which are linked along each of the six edges by the bis(bidentate) ligands $(L^{10})^{2-}$, so that each of the four magnesium(II) ions is octahedrally coordinated. Charge compensation of the tetraanionic core $(\mathbf{31})^{4-}$, to give $[(NH_4)_2(p\text{-}MeOC_6H_4CH_2NH_3)_2 \cap \{Mg_4(L^{10})_6\}]$ (**31**), is achieved by two ammonium and two *p*-methoxybenzylammonium counterions, which are each hydrogen-bonded to three ideally oriented oxygen donors of the ligands at the triangular faces (Scheme 12, Fig. 12).

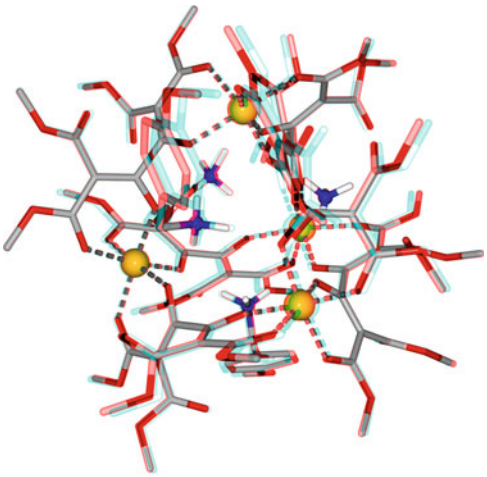

Fig. 11 Stereo representation of (Λ,Λ,Λ,Λ)-*fac*-$[(NH_4)_2(p\text{-}MeOC_6H_4CH_2NH_3)_2 \cap$-$\{Mg_4(L^{10})_6\}]$ (**31**)

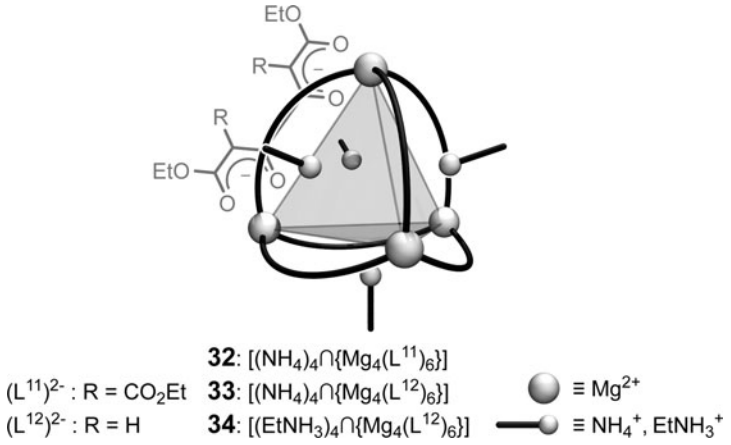

Scheme 12 Schematic representation of $[(NH_4)_4 \cap \{Mg_4(L^{11})_6\}]$ (**32**), $[(NH_4)_4 \cap \{Mg_4(L^{12})_6\}]$ (**33**), and $[(EtNH_3)_4 \cap \{Mg_4(L^{12})_6\}]$ (**34**)

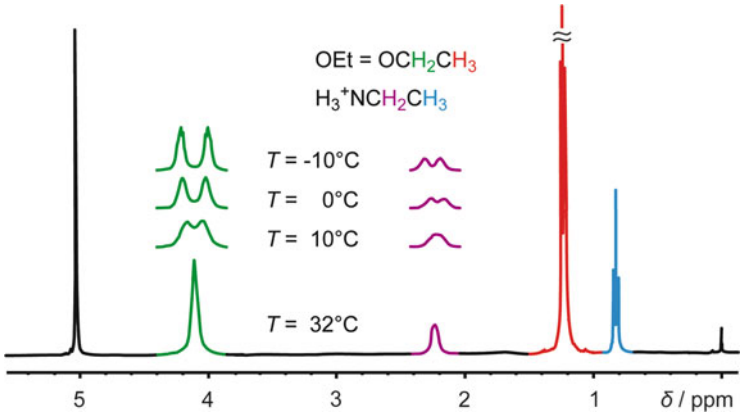

Fig. 12 Variable-temperature ^{1}H NMR spectrum of (Δ,Δ,Δ,Δ)/(Λ,Λ,Λ,Λ)-$[(EtNH_3)_4 \cap \{Mg_4(L^{12})_6\}]$ (**34**)

5.1 Enantiomerization of Tetrahedral Homochiral $[(RNH_3)_4 \cap \{Mg_4(L^{12})_6\}]$ Chelate Complexes: Enantiotopization of Diastereotopic Protons via Enantiomerization

So far we have described only the solid state structures of the tetrahemispheraplexes **29**–**31**. The question now was, is it possible to prove, whether

they are also stable in solution and do not fall apart. The most striking difference between $[(NH_4)_4 \cap \{Mg_4(L^{11})_6\}]$ (**32**) and $[(NH_4)_4 \cap \{Mg_4(L^{12})_6\}]$ (**33**) [106–108] is the fact that $(L^{12})^{2-}$ lacks the two bulky ester groups present in $(L^{11})^{2-}$ (Scheme 12).

Temperature-dependent ^{1}H NMR spectroscopy studies showed homochiral, racemic $(\Delta,\Delta,\Delta,\Delta)/(\Lambda,\Lambda,\Lambda,\Lambda)$-$[(NH_4)_4 \cap Mg_4(L^{11})_6\}]$ (**32**) to be kinetically stable on the NMR timescale. Owing to steric hindrance, rotation around the central C–C bond in $(L^{11})^{2-}$ is blocked, which prevents **32** from enantiomerization. The spectrum of **32** displays one triplet each for the ester and ether methyl groups and four multiplets for the corresponding diastereotopic methylene protons. Surprisingly, the ^{1}H NMR spectrum of racemic $(\Delta,\Delta,\Delta,\Delta)/(\Lambda,\Lambda,\Lambda,\Lambda)$-$[(NH_4)_4 \cap Mg_4(L^{12})_6\}]$ (**33**) reveals dynamic temperature dependence. The spectrum presents one sharp triplet for the ether methyl groups at 32 °C, but only one unresolved broad signal for the diastereotopic methylene protons. The triplet remains sharp over a temperature range from 32 °C to −10 °C, whereas the methylene protons at 32 °C are recorded as one broad signal and at −10 °C as two poorly resolved quartets. This phenomenon can be explained by simultaneous Bailar twists at the four octahedrally coordinated magnesium centers synchronized with sterically unhindered atropenantiomerization processes around the C–C single bonds of the six enolate ligands $(L^{12})^{2-}$, leading to the unprecedented enantiomerization $(\Delta,\Delta,\Delta,\Delta)$-(**33**) ⇄ $(\Lambda,\Lambda,\Lambda,\Lambda)$-(**33**). This profound, non-dissociative transformation monitored by NMR spectroscopy reflects the enantiotopization of the diastereotopic methylene protons [37, 106–111]. A prerequisite for the performance of the Bailar twists in **33** is its flexible $[Mg_4(L^{12})_6]^{4-}$ scaffold. This is guaranteed, since the ketipinate dianion $(L^{12})^{2-}$ allows sterically unhindered back and forth twists around the central C–C single bond and thus atropenantiomerization of the ligands. The enantiomerization of **33** occurs non-dissociatively without the formation of diastereoisomers, outlined by the sharp singlet for the olefinic protons, indicating the presence of only one product.

Supplementary support for the interpretation of the temperature-dependent dynamic ^{1}H NMR spectra of **33** is presented by additional studies of $(\Delta,\Delta,\Delta,\Delta)/(\Lambda,\Lambda,\Lambda,\Lambda)$-$[(EtNH_3)_4 \cap \{Mg_4(L^{12})_6\}]$ (**34**). In **33** and **34**, the methylene protons of the ligands exhibit identical VT NMR spectra. Moreover, the diastereotopic methylene protons (magenta) of the ethyl ammonium counterions of **34** display similar temperature-dependent coalescence as the ligand vinylether methylene protons (green). This is due to the fact that, even in solution, the ethyl ammonium groups are fixed to the tripodal calix-like surfaces of the $[Mg_4(L^{12})_6]^{4-}$ scaffold and therefore the methylene protons are in a chiral environment and display diastereotopicity.

6 Six- and Eight-Membered Iron(III) Coronates from Triethanolamine with Sodium- or Cesium-Ions as Endohedral Guests

When triethanolamine H_3L^{13} (**35**) was reacted with sodium hydride and iron(III) chloride, the hexanuclear centrosymmetric ferric wheel [Na⊂{$Fe_6(L^{13})_6$})Cl (**36**) was isolated. Amidst a set of possibilities in the template-mediated self-assembly of a supramolecular system, the one combination of building blocks is realized that leads to the best receptor for the substrate [112]. Therefore, the six-membered cyclic structure **36** is exclusively selected from all the possible iron triethoxyamine oligomers, when sodium ions are present. The iron(III) complex **36** is present as an S_6-symmetric wheel, with an encapsulated sodium ion in the center and a chloride counterion. Consequently, the trianion $(L^{13})^{3-}$ acts as a tripodal, tetradentate, tetratopic ligand, which each links three iron(III) ions and one sodium ion. In the presence of cations with different ionic radii, different structures are expected. Therefore, when triethanolamine H_3L^{13} (**35**) was reacted with cesium carbonate and iron(III) chloride, the octanuclear centrosymmetric ferric wheel [Cs⊂{$Fe_8(L^{13})_8$}]Cl (**37**) was isolated (Scheme 13) [113].

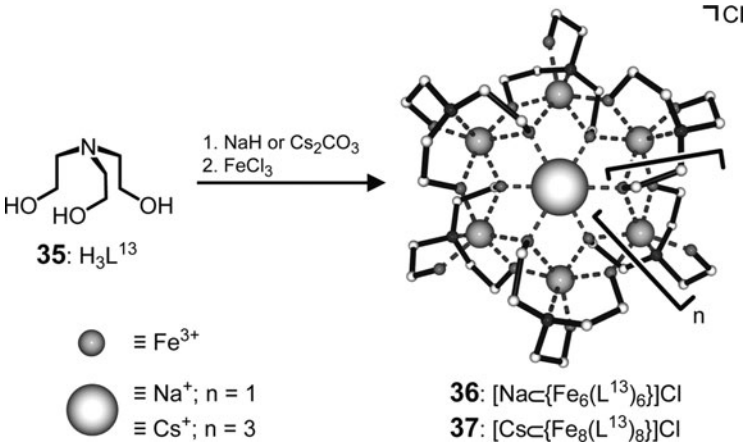

Scheme 13 Formation and schematic representation of [Na⊂{$Fe_6(L^{13})_6$})Cl (**36**) and [Cs⊂-{$Fe_8(L^{13})_8$}]Cl (**37**)

7 Six-Membered Iron(III) Coronands from N-Substituted Diethanolamines

7.1 Compartmentation Through Interdigitation

A common feature of the complexes $[Na\subset\{Fe_6(L^{13})_6\}]Cl$ (**36**) and $[Cs\subset\{Fe_8(L^{13})_8\}]Cl$ (**37**, Sect. 6) is that one μ_1-O^- ethoxide donor of the triethanolateamine ligands $[N(CH_2CH_2O^-)_2CH_2CH_2O^-]$ of $(L^{13})^{3-}$ does not participate in the formation of the ferric wheels. They function solely as ligands for the coordinative saturation of the iron centers. Therefore, any monoanionic donor, such as a chloride ion, could also be a candidate for this function. As expected, reaction of *N*-alkyldiethanolamines H_2L^{14-17} (**38**) with calcium hydride and iron(III) chloride yielded the neutral iron coronands $[Fe_6Cl_6(L^{14-17})_6]$ (**39**) with unoccupied centers (Scheme 14) [114–116].

In principle, all the six-membered ferric wheels $[Fe_6Cl_6(L^{14-17})_6]$ (**39**) are isostructural and have idealized S_6-molecular symmetry. However, there are fundamental differences concerning their crystal packing. For example, all the disk-like molecules of **39a** are arranged in parallel and are piled in cylindrical columns, with all the iron centers superimposed. Each column is surrounded by six parallel columns, which are alternately dislocated by 1/3 *c* and 2/3 *c* against the central one (Fig. 13).

An additional interesting feature of some ferric wheels is their readiness to create various superstructures, depending on the nature of their side arms. For instance, van der Waals interactions cause the side arms of $[Fe_6Cl_6(L^{15})_6]$ (**39b**) to interlock

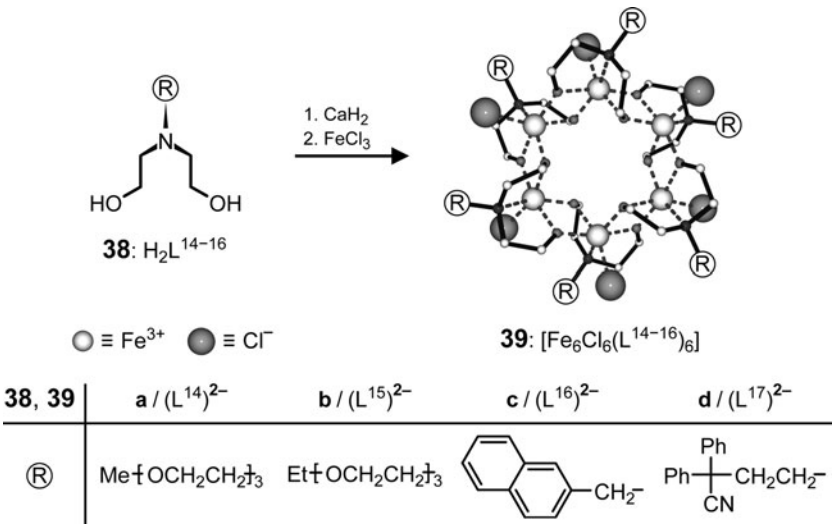

Scheme 14 Formation and schematic representation of $[Fe_6Cl_6(L^{14-17})_6]$ (**39**)

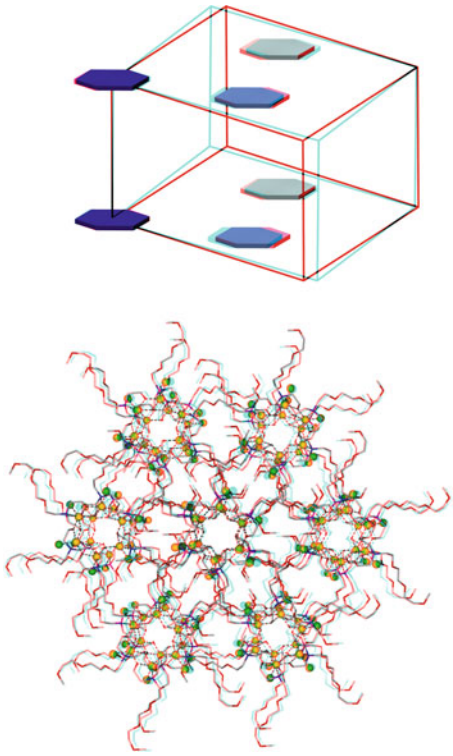

Fig. 13 Stereo representations of the schematic unit cell (*top*) and the crystal packing (*bottom*) of the ferric wheel $[Fe_6Cl_6(L^{14})_6]$ (**39a**), view along the *c* axis

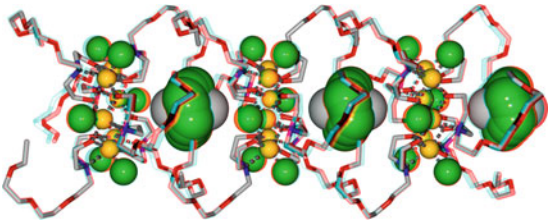

Fig. 14 Stereo representation of the columnar crystal packing of $[Fe_6Cl_6(L^{15})_6]$ (**39b**), highlighting the compartments with encapsulated disordered chloroform

and give rise to the formation of compartments occupied by disordered chloroform, respectively (Fig. 14).

7.2 Porosity of 3D-π–π-Stacked Ferric Wheels

An especially interesting example of crystal packing, leading to porous three-dimensional frameworks, is caused by π–π stacking of the naphthyl groups of the side arms of the ferric wheels $[Fe_6Cl_6(L^{16})_6]$ (**39c**) (Fig. 15).

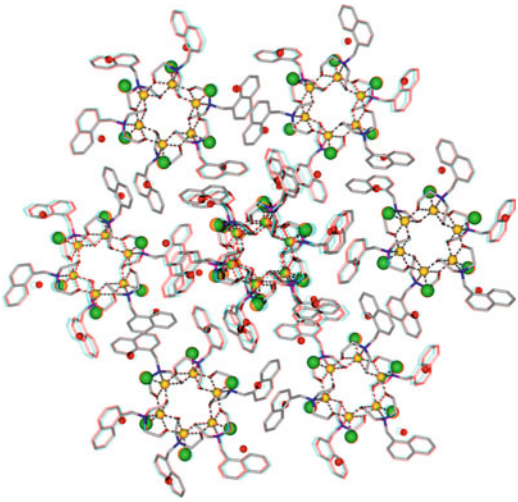

Fig. 15 Stereo representation of the crystal packing of $[Fe_6Cl_6(L^{16})_6]$ (**39c**), highlighting the π−π interactions together with the co-crystallized water molecules

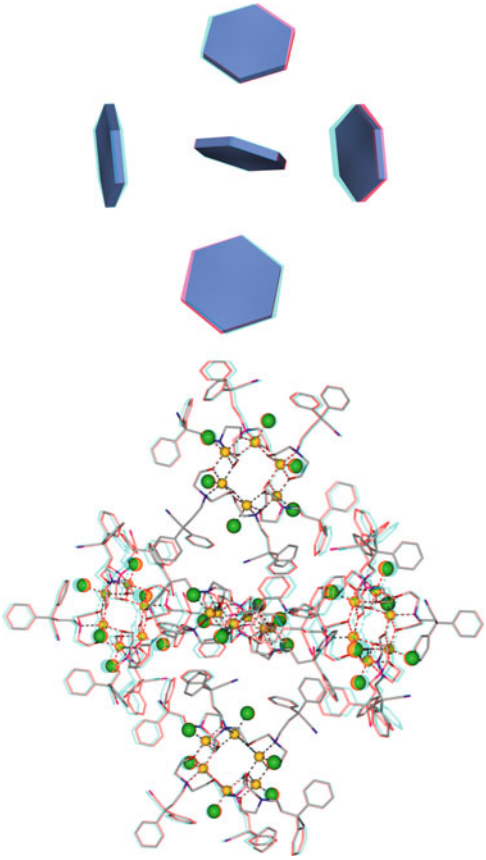

Fig. 16 Stereo representations of the schematic three-dimensional orthogonal arrangement of (*top*) and the crystal packing (*bottom*) of the ferric wheel $[Fe_6Cl_6(L^{17})_6]$ (**39d**)

Unlike $[Fe_6Cl_6(L^{14})_6]$ (**39a**) (Sect. 7.1), the ferric wheels of $[Fe_6Cl_6(L^{17})_6]$ (**39d**) are not arranged in parallel but rather are three-dimensionally perpendicular (Fig. 16) [114–116], a well-known arrangement for 3D-coordination polymers (Sect. 9.2, Fig. 18).

8 Metallodendrimers

Especially promising examples for the generation of three-dimensional interlocked systems are metallodendrimers such as $[M_6^{III}Cl_6(L^{dendrimer})_6]$ (**40**; $M^{III} = Fe^{3+}, In^{3+}$). Provided that the bridging ligands are flexible, these systems are not rigid, but rather undergo rapid, non-dissociative topomerization. This was shown by VT ^1H and ^{13}C NMR spectroscopy. The six indium centers experience inversion of configuration resulting in retention of the overall S_6 molecule symmetry (Fig. 17) [117].

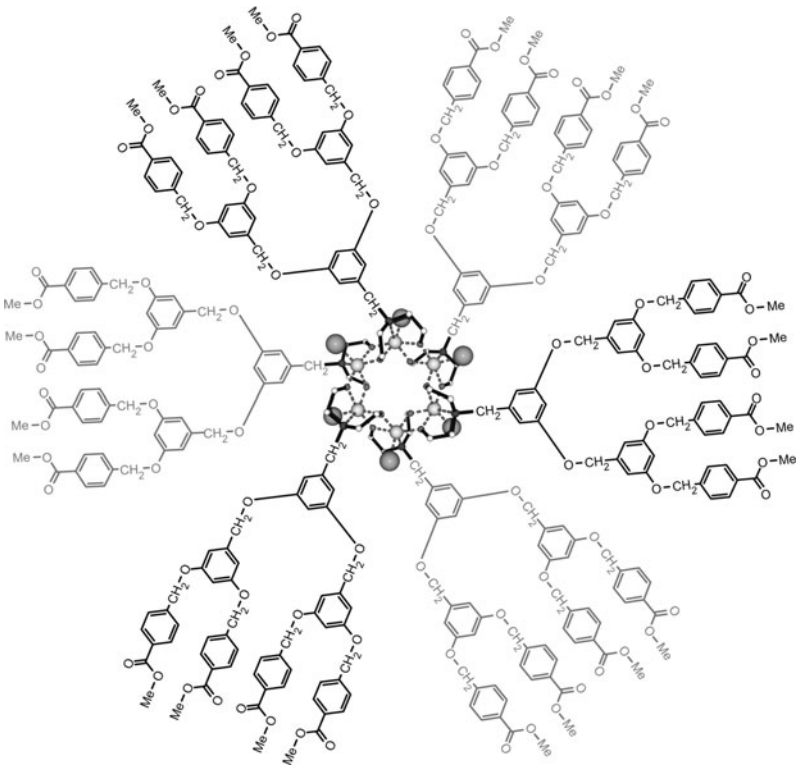

Fig. 17 Representation of metallodendrimer $[In_6Cl_6(L^{dendrimer})_6]$ (In-**40**)

9 Porous 1D-, 2D-, 3D-Metallo-Coordination Polymers – Tetrazolyl Enolate-, Pyrrolidinyl Enolate-, and Semicorrinate Anions as Chelate Ligands for Iron(II) and Copper(II) Ions: From Molecular to Collective Structures

9.1 Mononuclear- and Polynuclear Chelate Complexes of Iron(III)- and Iron(II) Ions

Naturally occurring and synthetically accessible siderophores (iron carriers) contain predominantly bidentate pyrocatechinato- or hydroxamato ligands and are of special interest because of their high affinity towards trivalent metal ions, especially towards iron(III) ions [5, 118–127]. The methyl *(E)*-2-(1-alkyl/aryl-4,5-dihydro-1*H*-tetrazol-5-ylidene)-2-cyanoacetates **41a–c**, first prepared by us [128], also appeared to be suitable as siderophores.

Upon reaction of the tetrazolyl enolates **41a–c** (HL^{18}) in ether with aqueous iron(III) chloride solutions, and after addition of *n*-hexane, the mononuclear complexes $[Fe(L^{18})_3]$ (**42a–c**) separate as deep blue microcrystals [129, 130].

The corresponding iron(III) complexes $[Fe(L^{18})_3]$ (**42d–f**) can be obtained analogously from the 1-(1-alkyl/aryl-1*H*-tetrazol-5-yl)-2-aIkanones **41d–f** (HL^{18}) [131]. Apparently, in both cases only the (Δ)/(Λ)-*mer*-isomers **42** of the two theoretically possible (Δ)/(Λ)-configurational isomers, are formed (Scheme 15) [129, 130].

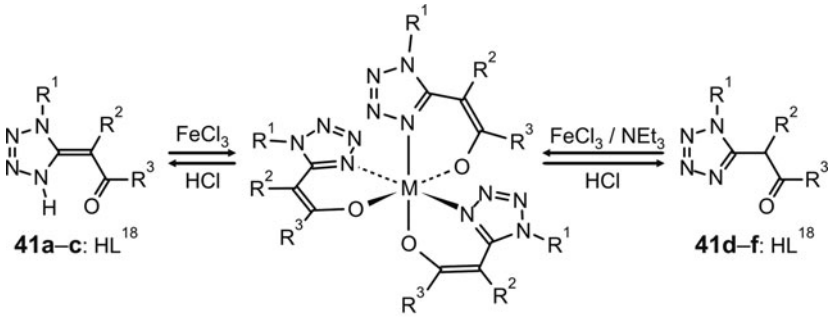

41, 42	a	b	c	d	e	f
R^1	Me_3CCH_2	$C_6H_5CH_2$	4-EtC_6H_4	Et	$Me(CH_2)_2$	Me_3C
R^2	CN	CN	CN	H	H	H
R^3	OMe	OMe	OMe	C_6H_5	C_6H_5	C_6H_5

Scheme 15 Formation of $[Fe(L^{18})_3]$ (**42**)

Scheme 16 Formation and schematic representation of $^{3}_{\infty}[Fe(L^{18})_2]$ (**43**)

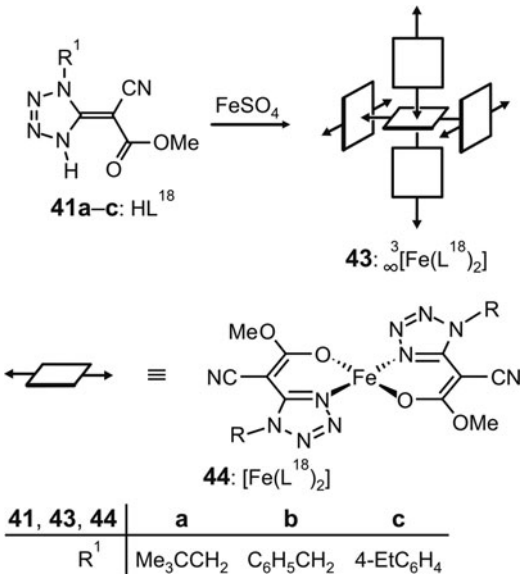

Whereas the enolates of **41a–c** function as bidentate ligands towards iron(III) ions and form the neutral *mer*-complexes **42a–c**, the enolates of the same compounds **41a–c** should function as tridentate ligands towards iron(II) ions and afford, by *spontaneous self-organization* [102, 103, 132], neutral three-dimensional coordination polymers [132–153].

Therefore we have carried out reactions of **41a–c** in diethyl ether with aqueous iron(II) sulfate solutions. The green precipitates obtained are almost insoluble in non-coordinating solvents. The analytical data obtained correspond with the general composition $^{3}_{\infty}[Fe(L^{18})_2]$, indicating the presence of polymers (Scheme 16). The formation of the coordination polymers $^{3}_{\infty}[Fe(L^{18})_2]$ (**43**) is understandable if the enolates of **41a–c** are considered as tridentate chelate ligands and if one assumes intermediary formation of the coordinatively unsaturated iron(II) building blocks **44**. The monomers are bidentate coordinating through the two CN donors, which leads to linking of monomers and to coordinative saturation at the iron(II) center of **44** with formation of the corresponding three-dimensional coordination polymers **43** [154]. In agreement with a polymeric structure of **43** is the fact that they are readily soluble in coordinating solvents such as pyridine, acetonitrile, etc., and are depolymerized.

In contrast to **41a–c**, the prerequisites for an "internal" coupling are lacking in **41d–f** because of the absence of additional CN donors.

An unequivocal assertion in favor of a 3D-linkage of the self-complementary monomers **44** is still missing, since it was hitherto not possible to grow single crystals of **43** suitable for X-ray analysis. However, an indirect proof of the structure of **43** is given in the case of copper(II) (Sect. 9.2).

9.2 3D- and 2D-Coordination Polymers of Copper(II)-Ions from Tetrazolyl- or Pyrrolinyl Enolates

Transition metal complexes are interesting as bio-inorganic model systems [155–157] and also because of their material properties (conductivity, magnetism, porosity) and as potential hosts for a variety of guests [156–161]. Whereas salt-like 2D-Cu^{II}-coordination polymers are well documented [158–162], far less is known about their neutral counterparts.

Reaction of tetrazolyl enole **45** with copper(II) acetate yields the 3D-coordination polymer $_{\infty}^{3}[Cu(L^{19})_2]$ (**46**), the structure of which is unequivocally established by single-crystal X-ray diffraction. The formation of **46** is understandable if the enolate of **45** is considered as tridentate chelate ligand and if the intermediate formation of the coordinatively unsaturated self-complimentary copper(II) building block **47** is assumed. The monomers **47** are bidentate coordinating by the two CN donors, which leads to linking of monomers and to coordinative saturation at the copper(II) center of **47** with formation of three-dimensional $_{\infty}^{3}[Cu(L^{19})_2]$ (**46**) (Scheme 17, Fig. 18) [163, 164].

In contrast to tetrazole **45** (HL^{19}) structurally analogous pyrrolidines **48** (HL^{20}) react with copper(II) acetate to give 2D-coordination polymers $_{\infty}^{2}[Cu(L^{20})_2]$ (**49**) rather than 3D-coordination polymers (Scheme 18). The structure of **49a** is established by single crystal X-ray diffraction (Fig. 19). The formation of 2D-coordination polymer **49a** is understandable if the enolate of **48a** is considered as tridentate chelate ligand and if an intermediate formation of the self-complimentary coordinatively unsaturated copper(II) building block **50a**, which reacts as metal and as well as ligand, is assumed [165].

Depolymerization of copper(II)/pyrrolidine-based 2D-polymer **49a** by 4,4'-bipyridyl and crystallization of the reaction product leads to two visually

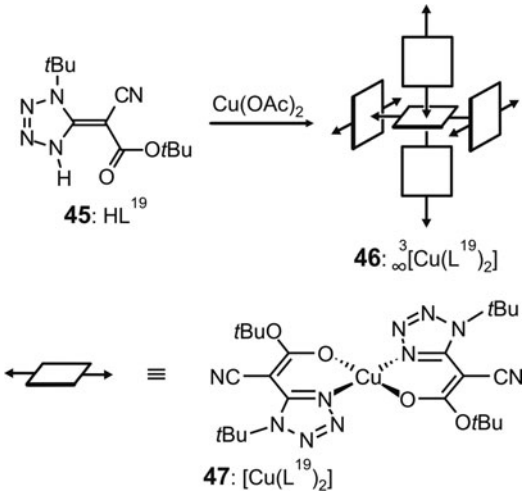

Scheme 17 Formation and schematic representation of $_{\infty}^{3}[Cu(L^{19})_2]$ (**46**)

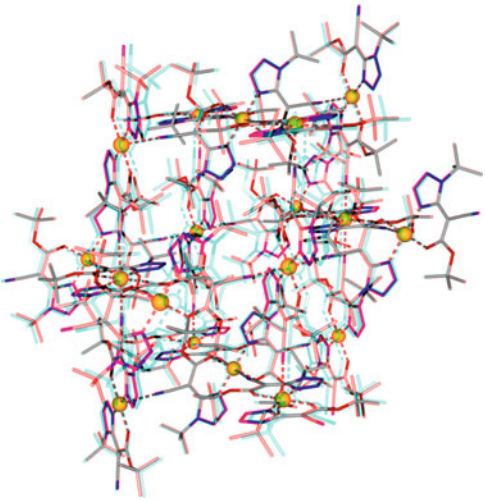

Fig. 18 Stereo representation of the structure determining motif of $_{\infty}^{3}[Cu(L^{19})_2]$ (**46**)

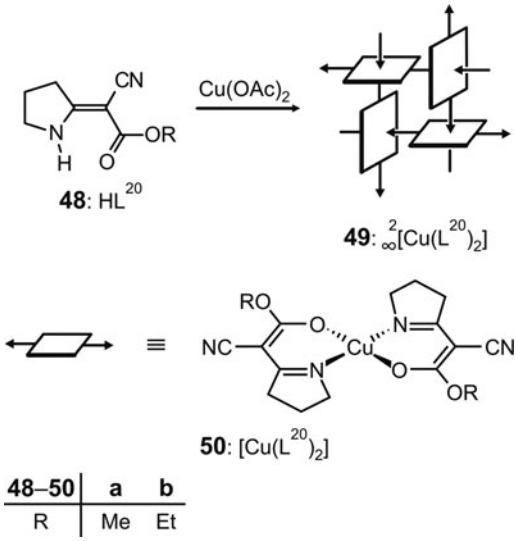

Scheme 18 Formation and schematic representation of $_{\infty}^{2}[Cu(L^{20})_2]$ (**49**)

distinguishable crystal charges, composed of dark green octahedral *meso*-**51** and light green rod-shaped crystals *racem*-**51** (Scheme 19, Fig. 20) [165]. Separation of the conglomerate of the morphologically different crystals is accomplished by pick out. The structure of the dinuclear complex *racem*-**51** has been established unambiguously by X-ray analysis.

The construction of supramolecular coordination polymers requires the ability to assemble small supramolecular units that can be further aggregated in a controlled

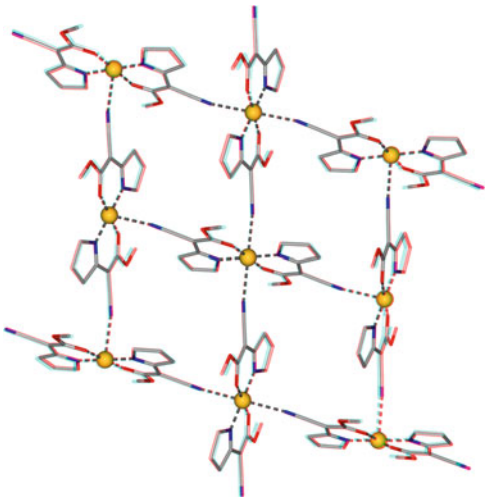

Fig. 19 Stereo representation of the structure determining motif of $^{2}_{\infty}[Cu(L^{20})_2]$ (**49a**)

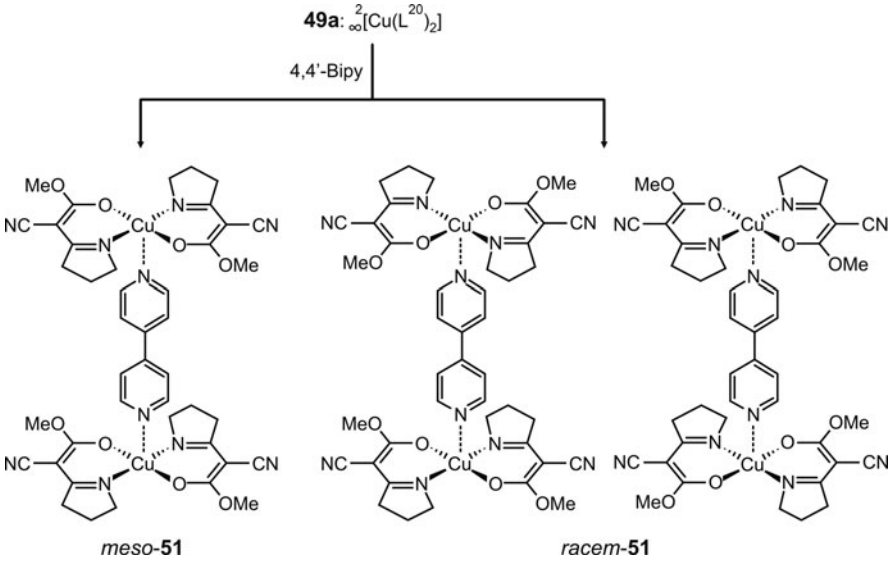

Scheme 19 Formation of *meso*-**51** and *racem*-**51**

fashion. Thus, during the crystallization of the 3D- and 2D-polymers, the role of the building blocks is twofold. They react both as metals and as ligands. This leads to *perpendicular* linking of the monomers and to coordinative saturation at the copper(II) centers. However, in order to study the effect of lateral substituents at the ligands on the dimensionality and geometry of the coordination polymers, we treated a methanolic solution of pyrrolidine **52** (HL^{21}) with copper(II) acetate and

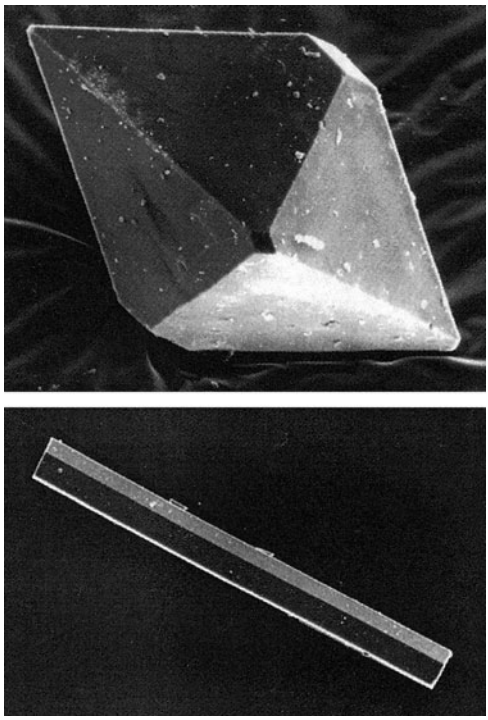

Fig. 20 Representation of crystals of *meso*-**51** (*top*: octahedron) and *racem*-**51** (*bottom*: rod)

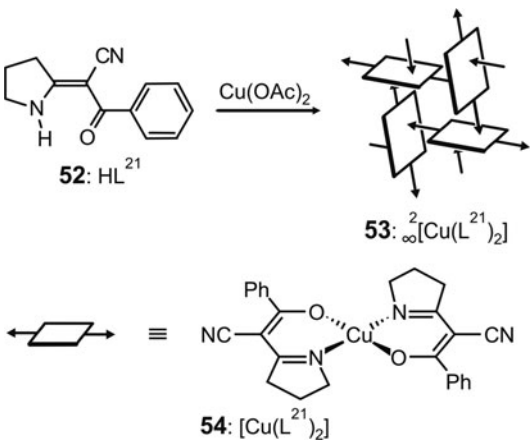

Scheme 20 Formation and schematic representation of $_{\infty}^{2}$[Cu(L^{21})$_2$] (**53**)

isolated crystals of $_{\infty}^{2}$[Cu(L^{21})$_2$] (**53**) (Scheme 20) [166]. Polymer **53** is generated from the self-complementary C_{2h}-symmetric building blocks (Cu(L^{21})$_2$) (**54**). Most interestingly, in this case, the cyano groups of monomer **54** are now bound to copper with a Cu–N–C angle of 117.0° (Fig. 21).

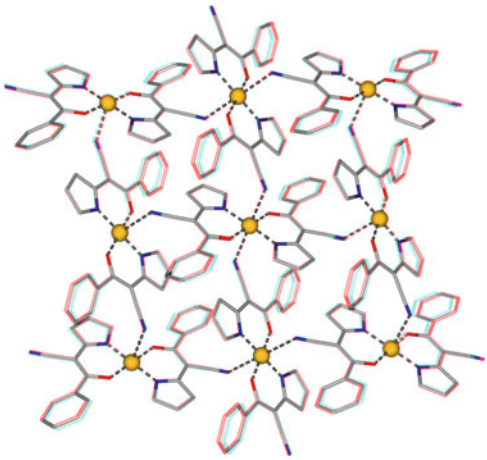

Fig. 21 Stereo representation of the structure determining motif of $^{2}_{\infty}[Cu(L^{21})_2]$ (**53**)

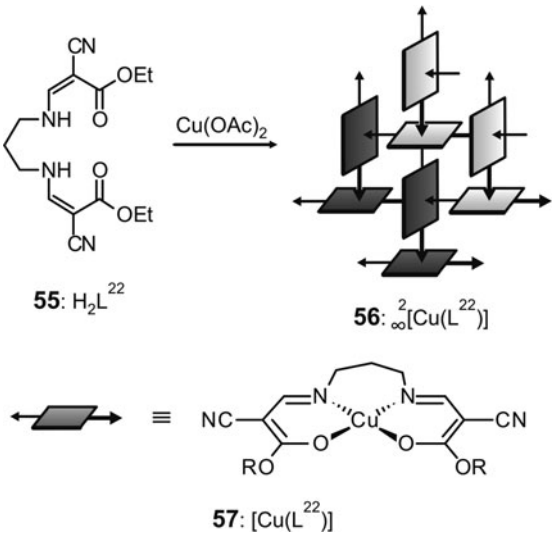

Scheme 21 Formation and schematic representation of $^{2}_{\infty}[Cu(L^{22})]$ (**56**)

The reaction of copper(II) acetate with ethyl aminomethylene cyanoacetate of type $H_2(L^{22})$ (**55**) provides highly stable polymer $^{2}_{\infty}[Cu(L^{22})]$ (**56**). The supramolecular 2D geometry of **56** depends basically on the lateral groups of the chelate ligand. The two cyano donors of monomer $[Cu(L^{22})]$ (**57**) coordinate differently, with the result that **56** is rather composed of zig-zag-1D-strands, linked among each other to give a 2D-network (Scheme 21) [167].

9.3 Ligand Programmed 1D-Coordination Polymers

In the 2D-, and 3D-coordination polymers discussed so far, a given monomer is surrounded by a total of four monomeric building blocks. Two of them are connected perpendicular to the axial position (Cu ← NC acceptor interaction), and two are connected equatorial (CN → Cu donor interaction) to the central monomer.

In contrast, when ethyl aminomethylene cyanoacetate of type **58** [$H_2(L^{23})$] is reacted with copper(II) acetate, a one-dimensional stair-like rather than a 2D- or 3D-coordination polymer $^{1}_{\infty}[Cu(L^{23})]$ (**59**) is generated. In **59**, the monomers [$Cu(L^{23})$] (**60**) are not arranged perpendicularly as in the 2D-/3D-case, but parallel, with the equatorial cyano donors coordinated axially to the copper centers (Scheme 22, Fig. 22) [168].

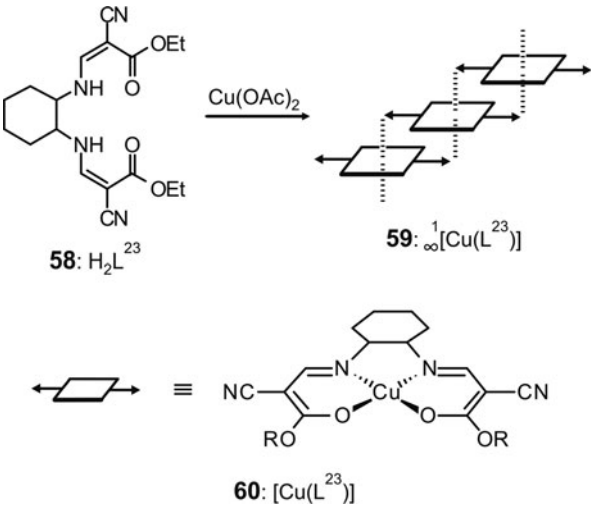

Scheme 22 Formation and schematic representation of $^{1}_{\infty}[Cu(L^{23})]$ (**59**)

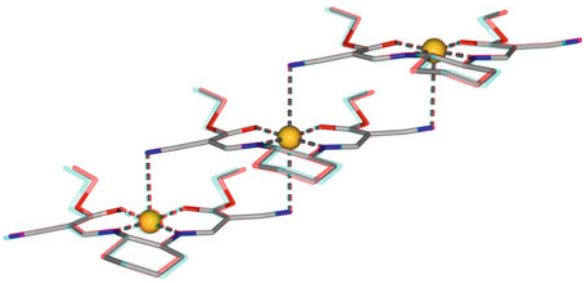

Fig. 22 Stereo representation of the structure determining motif of $^{1}_{\infty}[Cu(L^{23})]$ (**59**)

On the other hand, diethyl 1,4-butanediylbis(aminomethylene)-bis(cyanoacetate) $H_2(L^{24})$ (**61**) reacts with copper(II) acetate to give coordination polymer $_{\infty}^{1}[Cu(L^{24})]$ (**62**). In contrast to the hexacoordinate examples discussed so far, in **62** copper is only pentacoordinate. This leaves one cyano group of monomer $[Cu(L^{24})]$ (**63**) unoccupied and as in stair-like **59** leads to reduction of dimensionality resulting in a zig-zag 1D-structure for **62** (Scheme 23, Fig. 23) [168].

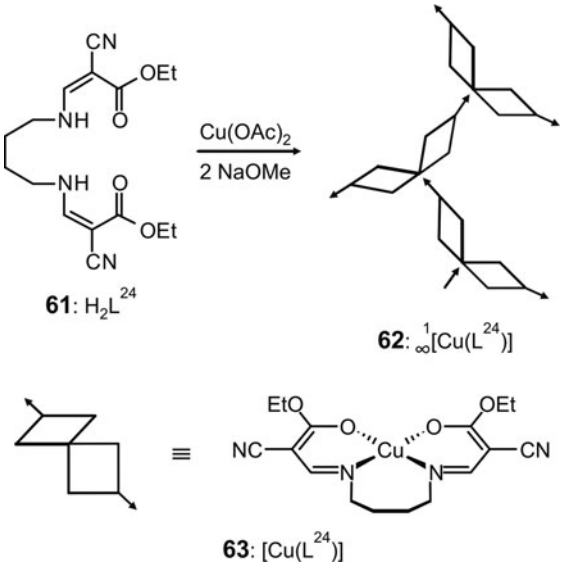

Scheme 23 Formation and schematic representation of $_{\infty}^{1}[Cu(L^{24})]$ (**62**)

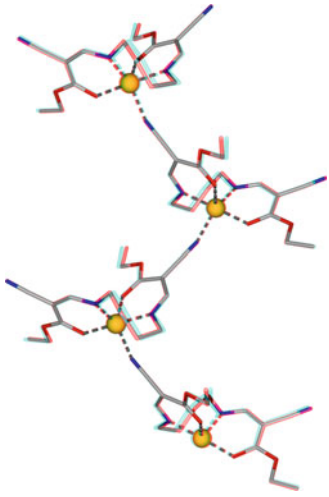

Fig. 23 Stereo representation of the structure determining motif of $_{\infty}^{1}[Cu(L^{24})]$ (**62**)

9.4 *Induction of Helicity via Stereogenic Centers: Asymmetric Synthesis of (*P*)- and (*M*)-1D-Coordination Polymers*

Reaction of a methanolic solution of copper(II) acetate and enantiomerically pure (*R*)/(*S*)-methyl(*E*)-4ethyl-2-oxazolidinylidene)cyanoacetate **64** leads to the coordinatively unsaturated C_2-symmetric intermediates (*R*,*R*)-**65** and (*S*,*S*)-**65**, which are sterically shielded at one side by two ethyl groups. Therefore, in contrast to the 2D- and 3D-coordination polymers, coordination of (*R*,*R*)/(*S*,*S*)-**65** with only one cyano donor is possible, resulting in the formation of polymers (*P*)-$^1_\infty$[Cu(L^R)$_2$] (*P*-**66**) and (*M*)-$^1_\infty$[Cu(L^S)$_2$] (*M*)-**66**) (Scheme 24) ([166, 169, 170]; for other chiral 1D-coordination polymers of our group, see [171, 172]). The X-ray crystal structure analysis of polymer (*P*)-**66** clearly proves a well-ordered infinite one-dimensional architecture. The central copper atoms in (*P*)-$^1_\infty$[Cu(L^R)$_2$] (*P*-**66**) are almost tetragonal-pyramidally coordinated, and in contrast to the 2D- and

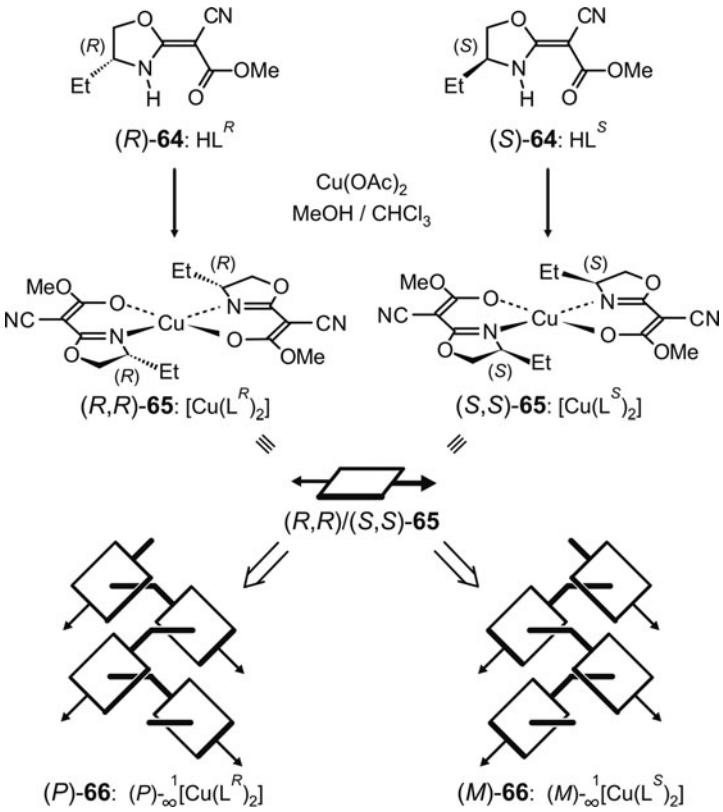

Scheme 24 Formation and schematic representation of (*P*)-$^1_\infty$[Cu(L^R)$_2$] (*P*)-**66** and (*M*)-$^1_\infty$[Cu-(L^S)$_2$] (*M*)-**66**

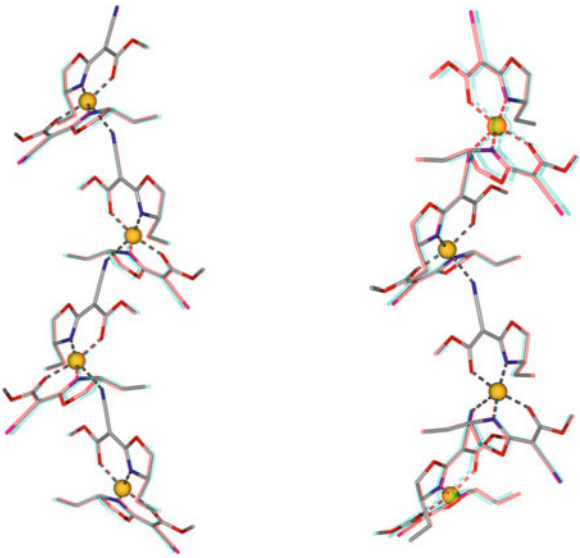

Fig. 24 Stereo representation of the structure determining motif of helical (*P*)-$^{1}_{\infty}$[Cu(L^{R})$_2$] (*P*)-**66** (*left*) and (*M*)-$^{1}_{\infty}$[Cu(L^{S})$_2$] (*M*)-**66** (*right*)

3D-polymers (Sects. 9.1–9.2), the monomers (*R*,*R*)-**65** in the helix polymer (*P*)-**66** are not positioned perpendicular to each other.

Consequently, the mononuclear building blocks (*S*,*S*)-**65** were obtained starting from (5*S*)-**64**, which during crystallization from chloroform afforded *left-handed helical* 1D-coordination polymer (*M*)-$^{1}_{\infty}$[Cu(L^{S})$_2$] (*M*-**66**). The structure of (*M*)-**66** was determined by X-ray crystal structure analysis (Fig. 24). In conclusion, it is demonstrated that stereogenic centers of ligands may induce stereospecifically helicity to 1D-coordination polymers. Thus (*R*)-**64** gives rise to (*P*)-**66** and (*S*)-**64** to mirror image (*M*)-**66** [166, 169–172].

9.5 *Reduction of Dimensionality by Using a Group 1 Metal*

Reaction of sodium hydride with tetrazole HL^{25} (**67**) in the presence of PMDETA (pentamethyldiethylenetriamine) in toluene leads to one-dimensional coordination polymer $^{1}_{\infty}$[Na(L^{25})(PMDETA)] (**68**) (Scheme 25) [173]. The generation of **68** is understandable if one assumes the intermediate formation of the coordinatively unsaturated, monomeric sodium building block [Na(L^{25})(PMDETA)] (**69**). The exact structure of neutral 1D-coordination polymer **68** was determined by X-ray crystallographic structural analysis. According to this analysis, the central sodium ion is coordinated by one tetrazolyl enolate ligand $(L^{25})^{-}$, tridentate PMDETA, and a CN group of a neighboring monomer, which completes the preferred sixfold coordination at sodium.

Scheme 25 Formation and schematic representation of $^{1}_{\infty}$[Na(L^{25})(PMDETA)] (**68**)

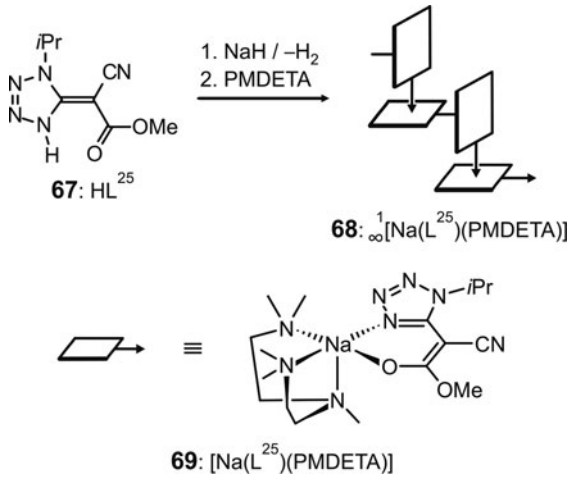

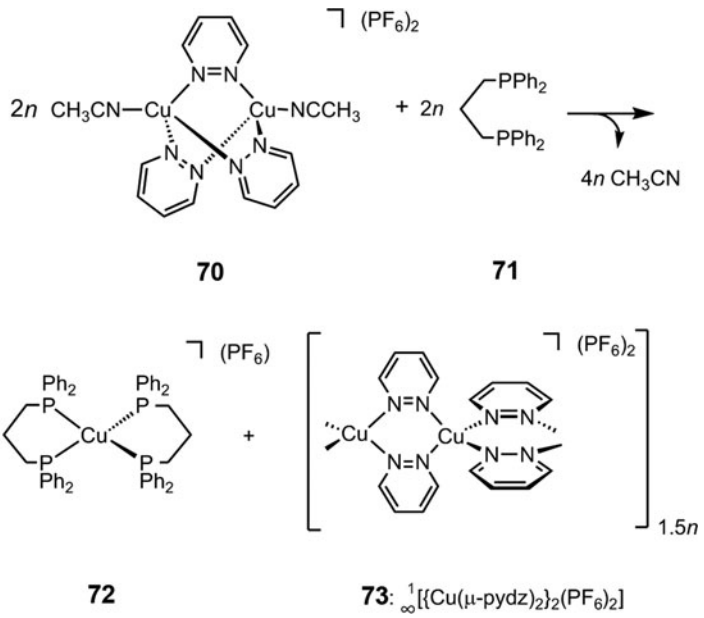

Scheme 26 Formation and schematic representation of *meso*-$^{1}_{\infty}$[{Cu(μ-pydz)$_2$}$_2$(PF$_6$)$_2$] (**73**)

9.6 A meso*-Helical 1D-Coordination Polymer*

Reaction of achiral [Cu$_2$(H$_3$CCN)$_2$(μ-pydz)$_3$][PF$_6$]$_2$ (**70**) (pydz = pyridazine) with bidentate 1,3-bis(diphenyl phosphanyl)propane **71** in acetonitrile at room temperature in a 1:1 ratio yielded the mononuclear copper(I) complex

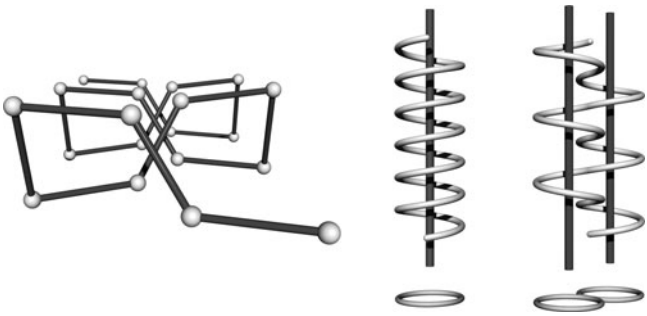

Fig. 25 *Left*: Schematic representation of the location of the copper(I) centers of coordination polymer *meso*-$^{1}_{\infty}$\{[Cu(μ-pydz)$_2$[PF_6]\} (**73**). In order to clarify the *meso*-helical arrangement, the positions of the copper centers were scaled along c by a factor of 0.125. *Right*: Generation of a helix and a *meso*-helix from a circle and a lemniscate

[Cu\{CH_2(CH_2PPh_2)$_2$\}$_2$][PF_6] (**72**) together with new one-dimensional coordination polymer $^{1}_{\infty}$\{[Cu(μ-pydz)$_2$][PF_6]\} (**73**) (Scheme 26) [174–188].

The one-dimensional coordination polymer **73** exhibits as an outstanding feature the rare structure of a *meso*-helix. Detailed analysis of the one-dimensional infinite framework of **73** revealed that finally eight copper centers constitute the repeating unit, creating the extraordinary *meso*-helix **73** with its points of contrareflexure (Fig. 25).

10 Summary and Perspectives

To see or to cognize

This review impressively demonstrates the paramount synthetic versatility of supramolecular coordination chemistry to get access to coronands, coronates, spherical containers, bowl-shaped surfaces, porous 1D-, 2D-, and 3D-metallo-coordination polymers, and even metallo-dendrimers. These systems altogether have high potentials for applications and because of the interdisciplinary assignment of tasks are best suited to train young chemists. They combine organic, inorganic, and physical aspects. Especially the incorporated metal ions assign redox or single molecular magnetic properties to these supramolecular coordination species.

It is evident that the majority of different structures given above provides excellent sources for further development, as illustrated exemplarily by the ferric wheels. A general feature of the metallo-coronands [$Fe_6Cl_6(L)_6$] (**39**; Sect. 7) is the fact that the N-alkyl substituents are alternately arranged above and below the plane of the six iron ions. Interestingly, this molecular geometry offers the possibility to construct container molecules.

In our modern world of visualization we have to deal cautiously with the suggestive power of pictures. If you want to present something new to students, you are often disappointed about the impact because they make you feel that they have seen this already.

However, there is a fundamental difference between whether you have only seen something or you have cognized (experienced) the issue. Therefore we have put much effort in the graphical 3D presentation of the supramolecular structures. The blue-red presentations, looked at with the inexpensive paper-back spectacles, impressively reveal the 3D world even of these complex structures and give you an unexpected insight and understanding.

What is meant by "to see or to cognize" is best illustrated by the art work of Albrecht Dürer (*Betende Hände*) [189] and by Auguste Rodin (*La Cathedrale*) [190]. The obvious fact which makes Rodin's *La Cathedrale* so special is that it is two right hands.

Acknowledgments This work was supported by the Deutsche Forschungsgemeinschaft [SPP 1137 "Molecular Magnetism" (SA276/26-1–3), SA276/27-1–2, SA276/29-1, SFB583, GK312], the Bayerisches Langzeitprogramm Neue Werkstoffe, and the Fonds der Chemischen Industrie. Generous allocation of premises after my retirement by Prof. Dr. K. Meyer, Department Chemie und Pharmazie, Anorganische Chemie, Universität Erlangen-Nürnberg, is gratefully acknowledged. Particular thanks are due to the enthusiastic co-workers mentioned in the references, who actively have taken part in our own research and developed innumerous number of cartoons, especially Dr. Harald Maid.

References

1. Saenger W (1984) Principles of nucleic acid structure. Springer, New York, pp 141–143
2. Fraenkel-Conrat H, Williams RC (1955) Proc Natl Acad Sci U S A 41:690–698
3. Klug A (1983) Angew Chem 95:579–596; Angew Chem Int Ed Engl 22:565–582
4. Lehn J-M (1990) Angew Chem 102:1347–1362; Angew Chem Int Ed Engl 29: 1304–1319
5. Vögtle F (1989) Supramolekulare chemie. B. G Teubner-Verlag, Stuttgart
6. Lehn J-M (1985) Science 227:849–856
7. Lehn J-M (1980) Pure Appl Chem 52:2441–2459
8. Tomalia DA, Naylor AM, Goddard WA III (1990) Angew Chem 102:119–157; Angew Chem Int Ed Engl 29:138–175
9. Lehn J-M (2007) Chem Soc Rev 36:151–160
10. Lehn J-M (2005) Prog Polym Sci 30:814–831
11. Lehn J-M (2002) Science 295:2400–2403
12. Machado VG, Baxter PNW, Lehn J-M (2001) J Braz Chem Soc 12:431–462
13. Lehn J-M (1999) Chem Eur J 5:2455–2463
14. Lehn J-M (1995) Supramolecular chemistry: concepts and perspectives. VCH, Weinheim
15. Lehn J-M (1978) Acc Chem Res 11:49–57
16. Wiester MJ, Ulmann PA, Mirkin CA (2011) Angew Chem 123:118–142; Angew Chem Int Ed 50:114–137
17. Timco GA, Faust TB, Tuna F, Winpenny REP (2011) Chem Soc Rev 40:3067–3075
18. Breiner B, Clegg JK, Nitschke JR (2011) Chem Sci 2:51–56

19. Khutia A, Sanz Miguel PJ, Lippert B (2011) Chem Eur J 17:4195–4204
20. Cornia A, Mannini M, Sainctavit P, Sessoli R (2011) Chem Soc Rev 40:3076–3091
21. Long D-L, Tsunashima R, Cronin L (2010) Angew Chem 122:1780–1803; Angew Chem Int Ed 49:1736–1758
22. Mellet CO, Benito JM, Ferández JMG (2010) Chem Eur J 16:6728–6742
23. Piguet C (2010) Chem Commun 46:6209–6231
24. Ward MD (2009) Chem Commun 4487–4499
25. Petukhov K, Alam MS, Rupp H, Strömsdörfer S, Müller P, Scheurer A, Saalfrank RW, Kortus J, Postnikov A, Ruben M, Thompson LK, Lehn J-M (2009) Coord Chem Rev 253:2387–2398
26. Yoshizawa M, Klosterman JK, Fujita M (2009) Angew Chem 121:3470–3490; Angew Chem Int Ed 48:3418–3438
27. Aromí G, Gamez P, Reedijk J (2008) Coord Chem Rev 252:964–989
28. Northrop BH, Yang H-B, Stang PJ (2008) Chem Commun 5896–5908
29. Koblenz TS, Wassenaar J, Reek JNH (2008) Chem Soc Rev 37:247–262
30. Albrecht M, Fröhlich R (2007) Bull Chem Soc Jpn 80:797–808
31. Mezei G, Zaleski CM, Pecoraro VL (2007) Chem Rev 107:4933–5003
32. Pluth MD, Raymond KN (2007) Chem Soc Rev 36:161–171
33. Boyer JL, Kuhlman ML, Rauchfuss TB (2007) Acc Chem Res 40:233–242
34. Thomas JM (2007) Chem Soc Rev 36:856–868
35. Pariya C, Sparrow CR, Back C-K, Sand G, Fronczek FR, Maverick AW (2007) Angew Chem 119:6421–6424; Angew Chem Int Ed 46:6305–6308
36. Gimeno N, Vilar R (2006) Coord Chem Rev 250:3161–3189
37. Seeber G, Tiedemann BEF, Raymond KN (2006) Top Curr Chem 265:147–183
38. Swiegers GF, Malefetse TJ (2002) Coord Chem Rev 225:91–121
39. Scarso A, Rebek J Jr (2002) Angew Chem 114:1556–1578; Angew Chem Int Ed 41:1488–1508
40. Albrecht M (2001) Chem Rev 101:3457–3497
41. Granzhan A, Schouwey C, Riis-Johannessen T, Scopelliti R, Severin K (2011) J Am Chem Soc 133:7106–7115
42. Ahamed BN, Arunachalam M, Ghosh P (2011) Inorg Chem 50:4772–4780
43. Costa JS, Craig GA, Barrios LA, Roubeau O, Ruiz E, Gómez-Coca S, Teat SJ, Aromí G (2011) Chem Eur J 17:4960–4963
44. Li S, Jia C, Wu B, Luo Q, Huang X, Yang Z, Li Q-S, Yang X-J (2011) Angew Chem 123:5839–5842; Angew Chem Int Ed 50:5721–5724
45. Clegg JK, Li F, Jolliffe KA, Meehan GV, Lindoy LF (2011) Chem Commun 47:6042–6044
46. Gupta D, Rajakannu P, Shankar B, Shanmugam R, Hussain F, Sarkar B, Sathiyendiran M (2011) Dalton Trans 40:5433–5435
47. Lim CW, Hong J-I (2011) Bull Korean Chem Soc 32:1030–1032
48. Seidel RW, Dietz C, Oppel IM (2011) Z Anorg Allg Chem 637:94–101
49. Albrecht M, Stöckel BA (2011) Synlett 121–123
50. Meng W, Breiner B, Rissanen KJ, Thoburn D, Clegg JK, Nitschke JR (2011) Angew Chem 123:3541–3545; Angew Chem Int Ed 50:3479–3483
51. Glasson CRK, Clegg JK, McMurtrie JC, Meehan GV, Lindoy LF, Motti CA, Moubaraki B, Murray KS, Cashion JD (2011) Chem Sci 2:540–543
52. Hashimoto T, Nishimura T, Lim JM, Kim D, Maeda H (2010) Chem Eur J 16:11653–11661
53. Cangelosi VM, Zakharov LN, Johnson DW (2010) Angew Chem 122:1270–1273; Angew Chem Int Ed 49:1248–1251
54. Liu T, Liu Y, Xuan W, Cui Y (2010) Angew Chem 122:4215–4218; Angew Chem Int Ed 49:4121–4124
55. Jankolovits J, Kampf JW, Maldonado S, Pecoraro VL (2010) Chem Eur J 16:6786–6796
56. Arribas CS, Wendt OF, Sundin AP, Carling C-J, Wang R, Lemieux RP, Wärnmark K (2010) Chem Commun 46:4381–4383

57. Liao P, Langloss BW, Johnson AM, Knudsen ER, Tham FS, Julian RR, Hooley RJ (2010) Chem Commun 46:4932–4934
58. Bogdan ND, Matache M, Meier VM, Dobrotă C, Dumitru I, Roiban GD, Funeriu DP (2010) Chem Eur J 16:2170–2180
59. Chen Q, Zeng M-H, Wei L-Q, Kurmoo M (2010) Chem Mater 22:4328–4334
60. Hastings CJ, Pluth MD, Bergman RG, Raymond KN (2010) J Am Chem Soc 132:6938–6940
61. Adarsh NN, Tocher DA, Ribas J, Dastidar P (2010) New J Chem 34:2458–2469
62. Liu Y, Lin Z, He C, Zhao L, Duan C (2010) Dalton Trans 39:11122–11125
63. Zhang Q, He L, Liu J-M, Wang W, Zhang J, Su C-Y (2010) Dalton Trans 39:11171–11179
64. Lemus L, Guerrero J, Costamagna J, Estiu G, Ferraudi G, Lappin AG, Oliver A, Noll BC (2010) Inorg Chem 49:4023–4035
65. Misaki H, Miyake H, Shinoda S, Tsukube H (2009) Inorg Chem 48:11921–11928
66. Mahata K, Schmittel M (2009) J Am Chem Soc 131:16544–16554
67. Saalfrank RW, Maid H, Scheurer A (2008) Angew Chem 120:8924–8956; Angew Chem Int Ed 47:8794–8824
68. Saalfrank RW, Löw N, Kareth S, Seitz V, Hampel F, Stalke D, Teichert M (1998) Angew Chem 110:182–184; Angew Chem Int Ed 37:172–175
69. Saalfrank RW, Löw N, Hampel F, Stachel H-D (1996) Angew Chem 108:2353–2354; Angew Chem Int Ed Engl 35:2209–2210
70. Saalfrank RW, Scheurer A, Puchta R, Hampel F, Maid H, Heinemann FW (2007) Angew Chem 119:269–272; Angew Chem Int Ed 46:265–268
71. Saalfrank RW, Dresel A, Seitz V, Trummer S, Hampel F, Teichert M, Stalke D, Stadler C, Daub J, Schünemann V, Trautwein AX (1997) Chem Eur J 3:2058–2062
72. Saalfrank RW, Seitz V, Caulder DL, Raymond KN, Teichert M, Stalke D (1998) Eur J Inorg Chem 1313–1317
73. Saalfrank RW, Seitz V, Heinemann FW, Göbel C, Herbst-Irmer R (2001) J Chem Soc Dalton Trans 599–603
74. Caulder DL, Raymond KN (1999) J Chem Soc Dalton Trans 1185–1200
75. Puchta R, Roling B, Scheurer A, Weiskopf V, Hampel F, van Eikema Hommes NJR, Hummel H-U (2008) Solid State Ionics 179:489–494
76. Sanders J (2007) 21st Solvay conference on chemistry, Brussels, Belgium 28–30 Nov 2007
77. Brady PA, Sanders JKM (1997) Chem Soc Rev 26:327–336
78. Saalfrank RW, Maid H, Mooren N, Hampel F (2002) Angew Chem 114:323–326; Angew Chem Int Ed 41:304–307
79. Saalfrank RW, Mooren N, Scheurer A, Maid H, Heinemann FW, Hampel F, Bauer W (2007) Eur J Inorg Chem 4815–4822
80. Saalfrank RW, Burak R, Breit A, Stalke D, Herbst-Irmer R, Daub J, Porsch M, Bill E, Müther M, Trautwein AX (1994) Angew Chem 106:1697–1699; Angew Chem Int Ed Engl 33:1621–1623
81. Breit A (2001) Ph.D. Thesis, Universität Erlangen-Nürnberg
82. Saalfrank RW, Hörner B, Stalke D, Salbeck J (1993) Angew Chem 105:1223–1225; Angew Chem Int Ed Engl 32:1179–1182
83. Beissel T, Powers RE, Raymond KN (1996) Angew Chem 108:1166–1168; Angew Chem Int Ed Engl 35:1084–1086
84. Caulder DL, Powers RE, Parac TN, Raymond KN (1998) Angew Chem 110:1940–1943; Angew Chem Int Ed 37:1840–1843
85. Hörner B (1993) PhD Thesis, Universität Erlangen-Nürnberg
86. Saalfrank RW, Glaser H, Demleitner B, Hampel F, Chowdhry MM, Schünemann V, Trautwein AX, Vaughan GBM, Yeh R, Davis AV, Raymond KN (2002) Chem Eur J 8:493–497
87. Johnson DW, Xu J, Saalfrank RW, Raymond KN (1999) Angew Chem 111:3058–3061; Angew Chem Int Ed 38:2882–2885

88. Brückner C, Powers RE, Raymond KN (1998) Angew Chem 110:1937–1940; Angew Chem Int Ed 37:1837–1839
89. Caulder DL, Brückner C, Powers RE, König S, Parac TN, Leary JA, Raymond KN (2001) J Am Chem Soc 123:8923–8938
90. Yamaguchi T, Fujita M (2008) Angew Chem 120:2097–2099; Angew Chem Int Ed 47:2067–2069
91. Albrecht M, Janser I, Fröhlich R (2005) Chem Commun 157–165
92. Albrecht M, Janser I, Runsink J, Raabe G, Weis P, Fröhlich R (2004) Angew Chem 116:6832–6836; Angew Chem Int Ed 43:6662–6666
93. Albrecht M, Janser I, Meyer S, Weis P, Fröhlich R (2003) Chem Commun 2854–2855
94. Müller IM, Robson R, Separovic F (2001) Angew Chem 113:4519–4520; Angew Chem Int Ed 40:4385–4386
95. Müller IM, Möller D (2005) Angew Chem 117:3029–3033; Angew Chem Int Ed 44:2969–2973
96. Müller IM, Spillmann S, Franck H, Pietschnig R (2004) Chem Eur J 10:2207–2213
97. Hiraoka S, Harano K, Shiro M, Ozawa Y, Yasuda N, Toriumi K, Shionoya M (2006) Angew Chem 118:6638–6641; Angew Chem Int Ed 45:6488–6491
98. Glaser T, Heidemeier M, Weyhermüller T, Hoffmann R-D, Rupp H, Müller P (2006) Angew Chem 118:6179–6183; Angew Chem Int Ed 45:6033–6037
99. Oppel IM (née Müller), Föcker K (2008) Angew Chem 120:408–411; Angew Chem Int Ed 47:402–405
100. Saalfrank RW, Maid H, Scheurer A, Heinemann FW, Puchta R, Bauer W, Stern D, Stalke D (2008) Angew Chem 120:9073–9077; Angew Chem Int Ed 47:8941–8945
101. Saalfrank RW, Maid H, Scheurer A, Puchta R, Bauer W (2010) Eur J Inorg Chem, 2903–2906
102. Saalfrank RW, Stark A, Peters K, von Schnering HG (1988) Angew Chem 100:878–880; Angew Chem Int Ed Engl 27:851–853
103. Saalfrank RW, Stark A, Bremer M, Hummel H-U (1990) Angew Chem 102:292–295; Angew Chem Int Ed Engl 29:311–314
104. Saalfrank RW, Demleitner B, Glaser H, Maid H, Reihs S, Bauer W, Maluenga M, Hampel F, Teichert M, Krautscheid H (2003) Eur J Inorg Chem 822–829
105. Stark A (1990) Ph.D. Thesis, Universität Erlangen-Nürnberg
106. Saalfrank RW, Löw N, Demleitner B, Stalke D, Teichert M (1998) Chem Eur J 4:1305–1311
107. Saalfrank RW, Demleitner B, Glaser H, Maid H, Bathelt D, Hampel F, Bauer W, Teichert M (2002) Chem Eur J 8:2679–2683
108. Glaser H (2002) Ph.D. Thesis, Universität Erlangen-Nürnberg
109. Beissel T, Powers RE, Parac TN, Raymond KN (1999) J Am Chem Soc 121:4200–4206
110. Mal P, Schultz D, Beyeh K, Rissanen K, Nitschke JR (2008) Angew Chem 120:8421–8425; Angew Chem Int Ed 47:8297–8301
111. Albrecht M, Kotila S (1996) Angew Chem 108:1299–1300; Angew Chem Int Ed Engl 35:1208–1210
112. Hasenknopf B, Lehn J-M, Kneisel BO, Baum G, Fenske D (1996) Angew Chem 108:1987–1990; Angew Chem Int Ed Engl 35:1838–1840
113. Saalfrank RW, Bernt I, Uller E, Hampel F (1997) Angew Chem 109:2596–2599; Angew Chem Int Ed Engl 36:2482–2485
114. Saalfrank RW, Deutscher C, Sperner S, Nakajima T, Ako AM, Uller E, Hampel F, Heinemann FW (2004) Inorg Chem 43:4372–4382
115. Saalfrank RW, Bernt I, Chowdhry MM, Hampel F, Vaughan GBM (2001) Chem Eur J 7:2765–2769
116. Ako AM, Maid H, Sperner S, Zaidi SHH, Saalfrank RW, Alam MS, Müller P, Heinemann FW (2005) Supramol Chem 17:315–321
117. Saalfrank RW, Deutscher C, Maid H, Ako AM, Sperner S, Nakajima T, Bauer W, Hampel F, Heß BA, van Eikema Hommes NJR, Puchta R, Heinemann FW (2004) Chem Eur J 10:1899–1905

118. Matzanke BF, Müller-Matzanke G, Raymond KN (1989) Siderophore-mediated iron transport. In: Loehr TM (ed) Physical bioinorganic chemistry series: iron carriers and iron proteins, VCH, pp 1–121
119. Ebmeyer F (1990) F. Vögtle. In: Duglas H (ed) Bioorganic chemistry frontiers, vol 1. Springer, Berlin, pp 143–159
120. Kiggen W, Vögtle F, Franken S, Pulf H (1986) Tetrahedron 42:1859–1872
121. Hancock RD, Martell AE (1989) Chem Rev 89:1875–1914
122. Sun Y, Martell AE (1990) Tetrahedron 46:2725–2736
123. Miller MJ, McKee JA, Minnick AA, Dolence EK (1991) Biol Metals 4:62–69
124. Garrett TM, McMurry TJ, Hosseini MW, Reyes ZE, Hahn FE, Raymond KN (1991) J Am Chem Soc 113:2965–2977
125. Pierre JL, Baret P, Gellon G (1991) Angew Chem 103:75–76; Angew Chem Int Ed Engl 30:85–86
126. Giroud-Godquin A-M, Maitlis PM (1991) Angew Chem 103:370–398; Angew Chem Int Ed Engl 30:375–402
127. Ahmet MT, Frampton CS, Silver J (1988) J Chem Soc Dalton Trans 1159–1163
128. Saalfrank RW, Lurz C-J, Hassa J, Danion D, Toupet L (1991) Chem Ber 124:595–608
129. Saalfrank RW, Lurz C-J, Schobert K, Struck O, Bill E, Trautwein AX (1991) Angew Chem 103:1499–1501; Angew Chem Int Ed Engl 30:1494–1496
130. Saalfrank RW, Reihs S, Hug M (1993) Tetrahedron Lett 34:6033–6036
131. Chakrasali RT, Ila H, Junjappa H (1988) Synthesis 6:453–455
132. Hvastijová M, Kohout J, Köhler H, Ondrejovič G (1988) Z Anorg Allg Chem 566:111–120
133. Leong WL, Vittal JJ (2011) Chem Rev 111:688–764
134. Zheng X-D, Lu T-B (2010) CrystEngComm 12:324–336
135. Masci B, Pasquale S, Thuéry P (2010) Cryst Growth Des 10:2004–2010
136. Vigato PA, Peruzzo V, Tamburini S (2009) Coord Chem Rev 253:1099–1201
137. Zhao X-X, Ma J-P, Shen D-Z, Dong Y-B, Huang R-Q (2009) CrystEngComm 11:1281–1290
138. Robson R (2008) Dalton Trans 5113–5131
139. Vittal JJ (2007) Coord Chem Rev 251:1781–1795
140. Biradha K, Sarkar M, Rajput L (2006) Chem Commun 4169–4179
141. Robin AY, Fromm KM (2006) Coord Chem Rev 250:2127–2157
142. Sokolov AN, MacGillivray LR (2006) Cryst Growth Des 6:2615–2624
143. Chen C-L, Kang B-S, Su C-Y (2006) Aust J Chem 59:3–18
144. Han L, Hong M (2005) Inorg Chem Commun 8:406–419
145. Kitagawa S, Uemura K (2005) Chem Soc Rev 34:109–119
146. Janiak C (2003) Dalton Trans 2781–2804
147. Serrano JL, Sierra T (2003) Coord Chem Rev 242:73–85
148. Moulton B, Zaworotko MJ (2001) Chem Rev 101:1629–1658
149. Eddaoudi M, Moler DB, Li H, Chen B, Reineke TM, O'Keeffe M, Yaghi OM (2001) Acc Chem Res 34:319–330
150. Khlobystov AN, Blake AJ, Champness NR, Lemenovskii DA, Majouga AG, Zyk NV, Schröder M (2001) Coord Chem Rev 222:155–192
151. Swiegers GF, Malefetse TJ (2000) Chem Rev 100:3483–3538
152. Blake AJ, Champness NR, Hubberstey P, Li W-S, Withersby MA, Schröder M (1999) Coord Chem Rev 183:117–138
153. Yaghi OM, Li H, Davis C, Richardson D, Groy TL (1998) Acc Chem Res 31:474–484
154. Fritschi H, Leutenegger U, Siegmann K, Pfaltz A, Keller W, Krathy C (1988) Helv Chim Acta 71:1541–1552
155. Petty RH, Welch BR, Wilson LJ, Bottomley LA, Kadish KM (1980) J Am Chem Soc 102:611–620
156. Brown DB, Hall JW, Helis HM, Walton EG, Hodgson DJ, Hatfield WE (1977) Inorg Chem 16:2675–2680
157. Julve M, De Munno G, Bruno G, Verdaguer M (1988) Inorg Chem 27:3160–3165

158. Phelps DW, Losee DB, Hatfield WE, Hodgson DJ (1976) Inorg Chem 15:3147–3152
159. Darriet J, Haddad MS, Duesler EN, Hendrickson DN (1979) Inorg Chem 18:2679–2682
160. Guillou O, Oushoorn RL, Kahn O, Boubekeur K, Batail P (1992) Angew Chem 104:658–660; Angew Chem Int Ed Engl 31:626–628
161. Hanack M, Hirsch A, Lehmann H (1990) Angew Chem 102:1499–1501; Angew Chem Int Ed Engl 29:1467–1468
162. Sekizaki M (1973) Acta Crystallogr Sect B Struct Crystallogr Cryst Chem B29:327–331
163. Saalfrank RW, Struck O, Peters K, von Schnering HG (1993) Chem Ber 126:837–840
164. Saalfrank RW, Struck O, Nunn K, Lurz C-J, Harbig R, Peters K, von Schnering HG, Bill E, Trautwein AX (1992) Chem Ber 125:2331–2335
165. Saalfrank RW, Struck O, Peters K, von Schnering HG (1994) Z Naturforsch 49b:1410–1414
166. Saalfrank RW, Maid H, Hampel F, Peters K (1999) Eur J Inorg Chem 1859–1867
167. Saalfrank RW, Struck O, Danion D, Hassa J, Toupet L (1994) Chem Mater 6:1432–1436
168. Saalfrank RW, Danion D, Hampel F, Hassa J, Struck O, Toupet L (1994) Chem Ber 127:1283–1286
169. Saalfrank RW, Struck O, Peters K, von Schnering HG (1994) Inorg Chim Acta 222:5–11
170. Saalfrank RW, Decker M, Hampel F, Peters K, von Schnering HG (1997) Chem Ber Recueil 130:1309–1313
171. Alam MS, Scheurer A, Saalfrank RW, Müller P (2008) Z Naturforsch 63b:1443–1446
172. Scheurer A, Maid H, Hampel F, Saalfrank RW, Toupet L, Mosset P, Puchta R, van Eikema Hommes NJR (2005) Eur J Org Chem 2566–2574
173. Saalfrank RW, Struck O, Davidson MG, Snaith R (1994) Chem Ber 127:2489–2492
174. Plasseraud L, Maid H, Hampel F, Saalfrank RW (2001) Chem Eur J 7:4007–4011
175. Liu W, Yu J, Jiang J, Yuan L, Xu B, Liu Q, Qu B, Zhang G, Yan C (2011) CrystEngComm 13:2764–2773
176. Liu J-Q, Wang Y-Y, Jia Z-B (2011) Inorg Chem Commun 14:519–521
177. Wang X-J, Huang T-H, Tang L-H, Cen Z-M, Ni Q-L, Gui L-C, Jiang X-F, Liu H-K (2010) CrystEngComm 12:4356–4364
178. Muñoz MC, Blay G, Fernández I, Pedro JR, Carrasco R, Castellano M, Ruiz-García R, Cano J (2010) CrystEngComm 12:2473–2484
179. Dong Z, Wang Y-Y, Liu R-T, Liu J-Q, Cui L, Shi Q-Z (2010) Cryst Growth Des 10:3311–3314
180. Huang K-L, Liu X, Li J-K, Ding Y-W, Chen X, Zhang M-X, Xu X-B, Song X-J (2010) Cryst Growth Des 10:1508–1515
181. Grünwald KR, Saischek G, Volpe M, Belaj F, Mösch-Zanetti NC (2010) Eur J Inorg Chem 2297–2305
182. Zang S-Q, Liang R, Fan Y-J, Hou H-W, Mak TCW (2010) Dalton Trans 39:8022–8032
183. Santillan GA, Carrano CJ (2009) Cryst Growth Des 9:1590–1598
184. Gu Z-G, Sevov SC, (2009) J Mater Chem 19:8442–8447
185. Xiao D, Yuan R, Sun D, Zhang G, Chen H, He J, Wang E, (2009) J Mol Struct 936:264–269
186. Zhang C, Pang H, Hu M, Li J, Chen Y (2009) J Solid State Chem 182:1772–1779
187. McMorran DA (2008) Inorg Chem 47:592–601
188. Domasevitch KV, Solntsev PV, Gural'skiy IA, Krautscheid H, Rusanov EB, ChernegaAN, Howard JAK (2007) Dalton Trans 3893–3905
189. Betende Hände (Studie zu einer Apostelfigur des "Heller"-Altars), by Albrecht Dürer, ca. 1508, current location: Albertina, Vienna; cf.: http://de.wikipedia.org/wiki/Betende_Hände (accessed November 4, 2011)
190. La Cathedrale (The Cathedral), by Auguste Rodin, 1908, current location: Musée Rodin, Paris; cf.: http://www.musee-rodin.fr/en/collections/sculptures/cathedral (accessed November 4, 2011)

Index